



**HAL**  
open science

**Molecular analysis of the interactions of the cell-penetrating peptide Penetratin and lipid membranes. Contributions of the lipid PIP2, biophysical approaches and benzophenone photoreactivity in model membranes**

Leïla Bechtella

► **To cite this version:**

Leïla Bechtella. Molecular analysis of the interactions of the cell-penetrating peptide Penetratin and lipid membranes. Contributions of the lipid PIP2, biophysical approaches and benzophenone photoreactivity in model membranes. Biochemistry [q-bio.BM]. Sorbonne Université, 2019. English. NNT : 2019SORUS045 . tel-03381780

**HAL Id: tel-03381780**

**<https://theses.hal.science/tel-03381780>**

Submitted on 18 Oct 2021

**HAL** is a multi-disciplinary open access archive for the deposit and dissemination of scientific research documents, whether they are published or not. The documents may come from teaching and research institutions in France or abroad, or from public or private research centers.

L'archive ouverte pluridisciplinaire **HAL**, est destinée au dépôt et à la diffusion de documents scientifiques de niveau recherche, publiés ou non, émanant des établissements d'enseignement et de recherche français ou étrangers, des laboratoires publics ou privés.

# Sorbonne Université

Ecole doctorale de Chimie moléculaire Paris Centre (ED 406)

*UMR 7203 Laboratoire des BioMolécules (LBM)*

## Molecular analysis of the interactions of the cell-penetrating peptide Penetratin and lipid membranes.

*Contributions of the lipid PIP<sub>2</sub>, biophysical approaches and  
benzophenone photoreactivity in model membranes.*

Leïla Bechtella

Ph.D. thesis of Molecular chemistry

Supervised by Emmanuelle Sachon and Astrid Walrant

Presented and defended publicly on the 16 of October 2019

Committee members:

Prof Christine Enjalbal  
Prof Antoinette Killian  
Prof Mélanie Etheve-Quelquejeu  
Dr Alain Joliot  
Prof Giovanni Poli  
Dr Emmanuelle Sachon  
Dr Astrid Walrant

Reviewer  
Reviewer  
Jury member  
Jury member  
Jury member  
Ph.D. Director  
Ph.D. Co-Director, invited member



## Acknowledgements

*This Ph.D. work has been achieved at Sorbonne University, in the Laboratoire des BioMolécules (UMR 7203), directed by Sandrine Sagan.*

*First, I would like to thank Prof Christine Enjalbal and Prof Antoinette Killian for agreeing to evaluate this work and to be part of my Ph.D. committee in the quality of reviewers. I also thank Prof Mélanie Etheve-Quelquejeu, Dr Alain Joliot and Prof Giovanni Poli for accepting to be part of my Ph.D. committee.*

*These three years have been an incredible experience, both scientifically and personally, thanks to the good atmosphere and scientific dynamism of the laboratory, and thanks to all the persons with whom I have been able to interact during this thesis.*

*I would like to thank Sandrine Sagan for welcoming me to the laboratory, for her kindness, for her support and for her constructive suggestions on the project.*

*I would like to express my deep gratitude to my two wonderful supervisors, Astrid Walrant and Emmanuelle Sachon, for their dedication, useful advices and constant support. Working with you has greatly contributed to make of these three years a rewarding and exciting scientific experience. I have learned a lot from your great knowledge, enthusiasm and persistence. I truly appreciated to be part of your small team, thank you for your warm welcome, for the dinners and nice times in your company.*

*I would like to thank all the persons who have contributed in any way to this project. The interdisciplinarity and sharing of knowledge between the different teams of the lab has led to fruitful discussions and experiments. I thank Patrick Fuchs and Paula Milán Rodríguez for their beautiful molecular modelization, and Olivier Lequin and Edward Chalouhi for their expertise in NMR simulation.*

*I thank the team from the MS and Proteomics Platform IBPS (SU) for sharing their knowledge and sympathy. I thank Gérard Bolbach for sharing his great knowledge in mass spectrometry and for his helpful advices. I thank Lucrèce Matheron for her help in ESI experiments, useful comments on the article and for welcoming me to her peaceful office during the writing period. I thank Gilles Clodic for helping me to use the MS instruments and for his nice company.*

*I also thank Denis Lesage, Yves Gimbert, Giovanni Poli, and Alexandre Pradal from IPCM (SU) for the fruitful discussions.*

*I would like to thank all the internship students who have participated to this work: Carla Kirschbaum, Samy Leprévost and Marine Cosset. Thank you for your enthusiasm and interest.*

*I am grateful to the people from the Team 2 for their warm welcome and for giving to the 4<sup>th</sup> floor lab its nice working atmosphere.*

*Special thoughts go to Françoise Illien and Delphine Ravault who offered me their help and wise advises during my lab work. Thank you also for your smiles and kindness. Thank you Claire Lacombe to illuminate the lab with your joy and laughs. Thank you Nicolas Rodriguez and Sophie Cribier for your kindness and chocolates. I also thank Haifei Gao, Fabienne Burlina, Karine Guitot, Nicolas Pietrancosta, Thierry Drujon and Jesus Ayala-Sanmartin. Thank you for the fruitful discussions we could have. It has been a real pleasure working with you all.*

*Assistance provided by Eliane Moulinié and Karine Gherdi was also greatly appreciated. Thank you for your availability and your help for the (sometimes complicated) administrative tasks.*

*Thanks also to all the people from the other teams with whom I had the opportunity to discuss about work or other subjects. Thanks to Rodrigue MARQUANT for his help with the HPLC and for the lab security aspects, and to Ludovic CARLIER for his help in protein production.*

*I also thank all the Ph.D. students for the good moments, in the lab, in congress or in the weekends, thank you Agathe, Alexandre, Benjamin, Bingwei, Claudia, Damien, Didier, Edward, Koutedja, the 2 Mathildes, Nathalie, Paula, Pauline, Rachel, Roxanne, Sébastien, Shadai, Simon, Soha and Taleen. I am sure we will meet again soon and I wish good luck to the next ones !*

*Last but not least, I thank my family and friends for always being by my side and for supporting me along the way.*



# TABLE OF CONTENT

Acknowledgements.....	3
Table of content.....	6
Abbreviations .....	10
GENERAL INTRODUCTION.....	14
PART 1: PIP <sub>2</sub> CONTRIBUTIONS FOR THE INTERNALIZATION OF PENETRATIN .....	18
Introduction .....	19
1. Plasma membrane and phosphatidylinositol-4,5-biphosphate (PIP <sub>2</sub> ) .....	19
1.1. The plasma membrane .....	19
1.2. Phosphoinositides and PIP <sub>2</sub> functional properties and roles .....	39
1.3. PI(4,5)P <sub>2</sub> binding with proteins .....	44
1.4. Model membranes to study peptide-lipid interactions .....	45
2. The cell-penetrating peptide Penetratin.....	49
2.1. Penetratin sequence and structure .....	50
2.2. CPP classification by physicochemical properties.....	51
2.3. Cell entry mechanisms.....	54
3. PIP <sub>2</sub> and Penetratin internalization in the literature .....	62
3.1. Sequestration of PIP <sub>2</sub> by proteins basic binding-site or by basic peptides .....	62
3.2. CPPs can remodel the actin cytoskeleton.....	64
3.3. PIP <sub>2</sub> implication in the internalization mechanism of Engrailed .....	65
3.4. PIP <sub>2</sub> could play a role in Penetratin internalization.....	66
Results and discussion.....	68
1. Influence of the PIP <sub>2</sub> polar head blockage on the Penetratin internalization in cells	69
1.1. Internalization quantification by mass spectrometry .....	69
1.2. Contribution of PIP <sub>2</sub> in the internalization efficiency of Penetratin.....	70
2. Effect of Penetratin on the thermotropic phase behavior of PIP <sub>2</sub> -containing liposomes	72
2.1. Differential Scanning Calorimetry (DSC) .....	72
2.2. DSC data interpretation for studying CPP-lipid interaction .....	73
2.3. Penetratin effect on thermotropic phase behavior of PIP <sub>2</sub> -containing lipid vesicles	75
3. Penetratin-PIP <sub>2</sub> binding affinity.....	81
3.1. Fluorescence spectroscopy.....	81

3.2.	Binding affinity of Penetratin for PIP <sub>2</sub> -containing lipid vesicles .....	81
4.	Identification of lipid interaction partners of Penetratin in PIP <sub>2</sub> -containing liposomes	84
4.1.	Control experiment on zwitterionic lipid PC MLVs .....	86
4.2.	Binary lipid compositions: The presence of negatively charged lipids triggers the photo-cross-linking reaction .....	86
4.3.	Tertiary lipid compositions: PIP <sub>2</sub> photo-cross-linking over PS .....	89
	Conclusion.....	91
PART 2: BENZOPHENONE PHOTOREACTIVITY IN A LIPID BILAYER TO PROBE CPP/LIPID MEMBRANE INTERACTIONS .....		95
	Introduction .....	96
1.	CPPs and the membrane fluidity.....	96
1.1.	Penetratin structuration .....	96
1.2.	Penetratin positioning in lipid bilayers .....	97
1.3.	Penetratin influence on membrane organization: fluidity and curvature .....	98
2.	Benzophenone as a photoactivable probe in model membranes .....	101
2.1.	Radical hydrogen abstraction .....	102
2.2.	Paternò-Büchi reaction.....	103
2.3.	Triplet sensitized dimerization.....	103
2.4.	Double bond formation .....	104
3.	Characterization of the Penetratin photoadducts in gas-phase fragmentation .....	105
3.1.	Peptide fragmentation pathways .....	106
	Results and discussion.....	118
1.	CPP properties of Bzp-functionalized peptides.....	121
1.1.	Internalization efficiency of the Penetratin analogues .....	121
1.2.	Effect of the Penetratin analogues on thermotropic phase behavior of PIP <sub>2</sub> -containing liposomes.....	122
1.3.	Photo-cross-linking efficiency of the Bzp-functionalized Penetratin analogues on DMPG liposomes .....	124
1.4.	Effect of Bzp-functionalized Penetratin and (R/W) <sub>9</sub> on thermotropic phase behavior of DMPG liposomes .....	125
2.	Mapping of the benzophenone photoreactivity in lipid membranes .....	129
2.1.	General methodology .....	131
2.2.	Benzophenone-induced in-source decay (ISD) .....	132
2.3.	UV-induced redox reactions involving Bzp .....	134



2.4.	UV-induced covalent bond formation and rupture .....	136
2.5.	Bzp-induced photosensitization .....	146
2.6.	Radical oxygen species-induced oxidation reactions.....	148
3.	New insights in Pen preference for fluid-phase bilayers.....	151
4.	Analytical workflow and application of the methodology.....	152
5.	Formation of unusual c ions during the fragmentation of the Penetratin sequence by high energy CID (MALDI-TOF/TOF).....	156
5.1.	Mechanisms for the formation of c ions by CID MS/MS in the literature and comparison with our observations on the Penetratin sequence.....	158
5.2.	Peptide protonation state .....	163
5.3.	Peptide structuration.....	164
5.4.	Pursuance of the project to elucidate the c ions formation .....	166
	Conclusion.....	168
	GENERAL CONCLUSION .....	170
	MATERIAL AND METHODS.....	175
1.	Material.....	176
1.1.	Lipids.....	176
1.2.	Liposomes preparation .....	178
1.3.	Peptides .....	178
1.4.	Photo-cross-linking reagents .....	179
1.5.	Cell transfection.....	179
1.6.	Mass spectrometry matrices .....	180
2.	Peptide synthesis .....	180
3.	Lipid vesicles preparation.....	182
3.1.	Multilamellar vesicles (MLVs) .....	182
3.2.	Large unilamellar vesicles (LUVs).....	183
4.	Penetratin interaction with model membranes.....	183
4.1.	DSC.....	183
4.2.	Fluorescence spectroscopy.....	183
5.	CPP internalization in cells and quantification by MALDI-TOF mass spectrometry .	183
5.1.	Cells transfection with the plasmid GFP-PH .....	184
5.2.	Cells incubation with the peptide .....	184
5.3.	Streptavidin-functionalized magnetic beads preparation .....	185
5.4.	Purification.....	185

5.5.	Mass spectrometry analysis.....	185
6.	Identification of lipid interaction partner of Penetratin in PIP <sub>2</sub> -containing liposomes	185
6.1.	Model membranes photo-cross-linking.....	185
6.2.	Streptavidin-functionalized magnetic beads preparation .....	186
6.3.	Purification.....	186
6.4.	Photoadduct characterization .....	186
6.5.	Mass spectrometry analysis.....	187
6.6.	Studies and simulations of isotopic distributions. ....	187
	REFERENCES.....	188
	APPENDIX.....	209

## Abbreviations

18:1 ( <i>trans</i> $\Delta$ 9) PG	Dielsalidoyl phosphatidylglycerol
AA	Amino acid
ACN	Acetonitrile
AFM	Atomic force microscopy
AMP	Antimicrobial peptide
Apa	Aminopentanoic acid
Biot	Biotin
Biot(O <sub>2</sub> )	Biotin sulfone
Boc	tert-butoxycarbonyl
BSA	Bovine Serum Albumine
Bzp	Benzophenone
CAD or CID	Collision-activated dissociation or Collision-induced dissociation
CALM	Clathrin assembly lymphoid myeloid leukemia
CD	Circular dichroism
CG	Coarse-grained
CHCA	$\alpha$ -cyano-4-hydroxycinnamic acid
CHO-cell	Chinese hamster ovary cell
Chol	Cholesterol
Cp	Specific heat capacity
CPP	Cell-penetrating peptide
DCM	Dichloromethane
DIEA	N-N-diisopropylethylamine
DLoPG	1,2-dilinoleoyl-sn-glycero-3-phosphatidylglycerol
DMEM	Dulbecco's Modified Eagle Medium
DMF	Dimethylformamide
DMPC	1,2-dimyristoyl-sn-glycero-3-phosphocholine
DMPG	1,2-dimyristoyl-sn-glycero-3-phosphatidylglycerol
DMPS	1,2-dimyristoyl-sn-glycero-3-phosphatidylserine
DOPC	1,2-dioleoyl-sn-glycero-3-phosphatidylcholine
DOPG	1,2-dioleoyl-sn-glycero-3-phosphatidylglycerol
DOPIP <sub>2</sub>	1,2-dioleoyl-sn-glycero-3-phosphatidylinositol-(4,5)-biphosphate
DOPS	1,2-dioleoyl-sn-glycero-3-phosphoserine
DPPG	1,2-dipalmitoyl-sn-glycero-3-phosphatidylglycerol
DPPIP <sub>2</sub>	1,2-dipalmitoyl-sn-glycero-3-phosphatidylinositol-(4,5)-biphosphate
DPPS	1,2-dipalmitoyl-sn-glycero-3-phosphatidylserine
DSC	Differential Scanning Calorimetry
DTT	Dithiothreitol
$\Delta H_m$	Main transition enthalpy $P\beta' \rightarrow L\alpha$
$\Delta H_{pre}$	Pre-transition enthalpy $L\beta' \rightarrow P\alpha'$
$\Delta m$	mass difference
$E_{int}^0$	Initial internal energy

EA	Elaidic acid
ECD	Electron-capture dissociation
ECID	Electron capture-induced dissociation
$E_{CM}$	Center of mass energy
$E_k$	Kinetic energy of the incident precursor ion
En-2	Engrailed protein
ENTH	Epsin N-terminal homology
ESI	Electrospray ionization
ESR	Electron spin resonance
ETD	Electron-transfer dissociation
ExD	Electron-mediated dissociation
FERM	4.1 protein ezrin/radixin/moesin
FIA	Flow-injection analysis
FT-ICR	Fourier-transform ion cyclotron resonance
FWHM	Full width at half maximum
GAG	Glycosaminoglycan
GFP	Green fluorescent protein
GPI	Glycosylphosphatidylinositol
GPMV	Giant plasma membrane vesicle
GUV	Giant unilamellar vesicle
HBR	Highly basic region
HBSS	Hank's Buffered Salt Solution
HBTU	O-(benzotriazol-1-yl)-N, N, N', N'-tetramethyluronium hexafluorophosphate
HF	Hydrofluoric acid
$H_{II}$	Hexagonal phase
HIV-1	Human immunodeficiency virus-1
HPLC	High-performance liquid chromatography
ISD	In-source decay
IT	Ion trap
ITC	Isothermal titration calorimetry
LDL	Low-density lipoprotein
LoA	Linoleic acid
LTQ	Linear Triple Quadrupole
LUV	Large Unilamellar Vesicle
MA	Myristic acid
MALDI	Matrix-assisted laser desorption/ionization
MARCKS	Myristoylated alanine-rich C kinase substrate
MBHA	4-Methylbenzhydramine
$M_{gas}$	Mass of the inert gas
MIC	Minimal inhibitory concentration
$M_{incident\ precursor\ ion}$	Mass of the incident precursor ion
MLV	Multi Lamellar Vesicle
MS	Mass spectrometry
NMR	Nuclear magnetic resonance

OA	Oleic acid
P/L	Peptide/lipid molar ratio
PA	Palmitic acid
PA	Phosphatidic acid
P-B	Paternò-Büchi
PBS	Phosphate Buffered Saline
PC	Phosphatidylcholine
PE	Phosphatidylethanolamine
Pen	Penetratin
PG	Phosphatidylglycerol
PH	Pleckstrin homology
PI	Phosphoinositide
PI(4,5)P <sub>2</sub> or PIP <sub>2</sub>	Phosphatidylinositol-(4,5)-biphosphate
PKC	Protein kinase C
PLC <sup>δ</sup>	Phospholipase C delta
POPC	1-palmitoyl-2-oleoyl-sn-glycero-3-phosphocholine
PPII	polyproline II
PS	Phosphatidylserine
PSD	Post-source decay
PTD	Protein translocation domain
ROS	Radical oxygen species
S/N	Signal-to-noise
SDS	Sodium dodecylsulfate
SM	Sphingomyelin
SPR	Surface plasmon resonance
SUV	Small Unilamellar Vesicle
TFA	Trifluoroacetic acid
TIRF	Total internal reflection fluorescence microscopy
T <sub>m</sub>	Main transition temperature $P\beta' \rightarrow L\alpha$
TOF	Time-Of-Flight
T <sub>pre</sub>	Pre-transition temperature $L\beta' \rightarrow P\alpha'$
TQ	Triple quadrupoles
TRIS	Tris(hydroxymethyl)aminomethane
vdW	van der Waals



# GENERAL INTRODUCTION

Cell-penetrating peptides (CPP) can cross cell membranes and deliver biologically active molecules into cells. Understanding their internalization mechanisms is of first interest for an appropriate use in the medical field or for biotechnological applications. These peptides have been found to follow two distinct pathways for their internalization in cells: endocytosis and direct translocation. They can use these two routes concomitantly at various ratios, depending on their nature, cell type and various environmental factors. Endocytosis is an energy-dependent mechanism, responsible for the membrane vesicular traffic, that has been already described for the passage of large and polar molecules such as proteins, peptides or nucleic acids through the hydrophobic cell membrane. Direct translocation is an energy-independent pathway that is not yet understood. Many models have been proposed to explain how CPPs could cross the hydrophobic core of the plasma membrane without involving receptor recognition. A first recognition step of the peptide would imply electrostatic interaction with negatively charged lipids of the plasma membrane. This particular step and the methods to investigate it at the molecular level are the subject of this thesis.

Previous work showed that some CPPs could remodel the actin cytoskeleton,<sup>1,2</sup> interacted strongly with negatively charged lipids<sup>3</sup> and that phosphatidylinositol-(4,5)-biphosphate (PIP<sub>2</sub>) could play a role in Penetratin internalization<sup>4</sup>. The primary aim of this Ph.D. project is to analyze the role of the negatively charged lipid PIP<sub>2</sub>, a known regulator of actin polymerization, as a binding partner of the CPP Penetratin and as a potential effector of Penetratin internalization. This work will be presented in the Part 1 of the manuscript.

Internalization of Penetratin in Chinese hamster ovary (CHO)-cells will be studied. In particular, the role of PIP<sub>2</sub> in the internalization will be studied, by adding molecules that interact strongly with PIP<sub>2</sub>. In parallel, Penetratin interactions with model membranes will be studied. Model membranes are useful systems to study interactions between membrane-active peptides and lipids as they allow total control of the lipid composition. Model membranes such as PIP<sub>2</sub>-containing lipid vesicles will be used to estimate the effect of Penetratin on the thermotropic phase behavior of such liposomes. Penetratin binding affinity for PIP<sub>2</sub>-containing lipid vesicles will be estimated using tryptophan fluorescence. The binding affinity for PIP<sub>2</sub> will be compared to the one for PS, the most abundant negatively charged lipid in the cell membrane, by the same method.

Affinity photo-cross-linking coupled to mass spectrometry (MS), using benzophenone-functionalized peptides, was used to study the non-covalent interactions of CPPs and lipid membranes at a molecular level. Upon irradiation, benzophenone-functionalized Penetratin can be covalently bound to lipid fatty acid chains in its immediate environment.<sup>5</sup> This method allows us to identify Penetratin interaction partners using MS. Using this technique, we studied the interactions of Penetratin with negatively charged lipids, focusing on PIP<sub>2</sub>-containing liposomes with compositions including phosphatidylcholine (PC), phosphatidylserine (PS) and PIP<sub>2</sub>.

During our photo-cross-linking experiments, we encountered unexpected results, which we decided to investigate more in depth. This method has been further developed and exploited to retrieve valuable information on the peptide-model membrane non-covalent interactions. This study will be exposed in the Part 2 of this manuscript.



Highly informative secondary reactions occurring during UV irradiation were revealed, whose products were unequivocally identified by MS using Matrix-assisted laser desorption/ionization-Time-Of-Flight (MALDI-TOF) or Electrospray ionization (ESI)-Orbitrap MS and MALDI-TOF/TOF MS/MS. This work shows how to exploit in an original way the different reactivities of benzophenone in the context of a lipid membrane. An analytical workflow has been established for the interpretation of MS spectra, giving access to information on the CPP/lipid interaction at a molecular level such as depth of insertion or membrane fluidity in the CPP vicinity. An application of this workflow illustrates the role of cholesterol in the CPP/lipids interaction. This work represents a noteworthy improvement for the characterization of interacting partners such as CPPs and membrane lipids using benzophenone photo-cross-linking. This work is presented in an article published in *Analytical Chemistry* (see in Appendix).<sup>6</sup> In addition, during our study, we encountered unconventional collision-induced dissociation (CID) gas-phase fragmentation of Penetratin by MALDI-TOF/TOF. This point will also be discussed in Part 2.

Parts 1 and 2 of this manuscript are intimately linked. The methods for biophysical study such as calorimetry and for quantification of cell internalization will be presented in Part 1 to evaluate the Penetratin-PIP<sub>2</sub> interaction. The same methods will be reused in Part 2 for evaluation of benzophenone-functionalized Penetratin analogues used for the photo-cross-linking study. Moreover, the benzophenone-induced photo-cross-linking is used in Part 1 to evaluate Penetratin lipids preferences using liposomes of binary or multiple composition, including PIP<sub>2</sub>. The technique is developed in a methodological point of view in Part 2, for describing the benzophenone photoreactivity in lipid bilayers. Cross-references to the relevant points will be made when needed in the text.



# PART 1: PIP<sub>2</sub> CONTRIBUTIONS FOR THE INTERNALIZATION OF PENETRATIN

# Introduction

## 1. Plasma membrane and phosphatidylinositol-4,5-bisphosphate (PIP<sub>2</sub>)

PIP<sub>2</sub> is a minor lipid of the plasma membrane. However, probably because of its localized and high density of charge, it is implied in many cell processes. In this chapter, first a general description of the membrane composition, structure and dynamic will be given. The various transport pathways through the membrane will be approached, as well as model systems used for membranes study. Then, phosphoinositides (PIs) and PIP<sub>2</sub> properties and roles will be detailed. Their localization in the plasma membrane will be discussed. Finally, their binding abilities with proteins will be highlighted.

### 1.1. The plasma membrane

In all cells, prokaryotic or eukaryotic, from plants or animals, membranes play an essential role of separation. The plasma membrane, like all biological membranes, has for role to separate two environments of different compositions. Thereby, it constitutes a barrier between the cytoplasm contained in the cell and the extracellular environment. This property of separation is imparted from membrane lipids, whose organization in lipid bilayer allows to delimit the inside of the cell from its external environment. Lipids fatty acid chains form the hydrophobic core of the membrane, from 3 to 4 nm thick in general. This hydrophobic core constitutes an impermeable barrier to hydrophilic molecules.

Membranes also have a communication role between the two environments they separate. Biological membranes permeability is controlled by membrane proteins. With the contribution of transport proteins and vesicular traffic, membranes are able to regulate the passage of specific molecules from one to another environment.

Membranes have as well a structural role. Biomembranes of different cell types present various shapes, thus adapting to the particular functions of each cell. These various structures are given by the actin cytoskeleton, which mechanically support the membrane. The cytoskeleton proteins are among the most abundant proteins as this association of three classes of filaments form a thick network where associated proteins groups can be anchored.

Finally, most of the cell activity is proven to be held in the core or at proximity of the membrane. This last role of cell activity support highly depends on the membrane composition in lipids and proteins, as well as the way they are associated to each other.

The plasma membrane model organized in “fluid-mosaic”, described by Singel and Nicolson in 1972,<sup>7</sup> is still relevant today (Figure 1). This model, based on the thermodynamic study of the membrane principal components organization, presents a membrane constituted of proteins and glycoproteins inserted in a fluid lipid bilayer. This membrane is asymmetric and dynamic, proteins and lipids composing it are mobile and can diffuse in the bilayer through lateral and rotational movements.

In 40 years, the model has been enriched by many studies. In particular, the membrane fluidity has been discussed.<sup>8</sup> The membrane appears to be more structured than the model described

in 1972. The principal advancement, done by Simons and Ikonen<sup>9</sup> and Brown and London<sup>10</sup> in 1997, highlights the existence of relatively organized lipid micro domains, also called lipid rafts. These micro domains are mainly composed of sphingolipids and cholesterol, forming a sort of platform able to move in the fluid lipid bilayer. This platform hosts proteins which confer it various functions. In particular, these domains are implied in signalization,<sup>11</sup> fusion and membrane transport<sup>12</sup> activities. They can interact as well with structures present outside the membrane, such as the cytoskeleton.<sup>13</sup>

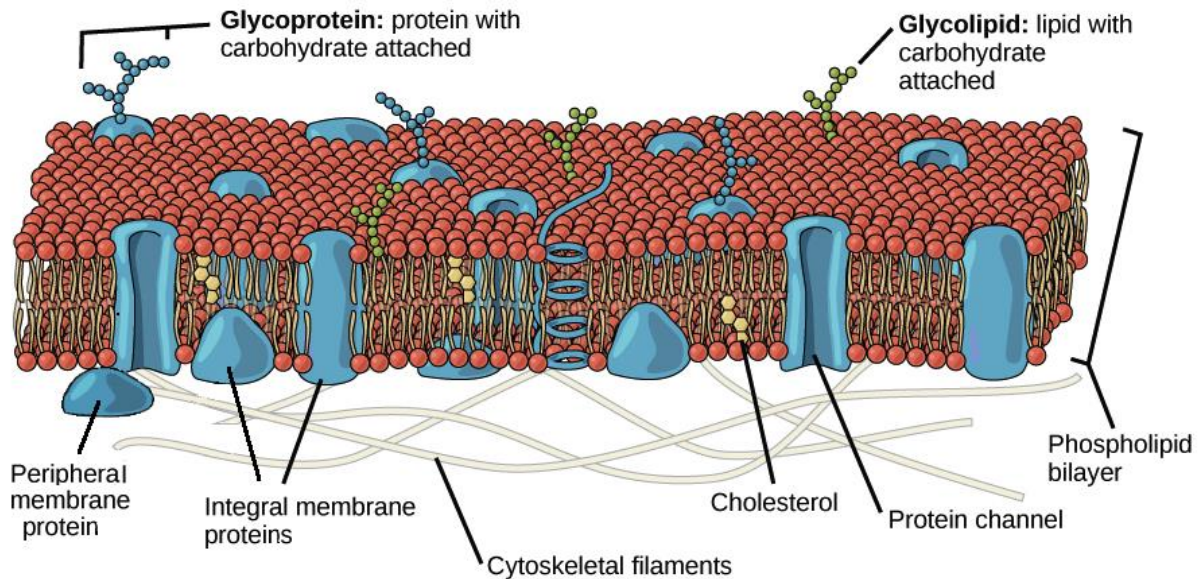


Figure 1. The fluid-mosaic model of the plasma membrane described by Singer and Nicolson.

Lipids and proteins diffusion is actually limited by interactions inside the membrane and by interactions held between the membrane and the cellular environment.

Lipids and proteins are the two principal components of the plasma membrane. Carbohydrates are also present in the membrane, but they are not found in their free form, they are systematically associated to lipids or proteins and they are present at the external leaflet only.

#### 1.1.1. Membrane lipid composition and structure

Lipids are the major constituents of the plasma membrane, their proportion varying according to the cell type studied. They principally have a structure and separation role, thanks to their organization in lipid bilayer. Certain lipids also have important functional roles. They can play a role in the proteins anchoring at the membrane, in proteins activities modification and in signal transduction to the cytoplasm. Membrane lipids are classified in 4 principal categories: phospholipids, sphingolipids, sterols and glycolipids. All these lipids are amphiphilic molecules, with a polar head and a hydrophobic tail. They auto-assemble in a bilayer held by hydrophobic and van der Waals interactions between their fatty acid chains.

#### LIPIDS CLASSES

##### Phospholipids

Phospholipids (or diacylphosphoglycerides) are the prevailing membrane lipids in eukaryotic cells. They are composed of a glycerol group linked to two fatty acids and to the lipid polar head

consisting in a phosphate group bearing a polar group (Figure 2). Their amphiphilic nature is behind their organization in lipid bilayer, forming the basic structure of the biological membrane. Length and degree of unsaturation, as well as the polar head nature, can vary. From these parameters ensue the physicochemical properties proper to each phospholipid.

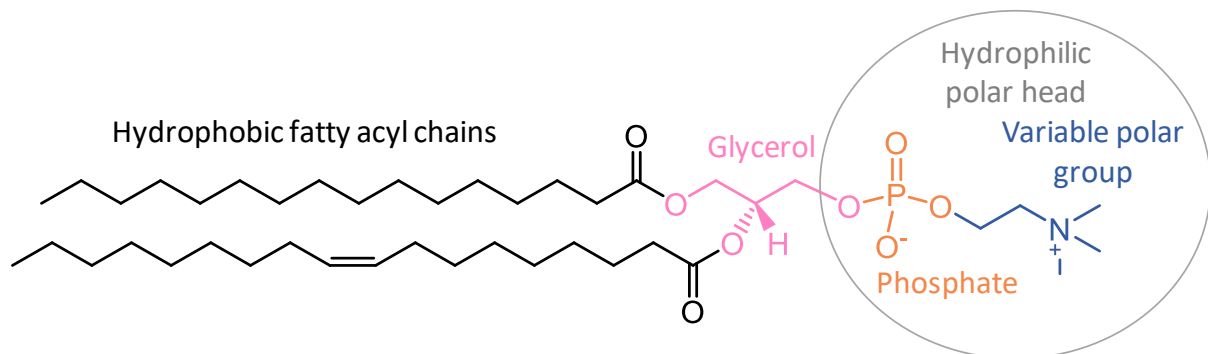


Figure 2. General structure of phospholipids, here with the example of 1-palmitoyl-2-oleoyl-sn-glycero-3-phosphocholine. In black, the fatty acyl chains, in pink, the glycerol group, in orange, the phosphate group, and in blue, the variable polar head (here, the choline group, predominant in number in the plasma membrane).

Phospholipids nature is determined by their polar group. The pKa of the phosphate group is included between 1 and 2. At physiological pH, it has a negative charge. The phospholipid global charge depends on the polar group. If this one is neutral (PS, PG, PI, PA), the global charge of the lipid is negative. If this one is positively charged (PC, PE), the phospholipid is electrically neutral. Neutral phospholipids are necessarily zwitterionic molecules. This particularity enhances the polarity of the phospholipids hydrophilic head, which strongly interact with the aqueous environment. The most frequently encountered phospholipids are presented in Figure 3.

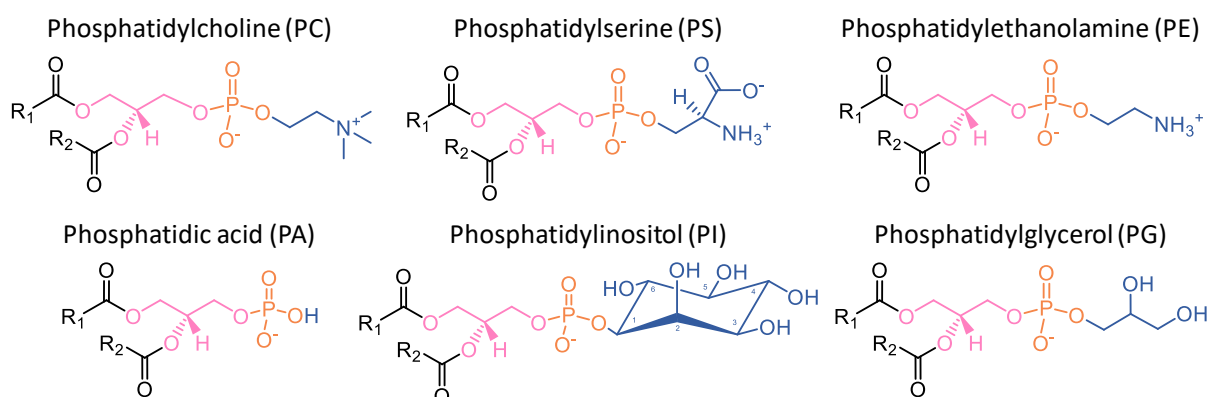


Figure 3. Principal polar groups of phospholipids found in the plasma membrane of eukaryotic cells, except for PG, of bacterial origin, however commonly used in model membranes. R<sub>1</sub> and R<sub>2</sub> are various saturated or unsaturated fatty acid chains.

Phosphatidylcholines (PC) are the most abundant phospholipids in the plasma membrane. The polar head group is constituted by a choline, a positively charged alcohol. PC are zwitterionic lipids, globally neutral. They represent more than 50% of total membrane phospholipids. They are located at 75% at the external leaflet.

Phosphatidylserines (PS) bear a negative charge and are mostly found at the internal leaflet. They represent most part of the negatively charged phospholipids in the plasma membrane of eukaryotic cells.

Phosphatidylethanolamines (PE) are zwitterionic lipids that we encounter especially at the internal leaflet. They constitute the principal lipid components at the internal leaflet.

Phosphatidic acids (PA) present the simplest polar substituent. These lipids are not much present in the plasma membrane. They are mainly present in the inside of the cell as they are intermediaries for the other phospholipids biosynthesis.

Phosphatidylglycerols (PG) are negatively charged bacterial lipids, which are not found in the eukaryotic membranes. However, they are ideal lipids for the *in vitro* study of membranes, using negatively charged model membranes, as they are easily available with a wide variety of acyl chains composition.

Phosphatidylinositols (PIs) and their derivatives are minor lipids of the plasma membrane. PIs bear a negative charge. PI derivatives are phosphorylated at the inositol hydroxyl groups (PIP, PIP<sub>2</sub>, PIP<sub>3</sub>), and thus can have several negative charges.

Fatty acyl chains of phosphoglycerides can be of various length and unsaturation degree. In biological membranes, fatty acid chains present most usually even numbers of carbons, varying from 14 to 24 carbons. Fatty acid chain lengths are most often C16, C18 and C20.<sup>14</sup> These different chain lengths induce differences in thickness and in rigidity in the membrane. Acyl chains can be saturated or unsaturated. The most common unsaturated species are 18:1, 18:2, 18:3 and 20:4, where the first number corresponds to the chain length and the second number reflects the number of double bonds. Natural unsaturated lipids mainly have *cis* double bonds rather than *trans*, which generates a defect in the membrane and prevents ordered acyl packing, increasing the membrane local fluidity. Moreover, membrane lipids often present an asymmetry with one saturated chain and one unsaturated chain.

### Sphingolipids

The different types of sphingolipids are presented in Figure 4. They have a similar structure to phospholipids and can be organized in mixed lipid bilayer with phospholipids. Sphingolipids all derive from the sphingosine, attached to a fatty acid chain by the amino group, also called a ceramide. Ceramide is the basic constituent of all sphingolipids.

Sphingolipids can be substituted by the same hydrophilic groups as the glycerophospholipids. The most abundant sphingolipid is the sphingomyelin (SM), which presents a phosphocholine group linked to the hydroxyl group of the sphingosine and thus is also a phospholipid.

Glycosphingolipids are ceramide derivatives linked to a sugar or to oligosaccharides. They are mainly located at the membrane outer leaflet. Their acyl chains are inserted in the lipid bilayer while their hydrophilic saccharide groups are outside the cell. This saccharide part confers them numerous recognition functions. The simplest is the glucocerebroside. It only presents one glucose unit linked to the sphingosine. More complex structures called gangliosides have one or two ramified sugar chains.

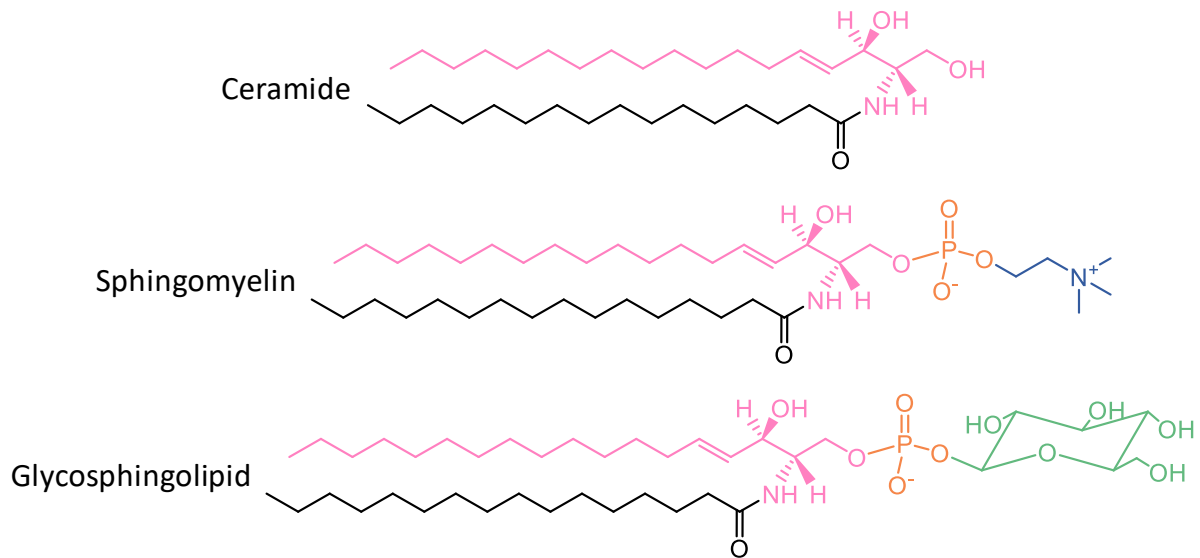


Figure 4. The different types of sphingolipids. In black, the fatty acids, in pink, the sphingosine, in orange, the phosphate group, in blue, the variable polar head (here, the choline group) and in green, the variable saccharide group (here, the glucose, forming the glucosylceramide or glucocerebroside).

### Sterols and their derivatives

Sterols are hydrophobic and compact molecules. The elementary structure is a tetracyclic hydrocarbon. Cholesterol (Figure 5) is the most common sterol in eukaryotic plasma membranes. It constitutes 30% in mass of all the membrane lipids. The molecule inserts almost entirely in the lipid bilayer, only the hydroxyl polar group is left at the membrane surface.

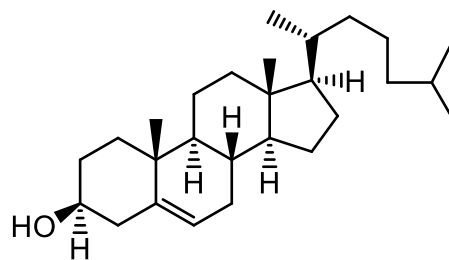


Figure 5. Cholesterol molecule.

### Glycolipids

Glycolipids (or diacylglycerides) are constituted of a glycerol group linked to two acyl chains and to one or several carbohydrates. These lipids are abundant in algae and plants photosynthetic membranes. They are hardly ever found in eukaryotic membranes. They have an amphiphilic nature and the more the glycoside part is important, the more polar will be the glycolipid.

## COMPOSITION AND DYNAMIC OF MEMBRANE LIPIDS

### Lipid membranes composition

Lipid composition in the different plasma membranes is wide. Some examples are given in Table 1. The different compositions in lipids give various properties to the membranes, structural, modulating their shape and contact points with the environment, or functional, as some lipids are implied in specific roles of signaling or vesicular transport for instance.



Table 1. Lipid composition of various biological membranes. Given in molar percentage of total lipid amount. N.D. stands for non-detected and « - » means non-analysed.<sup>15</sup>

Lipid	Human erythrocyte	CHO cell	Mitochondria		Endoplasmic reticulum	<i>Escherichia coli</i>
			External	Internal		
Cholesterol	25	-	N.D.	N.D.	20	N.D.
PC	19	51	46	38	46	N.D.
PE	18	21	33	24	21	75
SM	18	9	-	-	9	N.D.
Glycosphingolipid	10	-	-	-	-	N.D.
PS	9	7	1	4	2	<1
PI	1	8	10	16	2	N.D.
PG	0	1	N.D.	N.D.	-	20
Cardiolipin	0	2.3	6	16	-	5
PA	-	1	4	2	-	<2

Apart from the lipid classes diversity, the composition in hydrocarbon chains can also vary from one membrane to another (Table 2). SM presents long hydrophobic chains, up to 24 carbons, with low unsaturation. PC has mainly short fatty acid chains, from 16 to 18 carbons, also with low unsaturation. Anionic phospholipids PE and PS tend to have long and polyunsaturated chains, up to 6 double bonds. Combination of the different lipids and fatty acid chains provides numerous lipid species within one membrane.

Table 2. Gas phase chromatography analyses of the fatty acid chains composition of human erythrocytes. Data are expressed in % (w/w) of total phospholipids. The most representative percentage of chains (>10%) are highlighted in bold for each type of lipid.<sup>16</sup>

Chain length:unsaturation	Total phospholipids	SM	PC	PE	PS
16:0	20.1	<b>23.6</b>	<b>31.2</b>	<b>12.9</b>	2.7
18:0	17.0	5.7	<b>11.8</b>	<b>11.5</b>	<b>37.5</b>
18:1	13.3	<1	<b>18.9</b>	<b>18.1</b>	8.1
18:2	8.6	<1	<b>22.8</b>	7.1	3.1
20:0	<1	1.9	<1	<1	<1
20:3	1.3	<1	1.9	1.5	2.6
22:0	1.9	9.5	1.9	1.5	2.6
20:4	12.6	1.4	6.7	<b>23.7</b>	<b>24.2</b>
23:0	<1	2.0	<1	<1	<1
24:0	4.7	<b>22.8</b>	<1	<1	<1
22:4	3.1	-	<1	7.5	4.0
24:1	4.8	<b>24.0</b>	<1	<1	<1
22:5	2.0	-	<1	4.3	3.4
22:6	4.2	-	2.1	8.2	<b>10.1</b>

## Lipids physico-chemical properties and organization

Membrane lipids, mainly phospholipids, self-associate into bilayers in aqueous medium. Following the steric hindrance of both polar head and hydrophobic tails, lipids can take different orientations in the membrane. As presented in Figure 6, phospholipids organization in the bilayer is determined by geometric parameters:  $S$  the surface occupied by the lipid polar head,  $\Sigma$  the surface occupied by one fatty acid chain and  $\Phi$  the tilt angle. If the lipid has a large polar head, as it is the case for PC for instance, chains tilt allows to increase  $\Sigma$ , to optimize chains packing and to stabilize their interaction. Degree of tilt is also influenced by the bilayer hydration and presence of counterions.

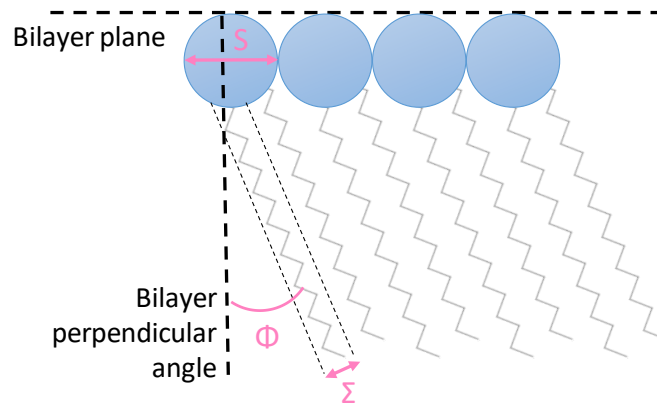
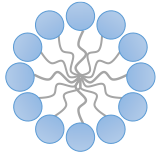
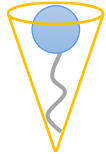
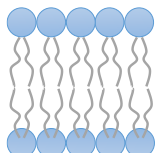
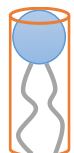
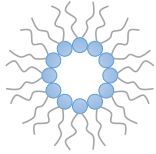
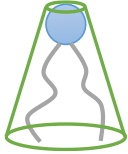


Figure 6. Illustration of lipids organization in the bilayer.

Lipids self-assembly is driven by interaction between the hydrophobic tails through van der Waals forces and hydrophobic effect. Hydrophilic polar heads are oriented towards the aqueous environment. Due to their various amphipathic properties and most of all geometric constraints, the different types of lipids associate in different polymorphic phase as shown in Table 3. Lipids adopt the shape that allows minimum contact between their hydrophobic moieties and the aqueous environment. These various shapes can be determined by the critical packing parameter ( $V/IS$ ), depending on the lipids geometry. It corresponds to the ratio of the volume  $V$  occupied by the hydrophobic tails over the chains length  $l$  multiplied by the surface  $S$  occupied by the lipid polar head. If the critical packing parameter is inferior to  $\frac{1}{2}$ , usually for lysophospholipids and most detergents, lipids have an inverted conical shape and adopt a micellar conformation. If the parameter is comprised between  $\frac{1}{2}$  and 1, lipids have a cylindrical shape and assemble in bilayer, also called lamellar phase. If the parameter is superior to 1, lipids have a conical shape and associate in hexagonal phase ( $H_{II}$ ).

Table 3. Polymorphic phases, molecular shapes and critical packing parameters of phospholipids. Geometric parameters: V is the volume occupied by the lipid fatty acid chains, l is the chain length and S the surface occupied by the lipid polar head. Adapted from <sup>17</sup>.

Lipid	Phase	Molecular shape	Critical packing parameter (V/S)
<p>Only one or 2 short hydrophobic tails</p> <p>Lysophospholipids</p> <p>Detergents</p>	 <p>Micellar</p>	 <p>Inverted conical</p>	$< \frac{1}{2}$
<p>Large polar head</p> <p>PC, SM, PS, PI, PG, PA, Cardiolipin</p>	 <p>Bilayer</p>	 <p>Cylindrical</p>	$\frac{1}{2} - 1$
<p>Small polar head and unsaturated fatty acid chains</p> <p>Unsaturated PE</p>	 <p>Hexagonal (H<sub>II</sub>)</p>	 <p>Conical</p>	$> 1$

Most of phospholipid have a cylindrical shape and associate in lamellar phase. Lamellar phases exist in different physical states which determine the lipids lateral order, molecular organization and fluidity in the bilayer (Figure 7).<sup>18</sup> Physicochemical factors such as temperature, pH, ionic strength have an impact on the physical state of a membrane. Presence of cholesterol in a lipid bilayer can as well influence the lamellar phase state.

In the gel phase ( $L_{\beta}'$  or  $L_{\beta}$  or  $S_o$  for solid-ordered), lipids chains are found in *trans* conformation and packing is optimized, which gives a very compact lipid structure. Lipid chains are also elongated at their maximum, forming a thick bilayer. Lateral diffusion and thus membrane fluidity are highly reduced.  $L_{\beta}'$  correspond to tilted chains while  $L_{\beta}$  corresponds to non-tilted chains. The tilt angle increases with membrane hydration, which makes the bilayer thickness decrease.

Ordered membranes can be brought to a disordered state by heating above the phase transition temperature  $T_m$  of the lipids, which will increase molecular agitation of the hydrophobic tails. This state is the fluid phase  $L_{\alpha}'$ , also called liquid-disordered phase ( $L_d$ ). Appearance of *trans-gauche* defaults give rise to much less ordered organization. Consequently, lipids lateral and rotational diffusion are favored. Bilayer thickness is also decreased compared to the gel phase, as the lipid chains are less elongated.

In the case of tilted lipids, an intermediate phase called the ripple phase ( $P_{\beta'}$ ) can be observed. The transition between the gel and ripple phases occurs at the pre-transition temperature  $T_{pre}$ . This pre-transition may be due to increase of the interaction between the polar head groups and the aqueous environment.<sup>19</sup>

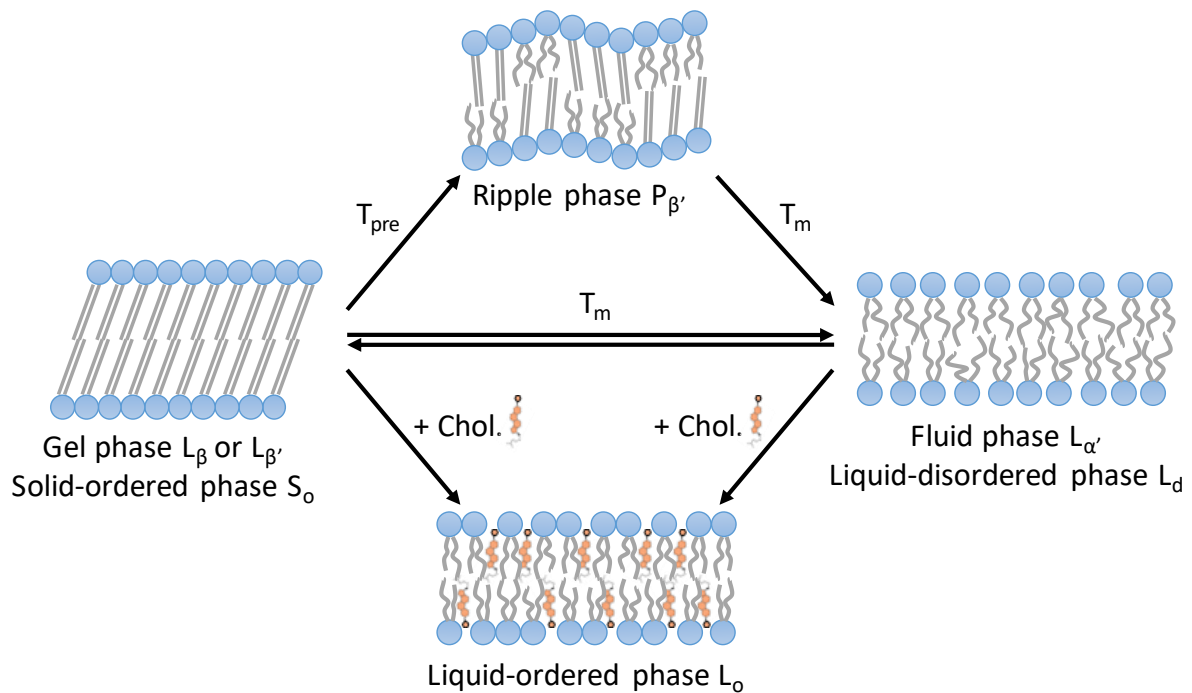


Figure 7. Illustration of the different physical states of a lipid lamellar phase in aqueous environment.

Thermotropic phase behavior of lipids are greatly influenced by the alkyl chains nature. Long and saturated chains tend to pack together through hydrophobic and van der Waals interactions, leading to a gel state of the membrane and a higher transition temperature. Short saturated chains have less surface for these interactions and thus induce a more fluid membrane. Tilt caused by an unsaturation in the fatty acid chain also leads to weaker interactions and consequently a higher fluidity. Polar head groups nature has also an impact on the phase transitions of lipids.

At physiologic temperatures, the inner leaflet of natural membranes is usually in a fluid phase. Cholesterol plays an important role in membrane fluidity. As previously mentioned, it is inserted between the phospholipids composing the bilayer. Considering a lipid membrane in fluid phase, its impact depends on concentration. For high concentrations in cholesterol, its presence tends to lower the membrane fluidity as the steroid part interacts with the hydrophobic tails of phospholipids. Cholesterol in large amounts promotes a typical liquid phase, the liquid-ordered ( $L_o$ ) phase, which is a fluid phase considering the lateral diffusion, but where the hydrophobic chains packing is highly organized (Figure 7). At low concentrations however, it tends to soften the membrane by increasing disorder.<sup>20</sup>

## Membrane asymmetry

The plasma membrane separates the cytosol from the extra cellular environment and present an asymmetric lipid composition. Most phospholipids are found in both leaflets but are more abundant in one or another.

In the plasma membrane of human erythrocytes (Figure 8), the outer leaflet is mainly uncharged, composed of zwitterionic lipids PC and SM while the inner leaflet is strongly negatively charged due to the presence of PS, PI and its phosphorylated derivatives. This contributes to the plasma membrane polarity, together with the difference in ionic concentration between the intra and extra cellular environments. This asymmetry is maintained by ATP-driven flippases that pump the anionic species from the outer to the inner leaflet.<sup>21,22</sup>

Asymmetry is also found in the fatty acid chains distribution. SM and PC, having rather long and saturated chains (Table 2), form a rigid and thicker lipid layer at the extracellular side of the membrane. Other phospholipids such as PE, PS, PI and its phosphorylated derivatives are more inclined to have unsaturated chains, which induces a more fluid organization of the cytosolic leaflet in which lateral diffusion occurs faster.

This asymmetry within the lipid bilayer also has an impact on the membrane local curvature. PE has a conical structure and thus is prone to form non lamellar membrane structures such as wells or vesicle buds at the inner leaflet of the membrane and can contribute to membrane fusion or transport pathways.



Figure 8. Lipid asymmetry of a human erythrocyte membrane. Left: Distribution for each phospholipid, in percentage of the considered phospholipid. Right: General distribution, in percentage of the total phospholipids amount. Adapted from <sup>23</sup>. Grouped data from: Bretscher (1971 a,b), Butikofer et al. (1990), Gascard et al. (1991), Gordesky et al. (1972, 1975), van Meer et al. (1981) and Verkleij et al. (1973).

Glycosphingolipids, implied in recognition functions, are mostly found at the extra-cellular leaflet. Repartition of cholesterol between the two leaflets is very uncertain and it is still not clear whether it is equally distributed or not.<sup>24</sup>

Finally, the plasma membrane asymmetry has important consequences in its functional roles. For instance, PS exposure on the cell surface serves as signal for phagocytosis and as a propagation signal in apoptosis and blood coagulation.<sup>22</sup>

### Lateral diffusion

Lipids lateral diffusion in the bilayer implies both lateral and rotational positions of lipids are continuously changing in the membrane. One lipid molecule can exchange laterally with one of its neighbors. This motion is called lateral diffusion and takes place about  $10^7$  times per second. Lateral diffusion coefficient ranges generally from  $10^{-7}$  to  $10^{-10}$   $\text{cm}^2 \cdot \text{s}^{-1}$ .<sup>18</sup> A lipid molecule can also rotate around its own axis, perpendicularly to the bilayer plane. This phenomenon occurs over times scale of nanoseconds. Proteins are also able to diffuse laterally within the plasma membrane, but their diffusion rate is a hundred times slower than lipid lateral diffusion.

Brownian motion of lipids in the fluid plasma membrane is however limited by lipid barriers and by interactions with proteins.<sup>25</sup> Actually, lipids distribution in the plasma membrane is not random and some lipids are locally enriched in the bilayer. The first observation of membrane lateral heterogeneity was made only one year after the fluid mosaic model was published by Singel and Nicolson and showed that detergent-labile and detergent-resistant fractions of the membrane could be isolated.<sup>26</sup> Numerous findings followed and gave rise to the lipid raft or microdomain hypothesis.<sup>10,27,28</sup> These rafts are enriched in sphingomyelin and cholesterol and form ordered platforms able to move laterally in the membrane. They would be present in liquid ordered phase ( $L_o$ ), a rigid and thick state induced by the presence of cholesterol, stabilizing the hydrophobic chains interactions. As confirmed by the use of biomimetic model membranes, certain lipids interact together to form large lateral domains through liquid-liquid phase separation.<sup>29</sup>

Such ordered domains existence *in vivo* is however controversial due to the lack of direct observation, mainly due to their very short lifetime of 10 ms of order, and to the unclear definition of such domains. A consensus definition suggests that rafts are heterogeneous, mostly composed of cholesterol and sphingomyelin, highly dynamic nanodomains of about 10-200 nm, which can form clusters larger than 300 nm generated by protein-protein and protein-lipid interactions.<sup>30</sup> These clusters present increased packing and order and decreased fluidity compared to the rest of the membrane, due to their enrichment in saturated phospholipids, sphingolipids, glycolipids and cholesterol. Some proteins like glycosylphosphatidylinositol (GPI)-anchored proteins and lipoproteins are anchored in these clusters and confer them functional roles.<sup>9</sup> As previously mentioned, these platforms are implied in signalization,<sup>11</sup> fusion and membrane transport<sup>12</sup> activities. They interact as well with membrane external structures such as the actin cytoskeleton which plays its part in the domains conservation and remodelling.<sup>13</sup> Furthermore, these domains are present in the inner and outer asymmetric membrane leaflets, probably coupled across leaflets,<sup>31,32</sup> which further impacts membrane organization. A representation of the membrane lateral heterogeneity is presented in Figure 9.

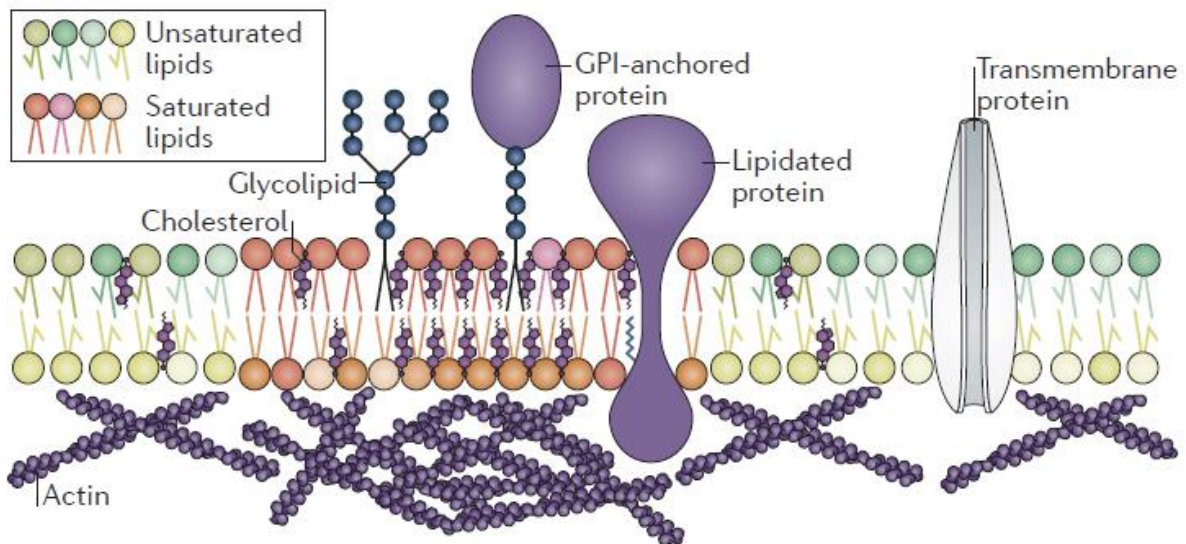


Figure 9. General overview of the plasma membrane lateral heterogeneity.<sup>25</sup>

Caveolae represents a third type of sphingolipid-cholesterol assembly (a subgroup of raft clusters), which is stabilized by polymerization of the caveolin protein. Caveolae are small invaginations of the membrane formed by self-association of caveolin proteins, forming a hairpin loop in the membrane. They are implied in endocytosis and exocytosis. Figure 10 shows how caveolin proteins associate to caveolae, with the N and C termini facing the cytoplasm, forming the intramembrane domain inserted within the bilayer. The caveolin scaffolding domain might interact with cholesterol through basic and bulky hydrophobic residues. The C-term domain, close to the intramembrane domain, is modified by palmitoyl groups embedded into the lipid bilayer. Interconnected caveolae structures can occupy a large area of the plasma membrane.<sup>33</sup>

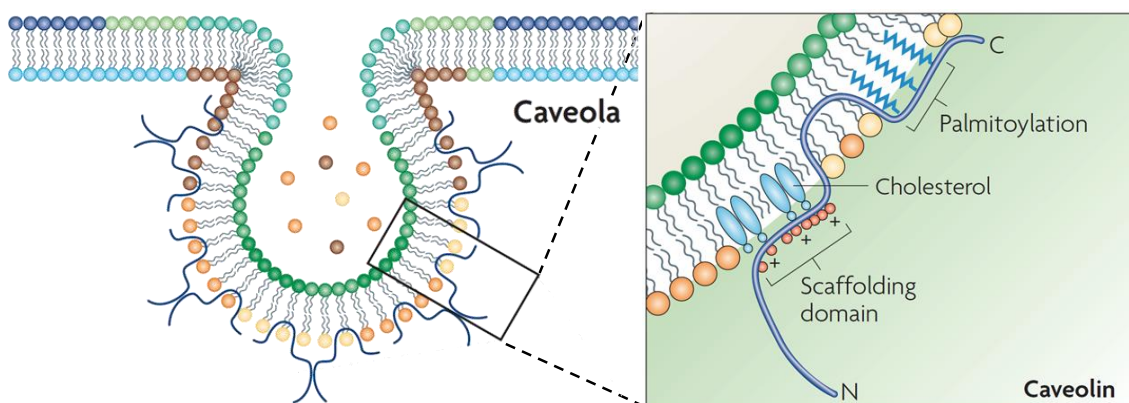


Figure 10. Caveolin proteins association with caveolae to form hairpin invaginations. Adapted from <sup>33</sup>.

### Transversal diffusion

The plasma membrane is known to be asymmetric. Phospholipids synthesis mostly takes place in the cytosolic leaflet of the endoplasmic reticulum. Transversal movement of lipids from one leaflet to the other is required to generate and maintain the heterogeneous composition of the membrane.<sup>34</sup> Moreover, various cell processes are dependent on the plasma membrane lipid

composition and its inherent asymmetry and dynamic. As an example, PS exposure at the cell surface regulates biochemical processes such as apoptosis, bone mineralization, cell-cell interactions and blood coagulation.<sup>22</sup> The transfer of one lipid from one leaflet of the membrane to the other is called transversal diffusion or flip-flop.

In pure lipid bilayers, phospholipids do not spontaneously diffuse transversally as this process is energetically unfavorable, implying the passage of the lipid polar head through the hydrophobic core of the bilayer. Passive diffusion of phospholipids in the plasma membrane is very slow and can take several hours to several days.<sup>18</sup> Only some lipid molecules such as cholesterol can undergo a fast flip-flop between the leaflets, in less than a second, probably due to their very small polar head consisting in a hydroxyl group.<sup>35,36</sup>

However, phospholipids transversal diffusion can be catalyzed by enzymes.<sup>37</sup> Flippases (lipid transfer towards the inward leaflet) and floppases (lipid translocation to the outward leaflet) are ATP-dependent that belong to the ABC transporter family and are able to selectively transfer lipids from a leaflet to the other. As an example, ABCB4, expressed in the liver and one of the most studied flippase, is able to move the PC from the cytosolic leaflet to the external leaflet.<sup>38</sup> Scramblases are energy-independent and calcium-dependent enzymes that are involved in transbilayer movement of phospholipids. They are non-selective and can catalyze non-specific lipid transversal diffusion across the bilayer.<sup>21</sup>

Additionally, insertion of external agents such as detergents, lipids, proteins or even membrane-active peptides in one of the membrane monolayers were found to accelerate transversal lipid motion. These effects are likely to be induced by perturbation of the interfacial region of the membrane by formation of hydrophobic defects or pore formation.<sup>21</sup>

### 1.1.2. Membrane proteins

Proteins inserted in the plasma membrane are classified based on their position in the bilayer. They are responsible for the membrane functional activities. The quantity and type of proteins vary according to the cell type. Some proteins are completely inserted in the bilayer while other are anchored to one of the leaflets. They can be associated in protein domains. Usually, protein domains associated to the extracellular leaflet bind other molecules such as other signalization proteins, ions, glucose, fatty acids or adhesion molecules present in the external environment. Domains inserted in the bilayer, and in particular the ones forming canals and pores, allow the transport of molecules from one to the other side of the plasma membrane. Domains located at the cytosolic leaflet can be implied in various functions, from proteins anchoring to the membrane to intracellular signalization processes. Functional properties and location of proteins in the membrane are generally linked to their sequence and structural characteristics.

There are 3 main categories of membrane proteins: integral (or intrinsic) proteins, peripheral proteins and lipid anchored proteins (illustrated on Figure 11).



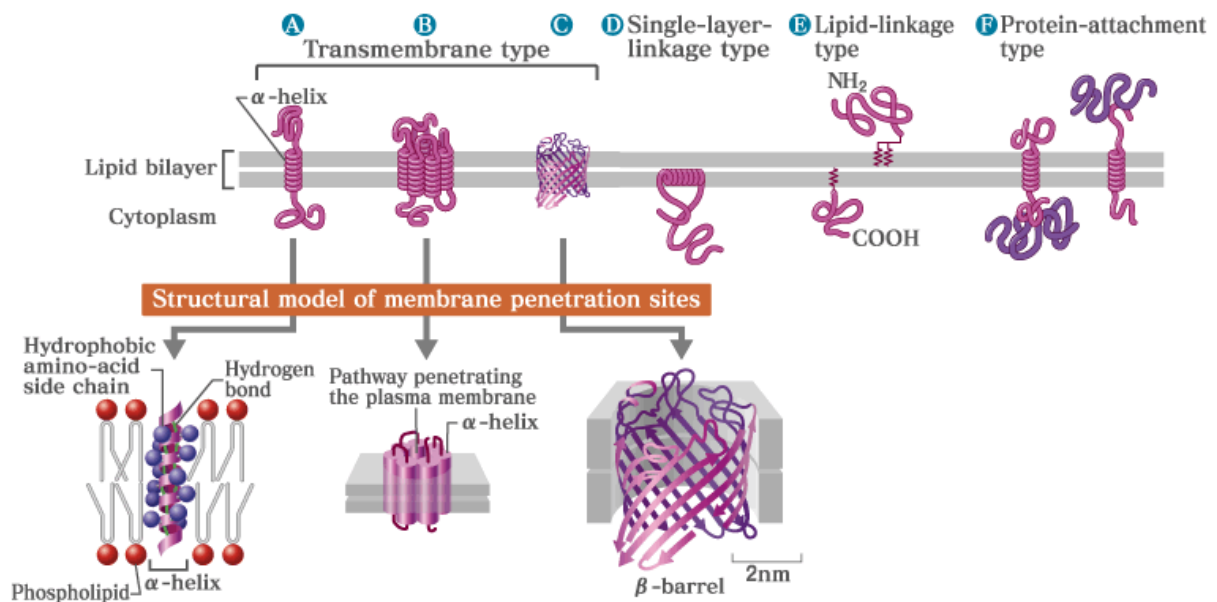


Figure 11. The different types of membrane proteins and their attachment mode.<sup>39</sup>

## INTEGRAL PROTEINS

Integral proteins can be transmembrane proteins or inserted in one single layer of the membrane (Figure 11). The transmembrane type crosses the 3 nm thick lipid bilayer. Integral proteins are completely inserted in the bilayer and are composed of 3 segments. One hydrophobic segment inserts in the lipid bilayer and the two other segments, whose external surfaces are more hydrophilic, extend to the external or cytosolic environments. The domain inserted in the bilayer is composed of hydrophobic amino acids interacting with the fatty acid chains of the phospholipids. They are usually structured in one or several  $\alpha$ -helix or in multiple  $\beta$ -sheets. Moreover, most of the integral proteins are glycosylated with complex ramified sugar groups systematically located at the extracellular side of the membrane.

Soluble proteins can fold locally with a wide variety of secondary structures. Intrinsic proteins, and more precisely their inserted domain in the hydrophobic core of the membrane, have a very limited panel of folding structures. They are mostly structured in one or more  $\alpha$  helix.

### $\alpha$ helix inserted in the membrane

$\alpha$  helix are embedded in the membrane through hydrophobic interactions with the fatty acid chains of some specific phospholipids and probably also through ionic interactions with their polar head groups. One example is the transmembrane protein glycophorin A, which is the most abundant plasma membrane protein in erythrocytes. It is a single transmembrane  $\alpha$  helix protein, which means it crosses the membrane through only one  $\alpha$  helix. In general, an  $\alpha$  helix inserted in the bilayer is composed of 20 to 25 hydrophobic amino acids, which is about 3.75 nm and is sufficient to cross the plasma membrane. In the membrane, the  $\alpha$  helix of the glycophorin A is associated with the  $\alpha$  helix of another glycophorin A to form a dimer.<sup>40</sup> Such association of dimeric membrane proteins is very common and a lot of membrane receptors are activated by dimerization.

Other transmembrane proteins present a helix bundle, composed of several  $\alpha$  helices, usually parallel or anti-parallel to each other (Figure 11). One of the biggest class is defined by seven

transmembrane  $\alpha$  helices. More than 150 have already been identified. Among them are the receptors coupled to the G proteins, important for signal transduction. Ion channels are the second prevailing type of helix bundle membrane proteins. They are usually tetrameric, each of the 4 sub-units having two transmembrane helices. All the helices associated with each other form a central channel covered with hydrophilic amino acids, while the external surface of the channel is hydrophobic. Ion flows are regulated by reorientation of the  $\alpha$  helices.

### **$\beta$ sheets forming transmembrane barrels**

Porins are another type of transmembrane proteins. They are mainly hydrophilic and are trimers composed of three identical sub-units. Each sub-unit forms 16  $\beta$  sheets, which associate to form a transmembrane  $\beta$  barrel with a central pore (Figure 11). The inner part of the pore is composed of hydrophilic amino acids while its external surface is covered with hydrophobic residues. Porins allow the absorption or the rejection of small hydrophilic molecules like nutrients or waste.

### **LIPID ANCHORED PROTEINS**

Lipid anchored proteins are covalently bound to one or several lipids. The hydrophobic tails of the lipids are inserted in the membrane and help to anchor the protein to the bilayer. In that case, the polypeptide chain is not inserted in the membrane. These proteins can be anchored to the membrane *via* three main types of lipids: saturated fatty acids, unsaturated fatty acids or GPIs (Figure 12). Their localization in the plasma membrane is dependent on the type of lipid they are bound to.

Saturated fatty acids anchored proteins are found at the cytosolic leaflet. Acylation of proteins with myristate (C14:0) or palmitate (C16:0) promotes the protein insertion in sphingolipids and cholesterol rich domains of the membrane.<sup>37</sup> The acyl group is linked to the N-terminal glycine residue.

Another group of cytosolic proteins is anchored to the membrane through an unsaturated and ramified fatty acid, attached to a cysteine residue in the C-terminal region. Farnesyl (C15) or geranylgeranyl (C20) tails are bound to the protein *via* a thioester bond to the -SH group of the cysteine. In the membrane, prenylated proteins are excluded from the sphingolipid–cholesterol domains.<sup>37</sup>

Certain proteins and glycosylated proteoglycans found at the cell surface are bound to the external side of the plasma membrane with a GPI group. They are mostly found in liquid-ordered ( $L_o$ ) domains. Although the exact structure of this type of anchor varies from one cell type to another, they always present a PI with two fatty acid chains inserted in the lipid bilayer and phosphoethanolamine (in green on Figure 12) binds covalently the anchor to the C-terminal end of the protein and several sugar units (represented in orange on Figure 12).

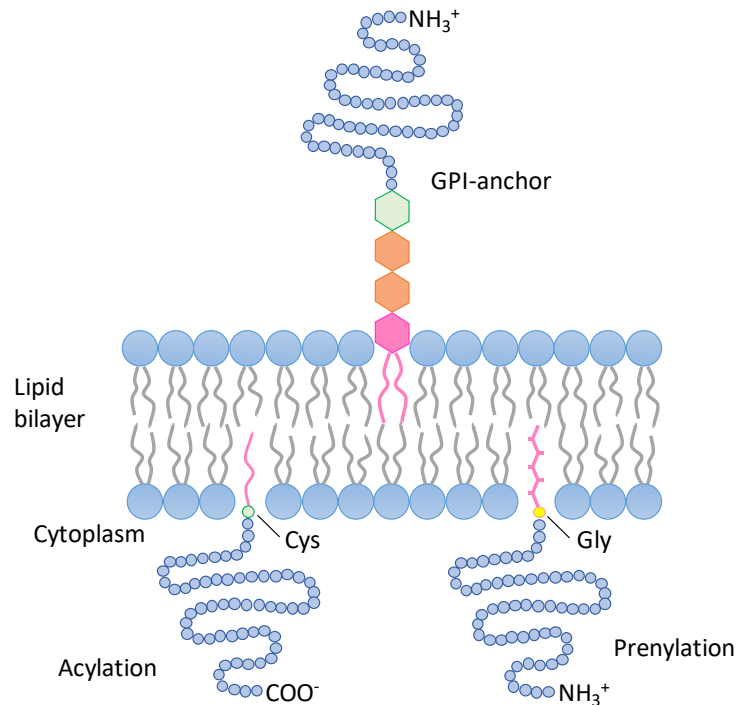


Figure 12. Lipid anchored protein. Adapted from <sup>37</sup>.

### PERIPHERAL PROTEINS

Peripheral proteins do not interact with the hydrophobic core of the lipid bilayer. They are generally bound indirectly to the membrane via non-covalent interactions with intrinsic proteins or with membrane lipids polar head groups. They can be localized at the extracellular or at the cytosolic leaflets of the membrane.

Further away from the plasma membrane are found some proteins associated more loosely to the membrane, such as the actin filaments forming the cytoskeleton. They are associated to the cytosolic side of the membrane through interactions with one or more membrane proteins or with adaptor proteins.

#### 1.1.3. Surface sugars

Glycoconjugates are a third essential class of constituents of the plasma membrane. They extend at the cell surface and form the glycocalyx, the most external layer of the membrane. Membrane sugars are covalently bound to lipids as glycolipids or to proteins as glycoproteins and proteoglycan. Glycans are involved in fundamental cell processes such as cell signaling, communication and cell–cell and cell-extra-cellular matrix interactions. In addition, various types of glycoconjugates interfere with key cancer cell processes and with the tumor environment, leading to cancer progression.<sup>41</sup> The membrane glycan composition is very diverse. They can be of various monosaccharide composition, they can present various saccharide bonds (between C1 and C3 or C1 and C4), various conformations, various ramifications, they can be substituted with several sulfation states and they can be bound to their lipid or protein (aglycone part) *via* different linkages (Figure 13). Glycoconjugates are basically defined by the nature of their aglycone part and by the type of linkage they are bound with.

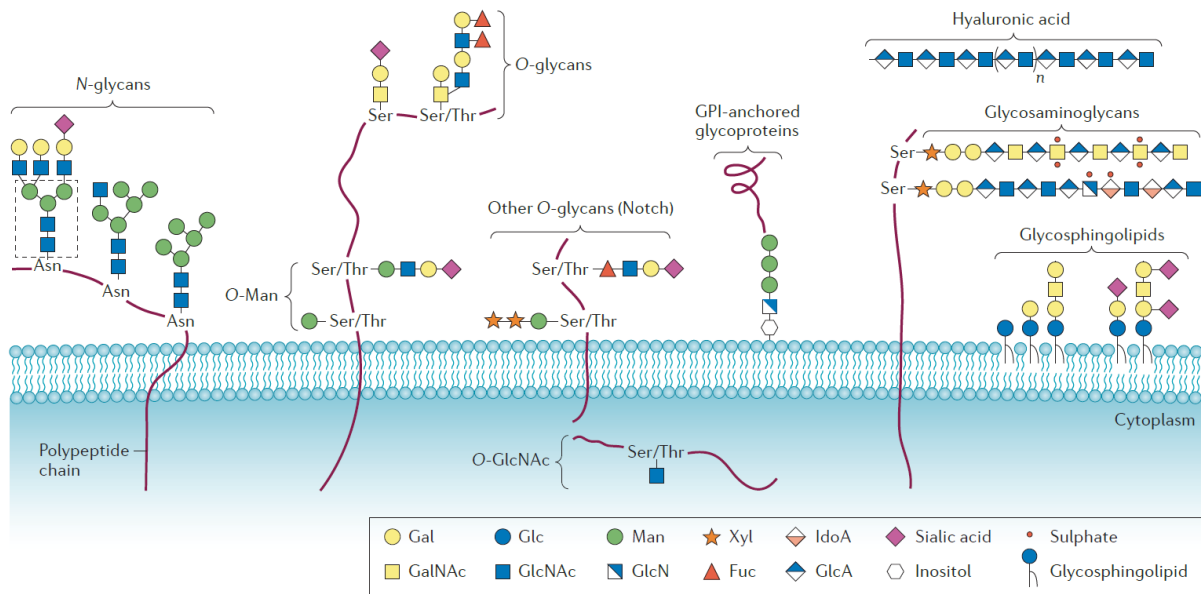


Figure 13. Common classes of glycoconjugates in mammalian cells.<sup>41</sup>

### GLYCOSPHINGOLIPIDS

Glycolipids and glycosphingolipids, briefly described in paragraph 1.1.1., are composed of a carbohydrate chain bound to a glycerol or a ceramide. Glycosphingolipids are the most common in mammalian cells and they are major components of the extra-cellular leaflet of the plasma membrane. They are always placed at the extracellular leaflet of the plasma membrane. Their classification is based on their glycan part. The ceramide is generally directly bound to a galactose (galactosylceramide) or to a glucose (glucosylceramide) *via* a  $\beta$  saccharide linkage. This first monosaccharide can be substituted with various units of glucose, galactose or sialic acid (Figure 13).

### GLYCOPROTEINS

As all glycoconjugates are found at the outer leaflet of the plasma membrane, glycoproteins are necessarily transmembrane proteins or GPI-anchored proteins, which are also considered as glycoproteins (detailed in paragraph 1.2.2.).

### O-glycans and N-glycans

Many transmembrane proteins present glycoside chains bound covalently *via* a nitrogen atom to lateral chains of asparagine (*N*-glycans) or *via* an oxygen atom to serine or threonine (*O*-glycans). They are called glycoproteins and they are always oriented such as the glycosylated part of the protein is located at the surface of the cell.

*O*-glycans can extend with various glucose and galactose monomers and can have diverse terminal structures, usually containing fucose and sialic acid. Other *O*-glycans are defined by the first saccharide unit bound to the protein. They include the *O*-mannose (*O*-Man), *O*-fucose (*O*-Fuc), *O*-galactose (*O*-Gal) and nucleocytoplasmic *O*-linked  $\beta$ -N-acetylglucosamine (*O*-GlcNAc).<sup>42,43</sup> Moreover, some proteins present a specific form of glycosylation, such as the Notch receptor, which is a type of *O*-glycan. The Notch receptor was shown to be important in cancer cell biology.<sup>44</sup>

*N*-glycans all present a common pentasaccharide core (Figure 13, dotted line box). This core can be further substituted with mannose polymers and modified in the terminal region with GlcNAc, Gal and sialic acid.<sup>41</sup>

### Proteoglycans

Proteoglycans are a sub-class of glycoproteins. They contain one or more polysaccharidic chains called glycosaminoglycans (GAGs). GAGs are long and linear polymers composed of specific disaccharide units, attached to the protein sequence through xylose bound to the hydroxyl group of a serine residue. Hyaluronic acid is an exception as it is the only GAG to be found in its free form in the extracellular matrix. Usually, one of the sugar is either a uronic acid (D-glucuronic acid or L-iduronic acid) or a D-galactose, the second sugar is either a N-acetylglucosamine or a N-acetylgalactosamine. One or the two sugars have at least one anionic group, carboxylate or sulfate. GAGs chains thus present a lot of negative charges and participate to the negative charge properties of the cell surface. Following their composition in disaccharide units, there are various types of GAGs: heparan sulfate/heparin, chondroitin sulfate, dermatan sulfate, keratan sulfate and hyaluronan. Heparin is the hyper sulfated form of heparan sulfate. On Figure 13 are shown the structures of chondroitin sulfate and heparan sulfate. Chondroitin sulfate contains disaccharide repeating units of *N*-acetylgalactosamine  $\beta$ 1-4 glucuronic acid (GlcNAc $\beta$ 1-4GlcA). It is called dermatan sulfate if the disaccharide units are *N*-acetylgalactosamine  $\beta$ 1-4 iduronic acid (GlcNAc $\beta$ 1-4IdoA). Heparan sulfate presents acidic disaccharide repeating units of *N*-acetylgalactosamine  $\alpha$ 1-4 glucuronic acid or iduronic acid (GlcNAc $\alpha$ 1-4GlcA or GlcNAc $\alpha$ 1-4IdoA).

#### 1.1.4. Transport pathways through the lipid membrane hydrophobic core

The phospholipid bilayer is impermeable to most of hydrophilic molecules, ions and water itself. It allows to maintain the compositions of the extra- and intra-cellular environments. Only gas such as CO<sub>2</sub>, N<sub>2</sub> and O<sub>2</sub>, and small polar and non-charged molecules such as ethanol and urea can easily cross a lipid bilayer by passive diffusion (Figure 14). These molecules can cross cell membranes without the help of a transport protein.

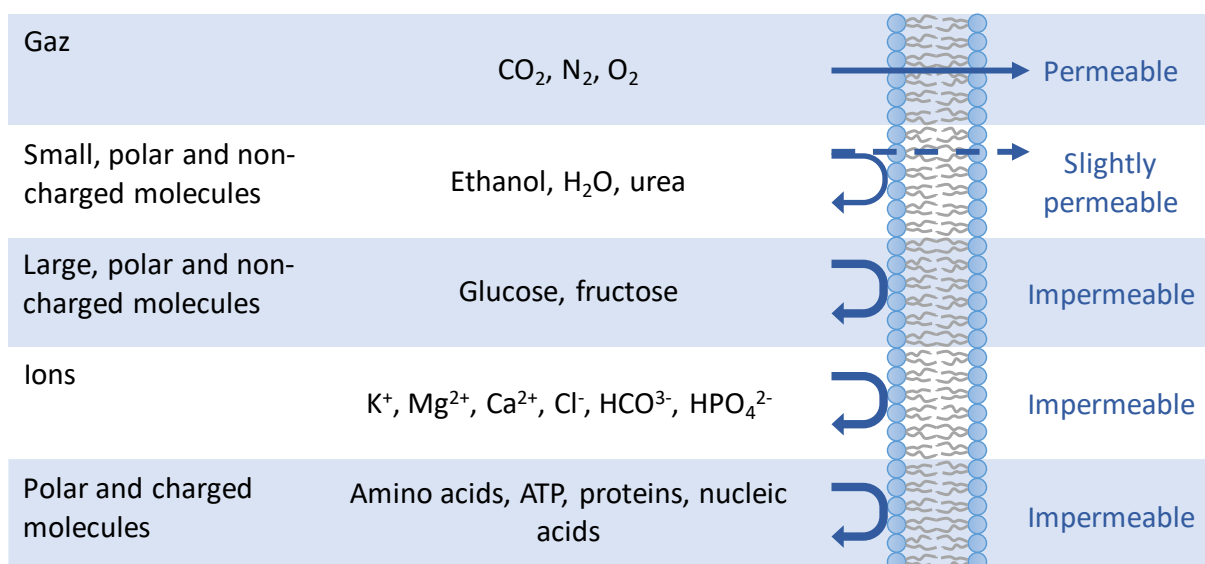


Figure 14. Relative permeability of a pure phospholipid bilayer for diverse molecules.

## ION CHANNELS AND SMALL MOLECULES TRANSPORTERS

For most of the molecules, specialized membrane proteins are required for transportation through the hydrophobic barrier that is the plasma membrane. They are always transmembrane proteins with multiple transmembrane segments, generally  $\alpha$  helices. They allow the passage of hydrophilic molecules and can be of several types (Figure 15).

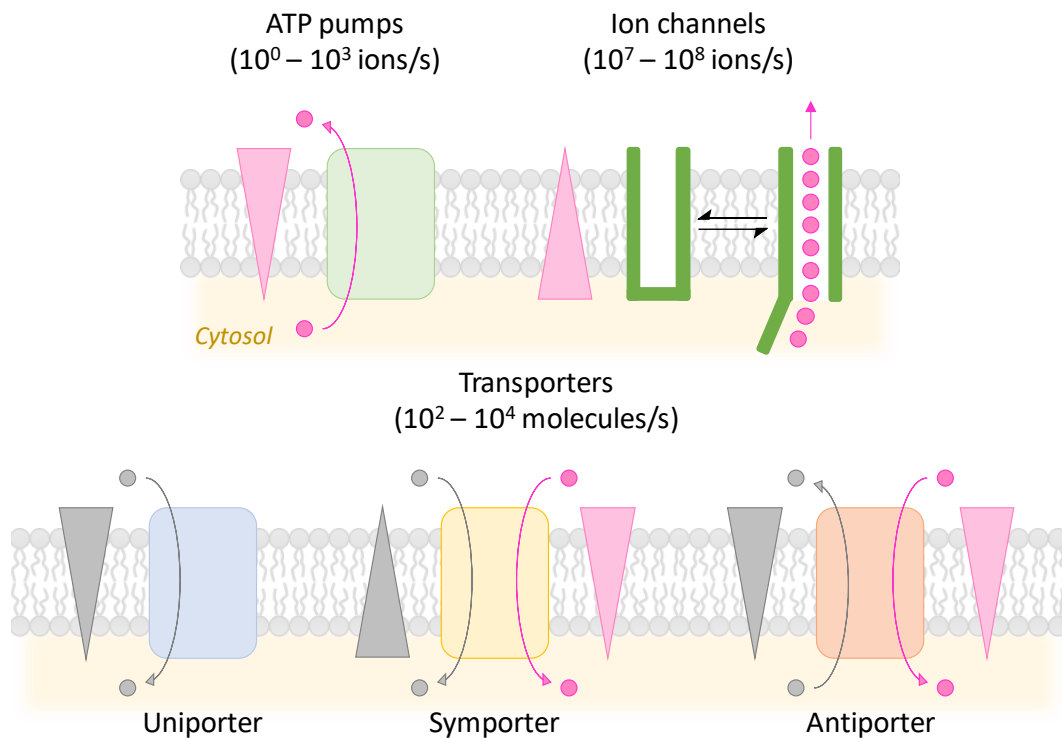


Figure 15. Transport membrane proteins. Adapted from <sup>45</sup>.

ATP pumps are ATPases using the energy produced by ATP hydrolysis to transport specific ions or small molecules through the membrane, against their concentration gradient or the electrical potential or both. It is an active transport.

Ion channels are pore-forming proteins that transport water, specific ions or small hydrophilic molecules in the direction of their electrochemical gradient. It can be called facilitated diffusion. Ion channels are open by chemical or electrical specific signals. They can be voltage-gated ion channels that open or close depending on the voltage gradient across the plasma membrane, or they can be ligand-gated ion channels that open or close following the binding of specific ligands ( $\text{Na}^+$ ,  $\text{Ca}^{2+}$ ,  $\text{K}^+$ , ... ) to the channel.

Transporters proteins insure the transmembrane transport of a lot of ions and molecules. There are 3 identified types of transporters: uniporters, symporters and antiporters. Uniporters transport a specific type of molecules in the direction of its concentration gradient. It is facilitated diffusion. Most of glucose molecules and amino acids cross the membrane thanks to this type of transporter.

Symporters and antiporters are co-transporters: they transport simultaneously two different molecules. One ion or molecule crosses the membrane against its concentration gradient while the other goes in the direction of its concentration gradient. Like for ATP pumps, co-

transporters couple the transport of two molecules, one that is energetically favorable and one that is unfavorable. The first one provides the energy needed for the second. Symporters transport the two molecules to the same side of the membrane while antiporters transport them in opposite directions (see Figure 15).

### VESICULAR TRAFFIC AND ENDOCYTOSIS

Vesicular traffic allows the passage of larger charged molecules, in particular proteins, peptides and nucleic acids, through the cell membrane and through the cell organelles membranes. In that way, vesicular traffic encompasses all the polar macromolecules movements following the secretory and endocytic pathways. They are very complex and regulated pathways, involving numerous protein and lipid partners.<sup>46</sup> The cargo molecules are trapped in lipid vesicles formed from the membrane of one compartment and deliver the molecules to the next compartment by membrane fusion. The pathway implied in the passage of the cell membrane is called endocytosis when it implies the entry in cells, while exocytosis concerns the secretion out of the cell. This section will be focused on the endocytosis pathways (Figure 16). In these processes, macromolecules are internalized by invagination of the plasma membrane. They first arrive in early endosomes, then late endosomes, and finally lysosomes from where they escape by the action of hydrolases.

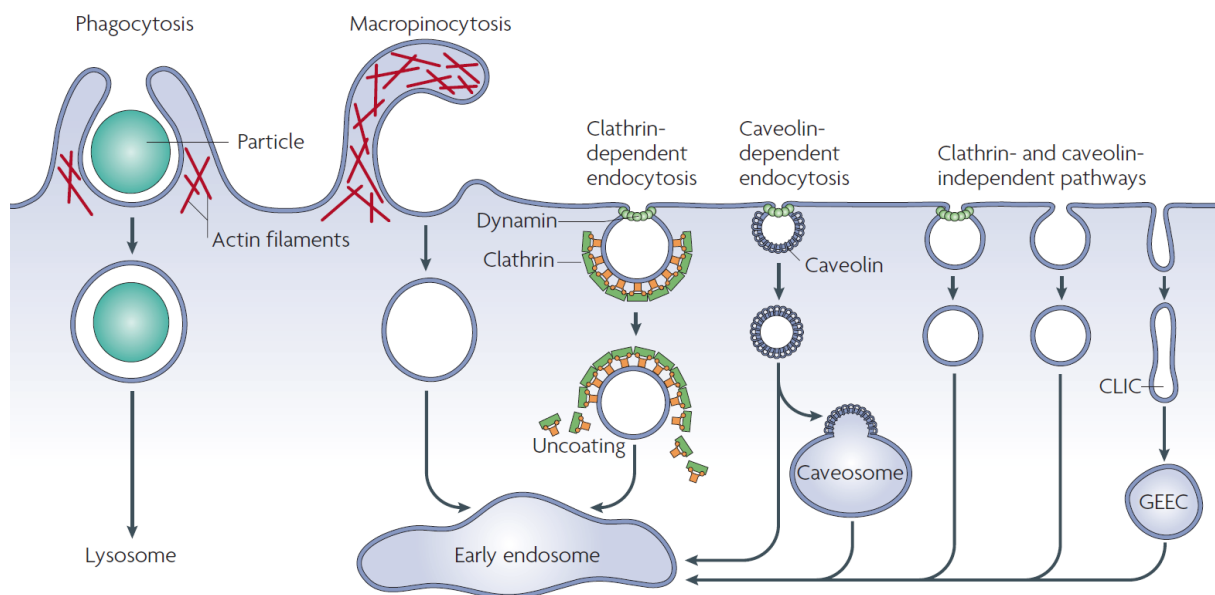


Figure 16. Pathways of endocytosis.<sup>47</sup>

Phagocytosis and macropinocytosis involve the remodeling of the cell membrane by actin filaments. They wrap their cargo and form larger vesicles (0.5 to 2  $\mu\text{m}$ ) compared to other endocytosis pathways (0.05 to 0.1  $\mu\text{m}$ ). Phagocytosis triggers the cellular uptake of large particles like bacteria while macropinocytosis carries the uptake of a large volume of fluid and the molecules that are dissolved in it like growth factors.

Some other endocytosis pathways are receptor-dependent. A cell receptor binds specifically to a macromolecule, the membrane forms a bud oriented to the inside of the cell, and by detaching from the membrane, the bud forms a lipid vesicle. These pathways generally drive the internalization of cholesterol-rich particles called low-density lipoprotein (LDL), of

transferrin, an iron-binding protein, of various hormones like insulin and of diverse glycoproteins.

Clathrin-dependent endocytosis implies the formation of clathrin-coated vesicles, arranged in the shape of a cage helping the bud formation. The membrane is pinched, and scission occurs by the action of dynamin, a large GTPase of about 100 kDa able to form tubules and to split membranes. After budding, the clathrin basket is removed by uncoating proteins and the naked vesicle is released in the cytosol.<sup>48,49</sup>

Caveolin-dependent endocytosis is driven by caveolae invaginations, which are cholesterol and sphingolipid rich domains (see paragraph 1.1.2.) containing specific receptors and signal transduction proteins. They are characterized by the presence of caveolins, which are transmembrane proteins forming a layer at the cytosolic surface of caveolae. Like for clathrin-dependent endocytosis, dynamin is responsible for membrane pinching and splitting.

In addition, several endocytosis pathways do not use clathrin or caveolin coats. They transport various cargoes and can sometimes be taken over by bacteria and viruses to enter the host cell.<sup>47</sup>

## 1.2. Phosphoinositides and PIP<sub>2</sub> functional properties and roles

Phosphatidylinositol-4,5-bisphosphate (PIP<sub>2</sub>) contributions for the internalization mechanism of the CPP Penetratin are the main interests of this work. This section aims to review the main physicochemical distinctive characteristics of PIP<sub>2</sub> and its implications, as well as some of the PIs family, in cell processes.

### 1.2.1. PIP<sub>2</sub> head group orientation

The orientation of the PIP<sub>2</sub> polar group with respect to the bilayer plane is unknown. Some works showed that PI is perpendicular to the membrane surface.<sup>50,51</sup> If PIP<sub>2</sub> presents the same conformation as PI, its polar head should be aligned with its hydrophobic tails and present a straight global orientation. This potentially cylindrical arrangement coupled with the large size and very polar head group of PIP<sub>2</sub> implies that it may extend further into the aqueous environment than other phospholipids.<sup>52</sup>

### 1.2.2. Charge of PIP<sub>2</sub>

PI derivatives (PIP, PIP<sub>2</sub>, PIP<sub>3</sub>) are phosphorylated at the inositol hydroxyl groups, and thus have several negative charges. The other negatively charged lipids of the plasma membrane bear only one charge, as it is the case for PS, the main negatively charged lipid of the plasma membrane. This confers very specific interaction properties to phosphorylated PIs. pKa values of the phosphate at positions 4 and 5 were found to be at 6.7 and 7.7, respectively.<sup>53</sup> Thus PIP<sub>2</sub> can have 3 to 5 charges at physiological pH,<sup>52</sup> as depicted on Figure 17. Besides, PIP<sub>2</sub> charge depends on several factors such as local pH and interactions with proteins. Presence of salts can also affect its number of charges.



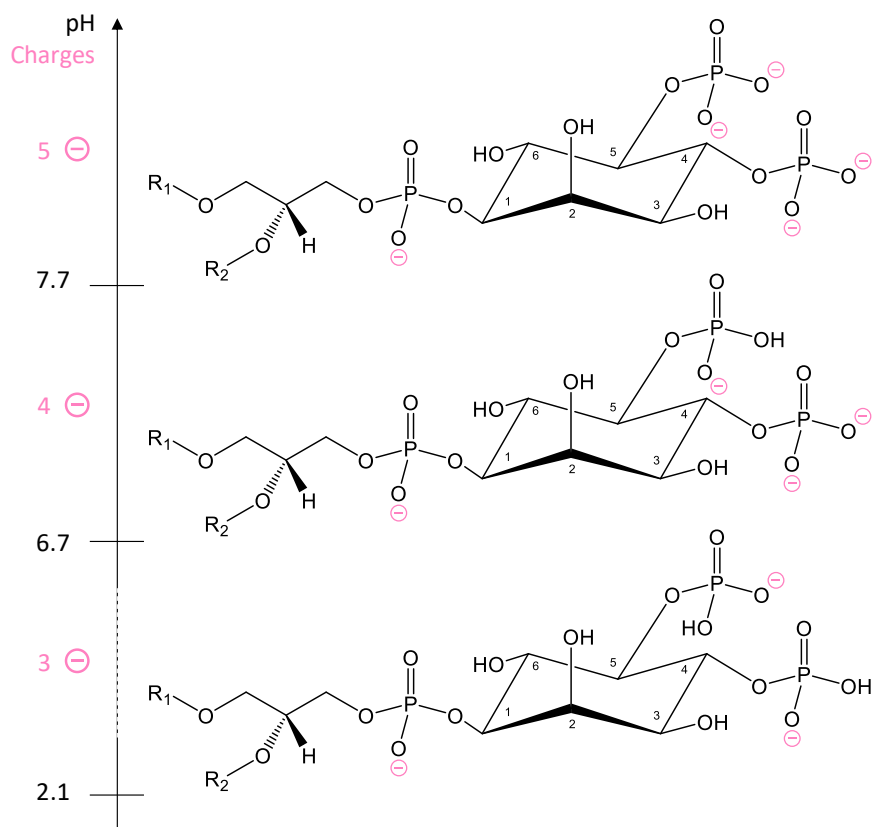


Figure 17.  $\text{PIP}_2$  number of charges.

### 1.2.3. $\text{PI}(4,5)\text{P}_2$ localization and lateral organization in the plasma membrane

$\text{PIP}_2$  is a minor negatively charged phospholipid of the plasma membrane.  $\text{PI}(4,5)\text{P}_2$  represents more than 99% of the doubly phosphorylated PIs,<sup>54</sup> and about 1% of phospholipids of the plasma membrane of human erythrocytes.<sup>52</sup> Known to be an inner leaflet phospholipid, it also has a significant fraction localized in the outer layer of the membrane ( $\sim 20\%$  of total  $\text{PIP}_2$ )<sup>23,55</sup> (Figure 8).

Although it is present in low amounts in the plasma membrane,  $\text{PIP}_2$  is implied in many cell functions. This can be explained by its peculiar distribution in the membrane. Indeed, it is not distributed uniformly and may be localized in raft domains. Specialized lipid domains rich in sphingolipids and cholesterol have been reported to concentrate  $\text{PIP}_2$ , up to half of the membrane  $\text{PIP}_2$  would be localized in these domains, the same domains where caveolin is gathered.<sup>56</sup> These  $\text{PIP}_2$ -enriched sites coordinate membrane fission and fusion processes, which are spatially localized events involving the actin cytoskeleton.  $\text{PIP}_2$ -enriched sites are also closely involved in membrane movement.<sup>57</sup>

Sequestration of  $\text{PIP}_2$  in these domains can occur either through localized synthesis of  $\text{PIP}_2$  or through  $\text{PIP}_2$  binding to clustering proteins. Experimentally, localization of  $\text{PIP}_2$  pools can be achieved using PIs-binding domains labelled with green fluorescent protein (GFP).<sup>58</sup> The pleckstrin homology (PH) domain is able to bind to  $\text{PI}(4,5)\text{P}_2$ ,  $\text{PI}(3,4,5)\text{P}_3$  or  $\text{PI}(3,4)\text{P}_2$ . Like other lipid-binding proteins, the PH domain anchors to the plasma membrane *via* specific interactions with inositide polar head groups as illustrated on Figure 18. In addition, other interactions could

contribute to the PH domain localization at the plasma membrane: insertion of hydrophobic residues in the lipid bilayer and electrostatic interactions with other acidic phospholipids.

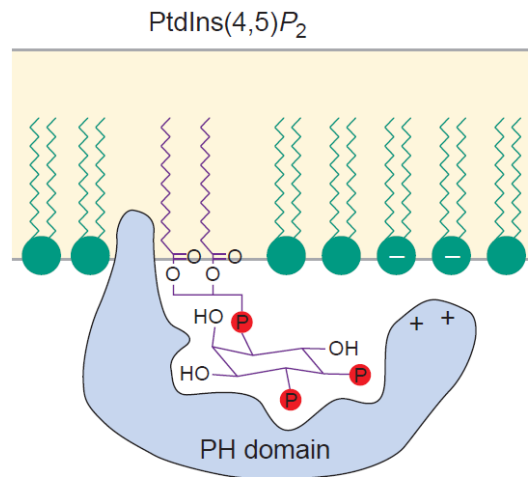


Figure 18. Anchoring of isolated pleckstrin homology (PH) (or other lipid-binding) domains to cellular membranes by inositide-specific interactions.<sup>58</sup>

PIs signaling are thought to be implicated in the cytoskeletal organization and modulate actin filaments assembly. Thanks to GFP probes, PIs pools dynamic concentration gradient or segregated domains could be correlated to activity of cellular functions. The PH domain of the phospholipase C delta (PLC<sup>δ</sup>) bound to a GFP was localized in actin-rich structures of the membrane and in cell peripheral protrusions in fibroblasts.<sup>59</sup> PIP<sub>2</sub> has also been localized, together with PI(4)P 5-kinase and F-actin, at sites of phagocytosis, which requires transient remodeling of the actin cytoskeleton.<sup>60</sup>

Another method using PI(4,5)P<sub>2</sub> antibodies have been used to detect discontinuous, nanodomains of clustered PI(4,5)P<sub>2</sub>. PIP<sub>2</sub> clusters co-localized with PIP<sub>2</sub>-binding proteins GAP43, myristoylated alanine-rich C kinase substrate (MARCKS) protein and CAP23 (GMC), probably in cholesterol-rich raft-like domains.<sup>61</sup>

Finally, branched actin networks anchored to membrane in PIP<sub>2</sub>-enriched domains has been evidenced using giant unilamellar vesicles (GUVs) observed in fluorescence microscopy.<sup>62</sup> Actin stress fibers were reported to induce spatial rearrangement in the lipid membrane, polymerization triggering lipid partitioning in initially homogenous liposomes. This behavior was found to depend only on the PIP<sub>2</sub>-N-WASP interaction linking the actin network to the membrane (Figure 19).

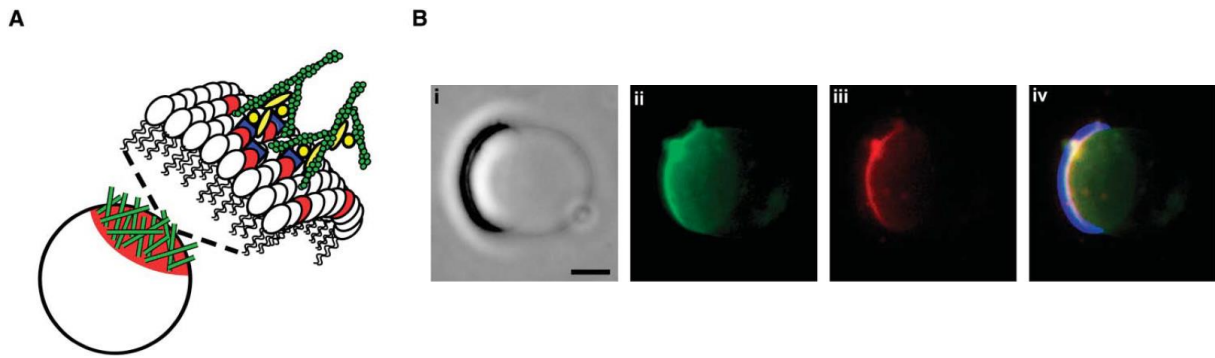


Figure 19. Assembly of actin networks on phase-separated GUVs. (A) Illustration of membrane-associated actin on a GUV (only the outer phospholipid bilayer is shown, not drawn to scale). The lipid  $\text{PIP}_2$  (in red), which binds to N-WASP (in blue) and then activates the Arp2/3 complex (in yellow) to initiate growth of a dendritic actin network at the surface of the vesicle. (B) Phase-separated vesicle with membrane-associated actin. (i) Optical phase contrast image showing the outline of the vesicle and phase-dense actin network. (ii) Epifluorescence image of fluo-DOPE that labels the  $L_d$  domain. (iii) Epifluorescence image of BODIPY TMR  $\text{PIP}_2$  showing localization of  $\text{PIP}_2$  within the  $L_d$  domain. (iv) Overlay of fluo-DOPE, TMR- $\text{PIP}_2$ , and optical phase contrast (optical phase-dense object is pseudo-colored in blue) images showing colocalization of the actin network on the  $L_d$  domain. Scale bars are 10  $\mu\text{m}$ .

Figure and legend adapted from <sup>62</sup>.

#### 1.2.4. $\text{PI}(4,5)\text{P}_2$ physiological functions

$\text{PIP}_2$  is an important signaling molecule in the membrane for the regulation of vesicle exo- and endocytosis and the modulation of the actin cytoskeleton organization.<sup>63,64</sup> It is involved in various cell functions of whom major ones are depicted in Figure 20.

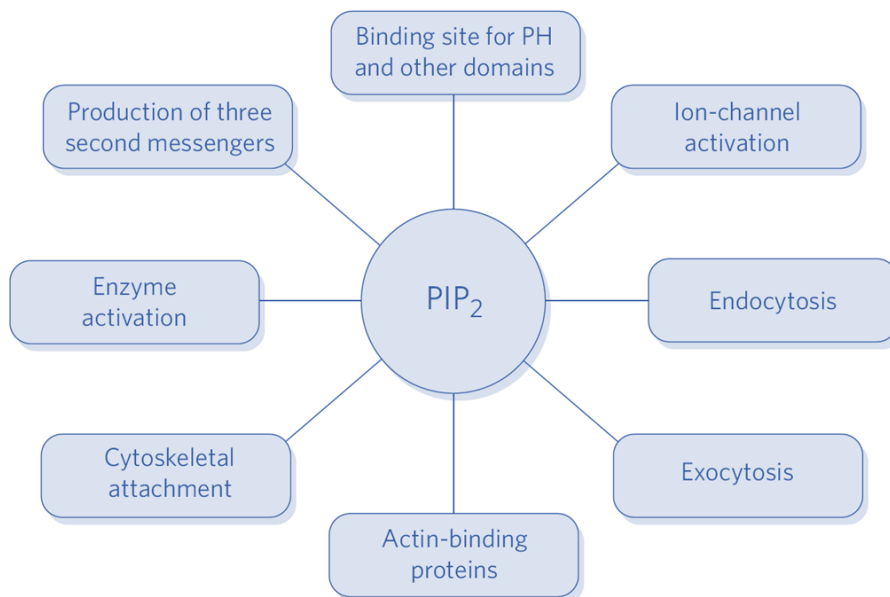


Figure 20. Functions of  $\text{PIP}_2$ . Adapted from <sup>65</sup>.

$\text{PIP}_2$  produces 3 second messengers, is responsible of many ion channels and enzymes activation, is an effector of actin polymerization and anchors proteins to the membrane. PIs are implied in the structural functions such as membrane budding and fusion.<sup>37</sup>

PIs in general are strongly involved in membrane transport and are effectors of translocation.<sup>66,67</sup> For example, PI<sub>3</sub>P located at the external leaflet mediates the internalization of pathogen effectors in plant and animal.<sup>68</sup> PI(4,5)P<sub>2</sub> is an actor of membrane trafficking. It has a role in vesicle exocytosis, endocytosis and motility as illustrated in Figure 21.<sup>57,69</sup> The ARF protein recruits PI kinases and synthesis of PIP<sub>2</sub> is supported by phospholipase D at localized sites of the membrane where PI(4,5)P<sub>2</sub> would be clustered in nanodomains and may form sites where exocytosis can occur (Figure 21a). After membrane fusion, PIP<sub>2</sub>-rich nanodomains recruit proteins required for clathrin-mediated endocytosis like for instance dynamin. Actin filaments association could help the membrane invagination involving profilin and syndapin, while pinocytosis and non-clathrin-mediated endocytosis would only depend on actin polymerization without coat recruitment (Figure 21b). PIP<sub>2</sub>-rich vesicles, activated by the WASP protein, would then promote an actin organization in “comet tail” to push the vesicle away from the membrane to the cytosol (Figure 21c). Finally, PIP<sub>2</sub> dephosphorylation by phosphatases such as synaptojanin would allow the vesicles uncoating and dissociation of the actin comet tail structure (Figure 21d).<sup>57</sup>

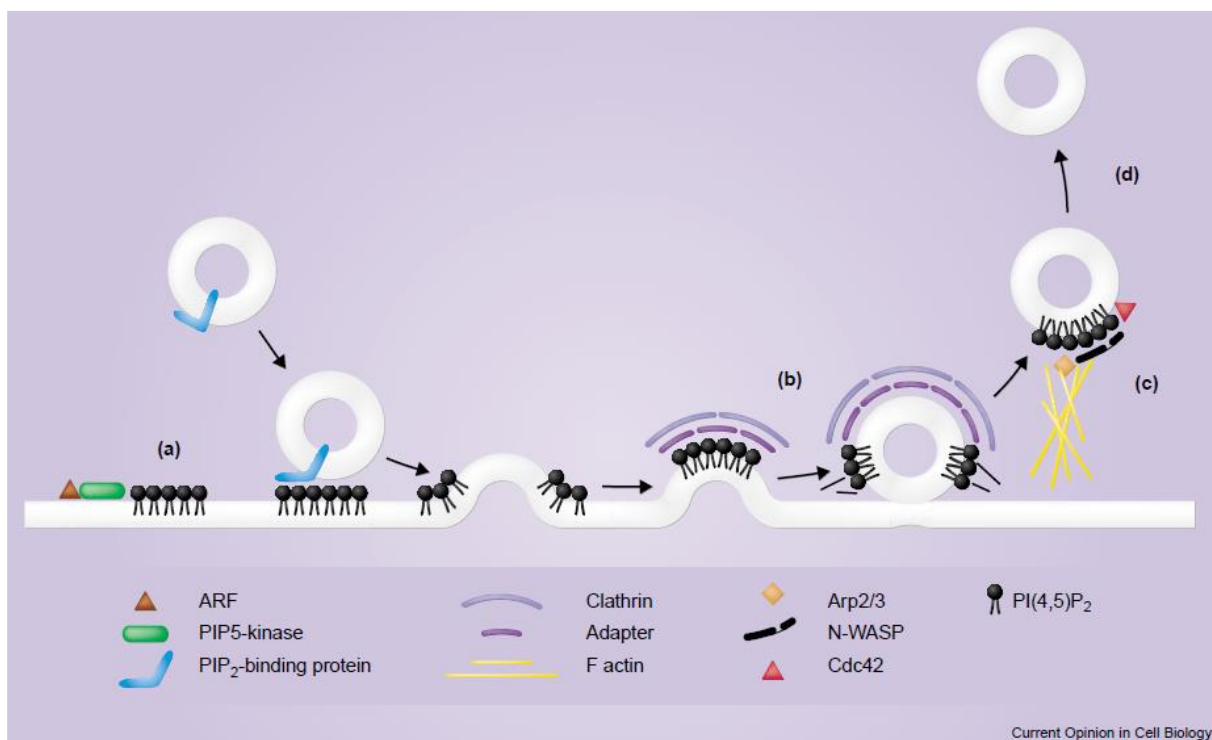


Figure 21. Possible roles for PI(4,5)P<sub>2</sub> in vesicle exocytosis, endocytosis and motility.<sup>57</sup>

PIP<sub>2</sub> signaling is also important for cell polarity and plays a role in cells motility and migration. Cell migration relies on the coordination of actin cytoskeleton dynamics and vesicular traffic to recruit and move the implicated proteins toward the location of migration. PIP<sub>2</sub>, as a signaling molecule, would be implicated in the regulation of cell polarity.<sup>69</sup>

The reasons why PIP<sub>2</sub> is implied in so many cell functions are still subject to query but its ability to form clusters might be a good explanation for its versatility.<sup>70</sup> Spatial segregation can indeed be generated through electrostatic binding with proteins.<sup>65</sup> This process is regulated by

cytoplasmic calcium local concentration. Some natively unfolded proteins containing cationic regions bind PIP<sub>2</sub> and release it if local Ca<sup>2+</sup> concentration increases.

### 1.3. PI(4,5)P<sub>2</sub> binding with proteins

Several cationic/aromatic domains are able to bind PIP<sub>2</sub> and serve proteins anchoring to the membrane. In this way, the PH domain and other domains anchor phospholipase C delta (PLC<sup>δ</sup>), C1 and C2 domains anchor protein kinase C (PKC). In these cases, PIP<sub>2</sub> serves as a passive membrane anchor.<sup>52</sup> Domains binding PIP<sub>2</sub> can be structurally diverse.

The example of the domain PH-PLC<sup>δ</sup> binding to the inositol triphosphate I(1,4,5)P<sub>3</sub> is illustrated on Figure 22. It binds 7 amino acids through direct hydrogen bonds. In particular, Lys 30 and Lys 57 appear to clamp the phosphate groups 4 and 5 in the binding pocket, each lysine binding with both phosphate groups.<sup>71</sup>

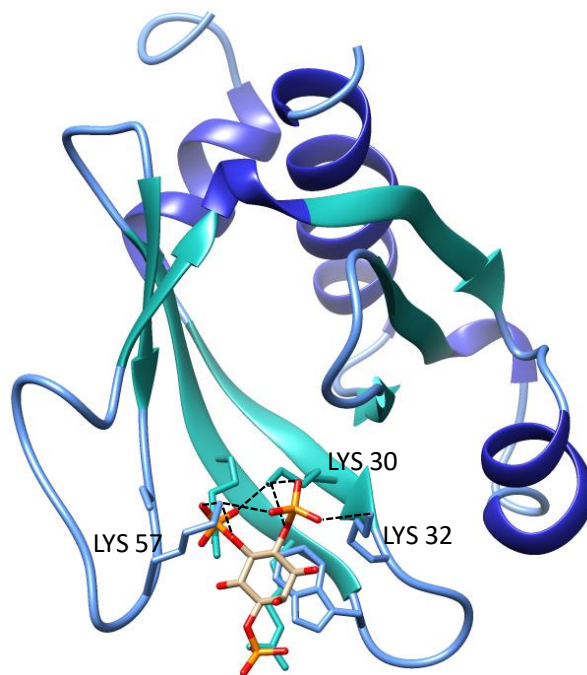


Figure 22. The I(1,4,5)P<sub>3</sub>-Binding site on the PH-PLC<sup>δ</sup> domain. Adapted from <sup>71</sup>.

The PH-PLC<sup>δ</sup> domain is known to have high specificity and affinity for PIP<sub>2</sub>, sufficiently to anchor the protein to the membrane.<sup>72</sup> Its affinity for PIP<sub>2</sub> was measured by calorimetry, using PC/PIP<sub>2</sub> liposomes. It binds PIP<sub>2</sub> with a K<sub>d</sub> = 2 μM.<sup>73</sup> It has to be noted that the PH-PLC<sup>δ</sup> domain binds 10-times more strongly to IP<sub>3</sub> than to PIP<sub>2</sub>.<sup>52</sup>

It seems that the specificity is closely related to the ability of the protein to form a structured domain. Such structured domains able to bind specifically PIP<sub>2</sub> are found in other anchored proteins like the epsin N-terminal homology (ENTH) domain, the binding domain of the clathrin assembly lymphoid myeloid leukemia (CALM) protein, or the 4.1 protein ezrin/radixin/moesin (FERM) domain. Epsin and CALM are proteins that regulate the clathrin network formation, necessary for endocytosis.<sup>57,74</sup> Proteins from the ERM family are, for their part, implicated in binding the actin filaments to the plasma membrane through interactions with CD44 for instance.

PIP<sub>2</sub> can bind with less specificity to unstructured small molecules such as neomycin or the peptide sequence corresponding MARCKS effector domain, both showing no specificity to PI(3,4)P<sub>2</sub> or PI(4,5)P<sub>2</sub>.<sup>52</sup>

#### 1.4. Model membranes to study peptide-lipid interactions

Simplified lipid systems modelling the membrane have been needed to better understand the complex biological processes occurring at the plasma membrane. Studying of membrane properties, structure and functioning have pushed the development of such biomimetic systems. They can be used to assess interactions between the lipid bilayer and membrane-active molecules, like peptides or drugs, or lipid organization and dynamics, for instance. Many model membranes exist, and they all have their advantages and drawbacks. The most common ones are lipid monolayers, micelles, planar lipid bilayers and liposomes.<sup>18</sup>

Lipid monolayers allow to detect membrane insertion of diverse amphipathic compounds for studying protein-lipid, drug-lipid or lipid-lipid interactions at the molecular level.<sup>18,75,76</sup> However, the most important limit is they are composed of only one layer of lipids, which represents a big difference with the plasma membrane bilayer organization.

Micelles and bicelles are the smallest objects mimicking the plasma membrane. Due to their small size, they are particularly adapted to the NMR structural studies, where the use of larger model systems is not possible. However, due to their small size, they have a high degree of curvature compared to the one of the plasma membrane, whose local curvature is negligible. Moreover, detergents and other molecules composing micelles are far from the lipid composition of the plasma membrane.

Supported lipid bilayers preparation is quite easy and they are very stable models. A nice advantage of this model is that it can be easily characterized by various surface techniques as it is deposited on a solid surface and not in suspension like vesicles. Stability and rigidity of this model allow its use for microscopy measurement like atomic force microscopy (AFM) or fluorescence microscopy to image lipid phase partitioning induced by interactions with proteins or other molecules, for instance. Evanescent field techniques like surface plasmon resonance (SPR) or total internal reflection fluorescence microscopy (TIRF) also require such a rigidly-supported bilayer.<sup>77</sup>

It is very important to pick the right model according to the kind of experiment pursued. Also, it can be noted that some of these model membranes can be adapted to some specific interaction studies. For instance, the actin cytoskeleton can be reconstituted in unilamellar liposomes or on supported lipid bilayers by using cytosol extracts to observe its behavior and interactions with lipid membranes.<sup>78</sup> In this work, liposomes have been chosen for their numerous advantages for the study of membranotropic peptide effect on thermotropic phase behavior of model membranes by calorimetry measurements, binding affinity studies using fluorescence and even identification of interactions peptide-lipid at the molecular level by photo-cross-linking coupled to MS. When possible, multilamellar vesicles (MLVs) are chosen due to their ease of preparation. In the case of fluorescence experiments, large unilamellar vesicles (LUVs) have been chosen for their low light scattering effects compared to MLVs and for their low curvature compared to small unilamellar vesicles (SUVs).

Liposomes or lipid vesicles are the mostly used model membranes for studying membrane phase behavior and processes. They are in suspension in an aqueous buffer and form spherical lipid bilayers entrapping an aqueous volume. Their lipid composition can be easily controlled, and they can be made of single lipid component or mixture of different types of lipids. Unlike lipid monolayers, their organization in two lipid leaflets better reflects the plasma membrane complexity. The different types of liposome structures are illustrated on Figure 23 and described below.

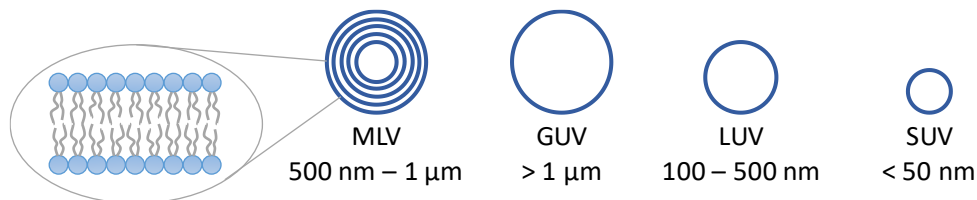


Figure 23. The different types of liposomes and their size.

### MULTI-LAMELLAR VESICLES (MLVS)

MLVs are made by hydrating under vigorous stirring a dried lipid film above its phase transition temperature. They are composed of several concentric spheres of lipid bilayers spaced by water molecules and their diameter is usually between 500 nm to 1  $\mu\text{m}$ . They are the easiest liposomes to prepare and their size is close to the one of a cell. They are used for biophysical studies on the membrane lipids organization and dynamic. However, their size distribution in a single suspension is wide, it is not possible to control their lamellar degree and only a small amount of the total lipid composing the MLV (about 10%) is located at the outermost layer. Also, their internal aqueous volume is relatively small in proportion to the quantity of lipids they are composed of.

### UNILAMELLAR VESICLES

Unilamellar vesicles are defined by a single lipid bilayer. There are various types depending on their size: small unilamellar vesicles (SUVs), large unilamellar vesicles (LUVs) and giant unilamellar vesicles (GUVs). Giant plasma membrane vesicles (GPMVs) are a particular type of unilamellar vesicles as they have a lipid composition very close to the one of the plasma membrane. The vesicles size determines specific parameters such as the lipid ratio between the two monolayers, the trapped volume of the enclosed aqueous solution, the number of phospholipid molecules per vesicle and the number of vesicles formed per quantity of lipids. These parameters are compared in Table 4 for SUVs of 25 nm size and for LUVs of 100 and 500 nm of diameter. Another important parameter that is related to the size of vesicle is the membrane curvature, which is clearly represented by the lipid ratio inner/outer monolayers. This ratio is low in small objects due to packing constrains in the bilayer.

Table 4. Some characteristics of SUVs (25 nm) LUVs (100 nm and 500 nm diameter). The calculations were made assuming a bilayer thickness of 4 nm and a surface area per phospholipid molecule of 0.6 nm<sup>2</sup>.<sup>16</sup>

Diameter (nm)	Inner monolayer/Outer monolayer (mole ratio)	Trapped volume (μL/μmol)	Number of phospholipid molecules/vesicle	Number of vesicles/μmol of lipids
25	0.46	0.3	4.8 x 10 <sup>3</sup>	1.3 x 10 <sup>14</sup>
100	0.85	2.5	9.7 x 10 <sup>4</sup>	6.2 x 10 <sup>12</sup>
500	0.97	15	2.6 x 10 <sup>6</sup>	2.3 x 10 <sup>11</sup>

#### SMALL UNILAMELLAR VESICLES (SUVS)

SUVs can be obtained by MLVs sonication. SUVs usually display a mean diameter of 25 to 50 nm. Due to their very small size, their membrane curvature is very high and their internal volume is lowered (Table 4), which prevents the use of SUVs for permeability studies. The lipid ratio in the outer layer over the inner layer can be up to 2:1. Lipids physical properties in such packing restrictions also limit the use of SUVs.

#### LARGE UNILAMELLAR VESICLES (LUVS)

LUVs show a larger diameter than SUVs and their ratio of lipids in the two monolayers is closer to 1:1. By this, they represent a better mimic for biological membranes. They are often chosen for spectroscopic studies as they induce little light diffusion compared to MLVs. The most common way to produce LUVs is to use an MLVs suspension. MLVs are subjected to several freeze-thaw cycles and extruded through a membrane of defined pore size to form LUVs at the chosen diameter. Size of LUVs varies from 100 to 500 nm. Moreover, there are methods to produce asymmetric LUVs, which are even better mimics for the plasma membrane.<sup>79,80</sup>

#### GIANT UNILAMELLAR VESICLES (GUVS)

Due to their large size, that ranges from 1 up to 100 μm, GUVs can be directly observed by optical microscopy. They are usually visualized in fluorescence or confocal microscopy to study molecular interactions with lipids.<sup>81</sup> Their size is very close to the size of cells. They can be obtained by two methods: the gentle hydration method or the electro formation method. The later allows the formation of higher yields of GUVs with low size distribution but is not compatible with high negatively charged lipids composition.<sup>82,83</sup> It consists in hydrating a dried lipid film above the phase transition temperature in presence of an electrical field. The gentle hydration method implies hydrating a dried lipid film above the phase transition temperature for a long time, about 36 h.

#### GIANT PLASMA MEMBRANE VESICLES (GPMVS)

GPMVs are derived directly from biological cells and thus have the same lipid composition as the plasma membrane. They contain the cell cytosol without the organelles and the actin cytoskeleton. Their size is comparable to the one of GUVs and sphingolipid and cholesterol rich domains can be observed in these models.<sup>84</sup> However, lipid membrane asymmetry is not conserved. GPMVs can be generated by several chemical treatments to obtain cell-attached GPMVs or cell-free GPMVs.<sup>85</sup> The most commonly used method to form cell-free GPMVs



consists in treating the cells with paraformaldehyde and DTT to induce plasma membrane vesiculation. An alternative method replaces paraformaldehyde and DTT by N-ethylmaleimide, known to induce GPMV formation.<sup>85,86</sup>

The cell membrane is a complex biological system. It is dynamic and diverse cell processes take place within or around it. The understanding of all aspects of these processes is only starting. Thanks to the use of model membranes, interactions of exogenous molecules with the plasma membrane can be studied at the molecular level. Membrantropic peptides, and among them CPPs, are an example of membrane-active molecules. In the next section, the CPP Penetratin, able to cross the cell membrane, will be presented and its internalization pathway will be discussed. Finally, an emphasis will be done on the Penetratin specific interaction partners involved in the cellular uptake.

## 2. The cell-penetrating peptide Penetratin

CPPs are short amino acid (AA) sequences (4-40 AAs) able to enter in cells through endocytosis and/or various translocation mechanisms (Figure 24). They are able to deliver biologically active molecules named cargoes such as nucleic acids, proteins, RNA, nanosized particles, drugs or diagnostic molecules, linked covalently, generally *via* disulfide bonds, or by complexation, in cells and tissues. They are also named “Trojan peptides” or protein translocation domains (PTDs). Such tools could be very helpful for drug delivery, gene therapy, cancer cells targeting and for biotechnological applications such as the study of intracellular processes. However, the CPP uptake mechanisms are still not clear and vary from one CPP sequence to another.

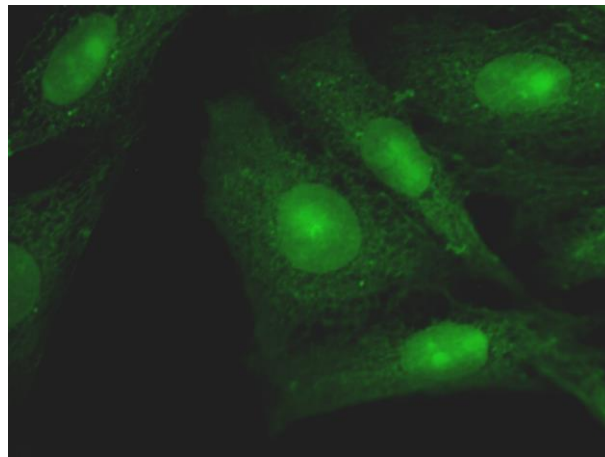


Figure 24. Microscope image of CPP Penetratin labelled with Alexa 488 internalized in CHO-K1 cells.

The first report of a protein able to undergo cell internalization was published in 1988 by two unrelated papers, for the HIV Tat protein.<sup>87,88</sup> It was followed in 1991 by the evidence of the ability to internalize of the 60 AAs Antennapedia homeodomain.<sup>89</sup> In 1994, it was reported that a short peptide sequence of 16 AAs, pAntp(43-58), called Penetratin, was responsible of this translocation.<sup>90</sup> These advancements set the ground for a new area of research in therapeutic delivery.

Since the first CPPs have been discovered, a lot of new sequences have been added to the CPP family, up to over 1800 sequences, which are reported in the *CPPsite 2.0* database.<sup>91</sup> All peptides of the CPP family are able to enter in cells but they can differ by several factors such as interaction partners at the plasma membrane, internalization mechanisms and generated cellular responses. Although their mechanism of entry is still not clear, numerous CPPs are being evaluated in preclinical and clinical trials. They constitute promising drug delivery systems by their low cell cytotoxicity and intracellular targeting.<sup>92</sup> One of the obstacles for CPP-cargo conjugates delivery and subsequent biological activity is the availability in the cytosol, often prevented by trapping of the cargo in endosomes.<sup>93</sup> Another limit for CPP application as therapeutic delivery is their lack of cell type specificity.

Besides, some CPPs are also antimicrobial peptides (AMPs). It is the case of Penetratin, which has a potent antimicrobial activity, showing a minimal inhibitory concentration (MIC) of 0.5 to 4  $\mu$ M, although it does not exhibit any cytotoxicity against eukaryotic cells.<sup>94</sup>

In general, CPPs show little similarity in their sequence. Most of them are built with L-AAs (80%) and are linear peptides.<sup>95</sup> CPPs can be classified based on their origin (protein-derived, chimeric and synthetic) or based on their physicochemical properties. The later classification will be described in this section, as physicochemical properties describe better the interactions of these peptides with membrane partners and their effects on the cell.

## 2.1. Penetratin sequence and structure

Homeoproteins are DNA-binding proteins of the large family of transcription factors, implied in various morphological cell processes. Their DNA-binding segment, named the homeodomain, is highly conserved among homeoproteins of living species in general and is composed of 60 AAs arranged in three  $\alpha$ -helices. The third helix is specific of DNA targeting recognition. It is separated from the helix 2 by a  $\beta$  turn.<sup>96</sup>

The Penetratin CPP is derived from the Antennapedia homeodomain, coming from *Drosophila*, and corresponds to its third  $\alpha$ -helix. It corresponds to a short peptide sequence of 16 AAs, pAntp(43-58), responsible of the protein translocation. Its complete sequence is: RQIKIWFQNRRMKWKK. This peptide is able to internalize in cells at 37 and 4 °C, is released in the cytoplasm, and accumulates in the cell nucleus. Internalization studies with shorter versions of this sequence, *i.e.* N-term or C-term deletions, showed that this sequence is necessary and sufficient for the cell uptake.<sup>90</sup>

Like many other CPPs, Penetratin has a high content in basic AA residues. It also presents two tryptophan residues which are necessary for the cellular uptake.<sup>90</sup> Interestingly, tryptophan 48 and Phenylalanine 49 are very well conserved in all the homeodomain sequences, and are important for the homeodomains structure.<sup>97</sup>

In aqueous solvent, Penetratin was suggested to adopt a random coil configuration as no evidence of a clear structure was observed by circular dichroism (CD) studies.<sup>98</sup> Another paper based on CD experiments reports the presence of a mixture of structural conformations and a low level of secondary structures.<sup>99</sup> NMR experiments allow to define more precisely the peptide behavior. Actually, the edges of the sequence would indeed be observed as random coil, but the center of the sequence would be found in a short  $\alpha$ -helical structure,<sup>100</sup> as illustrated on Figure 25.

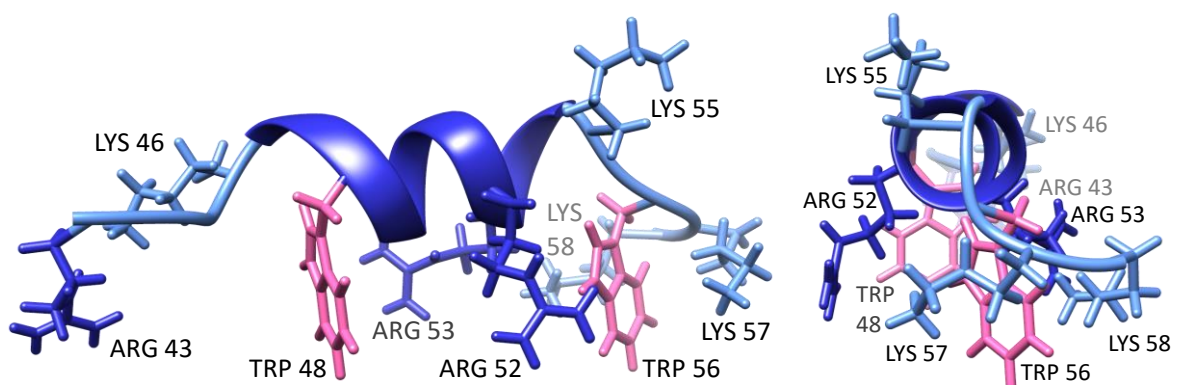


Figure 25. Penetratin  $\alpha$ -helix structure in solution, AAs in 3-letters code. Adapted from <sup>100</sup>.

Interaction with negatively charged lipids gives rise to a clear structuration of the peptide. In presence of negatively charged lipids, an amphipathic  $\alpha$ -helical structure is observed for low lipid to peptide ratios or a  $\beta$ -sheet structure for higher ratios.<sup>98</sup>

## 2.2. CPP classification by physicochemical properties

The charge, hydrophobicity and their distribution in the peptide sequence are the main characteristics used to classify the CPPs by physicochemical properties. They will thus be grouped as cationic, amphipathic and hydrophobic CPPs. This classification is well correlated with the advancements made on their uptake mechanism.<sup>101,102</sup> A majority of CPPs are positively charged at physiological pH (83%), while anionic CPPs are very few and are usually assigned to the other CPP groups individually.<sup>103</sup> Table 5 shows some examples of CPP sequences classified according to their physicochemical properties.

Table 5. Examples of CPPs classified according to physicochemical properties. Penetratin is highlighted in bold. Adapted from <sup>104,105</sup>. <sup>a</sup>N natural, C chimeric, S synthetic.

Type	Name	Peptide sequence	Origin <sup>a</sup>	Ref.
<b>Amphipathic</b>	Transportan	GWTLNSAGYLLGKINLKALAALAKKIL	C	106
	Pep-1	KETWWETWWTEWSQPKKRKRKV	C	107
	MPG	GALFLGFLGAAGSTMGAWSQPKSKRKRKV	C	108
	(R/W) <sub>9</sub>	RRWRRRWR	S	109
	MAP (Model Amphipathic Peptide)	KLALKLALKALKAALKLA	S	110
	pVEC	LLIILRRRIRKQAHASK	N	111
	ARF (1-22)	MVRRFLVTLRIRACGPPRVRV	N	112
<b>Cationic</b>	HIV-1 Tat protein, Tat(49–57)	RKKRRQRRR	N	113
	<b>Penetratin, pAntp(43-58)</b>	<b>RQIKIWFQNRMRMKWKK</b>	<b>N</b>	90
	Polyarginine	(R) <sub>n</sub> ; n = 6–12	S	114,115
	Engrailed-2	SQIKIWFQNKRAKIKK	N	116
<b>Hydrophobic</b>	C105Y	CSIPPEVKFNKPFVYLI	N	117
	Pep-7	SDLWEMMMVSLACQY	S	118
<b>Anionic</b>	p28, Azurin(50-77)	LSTAADMQGVVTDGMASGLDKDYLPDD	N	119
	PepNeg	SGTQEEY	S	120

### 2.2.1. Cationic CPPs

The cationic group includes strongly positively charged CPPs at physiological pH. In order to differentiate hydrophobic and amphipathic CPPs from the cationic ones, a CPP is considered cationic only if it presents a continuous stretch of basic residues that is essential for the peptide internalization, and if it does not form by folding to an amphipathic  $\alpha$ -helix conformation.<sup>105</sup>

The first CPP discovered is cationic. Tat(49–57) is derived from the human immunodeficiency virus-1 (HIV-1) protein Tat and its sequence (RKKRRQRRR) contains 8 basic residues. It has been shown by studies on arginine-based peptides composed of 3 to 12 residues that this number of charge is the minimal to induce efficient cell uptake<sup>114</sup> and that increasing the amount of arginine residues enhances the cellular uptake level. However, increasing the amount of basic residues also increases side effects like cytotoxicity and strong and irreversible interactions with the plasma membrane, which above 10 arginine residues diminishes the internalization efficiency. Arginine residues contribute to a higher extent to cellular uptake compared to lysine residues.<sup>121,122</sup> Lysine-based peptides show poor internalization properties. This is explained by

the ability of the arginine guanidinium moiety to form bidentate hydrogen bonds with negatively charged interaction partners of the cell membrane,<sup>123</sup> which can present carboxylic, sulfate or phosphate groups, as depicted on Figure 26. This particular binding would be of great importance for the cationic CPPs cellular uptake at physiological pH.<sup>115,124,125</sup> As lysine residues do not present a guanidinium group, the ability of lysine-based peptides to cross the cell membrane is lowered.

Basic residues are necessary but not always sufficient for internalization of cationic CPPs. The example of Penetratin demonstrates that other type of AAs can be essential. For this CPP, tryptophans play an important role in the cell uptake. It was shown that the two tryptophans of the Penetratin sequence are crucial for the cellular uptake and that replacement of the Penetratin W56 by a phenylalanine completely inhibits its internalization qualities.<sup>126-128</sup> Tryptophans also contribute significantly to cellular uptake of other cationic CPPs and they are essential for the internalization of CPPs containing less than 8 basic AAs.<sup>129,130</sup>

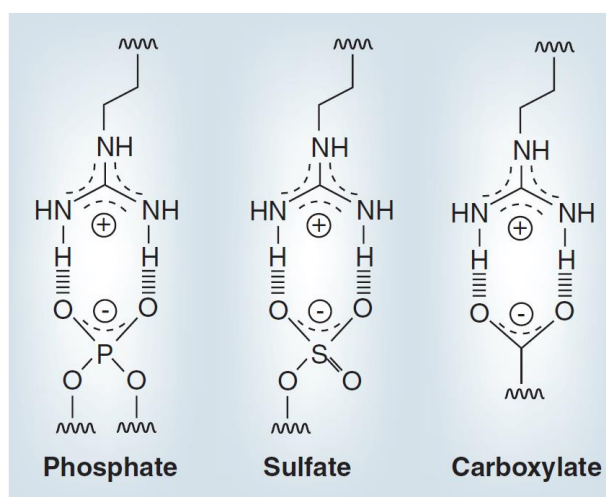


Figure 26. Favorable hydrogen bonds of the guanidinium group of arginine with phosphate, sulfate and carboxylate groups of the cell membrane.<sup>131</sup>

Polycationic stretches are often found in DNA-, RNA- and heparan-binding proteins coming from all kinds of organisms, which thus represent a wide source of cationic CPPs. An important group of cationic CPPs are protein-derived from homeodomains, like for instance Penetratin, Engrailed, oligo-arginines.<sup>132</sup>

### 2.2.2. Amphipathic CPPs

The amphipathic CPPs group is the most numerous, contributing to over 40% of the known CPP sequences and also include some anionic peptides.<sup>103</sup> They contain both hydrophilic and hydrophobic regions of AAs, generally forming two faces. The hydrophilic face is composed of lysines and arginines, while the hydrophobic face presents hydrophobic residues such as valine, leucine, isoleucine, and alanine.<sup>92</sup> Amphipathic CPPs can be classified into different groups, depending on their sequence, secondary structure and association with lipids<sup>102</sup>: primary, secondary  $\alpha$ -helical, secondary  $\beta$ -sheet and proline-rich amphipathic CPPs.<sup>103</sup>

### PRIMARY AMPHIPATHIC CPPS

In primary amphipathic CPPs, the two faces can exist either in the primary structure (MPG, Pep-1), or in a stable  $\alpha$ -helix structure (Transportan). In general, they are longer than cationic or secondary amphipathic CPPs, composed of over 20 AAs, so that they can extend through the hydrophobic core of a lipid membrane. They interact strongly with neutral or anionic bilayers and could disturb the lipid membrane organization.<sup>105</sup>

### SECONDARY AMPHIPATHIC CPPS

Secondary are generally shorter than primary amphipathic CPPs. They interact with anionic membranes, but not with neutral bilayers. They do not insert deeply in the membrane and thus disturb less the lipid membrane organization.

The secondary amphipathic CPPs are unfolded in solution. They take their amphipathic character by folding upon interaction with anionic molecules like negatively charged membrane lipids or GAGs.<sup>101</sup> Many peptides and proteins that bind to lipid membranes are amphipathic  $\alpha$ -helices, with two separated faces composed of hydrophobic AAs and hydrophilic AAs (cationic, anionic or polar). Thus, we can visualize their amphipathicity on helical wheel projections of the CPPs, as shown on Figure 27.

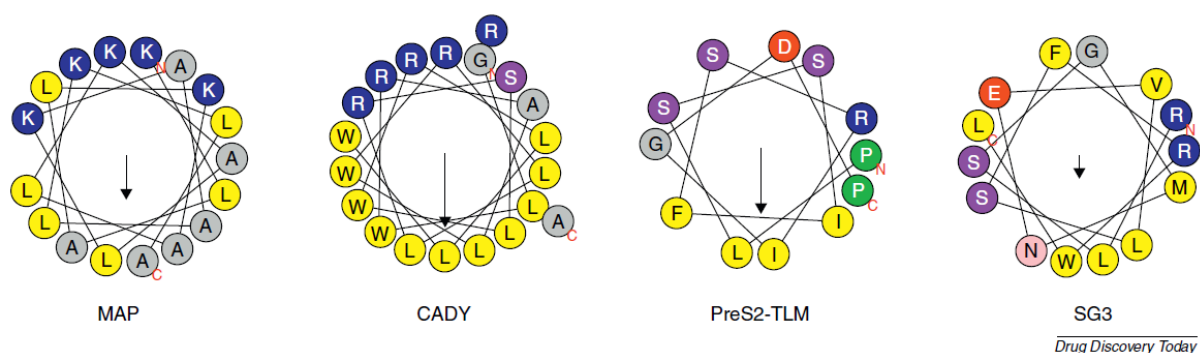


Figure 27. The helical wheel representation highlights peptide amphipathicity, with longer vector indicating a larger amphipathic moment. Amino acids are colored by amino acid class (yellow: hydrophobic; grey: apolar; purple: polar; blue: positively charged; red: negatively charged; green: proline).<sup>103</sup>

Most of the amphipathic CPPs are cationic but their translocation abilities would be attributed to their amphipathic character more than to their positive charge. Several studies have been trying to predict CPP  $\alpha$ -helical sequences by elucidation of the number of helix turns needed, peptide length, AAs degree of hydrophobicity or amphipathic moment but there is still no evidence of a reliable prediction model.<sup>103</sup>

### SECONDARY $\beta$ -SHEET AMPHIPATHIC CPPS

$\beta$ -sheet amphipathic CPPs arrange in a  $\beta$ -sheet structure when in contact with a lipid membrane. Like for  $\alpha$ -helical amphipathic CPPs, they present one hydrophobic and one hydrophilic regions of AAs. This  $\beta$ -sheet structure is essential for their cell penetration.<sup>133</sup>

### PROLINE-RICH AMPHIPATHIC CPPS

Proline-rich amphipathic CPPs are a specific subgroup of amphipathic CPPs. Proline has very unique properties compared to the other 20 natural AAs:

- It is very rigid due to its pyrrolidine ring;
- It cannot stabilize an  $\alpha$ -helix or  $\beta$ -sheet secondary structure through hydrogen bonds due to the lack of a hydrogen on its  $\alpha$  amino group, as it displays a tertiary nitrogen, unlike other AAs that present secondary nitrogen in their lateral chain;
- When abundant in a peptide sequence, it can form a typical secondary helical structure in water, polyproline II (PPII), a left-handed helix of 3.0 residues per turn (standard  $\alpha$ -helix is a right-handed helix of 3.6 residues per turn)

### 2.2.3. Hydrophobic CPPs

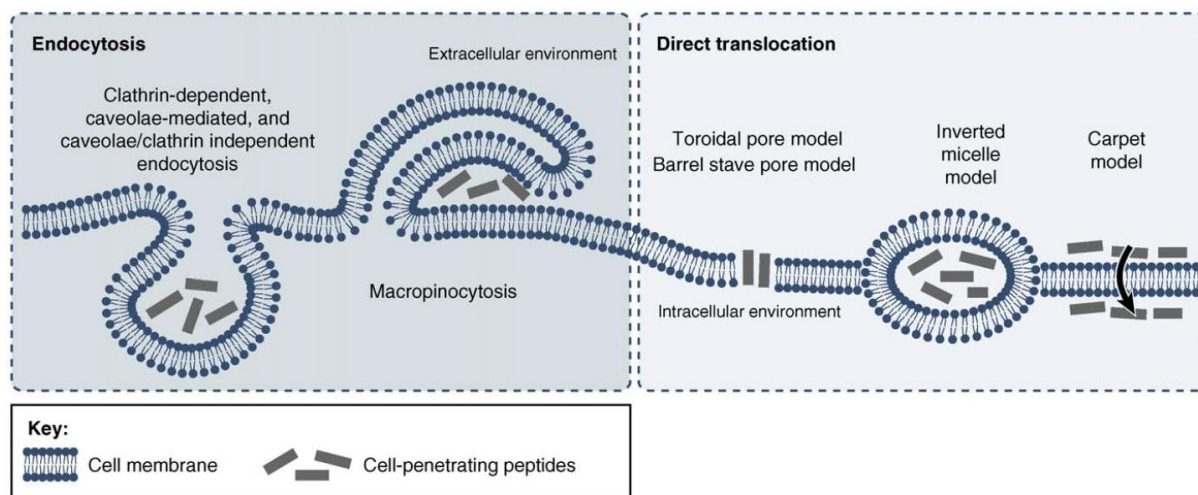
The hydrophobic CPPs group is the least represented among all CPP groups; it represents only 15% of the CPPs.<sup>103</sup> They comprise either uniquely non polar residues or very few charged AAs. These hydrophobic sequences have high affinity for the hydrophobic core of the plasma membrane, and that is probably crucial for their cell uptake. Hydrophobic CPPs have been discovered after cationic and amphipathic CPPs, which explains why there are only a limited number. As a consequence, their internalization pathways have been little investigated. Nevertheless, these CPPs could translocate through lipid bilayers via energy-independent pathways, thus contrasting with the other CPP groups internalization pathways.<sup>134</sup> The advantages of a direct translocation are that the peptide is immediately available in the cytosol, without any risk of endosomal entrapment or degradation. Some hydrophobic CPPs are based on natural AAs, such as the anionic and cationic BIP pentapeptides, the C105Y peptide, and its C-term cell-penetrating portion PFVYLI, and the Pep-7 peptide. Unlike cationic and amphipathic CPPs, scrambling the linear sequences of BIP pentapeptides or of the PFVYLI peptide does not significantly affect their internalization properties.<sup>135</sup> Hydrophobic CPPs also include peptides that are chemically modified by stapling to stabilize  $\alpha$ -helices<sup>136</sup>, prenylation to favor membrane interactions<sup>137</sup> or by forming pepducins that are CPPs able to bind to the cytosolic part of various transmembrane proteins like G proteins and thus remain anchored to the plasma membrane, where they can modulate receptor signal transduction.<sup>138</sup>

It can be noted that this classification is not resolute and the assignment of a CPP to one or another group sometimes vary from one paper to another. Also, some peptides are difficult to classify following this physicochemical classification, due to their secondary structure polymorphism. It is the case of Penetratin, classified here as a cationic peptide. In aqueous solvent, it is poorly structured, upon interaction with negatively charged lipids, it adopts an amphipathic  $\alpha$ -helical structure for low lipid to peptide ratios or a  $\beta$ -sheet structure for higher ratios.<sup>98</sup> In the case of Penetratin, the evidence that the  $\alpha$ -helical structure is not mandatory for its cell uptake<sup>139</sup> supports its classification as a cationic peptide.

## 2.3. Cell entry mechanisms

CPPs have been discovered 30 years ago and many investigations have been focused on their internalization mechanisms. However, the way CPPs cross the plasma membrane and enter in cells are still unclear. Difficulties arise from the fact that CPPs have very wide physicochemical properties, size, structure or nature of cargo, leading to different behavior and efficiency of cell uptake.<sup>140</sup> In particular, CPPs are able to exploit various routes to cross the plasma membrane and one CPP can use several routes concomitantly. The proportions of contribution of direct

translocation and endocytosis vary according to various factors such as the CPP sequence,<sup>4</sup> the CPP concentration, the cell type and the cellular differentiation state.<sup>141</sup> The various entry routes belong to two main categories: direct translocation (or direct penetration), an energy-independent pathway, and the energy-dependent endocytosis pathways (developed in the Chapter The plasma membrane, paragraph 1.1.2.). Figure 28 represents how wide are the CPPs entry mechanisms, involving these two main routes.



*TRENDS in Pharmacological Sciences*

Figure 28. Illustration of the probable CPPs internalization pathways. Direct translocation mechanisms are energy-independent processes including insertion of CPPs through pore formation and membrane destabilization in a carpet-like model or by inverted micelle formation. Endocytosis pathways are energy-dependent mechanisms.<sup>142</sup>

The evidence of the CPP penetration in cells at 4°C and 37°C strongly suggests that Penetratin is internalized by a receptor-independent mechanism.<sup>139</sup> Cell internalization being decreased at low temperatures, but not abolished, showed in addition that both direct translocation and endocytosis pathways are used concomitantly by the peptide to enter cells. Furthermore, introducing 1 to 3 proline residues does not affect the peptide internalization efficiency, demonstrating that the  $\alpha$ -helical structure is not crucial for the cell uptake. Using Penetratin analogues composed of D-enantiomer residues or composed of the same 6-AAAs positioned in the reversed order confirmed that no chiral receptor is implied in the internalization pathway of the CPP. This method allows to modify the  $\alpha$ -helix orientation without modifying the amphipathic properties of the peptide. The same study showed as well that the Penetratin uptake is very unlikely to imply a pore formation by an  $\alpha$ -helical conformation of the peptide. The inverted-micelle model for this peptide internalization is supported by several reasons. Pinocytosis, which is a receptor-independent pathway is not favored as endocytosis structures are not observed at the membrane.

### 2.3.1. Direct translocation

As it is an energy independent pathway, direct translocation can happen at low temperatures. It can also occur in the presence of endocytosis inhibitors. It entails multiple models of entry such as inverted micelles, electroporation-like model, carpet model, counterion model and other types of membrane destabilization like the ephemeral pore-like or tubule formation. In



general, these various mechanisms are initiated by interactions of the positively charged CPPs with negatively charged membrane partners like phospholipids or the glycocalyx, which are the first membrane components that the CPPs encounter before crossing the cell membrane.

### INVERTED MICELLES MODEL

The inverted-micelle (or hexagonal phase II) model was proposed in 1996 by Derossi *et al.*<sup>139</sup> (Figure 29) as a potential mechanism for the Penetratin internalization. Tryptophans, which are inducers of inverted-micelles,<sup>143</sup> were found to be necessary for the cellular uptake.<sup>90</sup> Finally, phosphore NMR studies showed that replacing tryptophans by phenylalanine residues in the Penetratin sequence prevents its ability to generate formation of hexagonal phases in phospholipids.<sup>144</sup>

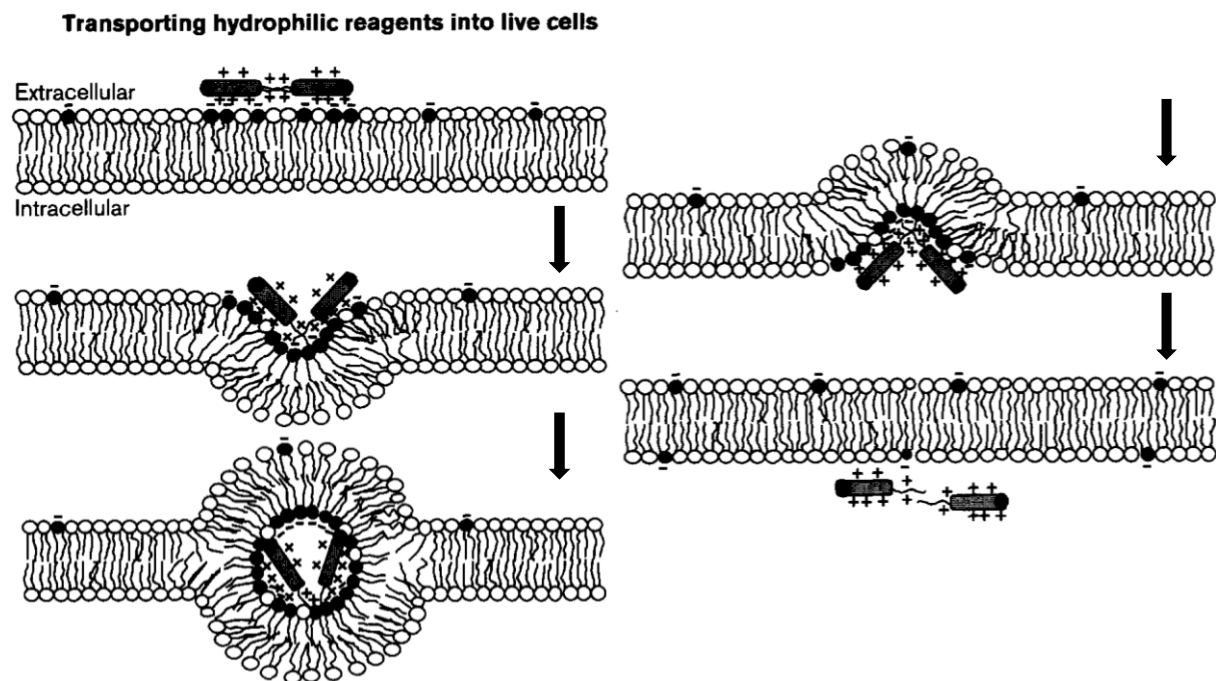


Figure 29. The inverted micelles/hexagonal phase II model, based on the known biological properties of Penetratin (*i.e.* no chiral receptor and internalization at 4°C) and on <sup>31</sup>P NMR studies.<sup>126</sup>

This inverted-micelle mechanism is based on the encapsulation of the CPP within an invagination of the phospholipid bilayer.<sup>145</sup> The CPP is then released from the micelle to the cytosol by inversion. It is probable that electrostatic interactions between the CPP and the lipid membrane induces a change in the peptide conformation leading to the modification of the membrane physicochemical properties.<sup>146</sup>

The mechanism is depicted in Figure 29. The cationic CPP would first lie at the negatively charged surface of the plasma membrane and destabilization of the membrane through curvature modification would then be induced by a tryptophan residue (tryptophan 48 in the case of Penetratin), forming an inverted-micelle. The later would then open to the other side of the membrane.<sup>126</sup>

### ELECTROPORATION-LIKE MODEL

The electroporation-like model is based on the transient existence of a transmembrane electrical field engendered by the asymmetrical distribution of the basic CPP located at the outer layer of the cell membrane. This would modify the transmembrane organization and impact its curvature until a point where the internalization would be triggered by ephemeral structures of inverted curvature in the membrane. This model has been proposed to explain the Penetratin cell uptake.<sup>147</sup>

### COUNTERION MODEL

The counterion model implies a local charge neutralization of guanidinium groups and was proposed to describe the cellular uptake mechanism of polyarginines.<sup>148</sup> Such basic CPPs following non-endocytic pathways have to overcome a high energy barrier. In this model, the translocation would be mediated by anion electrostatically bound to the guanidinium groups of arginines *via* bidentate hydrogen bonds (see Figure 26). Polyarginines guanidinium groups bind tightly to anionic counterions and can form thermodynamically stable complexes with anionic molecules of the plasma membrane. Herein, it was demonstrated that poly- and hexaarginine could be transferred from water to a hydrophobic solvent such as chloroform by forming complexes with amphiphilic anions (SDS, egg yolk PG, cholesterol sulfate, pyrenebutyrate and stearate), which was not possible for polylysine.<sup>149</sup> Moreover, the same study suggests that the same kind of complexes may contribute to the translocation of guanidinium-rich peptides through lipid bilayers. A same kind of mechanism is proposed for intracellular release from biomembranes, involving this time hydrophilic polyanions like heparin.<sup>148</sup>

The counterion model is also envisaged in the case of arginine-rich CPPs such as Penetratin. It was found by using water-octanol systems, that anionic phospholipids contribute to Penetratin partitioning into the octanol phase. A Penetratin analogue with arginine residues replaced by lysines shows considerable lower partition into octanol, while a Penetratin analogue enriched in arginine residues exhibits the highest partitioning effect.<sup>150</sup> These results also support the counterion mechanism involving the guanidinium groups for cell internalization.

### TRANSIENT PORE FORMATION

Transmembrane pore formation requires several CPP monomers to accumulate perpendicularly to the plasma membrane in the case of barrel-stave or toroidal pore models or organize in layer parallel to the membrane surface for the carpet-like model (Figure 30). These models are particularly described in the case of AMPs for explaining bacterial cells killing as they can lead to membrane leakage.

#### Barrel-stave model

The formation of transmembrane pores could be formed by aggregation of several amphipathic CPP monomers. In the same way as transmembrane proteins,  $\alpha$ -helical CPPs could associate with their hydrophobic residues facing and interacting with the hydrophobic core of the membrane, while their hydrophilic faces form the inside of the pore. This would engender an aqueous pore for the CPPs to be internalized and enable the passage of the hydrophilic CPPs.<sup>142</sup>

### Toroidal pore model

In this model, a transmembrane  $\alpha$ -helical structure is also involved, but the hydrophilic and positively charged section of the CPPs interact with the membrane phospholipid polar head groups that go along the pore. They insert in the bilayer and provoke the membrane rearrangement. In contrast with the barrel-stave model, the toroidal pore model does not imply peptide-peptide interactions.<sup>142</sup> The toroidal pore model was suggested to explain the internalization mechanism of the CPP Tat.<sup>151,152</sup>

### Carpet-like model

This model depicts the formation of a layer of peptide monomers lying parallel to the membrane surface. This carpet-like arrangement of the CPPs is thought to disrupt the lipid membrane packing, leading to slightly increased fluidity and membrane disruption.<sup>142</sup>

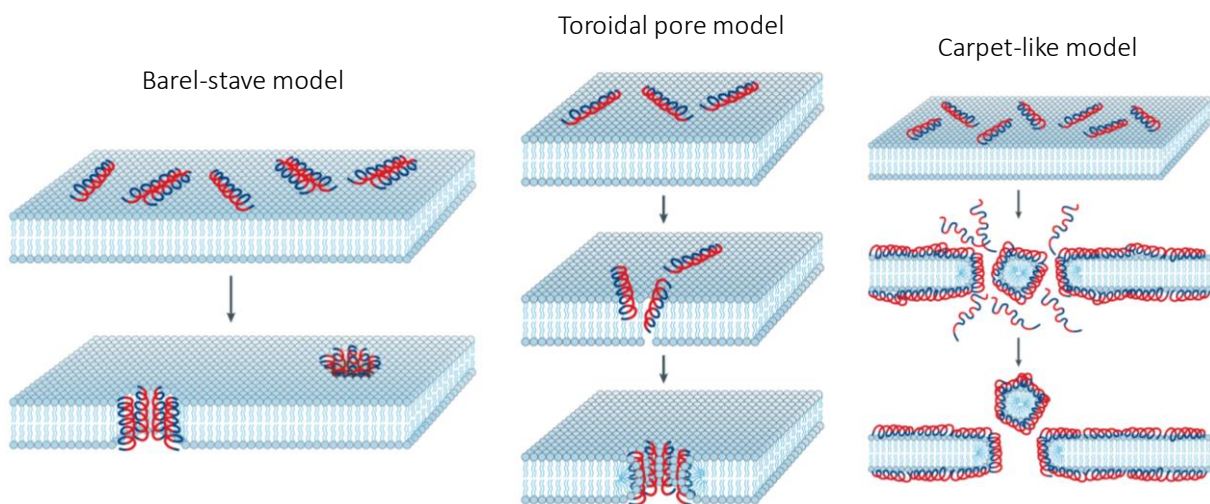


Figure 30. The transient pore formation models. Peptides hydrophilic regions are shown in red, hydrophobic regions are in blue. Adapted from <sup>153</sup>.

An alternative model is proposed in the case of Penetratin translocation (Figure 31). Penetratin monomers initially in unstructured random coil in solution would undergo a  $\beta$ -turn conformation upon association with negatively charged phospholipids at the membrane surface (Figure 31a). Accumulation of the peptide monomers would lead to membrane thinning and partial neutralization of the bilayer surface charge implying that other CPPs binding to the membrane surface would become unfavorable. A transition to  $\alpha$ -helical conformation of CPPs allows transmembrane positioning of peptides *via* transient pore formation (Figure 31b) and consequent translocation (Figure 31c).<sup>154</sup>

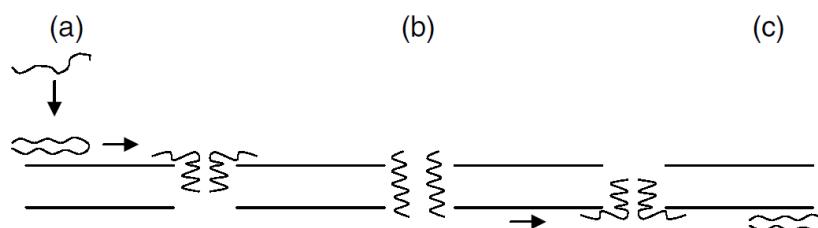


Figure 31. Model for the Penetratin translocation proposed by Clayton *et al.*<sup>154</sup>

### 2.3.2. Endocytosis

The endocytosis pathways are described in the previous section on the plasma membrane (paragraph 1.1.4.). Depending on the CPP sequence and type of cargo, all endocytosis types can be employed by CPPs: clathrin-dependent, caveolae-dependent, and caveolae- and clathrin-independent endocytosis and macropinocytosis. Endocytosis pathways can be easily distinguished from direct translocation as it involves the formation of vesicles and endosomes at the internal membrane proximity. Thus, using a fluorescently-labelled CPP, endocytosis pathways should result in a granular pattern as the peptide is trapped in the vesicles. As for translocation, one should observe a uniform labelling of cells.<sup>105</sup> However, both patterns can be observed for the same CPP sequence, showing the versatility of the CPP internalization mechanism. Various factors and environmental conditions influence these results: CPP physicochemical properties, type of cargo, cell line and conditions (confluence, viability), plasma membrane composition, extracellular environment, temperature, ionic strength and pH.<sup>155</sup>

Although many studies have evidence direct translocation as a pathway for the Penetratin internalization, there is no reason to put the endocytosis route aside. Recent studies have revealed that the cellular uptake of Penetratin is a more complex process. In this process, GAGs would be interaction partners of choice to induce Penetratin endocytosis, as it has been demonstrated by experiments using GAG-deficient cells.<sup>4</sup> Penetratin internalization at 4°C (*i.e.* direct translocation) was not hampered by the GAGs compositions of cells, while endocytic pathways efficiency (observed at 37°C) were significantly decreased.

Recruitment of Penetratin at the cell surface by GAGs, which were found to promote peptide aggregation and localized concentration,<sup>156</sup> would constitute a first recognition step before ignition of the endocytosis process. In addition, the endosomal escape of Penetratin has been interrogated by modelling in artificial vesicles.<sup>157</sup> It demonstrated that Penetratin was able to escape these endosome models, directed by a proton gradient. This also support the possibility of existence of the endocytic route for Penetratin uptake.

### 2.3.3. Molecular interaction partners of Penetratin involved in direct translocation

CPPs can follow all endocytic routes as well as direct membrane translocation to internalize. As mentioned earlier, contributions of these two internalization pathways vary according to the cell line, peptide sequence, but also many environmental factors such as temperature, pH, etc. In both types of pathway, the first step should lie in the CPP interaction with membrane components extending to the extracellular matrix. They would recognize CPPs with various affinity and selectivity according to their sequence. Internalization efficiency variability according to the cell type and peptide sequence implicates that CPPs associate with various interaction partners at the membrane surface.

The negatively charged lipids and carbohydrates are considered to be the first molecular partners to be encountered by CPPs, which are mostly positively charged. Electrostatic interactions between CPPs and these cell surface components are the first step for cellular uptake mechanism.

As explained in the previous paragraph, GAGs interactions are envisaged in the endocytic pathways recognition step, but are not considered in the case of direct translocation mechanism. The following section will be focused on the phospholipid interaction partners of Penetratin, as it constitutes a prerequisite for the direct translocation pathway. Model membranes are widely used to evaluate these interactions. Thus, the interaction of Penetratin with negatively charged model membranes in general, and more specifically with liposomes, will also be approached.

### ZWITTERIONIC LIPIDS

Considering Penetratin interaction with zwitterionic lipid PC, results can lead to contradictory conclusions depending on the technique used. Using isothermal titration calorimetry (ITC),<sup>158</sup> electron spin resonance (ESR)<sup>156</sup> or differential scanning calorimetry (DSC),<sup>145</sup> several studies showed no interaction between Penetratin and zwitterionic membrane composed of DMPC, POPC or DOPC vesicles. Other studies suggest that cationic CPPs could interact with both anionic and zwitterionic lipids through bidentate hydrogen bonds between their arginine moieties and the lipid phosphate groups.<sup>159</sup> Phosphorous NMR experiments performed using the CPP Tat and DMPC vesicles also related a modification of the membrane organization upon interaction with the cationic peptide.<sup>160</sup> The presence of the peptide triggered the formation of isotropic structures in DMPC bilayers, while this effect was not observed with anionic DMPG vesicles. This structuration, presumably inverted-micelles, is attributed to interactions of the peptide with the lipid head group, rather than to electrostatic interactions. Finally, DSC and ITC experiments revealed that Penetratin interacts with DMPC liposomes in absence of salt, while it shows no interaction effects in physiological buffer conditions.<sup>3,145</sup> All together, these results suggest that the Penetratin interaction with zwitterionic lipid PC is rather weak, and could only be observed in particular *in vitro* conditions, that would not necessarily reflect the biological ones.

Other lipids could also be important to consider in the peptide-membrane interaction. For example, the zwitterionic lipid PE was found to have an effect on the Penetratin affinity for lipid bilayers composed of egg PC. Its presence triggered the binding affinity of the peptide for the liposomes.<sup>161</sup> As PE has a conical shape that induces a particular negative curvature in the membrane, these results highlight the importance of the membrane state in the interaction. Indeed, the membrane fluidity and curvature should also be a key factor when considering the interactions peptide to membrane. This particular point will be further introduced and discussed in the Part 2 of this manuscript.

### NEGATIVELY CHARGED LIPIDS

Penetratin, as a cationic CPP, is strongly suspected to form electrostatic interactions with anionic lipids of the plasma membrane through bidentate hydrogen bonds with the arginine residues (Figure 26). Several papers have reported this kind of interactions in model membranes composed of negatively charged lipids. The eukaryotic plasma membrane is composed mainly of the zwitterionic phospholipid PC, but also contains anionic lipids in lower amounts, such as PS or PI derivatives. The PG lipid is also widely used in model membranes to mimic anionic membranes, although it is mainly found in bacterial membranes. Consistence of

this use is supported by the fact that many CPPs, including Penetratin, also show antimicrobial activities, implying that they interact with bacterial membranes.<sup>94</sup>

Many studies have investigated the interaction of Penetratin with negatively charged model membranes through various methods. It is now clearly admitted that Penetratin strongly interacts with anionic lipids.<sup>3,158</sup> DSC experiments indicated that the peptide binds to the anionic lipid DMPG, inducing modifications of the lipid headgroup tilting and of the bilayer fluidity, suggesting peptide insertion between the hydrophobic chains.<sup>145</sup>

The importance of anionic lipids as CPP interaction partners at the cell surface has been raised by using *in vitro* experiments and model membranes. Considering the biological aspect, anionic lipids are in minority in the plasma membrane. Also, they are mostly found at the internal leaflet. Thus, significance of the interaction of Penetratin with negatively charged lipid to explain the biological process of internalization can be questioned. The fact remains that some of the negatively charged lipids are found also at the external leaflet. In addition, a hypothesis consists in the ability of cationic peptides to recruit several anionic lipids and thus form enriched negatively charged domains in the membrane.<sup>131</sup> Recruitment of negatively charged lipids at the cell surface would be a key factor for the CPP recognition step, before translocation can occur. The CPP would accumulate in these domains and translocate in this favorable and very localized region. Evidence of negatively charged lipids recruitment by cationic CPPs can be found in the literature. Experiments of DSC showed that Penetratin could recruit cardiolipin and that it induced partitioning in liposomes composed of DPPC and cardiolipin or PG lipids.<sup>162</sup>

In particular, electrostatic sequestration of PIP<sub>2</sub> by cationic peptides has been demonstrated.<sup>163,164</sup> This point will be further discussed in section 3. of this introduction. More generally, links that can be made between PIP<sub>2</sub> and Penetratin in the literature will be highlighted.

### 3. PIP<sub>2</sub> and Penetratin internalization in the literature

#### 3.1. Sequestration of PIP<sub>2</sub> by proteins basic binding-site or by basic peptides

As commented in section 1 of this introduction, PIP<sub>2</sub> clustering abilities are very likely to be a key factor for its versatility of function and its implication in many cell processes. Apart from localized synthesis of PIP<sub>2</sub> or PIP<sub>2</sub> binding to clustering proteins of the plasma membrane, the PIP<sub>2</sub> concentration at localized sites of the membrane can be driven by interactions with other partners, such as a membranotropic agents that can translocate through the plasma membrane.

A concrete example is the one of the unconventional secretion of the Fibroblast Growth Factor FGF2, whose vectorial translocation across the membrane is regulated by interactions with PIP<sub>2</sub> and heparan sulfates on opposing sides of the membrane.<sup>165</sup> In particular, FGF2 is able to bind simultaneously to several PIP<sub>2</sub>, through high affinity interaction with basic residues of its binding pocket, including arginine and lysine residues. Atomistic molecular dynamics simulations are pictured on Figure 32.

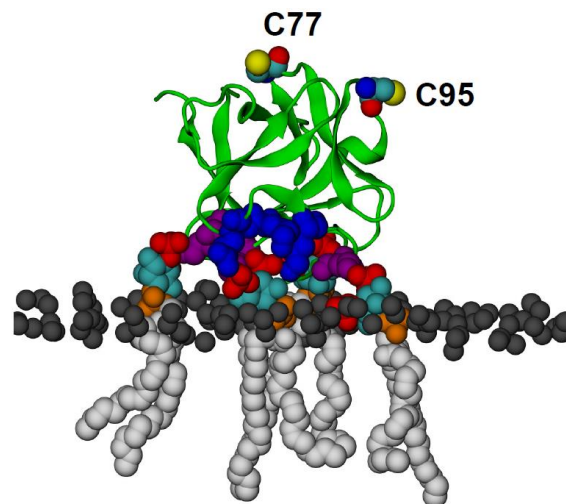


Figure 32. High-affinity orientation of FGF2 on the membrane surface, showing all the known PI(4,5)P<sub>2</sub>-binding site residues (K127, R128, K133) as well as the previously undetermined binding site residues (K34, K137, K143). FGF2 is rendered as green cartoon, and its C95 and C77 residues are shown as van der Waals (vdW) spheres and highlighted by text in the figure. The key binding pocket residues (K127, R128, K133) are shown as blue vdW spheres, and the additional binding site residues (K34, K137, K143) are shown as purple vdW spheres. Lipids are colored as gray vdW spheres (POPC phosphate atoms), red vdW spheres (PI(4,5)P<sub>2</sub> bisphosphates), cyan vdW spheres (inositol ring in PI(4,5)P<sub>2</sub>), orange vdW spheres (phosphate linking the fatty acid chains and the inositol ring in PI(4,5)P<sub>2</sub>), and white vdW spheres (fatty acid chains in PI(4,5)P<sub>2</sub>). Water molecules and ions are not shown for clarity. Figure and legend adapted from <sup>165</sup>.

Electrostatic recruitment of PIP<sub>2</sub> has also been reported to occur by interaction with the basic effector domain of the MARCKS protein.<sup>164</sup> This domain was found to bind to negatively charged lipids on the cytosolic leaflet of the membrane. Using model membrane containing a significant portion of monovalent phospholipid PS, MARCKS(151–175) was able to sequester

several PIP<sub>2</sub> (see Figure 33). Interaction with Ca<sup>2+</sup>/calmodulin or protein kinase C phosphorylation reverses this binding.

#### Electrostatic Sequestration of PIP<sub>2</sub>

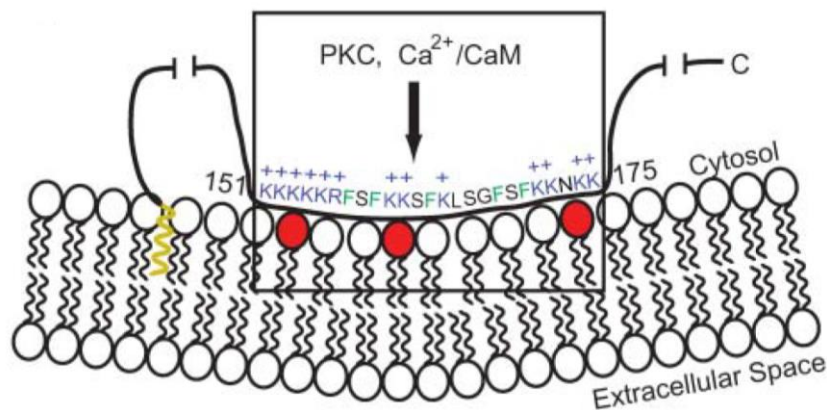


Figure 33. Cartoon of the “natively unfolded” MARCKS protein, shown as a black line, interacting with the inner leaflet of the plasma membrane. The N-terminal myristate, shown in yellow, inserts hydrophobically into the bilayer. The MARCKS effector domain (residues 151–175 of bovine MARCKS, shown in the box) interacts electrostatically with acidic lipids (3 PIP<sub>2</sub> shown in red) through its 13 basic residues (in blue with 1 signs) and hydrophobically through its five aromatic residues (in green).

Another example of PIP<sub>2</sub> lateral segregation is the one induced by interaction with the HIV-1 matrix domain (MA). This domain anchors to the intracellular leaflet of the plasma membrane. Coarse-grained simulations of the HIV-1 myristoylated MA protein interaction with the membrane revealed that PIP<sub>2</sub> head group binds with a highly basic region (HBR) of the domain *via* interactions with arginine and lysine residues (Figure 34).

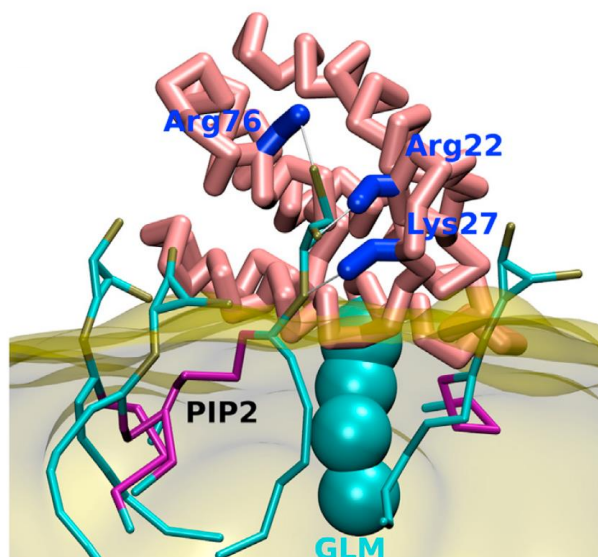


Figure 34. PI(4,5)P<sub>2</sub> head was binding with the myristoylated MA domain. Representative snapshots from an anchoring experiment of the Myr-MA protein to a membrane model; Myr residue at the N-terminus of HIV-1 MA was reported in blue spheres, whereas the membrane was reported in yellow surface. Water molecules were removed from the figure for more clarity.<sup>166</sup>



This work suggests that, after insertion of the myristoylated moiety and stabilization of the MA protein orientation, specific interaction between the PIP<sub>2</sub> polar head and the HBR motif leads to lateral segregation of PIP<sub>2</sub> in the membrane. It is advanced that the orientation of the protein favors the HBR motif positioning to interact preferably with PIP<sub>2</sub> than with PS, the main negatively charged phospholipid of the plasma membrane.

The propension of PIP<sub>2</sub> to form clusters in the plasma membrane has been evidenced through binding with specific proteins. These proteins usually contain clusters of basic residues that serve as binding site to interact electrostatically with acidic lipids of the plasma membrane, and in particular with PIP<sub>2</sub> polar head groups, recruiting several PIP<sub>2</sub> to form clusters. Cationic peptides have been found to induce this effect as well in model membranes.<sup>163</sup> Experiments using model membranes and analysis by fluorescence spectroscopy suggest that basic peptides are able to sequester multivalent PIP<sub>2</sub> but not monovalent PS, supposing that the density of charge of the PIP<sub>2</sub> polar heads is a key factor for such interactions and PIP<sub>2</sub> clustering. Using several basic peptide sequences, including MARCKS (151–175), they revealed that basic peptides interact with monovalent PS membranes through electrostatic interactions, without lateral redistribution of the lipids. Moreover, incorporating PIP<sub>2</sub> into the liposomes slow the diffusion of the membrane-bound peptides. The sequestered PIP<sub>2</sub> would produce an “electrostatic well” at the binding site, that would require significant energy for the peptide to desorb and diffuse freely in the membrane.

Altogether, these results strongly suggest that CPPs, as cationic AA sequences, could be able to recruit PIP<sub>2</sub> through electrostatic interactions and induce PIP<sub>2</sub> clustering. This effect could represent the first recognition step of the peptide, before it could be internalized. As the majority of PIP<sub>2</sub> is present at the cytosolic leaflet of the membrane, PIP<sub>2</sub> clustering could also step in at the end of the translocation, acting as a “magnet” by pulling the peptide towards the internal leaflet through electrostatic interactions. These two hypotheses are not contradictory and could contribute to the CPP internalization mechanism at different steps of the translocation.

### 3.2. CPPs can remodel the actin cytoskeleton

Possible role of PIP<sub>2</sub> in the internalization of CPPs can also be considered from a cellular function point of view by looking at the effect of cationic CPPs on the actin cytoskeleton. Indeed, recent studies strongly suggest that the actin cytoskeleton dynamics are implicated in the CPPs internalization.<sup>167,168</sup> In addition, several CPPs have been reported to have a remodeling effect on the actin network.

NIH-3T3/EWS-Fli cells transformed to tumoral cells exhibit important actin disorganization. Arginine- and/or tryptophan-rich CPP sequences, including (R/W)<sub>9</sub>, induce strong remodeling of the cytoskeleton structure of malignant fibroblasts, while they have no effect on non-tumoral fibroblasts.<sup>1</sup> This is also the reason why CPPs are usually considered as biologically inert molecules, as they do not have this effect on healthy cells. Different CPP sequences also induce different polymorphism effects, as shown in Figure 35. CPPs were reported to reverse the tumoral phenotype of EF cells to the non-tumoral phenotype of 3T3 cells, with the appearance of actin stress fibers after incubation with the CPP.

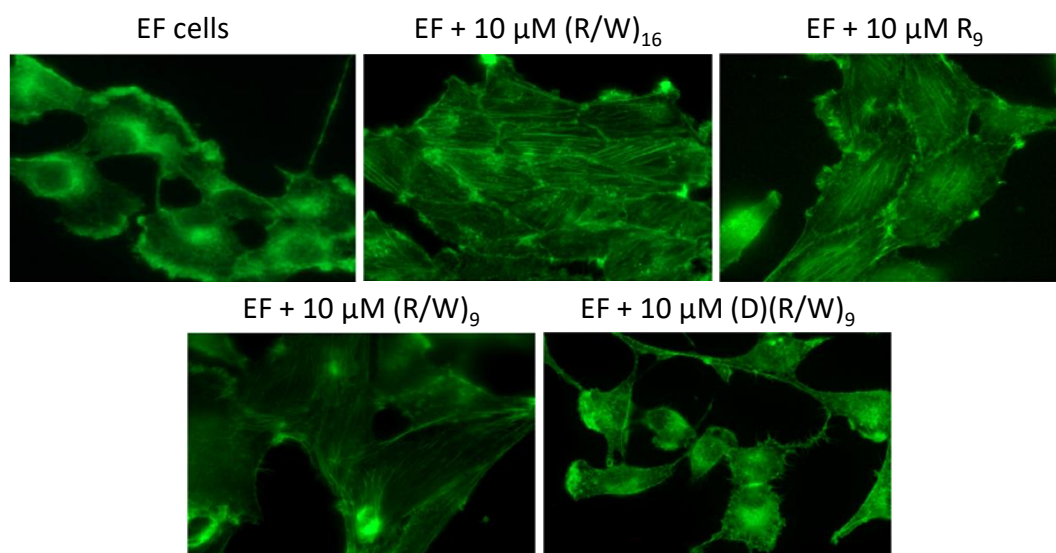


Figure 35. Actin organization in EWS-FLI1 expressing cells (EF cells). Fluorescence microscopy observation of actin (green) labeled with phalloidin-fluorescein isothiocyanate. EF cells were incubated for 18–24 h with 10  $\mu\text{M}$  (R/W)<sub>16</sub>, (R/W)<sub>9</sub>, R<sub>9</sub>, and (D)(R/W)<sub>9</sub>. Adapted from <sup>1</sup>.

As a consequence of this structural modification on the cells, it was revealed that CPPs reduces tumoral cells motility. This fact is particularly interesting for therapeutic purposes. Moreover, from a mechanistic point of view, this work shows that CPPs have protein partners inside the cell, such as actin, whose direct binding to the CPPs has been evidenced *in vitro* by NMR and by calorimetry experiments, using actin monomers.

The actin remodeling effect of (R/W)<sub>9</sub> has been further studied few years later by a proteomic approach.<sup>169</sup> First, they confirm the strong phenotype change of EF cells induced by the CPP using immunofluorescence experiments. Besides, their proteomic study showed that the remodeling effect of the CPP is not necessarily caused by important modifications of the EF cell proteins expression levels. They also point out the difficulties to link a phenotype change and proteome.

### 3.3. PIP<sub>2</sub> implication in the internalization mechanism of Engrailed

PIP<sub>2</sub> implication in unconventional secretion mechanisms has been evidenced by binding to basic section of proteins, such as for FGF2<sup>165</sup> or the HIV-1 Tat protein.<sup>170</sup> Recently, PIP<sub>2</sub> has been reported to be implied in the same kind of unconventional secretion pathway for the Engrailed protein (En-2).<sup>171</sup> Moreover, the same work showed, by using neomycin, that PIP<sub>2</sub> would also contribute to the Engrailed internalization mechanism, showing that the two pathways are not so different. Neomycin is an aminoglycoside antibiotic, positively charged, known to enter into cells and to bind specifically to PI(4,5)P<sub>2</sub>.<sup>172,173</sup> Co-incubation of neomycin during the internalization experiment decreased the internalization efficiency of En-2 (Figure 36). This work suggests a similarity in the secretion and internalization pathways, with contributions of interaction partners at both sides of the membrane.

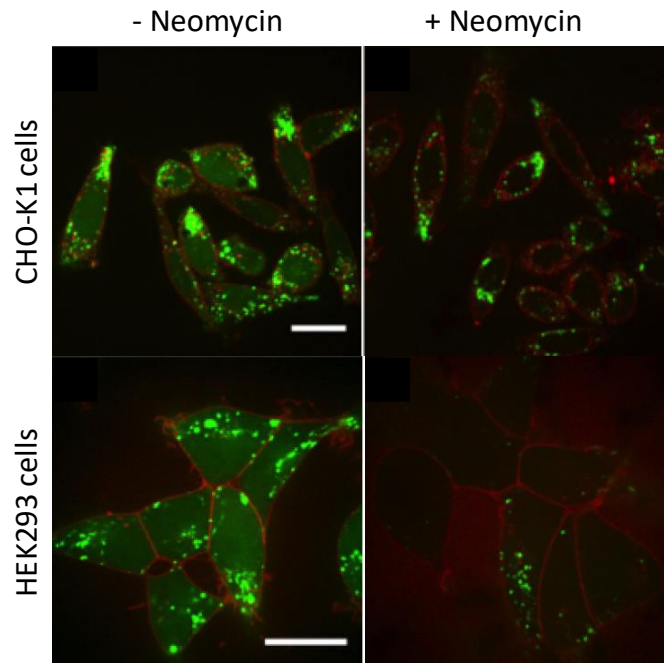


Figure 36. Influence of neomycin on the internalization of En-2. Observation, after addition of Trypan Blue in the cell medium, of the internalization of En-2 in CHO-K1 or HEK293 cells after 1 hour of incubation at 37°C, in presence or not of neomycin at 10 mM. Scale bars are 20 mm. Adapted from <sup>171</sup>.

### 3.4. PIP<sub>2</sub> could play a role in Penetratin internalization

Direct and clear evidence of a contribution of PIP<sub>2</sub> in the internalization of Penetratin has not yet been reported. However, recent work on cells suggest that it could take part in this mechanism.

Effect of preincubation of CHO-K1 cells with neomycin on the internalization efficiency of a Penetratin analogue (*i.e.* functionalized with a benzophenone photoprobe) was evaluated using a quantification method by MS.<sup>4</sup> In wild-type cells, the internalization rate was decreased in neomycin-treated cells after 15 min and 30 min of incubation with the peptide at 37°C, but the internalization efficiency was recovered after 1 hour of incubation. In GAG-deficient cells (pgsA-745), cells pre-treated with neomycin showed a constant and lower peptide uptake.

Pre-treatment with neomycin had an effect on the internalization kinetics of Penetratin at 37°C, which means it affected the endocytic pathway. These results indicate that PIP<sub>2</sub> would have a contribution in the internalization mechanism of Penetratin. Recovery after 1 hour incubation of an internalization rate close to the one of the non-treated cells could lead to several interpretations. Either the peptide has finally entered in the cell by following a route that do not imply interaction with PIP<sub>2</sub>, or, more likely, the binding affinity of neomycin for PIP<sub>2</sub> is lower than or close to the one of the Penetratin for PIP<sub>2</sub> and so these interactions are in competition. In the same way, neomycin could compete at PIP<sub>2</sub> binding sites with anchored proteins linking the membrane to the actin cytoskeleton, which would inhibit the endocytosis pathway.

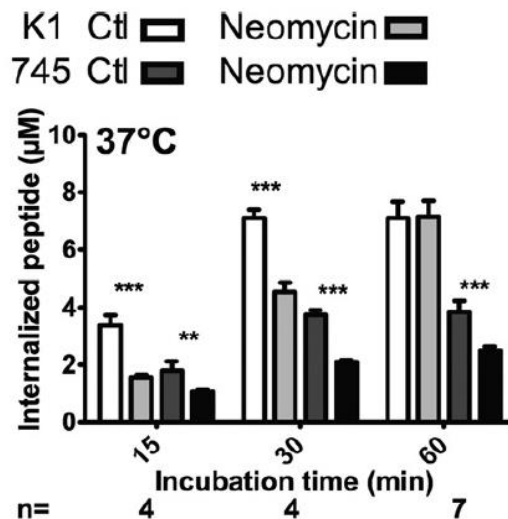


Figure 37. Effect of neomycin on peptide internalization. CHO-K1 or CHO-pgsA-745 cells were pretreated with 10 mM neomycin for 30 min, washed, and additionally incubated at 37 °C with 5 µM extracellular peptide Penetratin analogue for the indicated incubation times. *Error bars* are standard deviation obtained from n independent experiments. Figure and legend adapted from <sup>4</sup>.

To summarize, PIP<sub>2</sub> is a regulator of the actin polymerization and has been localized in the same membrane regions, probably in sphingolipid- and cholesterol-rich nanodomains, where actin is required for membrane trafficking and cell motility functions as discussed earlier. In addition, it is highly probable that Penetratin can recruit and form PIP<sub>2</sub> clusters, like other cationic peptides do. And finally, some CPPs interact with the actin cytoskeleton, whose dynamics seems to be implicated in the internalization mechanism. All these facts seem to converge to highlight the probable role of PIP<sub>2</sub> as a binding partner of Penetratin and as a potential effector of its internalization.

## Results and discussion

In the literature, several links can be made between Penetratin and PIP<sub>2</sub>. First, basic peptides promote PIP<sub>2</sub> clustering through electrostatic interactions, which is not the case when considering the monovalent phospholipid PS. Secondly, some CPPs are able to remodel the actin cytoskeleton, whose polymerization is regulated by PIP<sub>2</sub>.<sup>1,2</sup> In addition, Penetratin and more generally cationic CPPs interact strongly with negatively charged lipids.<sup>3</sup> Finally, some internalization experiments on cells showed that PIP<sub>2</sub> could play a role in Penetratin internalization.<sup>4</sup>

This Ph.D. project aims to analyze the role of the negatively charged lipid PIP<sub>2</sub> as a binding partner of the CPP Penetratin and as a potential effector of Penetratin internalization. Several methods have been employed to assess these questions.

First, the effect of PIP<sub>2</sub> on the internalization efficiency of Penetratin was quantified in cells, using the PH-PLC<sup>δ</sup> domain to block the PIP<sub>2</sub> polar heads. Secondly, Penetratin influence on the thermotropic phase behavior of PIP<sub>2</sub>- or PS-containing liposomes was evaluated using DSC measurements. Moreover, the binding affinity of Penetratin for PIP<sub>2</sub>- or PS-containing liposomes was estimated by fluorescence spectroscopy. Finally, a method coupling benzophenone-induced photo-cross-linking and MS analysis was exploited to identify lipid interaction partners of Penetratin in liposomes composed of PC, PS and PIP<sub>2</sub>. Results and discussion of this work are presented in this section.

## 1. Influence of the PIP<sub>2</sub> polar head blockage on the Penetratin internalization in cells

The contributions of PIP<sub>2</sub> in the internalization pathway of Penetratin was estimated in cells, by blocking the PIP<sub>2</sub> polar heads with the PH domain of PLC<sup>δ</sup> that has a high binding affinity for PIP<sub>2</sub>. Quantification of the internalized peptide was achieved by a MS method.

### 1.1. Internalization quantification by mass spectrometry

MALDI-TOF MS is used to quantify internalized peptides and to study the internalization pathway of Penetratin.<sup>174,175</sup> Complete protocol is depicted in Figure 38.

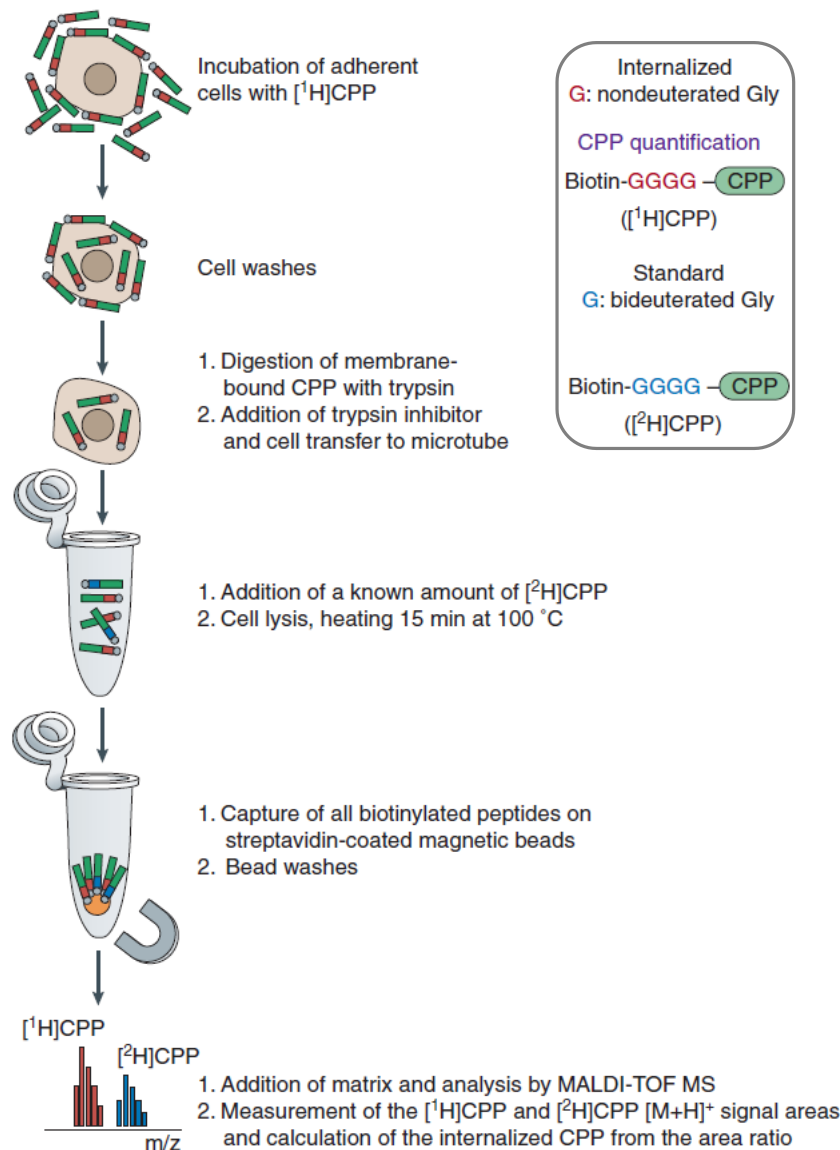


Figure 38. Steps of the CPP cellular uptake quantification protocol by MALDI-TOF MS.<sup>174</sup>

This method has already been used to study the internalization pathway of various CPPs.<sup>176</sup> It can be applied to CPPs of diverse sequences and also to CPPs linked to cargo molecules. Also, the method allows to distinguish the internalized peptide from the membrane-bound peptide. The method relies on the quantification of the internalized (<sup>1</sup>H) CPP by using a known amount

of the corresponding ( $^2\text{H}$ ) deuterated peptide as an internal standard. The isotopically-labeled peptide is synthesized by incorporating deuterated glycine residues at the N-term of the peptide sequence. MS is rarely used as a quantification technique as the signal intensity strongly depends on ionization efficiency of the molecules as well as on ions transmission and detection yields. Nevertheless, using a deuterated version of the peptide allows to obtain two molecules that are chemically equivalent and only differ by their mass. Thus, they are supposed to be ionized in the same way and to be transmitted and detected similarly. The two species will be separated on the mass spectra by the mass difference due to the number of incorporated deuterium in the deuterated sequence. The ratio of the areas of the two peptides signals is proportional to the ratio of their quantities and measuring the peptides signals areas allows to calculate the amount of internalized CPP.

## 1.2. Contribution of $\text{PIP}_2$ in the internalization efficiency of Penetratin

PH-PLC $^{\delta}$  binds to  $\text{PIP}_2$  with high affinity ( $K_d = 2 \mu\text{M}$  measured *in vitro*,<sup>73</sup> see Introduction, paragraph 1.3.). Transfecting cells with a plasmid GFP-PH, coding for this domain, allows intracellular blocking of  $\text{PIP}_2$  polar heads and to follow the transfection efficiency by fluorescence spectroscopy. Figure 39 shows a microscope image of CHO-K1 cells transfected with the GFP-PH plasmid. The PH domain is localized at the cell membrane. Flow cytometry was used to evaluate the transfection efficacy and showed a high yield of transfected cells, up to 70-80% of cells were transfected. Internalization results were corrected by the percentage of transfected cells.

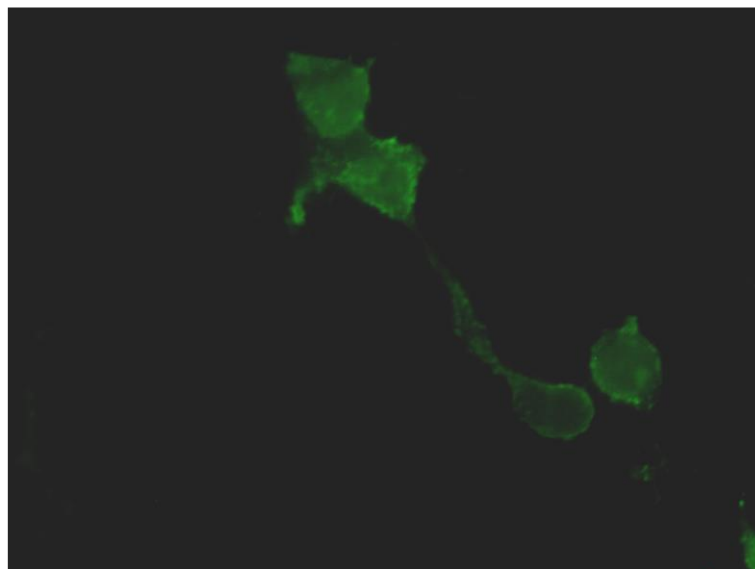


Figure 39. Microscope image of CHO-K1 cells transfected with a GFP-PH plasmid.

Internalization experiments were conducted on these transfected cells and show that the transfection clearly makes the internalization efficiency of Penetratin decrease (Figure 40).

Unlike the experiments using neomycin presented in introduction (paragraph 3.4.), internalization of Penetratin in transfected cells is always significantly lower than the control, even after 1 hour of incubation. It strongly suggests that results obtained in the study using neomycin reflected a competition between neomycin and Penetratin. The binding affinity of

the PH domain for PIP<sub>2</sub> is higher than the one of neomycin, thus the blocking of PIP<sub>2</sub> polar head groups is more efficient.

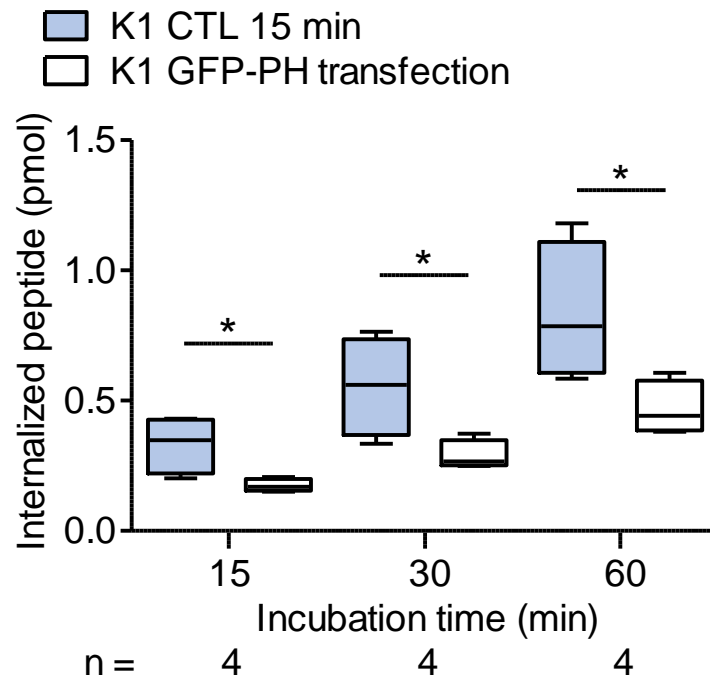


Figure 40. Intra-cellular PIP<sub>2</sub> contributions on Penetratin internalization at 37°C for various incubation times. CHO-K1 cells were pre-transfected with a GFP-PH plasmid for 24h before incubation with Penetratin. Error bars correspond to standard deviation obtained for n independent experiments.

Besides, as the PH domain is not able to cross the cell membrane, only the PIP<sub>2</sub> present at the cytosolic leaflet of the membrane is blocked in this experiment. Thus, these results show that the intra-cellular PIP<sub>2</sub> would contribute to the internalization pathway of Penetratin. This correlates with the hypothesis formulated in introduction, proposing that pools of PIP<sub>2</sub> at the internal leaflet of the membrane could attract the peptide to the cytosolic leaflet, thus playing a role as a step at the end of a direct translocation process.



## 2. Effect of Penetratin on the thermotropic phase behavior of PIP<sub>2</sub>-containing liposomes

As we established a role of PIP<sub>2</sub> for Penetratin translocation, we then characterized the molecular interactions of the two molecules more in depth.

Peptide/lipid interaction understanding using a biophysical approach is useful for deciphering the mechanism of action of membranotropic peptides. In particular, DSC is a method of choice to evaluate CPPs effect on the lipid phase transitions. The effect of CPPs on the thermotropic phase behavior of lipid membranes gives access to information on the way CPPs interact with model membranes.

### 2.1. Differential Scanning Calorimetry (DSC)

DSC is a thermal analytic method. It is based on the thermal heat difference between a reference cell and a measuring cell. The measuring cell contains the sample to analyze and the reference cell contains a component that is inert on the temperature range studied (water or buffer). The two cells are placed in a calorimeter subjected to a linear temperature gradient and thermal exchanges induced in the cells are measured. This method allows studying various systems such as synthetic polymers, liposomes, glass, etc. In particular, it gives access to phase transitions temperatures and thermodynamic parameters associated to them.

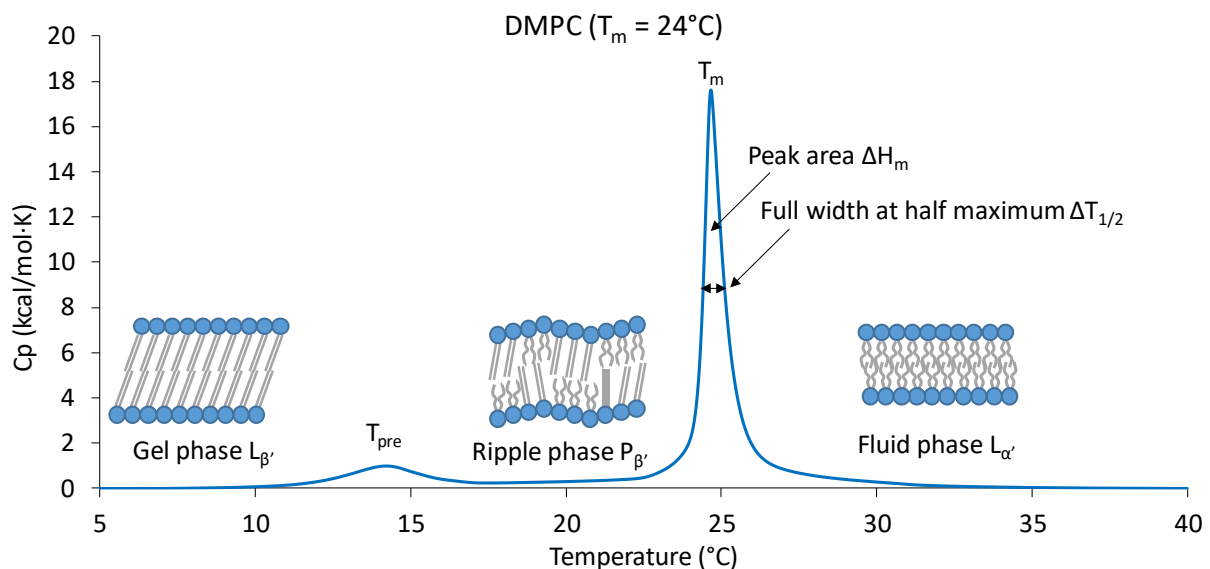


Figure 41. Thermogram of the lamellar phase transitions of DMPC MLVs showing the three typical lipid phases (gel phase L<sub>β</sub>, rippled phase P<sub>β</sub>, and fluid phase L<sub>α</sub>) and the corresponding temperature transitions (T<sub>pre</sub> and T<sub>m</sub>). Peak areas give access to the transition enthalpies.

Phospholipids organized in lamellar phase usually show two phase transitions (as introduced in paragraph 1.1.1.). The pre-transition corresponds to the transition between the gel phase and the ripple phase, while the main transition reflects the transition between the ripple phase and the fluid phase. Such physical transformations are observed by measuring the amount of heat absorbed or liberated during the transitions. The instrument controls the temperature difference and heats the sample cell more or less, depending on the endo- or exothermic effect,

so as to maintain its temperature equal to the one of the reference cell. The heat difference is converted in specific heat capacity ( $C_p$ ) and is usually presented in calories or Joules per mol per degrees Celsius or Kelvin, as a function of the temperature gradient. Peak areas give access to the corresponding transition enthalpies. An example of DSC thermogram is given in Figure 41, using MLVs of DMPC. Applying this method to lipid bilayers enables to study the interactions between a bilayer and an external element such as a CPP, for instance.

Presence of a membranotropic peptide can modify the DSC parameters. Indeed, if a CPP interacts with the lipid membrane, it can have an impact on the lipid phase transitions as it can affect lipids properties like lipids packing, membrane organization and fluidity. In general, the pre-transition is very sensitive to interactions of molecules with the lipid polar head groups as it is linked to the transition toward the ripple phase.<sup>177</sup> Thus, a perturbation of the pre-transition indicates an interaction of the peptide with the lipid polar head groups. A modification of the main transition temperature and/or enthalpy implies a stronger interaction with the membrane and is an indicator of the peptide impact on the lipid bilayer fluidity, and possibly of the peptide insertion below the polar heads level, between the lipid acyl chains.

If liposomes are composed of a mixture of lipids or if a membranotropic peptide is added, the transition signals can be affected. They can be broadened or a peak splitting can be observed. Separation of a transition signal into two peaks is assigned to a heterogeneous organization in the membrane that reflects domain formation. It can either be lipid-rich/lipid-poor domains or peptide-rich/peptide-poor domains. Deconvolution of the DSC signal can be useful in those cases to identify the thermodynamic parameters of the different domains.

Lipids miscibility is thus an important aspect when working with DSC experiments. Lipid mixtures are considered miscible when the transition temperatures  $T_m$  of the lipids are close. Their analysis in DSC results in a single phase transition peak, that is broad due to the heterogeneity of the membrane. When mixing lipids that present different  $T_m$ , the transition peaks of each lipid are well separated. In our study, we chose to focus on liposome compositions of miscible lipids, to observe the effect of the addition of the CPP Penetratin on the phase transitions of liposomes.

## 2.2. DSC data interpretation for studying CPP-lipid interaction

Membranotropic effects of peptides using DSC can give access to many interesting aspects on their mode of interaction. Careful interpretation of DSC thermogram is important to retrieve all relevant information one can obtain from these type of data. This section will be dedicated to the interpretation of thermotropic behaviors observed in DSC and what information can be extracted from each of the DSC parameters.

### 2.2.1. Pre-transition temperature $T_{pre}$

The pre-transition is not always visible on DSC thermograms. Most of the time it is only visible in pure lipid liposomes and tends to disappear when using model membranes composed of a mixture of lipids. A modification of the pre-transition temperature upon addition of a membranotropic peptide usually indicates an interaction of the peptide with the lipid polar head groups. Moreover, in liposomes composed of a lipid mixture, reappearance of the pre-

transition peak upon addition of a peptide can be an indicator of a lipid partitioning in the membrane.

### 2.2.2. Main transition temperature $T_m$

Transition at a higher temperature to the fluid phase comes with lipid disordering, a decrease in bilayer thickness and lateral expansion of lipids as they are less packed. The main transition occurs faster and is associated to a larger enthalpy difference compared to the pre-transition. Modification of the main transition temperature upon addition of the CPP indicates that the peptide has an impact on the lipid bilayer fluidity. If the  $T_m$  is increased, the peptide has a rigidifying effect and favors the gel phase. If the  $T_m$  is decreased, it means the peptide favors the transition and thus has a fluidifying effect on the lipid membrane.

### 2.2.3. Main transition enthalpy $\Delta H_m$

The enthalpy of main transition can be extracted from the area under the main transition peak. It is directly correlated with the van der Waals forces of interaction between the lipid hydrophobic tails. A decrease in the area of the main transition peak means that the peptide makes the van der Waals interactions decrease by perturbing the lipid acyl chains packing. It is an indicator of the peptide insertion in the lipid membrane, where it is intercalated between the lipid hydrophobic chains.<sup>178</sup>

### 2.2.4. Full width at half maximum (FWHM) or $\Delta T_{1/2}$

The full width at half maximum (FWHM) of the transition peak represents the cooperativity of the transition related with the number of molecules that undergo a transition simultaneously. Thus, sharpness of the transition peak is correlated with the lipid system purity. For example, a DSC thermogram of a single-lipid composition liposomes presents a sharp and symmetric transition peak, where FWHM values can be less than 0.1°C. If a lipid mixture is considered, transition peaks are usually asymmetric and broader, up to 10-15°C for complex lipid mixtures such as the ones found in biological membranes.<sup>179</sup> Besides, an increase of this parameter by addition of a CPP to a liposome suspension should indicate that the peptide inserts between the fatty acid chains of the lipids,<sup>178</sup> and induces heterogeneity in the membrane.

### 2.2.5. Shape of the transition peak

The shape of the transition peak, just like the FWHM, is related to the homogeneity of the system. Heterogeneity can be indicated by appearance of a shoulder or de-doubling of the transition peak or even appearance of new transition peaks. It can reflect heterogeneity of the peptide or of the lipid. For example, two phase transition peaks can correspond to peptide-poor or peptide-rich domains if the peptide is not homogeneously distributed in the lipid membrane. Otherwise, peak splitting or appearance of new transition peaks can reflect lipids partitioning in the membrane, forming domains of heterogeneous composition, for instance upon interaction with a membranotropic peptide.

### 2.3. Penetratin effect on thermotropic phase behavior of PIP<sub>2</sub>-containing lipid vesicles

DSC experiments were conducted using MLVs containing PC, PS and PIP<sub>2</sub> phospholipids. The polar head of the PS carries one negative charge, while the polar head of the PIP<sub>2</sub> can have 3, 4 or 5 negative charges at physiological pH, the pKa of the phosphate groups being close to 7 (see Introduction). For simplicity, an average number of 4 negative charges can be considered for PIP<sub>2</sub>. Here, the negatively charged proportions in the liposomes containing PS or PIP<sub>2</sub> is chosen so that the overall charge is the same. This way, comparison between PS- and PIP<sub>2</sub>-containing liposomes can be done for a same global charge of the model membranes. Liposomes composed of twice the percentage of PIP<sub>2</sub> were also used to observe a bigger effect. A control experiment was achieved with a zwitterionic lipid composition using liposomes of DMPC 100%.

The influence of Penetratin on the lipids phase transitions was measured on liposomes of the following compositions: DMPC 100%, DMPC/PS (80/20), DMPC/PIP<sub>2</sub> (95/5) and DMPC/PIP<sub>2</sub> (90/10). Brain PIP<sub>2</sub> and brain PS are used for these experiments. These results are presented in Figure 42. DSC thermodynamic parameters are reported in Table 6.

Comparison of the pure lipid liposomes thermograms shows that addition of PIP<sub>2</sub> or PS to DMPC liposomes decreases the main transition temperature. This is logical as brain PS and brain PIP<sub>2</sub> are composed of a heterogeneous composition in fatty acid chains, with a high level of unsaturated chains. As mentioned in introduction, presence of unsaturation on the fatty acid chains fluidifies the membrane and thus makes the transition temperature decrease.

In the case of DSC thermograms acquired in presence of MLVs of 100% DMPC, we do not observe a significant modification neither of the pre-transition temperature, nor of the main transition temperature and transitions enthalpies upon addition of Penetratin to the system. This indicates that Penetratin does not interact with lipids polar head groups and its presence does not impact the lipid bilayer fluidity and the fatty acid chains interactions.

The absence of pre-transition on DMPC/PS (80/20) thermograms is typical of liposomes with a heterogeneous lipid composition. The main transition peak is also wide, which is in accordance with the cooperativity of a lipid mixture. The addition of Penetratin to this system does not significantly affect the thermogram. In addition, the main transition temperature is not modified. If Penetratin partially interacts with the polar heads of the lipids of this composition, we cannot see it due to the dilution of the pre-transition signal. Still, the increase of the FWHM parameter suggests that the cooperativity of the main transition signal is decreased upon addition of Penetratin to the system, indicating an increase of the membrane heterogeneity. However, the non-modification of the main transition temperature allows us to conclude that Penetratin has no influence on the membrane fluidity of these liposomes. Moreover, the main transition enthalpy is not affected by the presence of the peptide, suggesting that the peptide does not insert in the membrane. Therefore, if Penetratin interacts with the polar heads of negatively PS-charged lipids, which is likely as it is a negatively charged phospholipid, this interaction would be weak and would not induce reorganization in the membrane.

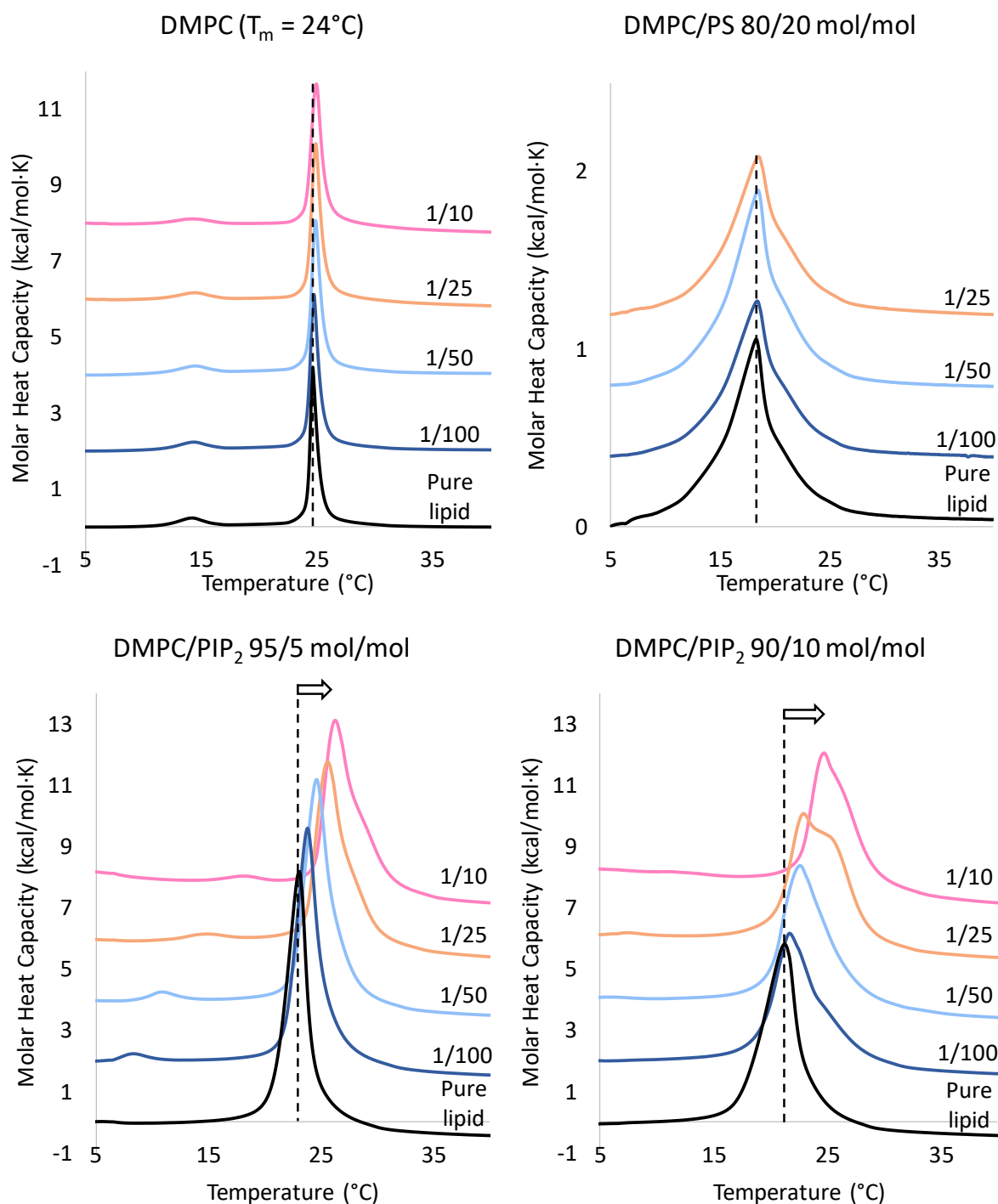


Figure 42. DSC thermograms illustrating the influence of Penetratin (Biot(O<sub>2</sub>)-Apa-pen) addition to MLVs of DMPC, DMPC/Brain PS 20% (mol/mol), DMPC/Brain PIP<sub>2</sub> 5% (mol/mol) and DMPC/Brain PIP<sub>2</sub> 10% (mol/mol), at 1 mg/mL, for ratios peptide/lipid from 0 to 1/10. Curves, from bottom to top, correspond to the MLVs solution alone (Pure lipid), and then to ratios peptide/lipid of 1/100, 1/50, 1/25 and 1/10.

Table 6. Thermodynamic parameters corresponding to DSC thermograms of phase behavior of DMPC, DMPC/Brain PS 20% % (mol/mol), DMPC/Brain PIP<sub>2</sub> 5% (mol/mol) and DMPC/ Brain PIP<sub>2</sub> 10% (mol/mol) in presence of Penetratin, for ratios peptide/lipid of 1/100, 1/50 and 1/25.

Pen/DMPC (n=1)	T <sub>pre</sub> (°C)	T <sub>m</sub> (°C)	ΔH <sub>m</sub> (kJ/mol)	FWHM (°C)
0	14.2	24.6	16.6	0.7
1/100	14.3	24.8	18.6	0.8
1/50	14.5	24.9	19.4	0.9
1/25	14.5	24.9	20.1	0.9
1/10	14.3	25.0	21.0	1.0
Pen/DMPC:PS 20% mol (n=1)	T <sub>pre</sub> (°C)	T <sub>m</sub> (°C)	ΔH <sub>m</sub> (kJ/mol)	FWHM (°C)
0	-	18.4	18.4	3.9
1/100	-	18.4	17.8	3.2
1/50	-	18.5	21.9	4.3
1/25	-	18.6	17.8	4.9
Pen/DMPC: PIP <sub>2</sub> 5% mol (n=2)	T <sub>pre</sub> (°C)	T <sub>m</sub> (°C)	ΔH <sub>m</sub> (kJ/mol)	FWHM (°C)
0	-	23.1 ± 0.1	20.4 ± 0.1	2.0 ± 0.0
1/100	8.4 ± 0.2	23.8 ± 0.1	19.7 ± 0.3	1.9 ± 0.3
1/50	10.5 ± 0.5	24.4 ± 0.2	20.4 ± 0.3	2.3 ± 0.2
1/25	13.2 ± 2.2	25.2 ± 0.6	18.9 ± 0.3	2.4 ± 0.5
1/10	15.4 ± 3.6	25.6 ± 1.0	18.3 ± 0.1	2.3 ± 0.5
Pen/DMPC: PIP <sub>2</sub> 10% mol (n=2)	T <sub>pre</sub> (°C)	T <sub>m</sub> (°C)	ΔH <sub>m</sub> (kJ/mol)	FWHM (°C)
0	-	21.4 ± 0.2	21.2 ± 2.6	3.1 ± 0.3
1/100	-	22.0 ± 0.5	18.7 ± 1.6	3.3 ± 0.8
1/50	6.4 ± 1.2	22.9 ± 0.5	17.8 ± 1.0	3.5 ± 0.9
1/25	8.2 ± 1.1	23.4 ± 0.7	19.8 ± 3.8	4.4 ± 1.2
1/10	11.4 ± 0.0	24.8 ± 0.1	15.9 ± 1.1	3.1 ± 0.8

Concerning the results obtained with MLVs containing PIP<sub>2</sub> at 5% and 10%, we can observe significant changes in the corresponding thermograms, influenced by the presence of Penetratin. Indeed, the addition of Penetratin to PIP<sub>2</sub>-containing MLVs causes modifications of the pre-transition and main transition, with a more pronounced effect on MLVs containing 10% PIP<sub>2</sub> and at high peptide/lipid ratios.

First, the absence of pre-transition typical of lipid mixtures is observed on scans acquired on MLVs alone. However, unlike PS-containing MLVs, the addition of Penetratin in the presence of PIP<sub>2</sub>-containing MLVs induces a reappearance of the pre-transition peak. An effect on the pre-transition indicates an interaction with the polar heads of lipids. In addition, the reappearance of the pre-transition peak on a lipid mixture suggests segregation at the membrane level, forming a heterogeneous organization with domains more or less enriched in certain lipids. The pre-transition signal is recovered already at a peptide/lipid ratio of 1/100 in the case of 5% PIP<sub>2</sub> MLVs, while it is recovered only for a 1/50 peptide/lipid ratio in liposomes of 10% PIP<sub>2</sub>. This

suggests that the pre-transition peak appears only when there are enough Penetratin molecules to recruit a significant fraction of PIP<sub>2</sub> and form clusters in the membrane.

After recovery of the pre-transition signal, addition of Penetratin at higher peptide/lipid ratios continues to impact the transition between the gel phase and the ripple phase. The pre-transition temperature increases upon addition of the peptide, showing that the peptide interacts with the lipid polar heads.

Furthermore, the modification of the main transition temperature to higher temperatures implies a significant modification of the Penetratin on the organization of the bilayer. The increase in this temperature after addition of the peptide shows that Penetratin promotes the gel phase and has a stiffening effect on these MLVs.

Regarding the MLVs of 5% PIP<sub>2</sub>, the slight decrease in enthalpy indicates that the peptide is inserted into the bilayer and disrupts the van der Waals interactions between the hydrophobic chains of phospholipids. This effect on enthalpy is not drastic, and is in agreement with the fact that Penetratin does not insert deeply into the model membranes.<sup>180</sup> This effect on the enthalpy is more pronounced on MLVs composed of 10% PIP<sub>2</sub>, where the main transition enthalpy decreases from 21.2 kJ/mol in the pure lipid system to 15.9 kJ/mol for a peptide/lipid ratio of 1/10.

In addition, thermograms obtained with 10% PIP<sub>2</sub> for a peptide/lipid ratio of 1/25 clearly show a separation of the main transition peak, confirming the appearance of lateral separation of the different lipids in the membrane. At this particular peptide/lipid ratio also, the FWHM is larger and the transition enthalpy (*i.e.* area under the peak) is increased. These effects are commonly observed when a membrane partitioning occurs. Deconvolution of the main transition signal, given in Figure 43, allowed to model the contributions corresponding to the two domains formed in the membrane.

The main transition signals of the DSC thermograms illustrating the Penetratin interaction with PIP<sub>2</sub>-containing liposomes at 10% were modeled thanks to the Nano Analyze software. The models fit well with the experimental curves.

Deconvolution of the main transition peak in liposomes composed of pure lipids gives two contributions with close maximum temperatures. An important contribution at 21°C is noticed, while the second contribution, at 20°C is rather low and the signal is spread over a large range of temperature. As the pure lipid is considered here, modeled contributions represent the cooperativity of the PC and PIP<sub>2</sub> lipids to the phase transition. However, none of these contribution fits with the DMPC values of enthalpy and T<sub>m</sub> that were obtained previously by DSC measurement, meaning that no DMPC-rich domain is observed and the membrane is quite homogeneous. The experimental peak is still narrow and no peak shoulder is observed, reflecting a good miscibility of the lipids.

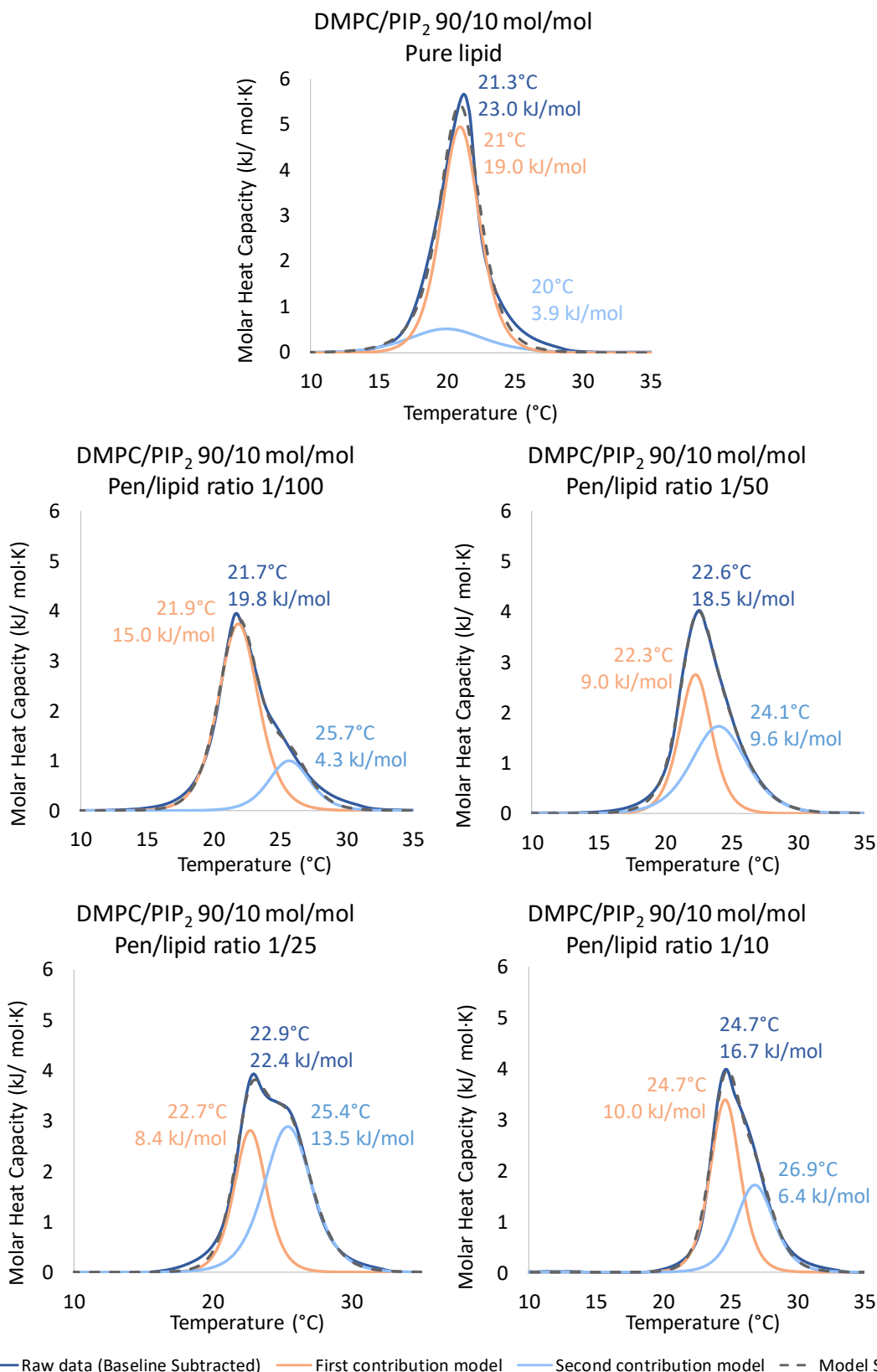


Figure 43. Deconvolution of the main transition signal of DSC thermograms obtain after Penetratin (Biot(O<sub>2</sub>)-Apa-pen) addition to MLVs of DMPC/Brain PIP<sub>2</sub> 10% (mol/mol), at 1 mg/mL, for ratios peptide/lipid from 0 to 1/10. Experimental data (corrected baseline) are in dark blue. The fitted model is shown as a dashed grey curve. Modeled contributions are in orange and light blue curves. The corresponding T<sub>m</sub> and ΔH<sub>m</sub> are also indicated on the graphs.



When adding Penetratin to these liposomes, contributions modeling indicate a clear partitioning in the samples, and this for all peptide/lipid ratios considered. The effect is enhanced upon addition of increasing ratios of peptide/lipid, until the most important effect observed at peptide/lipid ratio of 1/25. Then, at 1/10 peptide/lipid, partitioning seems to be less important. This suggests that the most important segregation in the membrane is obtained for peptide/lipid ratio of 1/25. It could be that the Penetratin binds to PIP<sub>2</sub> polar heads and recruits several PIP<sub>2</sub>, thus inducing partitioning in the membrane by forming PIP<sub>2</sub>-enriched domains. Penetratin addition amplifies the phenomenon by forming bigger clusters of PIP<sub>2</sub>, until every polar head groups of PIP<sub>2</sub> present in the membrane are occupied. Then, addition of Penetratin to the system might tend to break these big clusters in smaller ones, to favor the Penetratin binding to PIP<sub>2</sub>. Consequently, at higher percentage of Penetratin, PIP<sub>2</sub> clusters might be smaller and thus PIP<sub>2</sub> would be more dispersed in the membrane, which would result in a more homogeneous repartition of PIP<sub>2</sub> in the membrane (illustrated in Figure 44). Another hypothesis could be that adding excessive amounts of Penetratin (1/10 pen/lipid) forces the interaction with the PC lipids. In general, the ratio 1/10 membranotropic peptide over lipids is too high to observe a realistic effect.

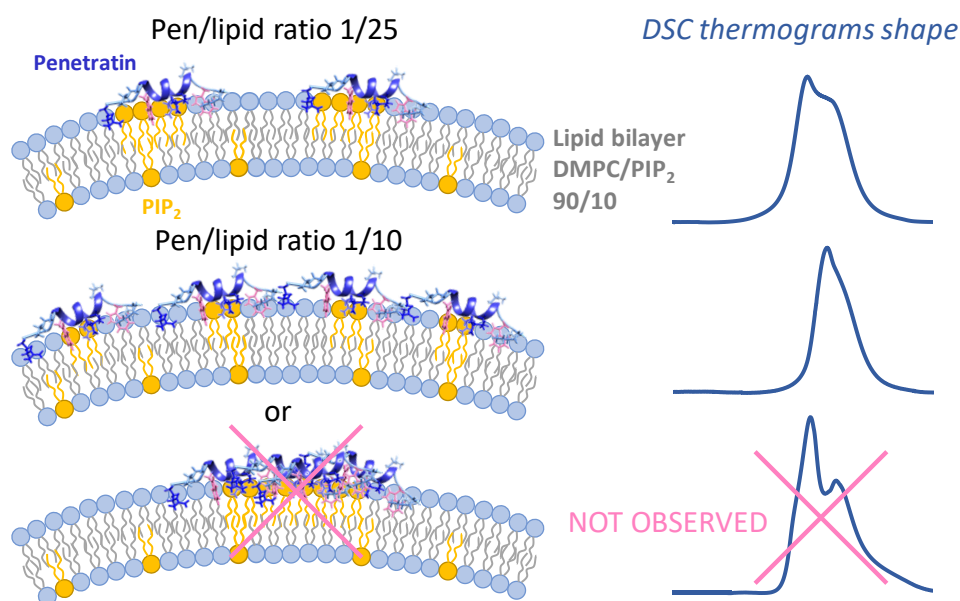


Figure 44. Illustration of the hypothesis to explain the DSC thermograms obtained.

These results are in line with studies carried out on the interactions between cationic peptides and negatively charged membranes, which show that these peptides are capable of recruiting several PIP<sub>2</sub> molecules and of forming PIP<sub>2</sub>-enriched regions. It had been shown that this effect is not possible with monovalent lipids PS.<sup>163</sup> Nevertheless, the ability of Penetratin to recruit PIP<sub>2</sub>, however strongly suspected, had not yet been assessed. Our results constitute the first asset of the Penetratin recruitment of PIP<sub>2</sub> and of its ability to form PIP<sub>2</sub> clusters. Again, this segregation induced by addition of Penetratin to liposome systems was not observed in the case of PS-containing vesicles, even though the amount of charge in the liposomes of 20% PS and 5% PIP<sub>2</sub> are equivalent. This highlights the specificity of interaction for PIP<sub>2</sub> and the importance of the charge concentration on the phospholipid polar head to induce clustering.

### 3. Penetratin-PIP<sub>2</sub> binding affinity

The binding affinity of Penetratin for PS- or PIP<sub>2</sub>-containing liposomes was evaluated by titration of a Penetration solution with increasing quantity of LUVs, and measured by fluorescence spectroscopy.

#### 3.1. Fluorescence spectroscopy

This titration method is based on the tryptophan fluorescence. The fluorescence emission intensity and wavelength of tryptophan is dependent on its environment hydrophobicity. The environment hydrophobicity of a tryptophan-containing CPP sequence can thus be evaluated by fluorescence spectroscopy. If the CPP interacts and inserts in the lipid bilayer of the liposomes, the tryptophan environment becomes more hydrophobic and a shift towards blue wavelengths, called blue-shift, is observed, as depicted on Figure 45. A saturation curve is obtained from which a partition coefficient can be calculated to estimate the CPP/lipid binding affinity.

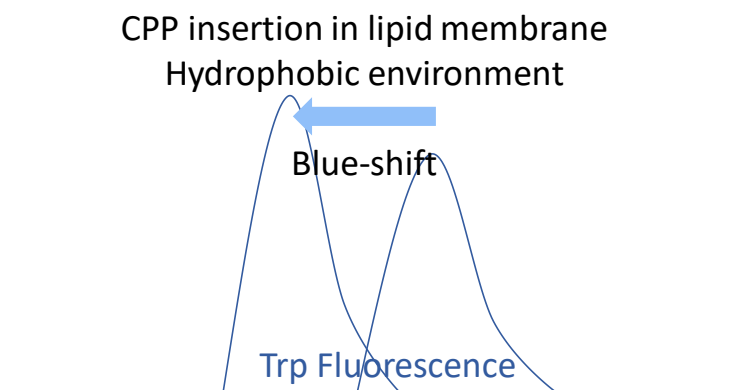


Figure 45. Illustration of the tryptophan fluorescence method for binding affinity evaluation of the CPP/lipid membrane interaction.

#### 3.2. Binding affinity of Penetratin for PIP<sub>2</sub>-containing lipid vesicles

LUVs are the most adapted liposomal system to use in fluorescence spectroscopy as they engender less diffusion issues compared to MLVs or SUVs. Moreover, the control of their size and the fact that they are unilamellar liposomes is an advantage compared to MLVs when working on titration experiments where the amount of accessible lipids at the external leaflet of the object is decisive and should be reproducible.

The titration experiments were conducted using LUVs containing PC, PS and PIP<sub>2</sub> phospholipids. The following LUV compositions were used: POPC 100%, POPC/DOPS (70/30), POPC/DOPS (60/40), POPC/DOPS (50/50) and POPC/PIP<sub>2</sub> (90/10). In order to compare the affinity of Penetratin for PIP<sub>2</sub> with that of Penetratin for PS, the most abundant negatively charged lipid in the plasma membrane, equivalent overall charged liposome compositions are studied. Thus, LUVs of POPC/DOPS (60/40) and POPC/PIP<sub>2</sub> (90/10) should be considered to compare results obtained with liposomes presenting the same amount of charge. Liposomes containing 30% and 50% PS were also studied, and liposomes composed of pure zwitterionic lipids (POPC 100%)

were used as a control. The blue-shift, which corresponds to the difference of the maximum wavelength with the one obtained for the Penetratin solution alone, is plotted as a function of the concentration in total phospholipids in Figure 46.

As expected, no relevant shifting of the tryptophan fluorescence is observed when the titration is achieved using LUVs composed of zwitterionic lipids POPC at 100%. Addition of anionic LUVs to the Penetratin solution induces a decrease of the maximum fluorescence wavelength toward the blue area. Saturation curves are obtained for negatively charged liposomes.

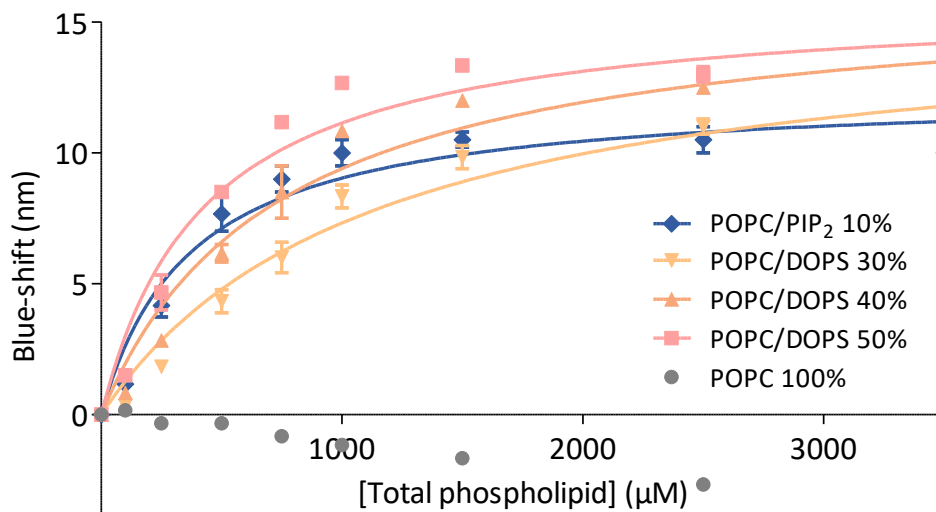


Figure 46. Saturation curves of the tryptophan fluorescence blue-shift observed upon addition of LUVs of POPC, POPC/DOPS 30%, POPC/DOPS 40%, POPC/DOPS 50% and POPC/PIP<sub>2</sub> 10% to a Penetratin solution at 20 μM, for ratios lipid/peptide from 0 to 400. Error bars correspond to standard deviation obtained for n independent experiments (n=3).

Molar partition coefficients were calculated from the saturation curves and are represented in Figure 47. Naturally, increasing the proportion of negatively charged lipids in the LUVs composition, from 30% to 50% in PS-containing liposomes, makes the partition coefficient decrease. In other words, the affinity of Penetratin for the liposomes is higher when the amount of negative charges in the liposomes is increased.

The partition coefficients extracted from these experiments are 377 μM for vesicles containing 10% PIP<sub>2</sub> and 757 μM for vesicles containing 40% PS, which is equivalent to a factor of 2. These results show that for an equivalent overall load, Penetratin has twice as much affinity for PIP<sub>2</sub> as for PS.

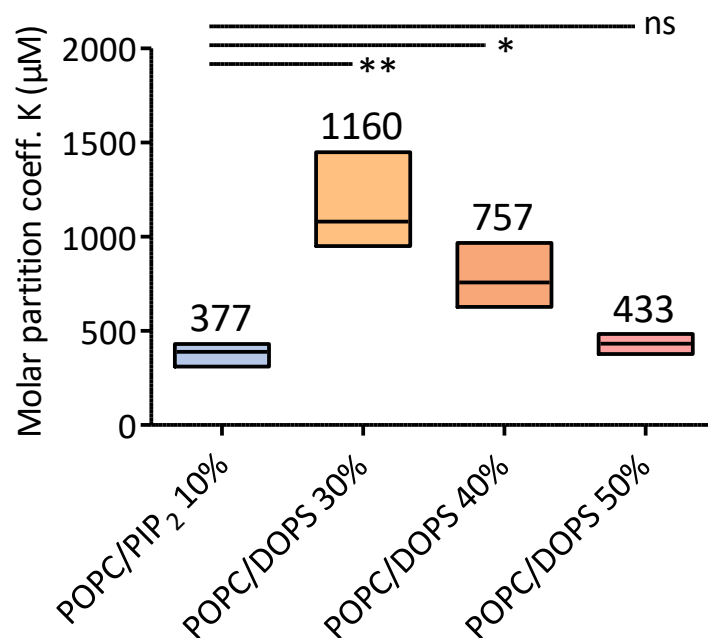


Figure 47. Molar partition coefficients calculated from the saturation curves obtained from the tryptophan fluorescence blue-shift observed upon addition of LUVs of POPC, POPC/DOPS 30%, POPC/DOPS 40%, POPC/DOPS 50% and POPC/PIP<sub>2</sub> 10% to a Penetratin solution at 20 μM, for ratios lipid/peptide from 0 to 400. n = 3 independent experiments.

The charge density on the polar head of PIP<sub>2</sub> could be an explanation for this phenomenon. To further investigate the binding affinity of Penetratin for PIP<sub>2</sub>, it would be interesting to know if this interaction is only linked to the concentration of charges on the PIP<sub>2</sub> polar head or if the conformation of the polar head also plays a role in the binding affinity. Indeed, in all our experiments, the interaction between Penetratin and PI(4,5)P<sub>2</sub> has been investigated. Using PI(3,4)P<sub>2</sub> or PI(3,5)P<sub>2</sub> could give more information on the type of interaction that is considered. In particular, it would inform us on the importance of the position of the phosphate groups, and thus position of the charges, on the inositol group of PIP<sub>2</sub>. Limits of this study is the accessibility of such lipids and the amount of material needed to conduct the tryptophan fluorescence-based titration as this experiment is lipid-consuming.

## 4. Identification of lipid interaction partners of Penetratin in PIP<sub>2</sub>-containing liposomes

The results presented in the previous sections allowed to compare the interaction of Penetratin with PIP<sub>2</sub>- or PS-containing liposomes. The next step is to build PIP<sub>2</sub>- and PS-containing liposomes to observe the behavior of Penetratin in presence of these two lipids, like it is in the plasma membrane. Evaluation of Penetratin preference for PIP<sub>2</sub> or PS in a single liposome system was achieved by identification of lipid interaction partners of Penetratin in liposomes of heterogeneous compositions.

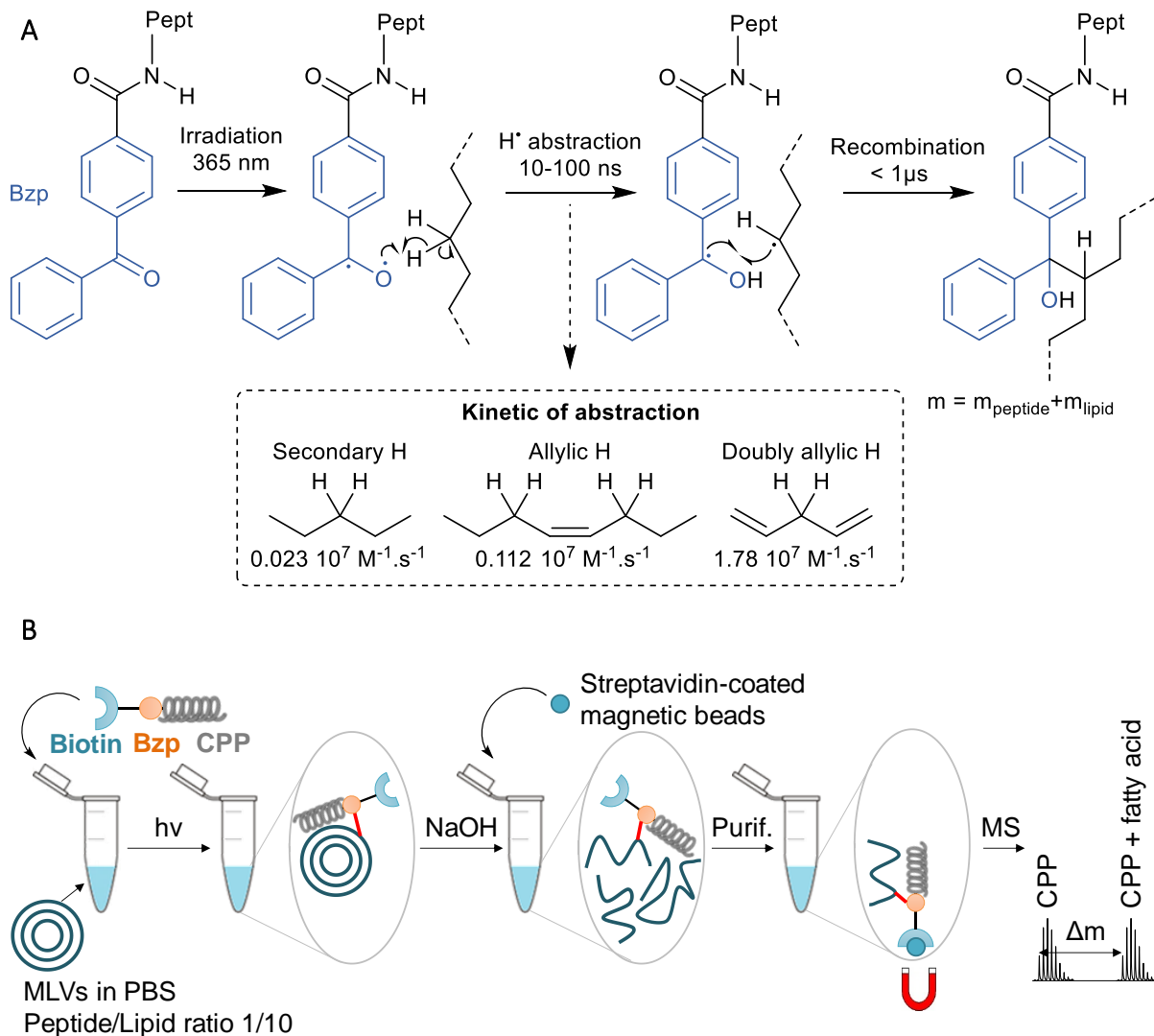


Figure 48. (A) Bzp-induced photo-cross-linking mechanism on phospholipids. Comparison of the kinetics of radical hydrogen ( $\text{H}^*$ ) abstraction for saturated, and (poly)unsaturated lipids.<sup>181</sup>  $m$ : total mass of the photoreactive peptide/lipid photoadduct. (B) Protocol for Bzp-induced photo-cross-linking between a biotinylated and photoreactive CPP and MLVs.

A photo-cross-linking method coupled with MS is used to identify lipid interaction partners of CPPs. This method is based on the photoreactivity of benzophenone (Bzp), which will be further described and developed in the Part 2 of this manuscript. A peptide functionalized with a Bzp can indeed be activated under UV irradiation. Bzp is then in an excited triplet state and is able

to abstract a radical hydrogen in its immediate environment. When the peptide is inserted into a membrane, the Bzp can abstract a H• from the fatty acid chain of a phospholipid. The kinetics of this H• abstraction step depends on the nature of the hydrogens.<sup>181</sup> The reaction is indeed faster on allylic hydrogens compared to secondary hydrogens that can be found in a membrane containing unsaturated and saturated lipids, respectively. Finally, a recombination step allows to create a covalent bond between the Bzp and the lipid (Figure 48). A more detailed description of the photochemistry will be given in the second part of the manuscript.

Photoadducts obtained with intact phospholipids are heteroadduct products known to be difficult to observe in MS. To allow better ionization and mass detection performance, phospholipid saponification was performed on the photoadducts prior to affinity purification of biotinylated species on magnetic streptavidin beads, which allowed the creation of photoadducts composed of the biotinylated peptide covalently linked to a simple fatty acid. The mass difference ( $\Delta m$ ) between the ionic signal of the non-photo-cross-linked peptide and the photoadduct allows to identify the fatty acid chain covalently bound to the peptide.

A previous study carried out in our laboratory showed that photo-cross-linking is more efficient on liposomes composed of negatively charged lipids, on lipids with unsaturated fatty acid chains, and of short length, in this order.<sup>5</sup> The first conclusion is directly linked to the fact that Penetratin interacts preferably with negatively charged lipids. The second results can be explained by two facts. Penetratin, and CPPs in general, have been found to interact preferably with disordered regions of the membrane.<sup>180</sup> Moreover, the kinetics of the H• abstraction step of the Bzp-induced photo-cross-linking drives the reaction to be more favorable on unsaturated lipids. Finally, short length phospholipids implies less interactions between their fatty acid chains compared to long chain phospholipids and thus gives rise to a less stiff membrane, in comparison. Indeed, DSC experiments have reported that Penetratin interacts preferably with shorter aliphatic chains.<sup>162</sup>

### Photoadducts theoretical masses and isotopic distributions

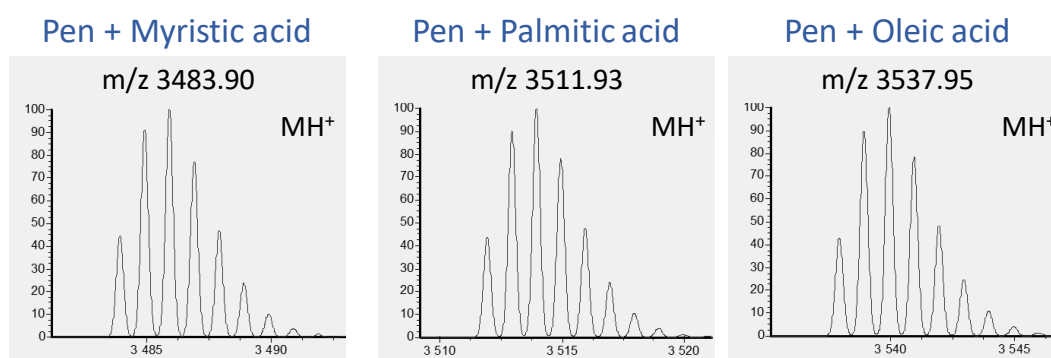


Figure 49. Photoadducts theoretical masses and isotopic distributions obtained with Isopro, corresponding to the Bzp-functionalized Penetratin (Pen) covalently bound to myristic acid, palmitic acid or oleic acid.

Liposomes of variable polar heads composition were used to identify interaction partners of Penetratin in the presence of PC, PS and PIP<sub>2</sub>. Variable compositions in fatty chains were also used: myristic acid (MA, 14:0), palmitic acid (PA, 16:0) and oleic acid (OA, 18:1). Irradiation was

performed at 45°C, to ensure that all lipids are in the fluid phase. The theoretical masses and isotopic distributions for photoadducts containing these lipids are presented in Figure 49.

#### 4.1. Control experiment on zwitterionic lipid PC MLVs

A control experiment was performed using MLVs of pure PC composition with different fatty acid chains: DMPC (14:0) and DOPC (18:1). Results are shown in Figure 50. No photoadduct was detected when using this composition of liposomes. It is likely that Penetratin does not interact with these zwitterionic lipids or that the interaction is so low that the peptide does not insert in the membrane, or at such a low level that it is found in the limit of the analysis detection. These MLV compositions represent a good negative control for our photo-cross-linking experiments.

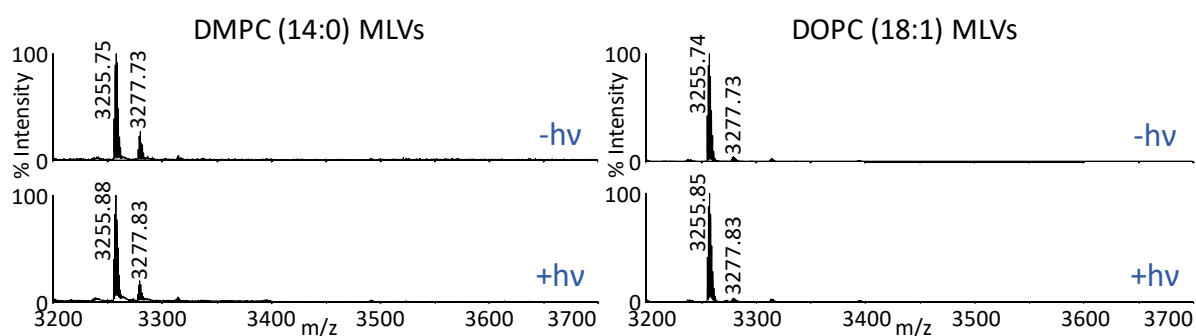


Figure 50. MALDI-TOF spectra of the Bzp-induced photolabeling between Biot(O<sub>2</sub>)-Apa-G<sub>5</sub>-K(Bzp)-RQIKIWFQNRRM(O)KWKK-CONH<sub>2</sub> (ApaPen) at m/z 3255 for the protonated [M+H]<sup>+</sup> molecule and MLVs composed of zwitterionic lipids DMPC and DOPC. Irradiation occurred for one hour at 45°C, where all lipids were in fluid phase. The ion at m/z 3277 corresponds to the [M+Na]<sup>+</sup>. All data were acquired by MALDI-TOF MS, in reflector positive ions mode, using a 2,5-dihydroxybenzoic acid (2,5-DHB) matrix supplemented with phosphoric acid at 1%.

External calibration was performed using a mixture of 5 peptides and optimization was performed on the Insulin chain B ion at m/z 3494.

#### 4.2. Binary lipid compositions: The presence of negatively charged lipids triggers the photo-cross-linking reaction

The photo-cross-linking experiment was applied to MLVs composed of PC and PIP<sub>2</sub>: DMPC/DOPIP<sub>2</sub> (95/5) and DMPC/DPPPIP<sub>2</sub> (90/10) (Figure 51).

The method limit of detection did not allow to use MLVs composition below 5% PIP<sub>2</sub>. In the first case, a photoadduct of oleic acid is obtained, corresponding to the fatty chains of DOPIP<sub>2</sub>. In the second case, the fatty chains of myristic acid and palmitic acid were photo-cross-linked, which corresponds to the photo-cross-linking of the fatty acids linked to both polar heads PC and PIP<sub>2</sub>. It can be noted that the control experiment was performed on MLVs composed of 100% DMPC where no photoadduct could be observed. We can thus deduce that the observation of photoadducts in experiments conducted on MLVs composed of lipids with PC and PIP<sub>2</sub> polar heads is possible by the presence of PIP<sub>2</sub> in the liposomes.

One can notice that the experimental first isotope of the photoadduct containing myristic acid and palmitic acid is shifted compared to the theoretical distribution given in Figure 48. The observed mass of the first isotope is at  $-2u$  compared to the theoretical one. This phenomenon led to detailed elucidation of the mass spectra and was attributed to the formation of a double bond (formal loss of  $2H$ ) on saturated lipids, induced by the Bzp photoreactivity in a constrained environment that is a saturated membrane. This point is further developed and discussed in the Part 2 of this manuscript.

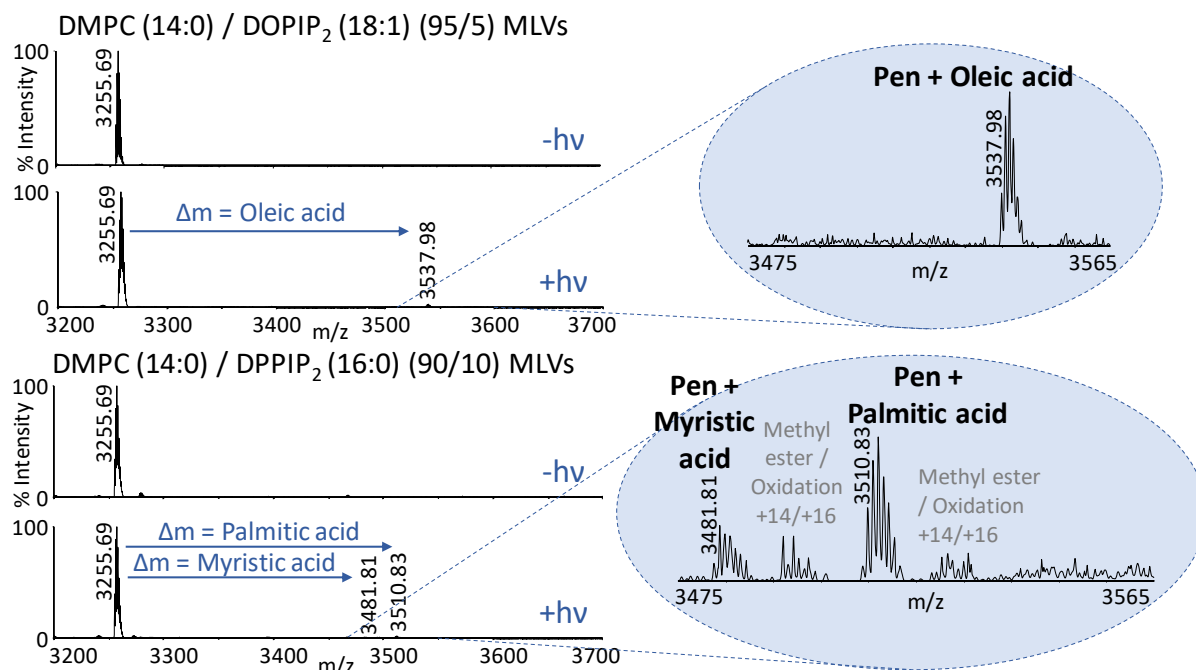


Figure 51. MALDI-TOF spectra of the Bzp-induced photolabeling between Biot(O<sub>2</sub>)-Apa-G<sub>5</sub>-K(Bzp)-RQIKIWFQNRRM(O)KWKK-CONH<sub>2</sub> (ApaPen, m/z 3255) and negatively charged MLVs of the following compositions: DMPC/DOPIP<sub>2</sub> (95/5) and DMPC/DPPIP<sub>2</sub> (90/10). Irradiation occurred for one hour at 45°C, where all lipids were in fluid phase. All data were acquired by MALDI-TOF MS, in reflector positive ions MLV mode, using a 2,5-DHB matrix supplemented with phosphoric acid at 1%. External calibration was performed using a mixture of 5 peptides and optimization was performed on the Insulin chain B ion at m/z 3494.

Photo-cross-linking experiments conducted with MLVs composed of PC and PS lipids gave comparable results (Figure 52). The MLVs compositions used are the following: DMPC/DOPS (70/30), DMPC/DPPS (70/30) and DOPC/DMPS (70/30). The percentage of PS in the liposomes was chosen so as to keep as much as possible the proportion PS/PIP<sub>2</sub> found in the plasma membrane composition.

In MLVs of DMPC/DOPS (70/30), a photoadduct of oleic acid is obtained predominantly and a small signal is detected for myristic acid. In the case of DMPC/DPPS (70/30), myristic acid and palmitic acid are photo-cross-linked. Concerning MLVs of DOPC/DMPS (70/30), only oleic acid photoadduct could be detected, which corresponds to the fatty acid chain of DOPC.

By comparing the results obtained for PIP<sub>2</sub>- and PS-containing vesicles, for similar fatty acid chain compositions, a tendency is already suggested. By comparing DMPC/DOPIP<sub>2</sub> (95/5) and



DMPC/DOPS (70/30), results show that only PIP<sub>2</sub> is labelled in the first case, while a small signal corresponding to the fatty acid chain of DMPC is detected in the latter case. Also, results obtained by using MLV compositions of DMPC/DPIP<sub>2</sub> (90/10) and DMPC/DPPS (70/30) reveals a different ratio of photo-cross-linking between myristic acid and palmitic acid. Indeed, for the same composition in fatty acid chains, the experiment with PIP<sub>2</sub> shows a higher photo-cross-linking signal on the palmitic acid, while the myristic acid signal is more intense in the case of the PS-containing MLVs. Data statistics are not sufficient to evaluate the contributions of each photo-cross-linking results. Still, in the case of PIP<sub>2</sub>, the photo-cross-linking efficiency is reversed compared to previous results as the palmitic acid is longer than the myristic acid.

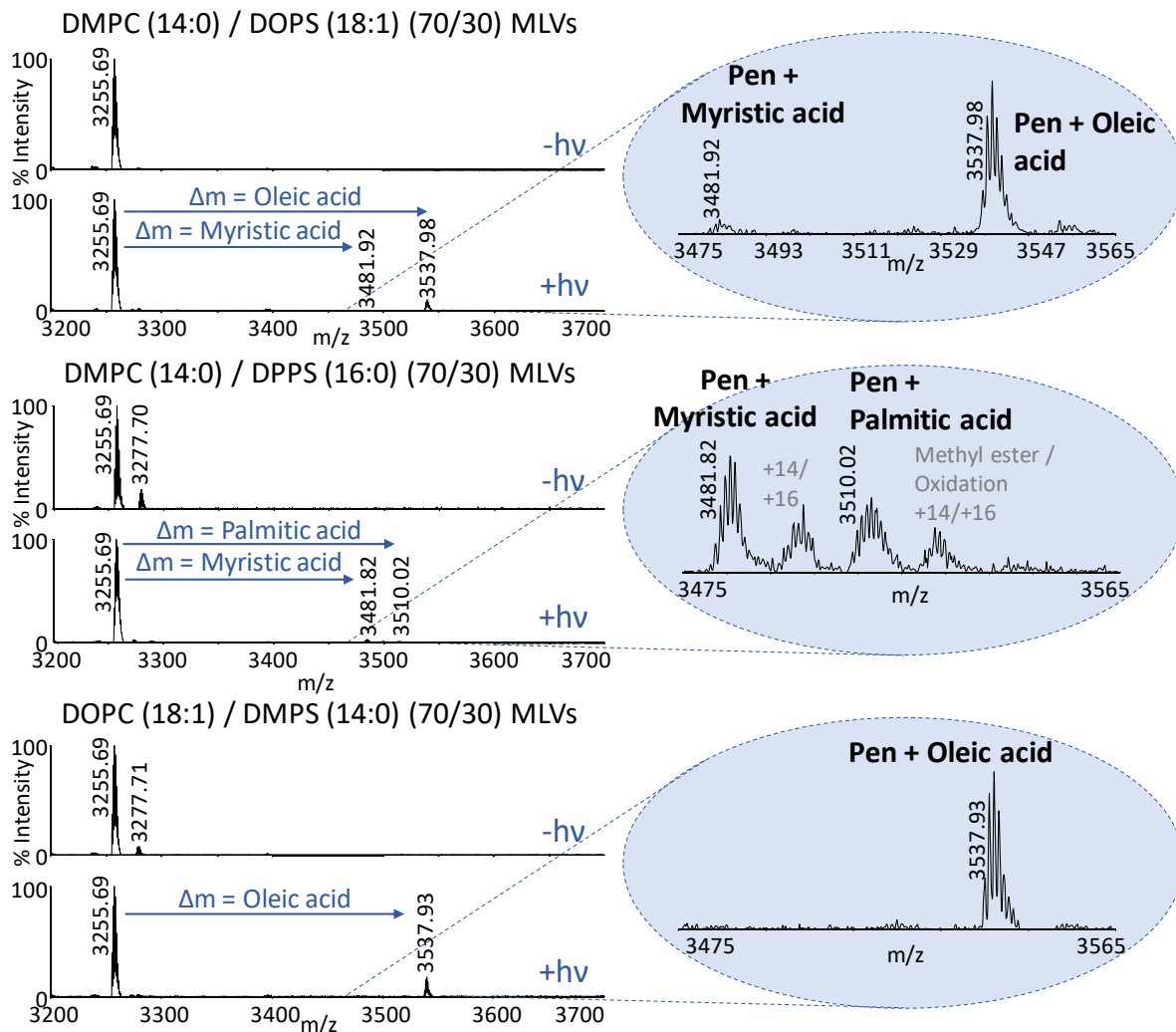


Figure 52. MALDI-TOF spectra of the Bzp-induced photolabeling between Biot(O<sub>2</sub>)-Apa-G<sub>5</sub>-K(Bzp)-RQIKIWFAQNRRM(O)KWKK-CONH<sub>2</sub> (ApaPen, m/z 3255) and negatively charged MLVs of the following compositions: DMPC/DOPS (70/30), DMPC/DPPS (70/30) and DOPC/DMPS (70/30). Irradiation occurred for one hour at 45°C, where all lipids were in fluid phase. All data were acquired by MALDI-TOF MS, in reflector positive ions mode, using a 2,5-DHB matrix supplemented with phosphoric acid at 1%. External calibration was performed using a mixture of 5 peptides and optimization was performed on the Insulin chain B ion at m/z 3494.

In general, photo-cross-linking products seem to be highly dependent on the nature of the phospholipids fatty acid chains and on the photo-cross-linking mechanism, no matter the polar

head group considered. Indeed, oleic acid chains are preferably labeled compared to the other types of hydrophobic chains. As no photoadducts were observed with liposomes composed of PC phospholipids only, the presence of the negatively charged phospholipids seems to be important to trigger the peptide-lipid interaction. Once, the peptide is inserted in the membrane, photo-cross-linking can occur in the environment of the Bzp, predominantly with the fatty acid chains that are the most favored for the photo-cross-linking reaction, *i.e.* unsaturated lipids. Still, experiments on MLVs of DMPC/DPPIP<sub>2</sub> (90/10) show a higher signal for the palmitic acid photoadduct, although the photo-cross-linking is supposed to be more efficient on the myristic acid due to its shorter length. In this example, PIP<sub>2</sub> appears to drive the photo-cross-linking preferably on the palmitic chains.

A supposition is that the clustering effect of Penetratin, highlighted by our calorimetry experiments, plays a role in the photo-cross-linking efficiency. Indeed, once the peptide is inserted in the membrane after PIP<sub>2</sub> clustering through electrostatic interaction with their polar heads, the peptide is surrounded by several PIP<sub>2</sub> phospholipids, which leads to a higher probability of photo-cross-linking on the fatty acid chains of PIP<sub>2</sub>.

#### 4.3. Tertiary lipid compositions: PIP<sub>2</sub> photo-cross-linking over PS

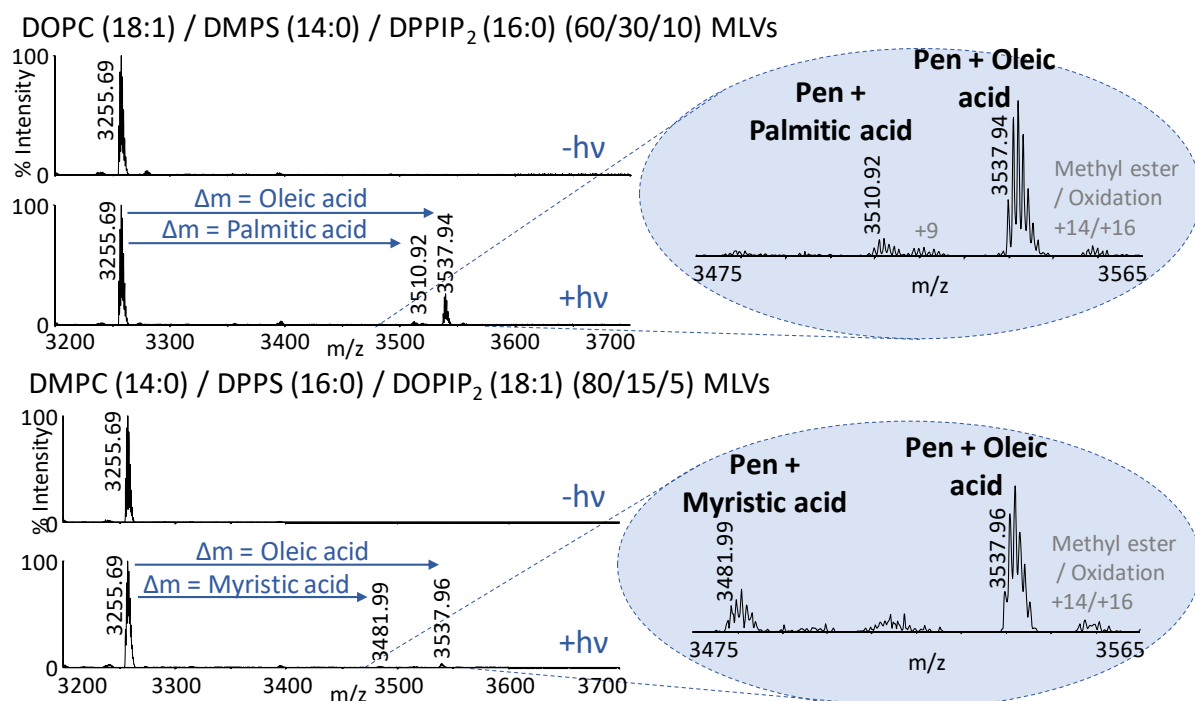


Figure 53. MALDI-TOF spectra of the Bzp-induced photolabeling between Biot(O<sub>2</sub>)-Apa-G<sub>5</sub>-K(Bzp)-RQIKIWFQNRRM(O)KWKK-CONH<sub>2</sub> (ApaPen, m/z 3255) and negatively charged MLVs of the following compositions: DOPC/DMPS/DPPIP<sub>2</sub> (60/30/10) and DMPC/DPPS/DOPIP<sub>2</sub> (85/15/5). Irradiation occurred for one hour at 45°C, where all lipids were in fluid phase. All data were acquired by MALDI-TOF MS, in reflector positive ions mode, using a 2,5-DHB matrix supplemented with phosphoric acid at 1%. External calibration was performed using a mixture of 5 peptides and optimization was performed on the Insulin chain B ion at m/z 3494.

The method was then applied to liposomes of a slightly more complex composition, including PS and PIP<sub>2</sub> in the same liposomes. PS is the most abundant negatively charged lipid in the plasma membrane and liposomes compositions were chosen so as to keep as much as possible the ratio PS/PIP<sub>2</sub> present in the plasma membrane. The percentage of PIP<sub>2</sub> in the liposomes is however limited to the detection limit of the method. Nevertheless, PIP<sub>2</sub> concentration in the plasma membrane is not homogeneous and evidence of PIP<sub>2</sub>-enriched regions in the plasma membrane has been highlighted in introduction. The lipid compositions used are as follows: DOPC/DMPS/DPPIP<sub>2</sub> (60/30/10) and DMPC/DPPS/DOPIP<sub>2</sub> (80/15/5) (Figure 53). In both cases the photo-cross-linked lipids correspond to the PC and PIP<sub>2</sub> lipids, and the oleic acid signal is the most intense. Very low intensity signal corresponding to the PS fatty acid chains might be perceived but low signal-to-noise (S/N) does not allow identification of a first isotope.

Bzp reacts on the fatty acid chains of lipids in its immediate environment, which makes it possible to identify the interaction partners of the peptide. We can therefore deduce from these results that Penetratin interacts preferentially with PIP<sub>2</sub> and is inserted into the liposome membrane close to the PIP<sub>2</sub> lipids. Once the peptide is inserted into the membrane, the photo-cross-linking reaction occurs on the surrounding lipids, which are PIP<sub>2</sub> and neighboring PC lipids, present in significant proportions in our model membranes.

## Conclusion

In this part of the project, the contributions of the phosphatidylinositol-(4,5)-biphosphate for the internalization of the cell-penetrating peptide Penetratin were evaluated. Our internalization studies on cells show the likely contribution of intracellular PIP<sub>2</sub> for the internalization of Penetratin. Blockage of the PIP<sub>2</sub> polar head groups by transfection of CHO-K1 cells by a GFP-PH-PLC<sup>δ</sup> plasmid prior to internalization experiments inhibited the cellular uptake of the peptide. In order to better define the interaction between Penetratin and the multivalent phospholipid PIP<sub>2</sub>, several experiments were conducted on model membranes containing PIP<sub>2</sub>. As Penetratin is known to interact with negatively charged phospholipids, an emphasis has been pursued on the comparison of the Penetratin interaction with PIP<sub>2</sub> and the Penetratin interaction with PS the negatively charged lipid the most abundant in the plasma membrane. Calorimetry measurements were used to assess the effect of Penetratin on the thermotropic phase behavior of such liposomes. It appears that Penetratin interacts strongly with PIP<sub>2</sub> and is able to induced PIP<sub>2</sub> clustering in model membranes, while it is not the case in PS-containing liposomes. In addition, the Penetratin binding affinity for PIP<sub>2</sub>- and PS-containing liposomes was estimated by fluorescence spectroscopy. It appears that Penetratin binds with 2 times more affinity for PIP<sub>2</sub>-containing vesicles compared to PS-containing vesicles, for a similar amount of charges in the liposomes. Finally, a method coupling photo-cross-linking to MS analysis allowed the identification of PIP<sub>2</sub> as a favored interaction partner of Penetratin in liposomes containing PC, PS and PIP<sub>2</sub>.

Figure 54 illustrates the conclusions obtained on the contributions of PIP<sub>2</sub> to the internalization of Penetratin evaluated using model membranes. A model membrane composed of PC, PS and PIP<sub>2</sub> in 80/15/5 proportions is considered.

In the presence of this negatively charged membrane, Penetratin is structured in  $\alpha$ -helix. We know from our fluorescence titration experiments that the affinity of Penetratin for PIP<sub>2</sub> is stronger than for PS. Penetratin will therefore interact preferentially with PIP<sub>2</sub>. In addition, our calorimetry results showed that Penetratin induces lateral separation in liposomes containing PIP<sub>2</sub>, strongly suggesting the formation of domains rich in PIP<sub>2</sub>. These results are supported by results from the literature, indicating that basic peptides are able to recruit multivalent PIP<sub>2</sub> lipids, but not monovalent PS lipids.<sup>163</sup> Penetratin then slightly inserts into the lipid bilayer, as suggested by our calorimetry results. Once inserted into the bilayer, the peptide is found in the vicinity of the fatty chains of the PIP<sub>2</sub> lipids with which it has interacted and the PC lipids which are in significant proportions in the membranes. This position of the peptide explains the results obtained by photo-cross-linking, with photoadducts corresponding to the hydrophobic chains of PIP<sub>2</sub> and PC.

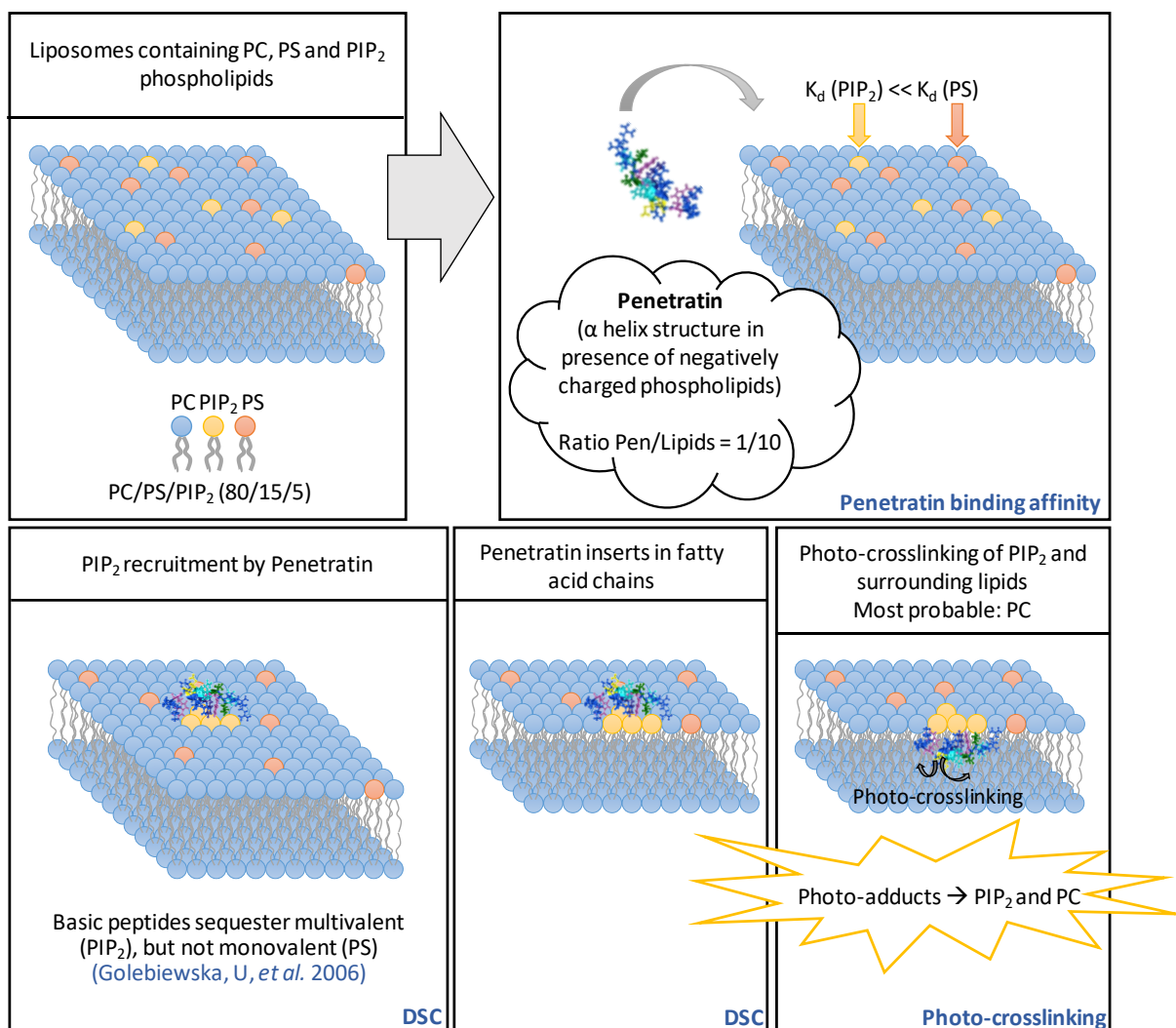


Figure 54. Illustration of the conclusions obtained on the contributions of PIP<sub>2</sub> to the internalization of Penetratin evaluated using model membranes.

A collaboration with the molecular modeling team of the laboratory allowed us to confirm the PIP<sub>2</sub> clustering effect of Penetratin by coarse-grained (CG) simulations. Coarse-graining consists in representing a system by merging several atoms into "beads". Due to the reduction in the number of degrees of freedom and elimination of fine interaction details, CG simulations require less resources compared to all-atom representation and improve sampling in general. They are well suited to understand protein/lipid interactions, particularly for finding what lipids preferentially bind to a membrane protein in a complex lipid mixture.<sup>182</sup> This work was performed in the context of the Ph.D. project of Paula Milán Rodríguez, supervised by Patrick Fuchs. Penetratin was embedded in a model membrane composed of POPC/POPS/POPIP<sub>2</sub> (80/15/5), by using a CG simulation with the MARTINI 2.2 force-field.<sup>183,184</sup> A box containing a lipid bilayer composed of 200 lipids for 2 Penetratin peptides, one on each leaflet, was constructed. The two leaflets have the same lipid composition. Having one Penetratin in each leaflet allowed us to double the statistics at no extra computational cost. Simulations of 10 microseconds were launched. Snapshots of the simulations are presented in Figure 55. The simulation box was repeated on each side to avoid visualization artefacts due to periodic

boundary conditions. Very rapidly, Penetratin recruits the PIP<sub>2</sub> lipids, up to 5 PIP<sub>2</sub> molecules per peptide (Figure 55B), while PS lipids seem to diffuse randomly in the membrane. A zoom on the Penetratin/PIP<sub>2</sub> cluster (Figure 55C) suggests that Penetratin basic residues (in blue) interact with the PIP<sub>2</sub> polar heads, while Tryptophan residues (in orange) insert deeper in the bilayer, just below the polar head groups.

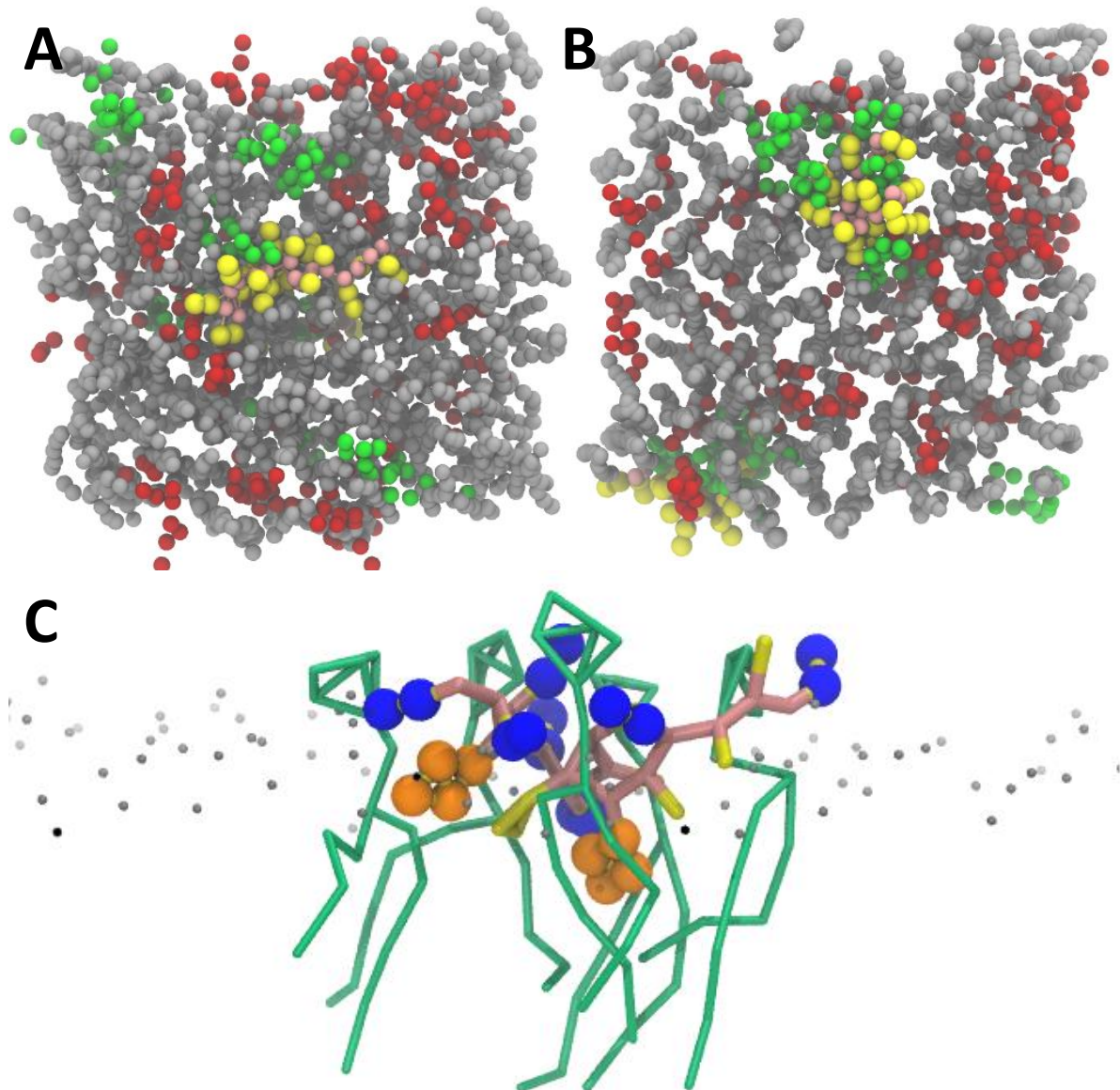


Figure 55. Representative snapshots from Penetratin forming PIP<sub>2</sub> clusters in a model membrane composed of POPC/POPS/POPIP<sub>2</sub> (80/15/5), obtained by MARTINI coarse-grained simulations. (A) Beginning of the simulation, after equilibration. (B) Snapshot at 4  $\mu$ s. PC polar heads are represented in grey, PS in red and PIP<sub>2</sub> in green. The Penetratin sequence is in pink (backbone) and yellow (lateral chains of the residues). Water molecules were removed from the figure for more clarity. (C) Snapshot of Penetratin binding 5 PIP<sub>2</sub> molecules at one of the membrane leaflets. The Penetratin backbone is in pink, the lateral chains of the AA residues are in yellow, except basic residues lateral chains that are highlighted with blue beads, and tryptophan residues that are highlighted with orange beads. PIP<sub>2</sub> lipids are in green. The phosphate groups of the phospholipids are shown with grey beads in order to localize the water/membrane interface. “Beads” are scaled for a better visualization. PC, PS lipids and water molecules were removed from the figure for more clarity.

*In vivo*, *in vitro* and *in silico* studies have been used to evaluate the Penetratin interaction with PIP<sub>2</sub>. Altogether, these results give more insight on the way Penetratin interacts with model membranes and on the direct translocation pathway of this peptide. Indeed, the first electrostatic interactions that the peptide has with the negatively charged molecules at the extracellular leaflet of the membrane must be a first recognition step, but interactions with the internal leaflet, which is more negatively charged, is of importance in the internalization pathway, probably by attracting the peptide toward the other side of the membrane. Furthermore, the Penetratin ability to form PIP<sub>2</sub> clusters is likely to be a key factor for the internalization to be possible. This clustering effect was evidenced by our calorimetry experiments and is also a good explanation for the stronger interactions toward PIP<sub>2</sub> observed in fluorescence and in photo-cross-linking results.

PART 2: BENZOPHENONE  
PHOTOREACTIVITY IN A LIPID  
BILAYER TO PROBE CPP/LIPID  
MEMBRANE INTERACTIONS



# Introduction

The benzophenone (Bzp) photoreactivity in the context of a lipid membrane will be extensively studied in this second part of the manuscript. As it has been mainly reported in solution, the reactivity of the Bzp triplet excited state can be impacted by the particular environment that is a model membrane. In addition, the Bzp probe being covalently bound to a CPP, the mode of interaction of the peptide with the lipid membrane could influence the photo-cross-linking properties. Parameters such as the peptide structuration at the membrane contact, its positioning in the lipid bilayer, and its interaction with the different physical states of the membrane – unsaturation degree, lamellar phase, curvature – are so many variables that could affect and direct the Bzp reactivity. In this introduction, we will attempt to describe the mode of interaction of CPPs with lipid membranes. Then, the classical photoreactivity of the Bzp probe will be described. Finally, a non-exhaustive description of peptide fragmentation pathways in MS/MS will be given, as this technique allowed us to characterize the Bzp-induced photo-cross-linking products.

## 1. CPPs and the membrane fluidity

Electrostatic interactions are not the only factor to be considered when studying the interaction of CPPs with lipid membranes. In fact, the membrane lamellar state and curvature also have an importance in this interaction.<sup>162,185</sup>

Studies of the interaction of membrane active peptides with model membranes can give precious information on various parameters such as the peptide structure, peptide partition and insertion and peptide-induced membrane perturbation.

### 1.1. Penetratin structuration

As mentioned earlier, Penetratin tends to adopt a defined secondary structure in contact with anionic lipid vesicles, while it has a mainly unstructured conformation in aqueous solution or in presence of uncharged membranes. Penetratin adopts an amphipathic  $\alpha$ -helical structure in presence of negatively charged lipids for low lipid to peptide ratios.<sup>98,128,145</sup> This secondary structure correlates well with the fact that Penetratin corresponds to the third  $\alpha$ -helix of the Antennapedia homeodomain. For higher ratios, and under specific salt concentration or vesicle aggregation, a  $\beta$ -sheet structure or a  $\beta$ -sheet / random coil mixt structure has been observed.<sup>98,99,186</sup> This latter configuration of the peptide would induce a stronger destabilization of the membrane. The secondary structure variability of Penetratin may be linked to different experimental conditions as regards to the peptide and lipid concentrations, buffer contents and temperature. It can be noted that the conditions of low peptide to lipid ratio where the  $\alpha$ -helical structuration is observed is closer to the biological conditions. Also, as commented in Part 1 introduction, the peptide structuration does not seem to be a crucial factor for the cell uptake efficiency.<sup>144</sup> Nonetheless, the secondary structure of Penetratin in live cells has been reported using Raman microscopy.<sup>187</sup> This method has shown a favored configuration in random coil and  $\beta$ -strand in the cytoplasm, and possibly in  $\beta$ -sheets in the nucleus. The limit of this method is it does not allow direct characterization when the peptide

is inside the cell membrane. Although the structuration of the peptide is not necessary for the cell uptake, it has been evidenced that the backbone rigidity and static presentation of guanidinium groups increases the internalization of arginine-rich CPPs.<sup>188</sup> Probably, the structuration allowing the good orientation of the guanidinium groups helps the peptide-membrane interaction in the first step of the internalization pathway.

Elucidation by NMR of the Penetratin structuration in presence of membrane models containing PIP<sub>2</sub> is an ongoing project at the laboratory, as part as the Ph.D. work of Edward Chalouhi, supervised by Olivier Lequin.

## 1.2. Penetratin positioning in lipid bilayers

Penetratin has been reported to insert superficially in model membrane, as it is not sufficiently hydrophobic to insert deeply into the phospholipid model membranes.<sup>128</sup> Studies on SDS vesicles by NMR showed that the peptide lies parallel to the micelle surface without insertion in the hydrophobic region.<sup>189,190</sup> This parallel orientation at the membrane surface has been confirmed using bicelles composed of PC and PG lipids. The same study showed that the tryptophan residues point toward the hydrophobic core of the bilayer, while the peptide seems to be located at the interface between the lipid polar head groups and their hydrophobic tails.<sup>191</sup> Similar results were obtained by tryptophan fluorescence, where the depth of insertion of the tryptophan residues was assessed using PC/PG or PC/PS SUVs. Indeed, Penetratin was found to be positioned parallel to the membrane, at the interface between lipids polar heads and their fatty acid chains, with tryptophan residues inserted deeper in the bilayer at 13.0 Å from the bilayer center, just below the lipid head groups, considering an average length of the acyl chains of the membrane bilayer to be 15 Å. Moreover, Trp 48 was found to be further inserted than Trp 56. Actually, a Penetratin variant where the Trp 48 was replaced by a Phe residue inserts only at 14.5 Å from the bilayer center.<sup>192,193</sup>

Although Penetratin does not affect PC liposomes phase transitions, DSC experiments conducted on PG liposomes showed that the peptide perturbs both the lipid head groups tilting and the main phase transition. It indicates that the peptide disrupts the van der Waals interactions between the hydrophobic chains, which means the peptide would insert at a certain level into those model membranes.<sup>145</sup>

Other studies, focusing on the (R/W)<sub>9</sub> CPP, have shown that the tryptophan residues are important for the cellular uptake efficacy, not only by their number, but also by their position in the peptide and by the size of the hydrophobic side they form. The same work estimated the peptide insertion in the lipid bilayer to around 10 Å from the membrane center, using the intrinsic Trp fluorescence and brominated lipid models of PC/PG LUVs.<sup>180</sup>

It is thus very likely that the cationic peptides containing tryptophan residues like Penetratin or (R/W)<sub>9</sub> are positioned at the water/membrane interface when in contact with negatively charged model membranes. Structured in an  $\alpha$  helix, their backbone should be positioned close to the lipid polar head groups, basic residues interacting with the negatively charged polar heads, while the tryptophan residues are further inserted in the membrane, just below the lipid polar heads. This positioning of tryptophan and basic residues at the water/membrane

interface has also been reported when considering the transmembrane proteins positioning in the plasma membrane.<sup>194</sup>

### 1.3. Penetratin influence on membrane organization: fluidity and curvature

X-ray diffraction allows to measure inter-lipid distance and was used to evaluate the effect of Penetratin on model membranes.<sup>195</sup> It showed that the peptide induces phase separation and lipid rearrangement in the lipid membrane. Using the Laurdan fluorescent probe, the same work reported that Penetratin induces de-packing of lipids in DMPC and DMPC/DMPG membranes. They also performed calorimetry (DSC) experiments using DMPC/DMPG liposomes, which showed that Penetratin favors the transition from the gel phase to the ripple phase (decrease of the pre-transition temperature). Altogether, these results suggest that the Penetratin-induced phase partitioning in the lipid membrane represents an important feature of membrane destabilization for the bilayer translocation, as the peptide favors the ripple phase, a heterogeneous lamellar state composed of gel-like and fluid-like parts.

Using three CPP sequences, Penetratin, R<sub>9</sub> and (R/W)<sub>9</sub>, and a cholesterol-pyrene probe, the same group showed more recently that the cholesterol-pyrene molecules dissociate from clusters upon the peptide-membrane interaction. Their results suggest that the peptide interaction with the membrane induces cholesterol redistribution and that the amphipathicity of the peptides increases membrane fluidity and might be important for membrane translocation.<sup>196</sup>

The use of DSC measurements has been very helpful to evaluate the interaction of CPPs with the different lamellar states of lipid membranes. Penetratin has been reported to interact favorably with lipids of shorter vs longer fatty acid chains and to recruit unsaturated fatty acids chains in a heterogeneous lipid composition.<sup>162</sup> This may be caused by their higher fluidity arising from their lower phase transition temperature. Indeed, when selective lipid interactions were observed in a binary mixture, the recruited lipid always corresponded to the one having the lowest phase transition temperature. The hierarchy in the segregation they report is the same as the one observed with Bzp-induced photo-cross-linking experiments:<sup>5</sup> the unsaturated lipids were preferentially recruited first, before lipids with shorter fatty acid chains. Unsaturated lipids always present a lower T<sub>m</sub>. Thus, such preference is likely to be related to the higher fluidity of these lipids, which better adapt to lipid rearrangements taking place during the cell translocation and/or perturbation of the lipid bilayer.<sup>162</sup>

CPP/lipid interaction is a cooperative process that can affect both partners. Indeed, Penetratin was found to adopt an  $\alpha$ -helical structure at the contact of negatively charged membranes. In the same manner, CPPs can also induce a remodeling of the membrane organization. In fact, it has been reported that Penetratin is able to generate a negative curvature in the lipid bilayer of GUVs, forming tubules that are favored in the disordered membrane regions.<sup>197</sup> This negative curvature can also lead to the formation of inverted micelle structures upon interaction of CPPs with model membranes.<sup>145</sup> Lipids segregation induced by CPPs also destabilizes the membrane by formation of boundary defects between the lipid domains.<sup>198,199</sup> A study related the ability of poly-lysines to induce domain formation and exploit the membrane destabilization to enter GUVs through defects in the membrane at the domains

boundary. The peptide translocation would be favored by the reduced surface tension in these boundary defects.<sup>200</sup>

Membrane defects can be found at lipid domains boundaries, but also in a curved region of the membrane and could facilitate the CPP/lipids interactions. The affinity of Penetratin for liposomes containing the zwitterionic lipid PE, prone to induce a negative curvature by its conical shape, is an indicator of the implication of such structuration of the membrane in the peptide/lipid bilayer interaction. Indeed, presence of PE in model membranes increased the Penetratin affinity for egg PC liposomes from 28 to 0.5  $\mu\text{M}$ , close to the affinity of Penetratin for negatively charged liposomes of egg PG, at 0.3  $\mu\text{M}$ .<sup>161</sup> Direct translocation could thus be favored in nanodomains of the membrane enriched in these conical-shaped lipid.<sup>201</sup>

Interaction of arginine-rich CPPs with curved membranes have been related to lipid packing defects induced by the membrane curvature.<sup>185</sup> Indeed, the loosening of lipid packing induced in the curved membrane would promote the cell entry of arginine-rich CPPs, as illustrated in Figure 56.<sup>202</sup>

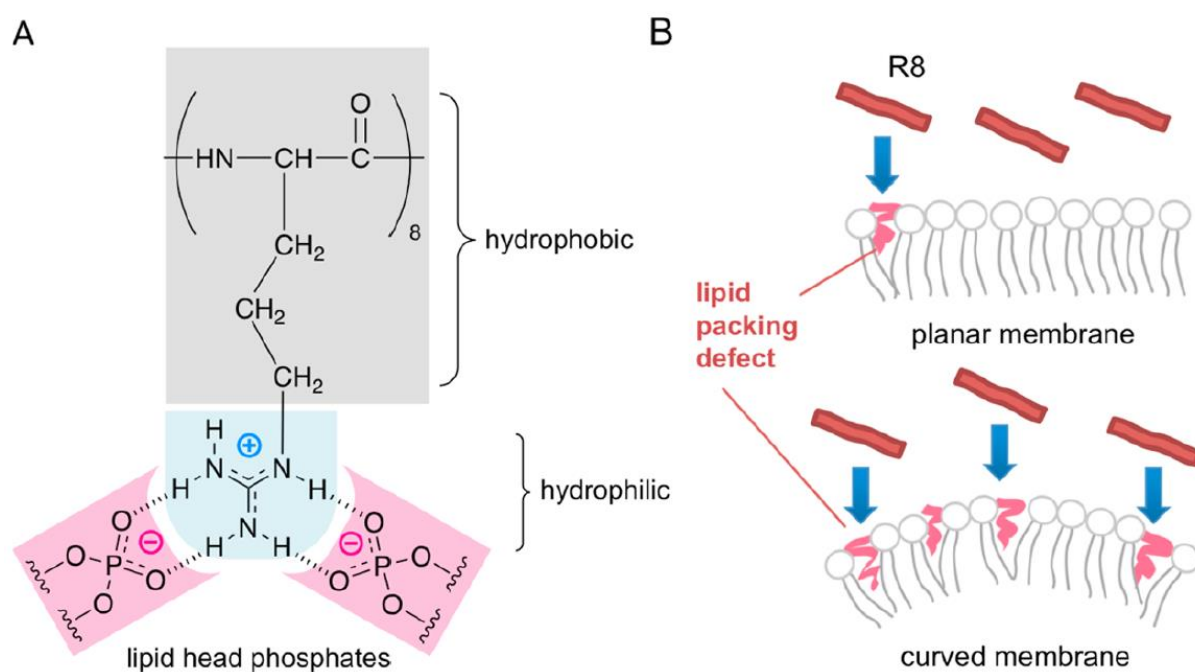


Figure 56. (A) Although the guanidino group of R8 is cationic and hydrophilic, other parts of the molecule are poorly hydrophilic. (B) Curved membranes should have more lipid packing defects than planar membranes, facilitating the interaction of R8 backbone with lipid core areas and the eventual translocation. Figure and legend from <sup>185</sup>.

Lipid packing defects would allow a better exposure of the hydrophobic chains of the lipids, that would favor the interaction with the hydrophobic backbone of the peptide, while the hydrophilic part of the peptide would interact through electrostatic binding with the lipids polar heads.

As the photo-cross-linking method we use is dependent on the CPP interaction with the lamellar state of the lipid membrane, it is important to consider the influence of membrane

fluidity and structure in our experiments. As previously mentioned, the Bzp photoreactivity on lipid substrates is dependent on the lipids unsaturation degree. In addition, insertion depth of the peptides could be a great advantage to consider in the same time with the interaction partner identification, for a better characterization of the system.

## 2. Benzophenone as a photoactivable probe in model membranes

The Bzp photoreactivity has been extensively described in the literature and the versatility of its triplet excited state is exploited for a wide diversity of applications in chemical biology, as illustrated in Figure 57.

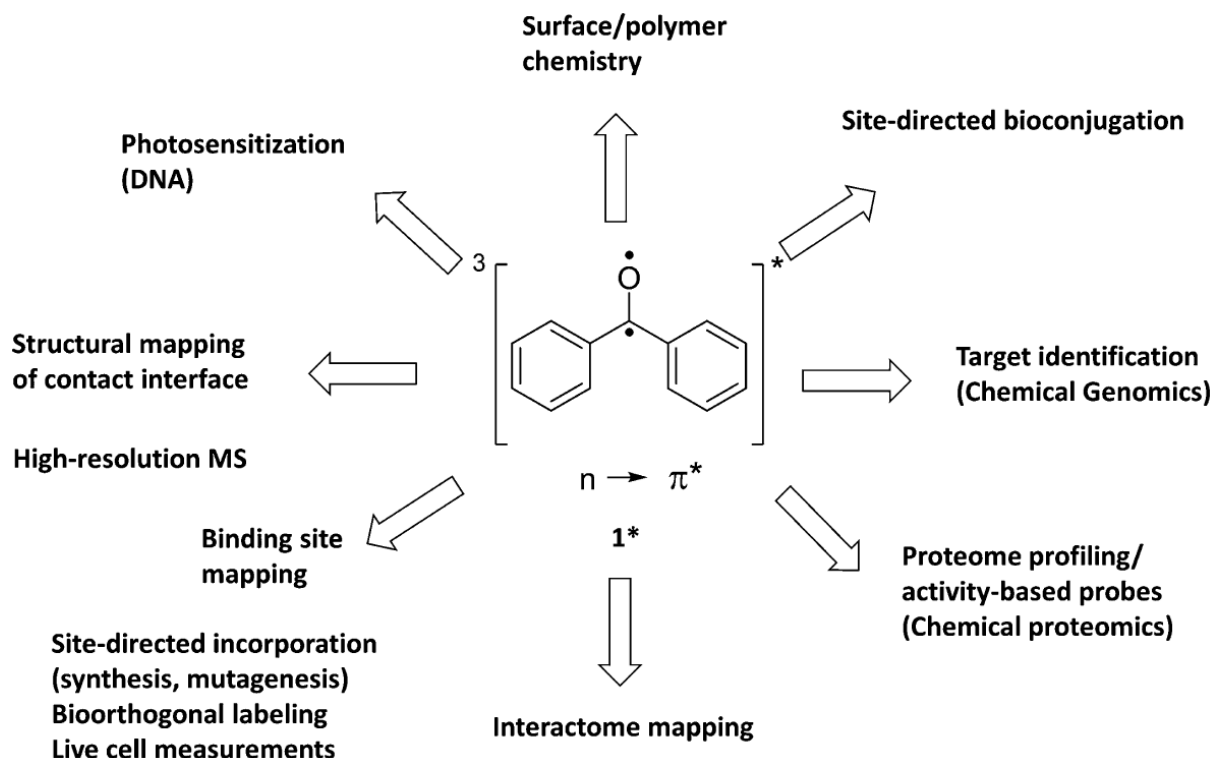


Figure 57. Diversity of applications of the Bzp photochemistry during the past 20 years, due in part to the rapid development of innovative technologies in chemical biology. 1\*: triplet excited state of Bzp, 3 Bzp\*.<sup>203</sup>

Upon irradiation, the Bzp chromophore can absorb a photon at >350 nm that promotes the transfer of a non-bonding  $n$  electron of the carbonyl oxygen into the  $\pi^*$  orbital of the carbonyl, leading to an  $n-\pi^*$  transition (Figure 58). The  $n-\pi^*$  triplet is often represented as a diradical and is the most reactive of the excited state species of Bzp.<sup>203</sup>

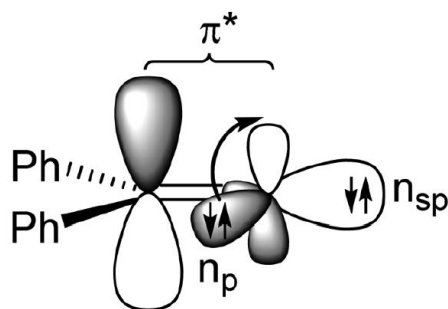


Figure 58.  $n-\pi^*$  transition of BP carbonyl upon irradiation.<sup>203</sup>

The most important photochemical reactions of the Bzp triplet excited state are hydrogen abstraction, [2+2] cycloaddition on a C=C double bond (Paternò-Büchi reaction, oxetane formation), and to a lower extent triplet sensitized dimerization.

## 2.1. Radical hydrogen abstraction

The  $n-\pi^*$  triplet excited state (Figure 59, molecule **1\***), which has both high energy and biradicaloid character, can abstract a radical hydrogen from an appropriate donor molecule, leading to the formation of Bzp ketyl radical (Figure 59, molecule **2**). Recombination of the radicals resulting from the  $H^\bullet$  abstraction and of the Bzp ketyl radical leads to the formation of a stable covalent bond between the substrate and a benzhydrol group (Figure 59, photo-cross-linked compound **9**).  $H^\bullet$  abstraction generally takes place within 10–100 ns, while recombination is slower ( $>1 \mu\text{s}$ ), and is considered as the rate-limiting step of the photo-cross-linking reaction. Two Bzp ketyl radicals **2** can also couple to form a benzopinacol (Figure 59, molecule **7**), but no such dimerization is reported for protein-Bzp<sup>203</sup> or peptide-Bzp<sup>204</sup>. The  $n-\pi^*$  triplet excited state is in equilibrium with the ground state, which provides a certain photostability of labeled molecules and is particularly adapted when studying biological systems that often require long incubation times. The  $n-\pi^*$  triplet excited state can also be reduced by compounds that are poor  $H^\bullet$ -donors but good electron donors, such as  $\text{H}_2\text{O}$ , leading to the hydrate molecule **12**, which can be further regenerated to the ketone molecule **1** that can again be excited.

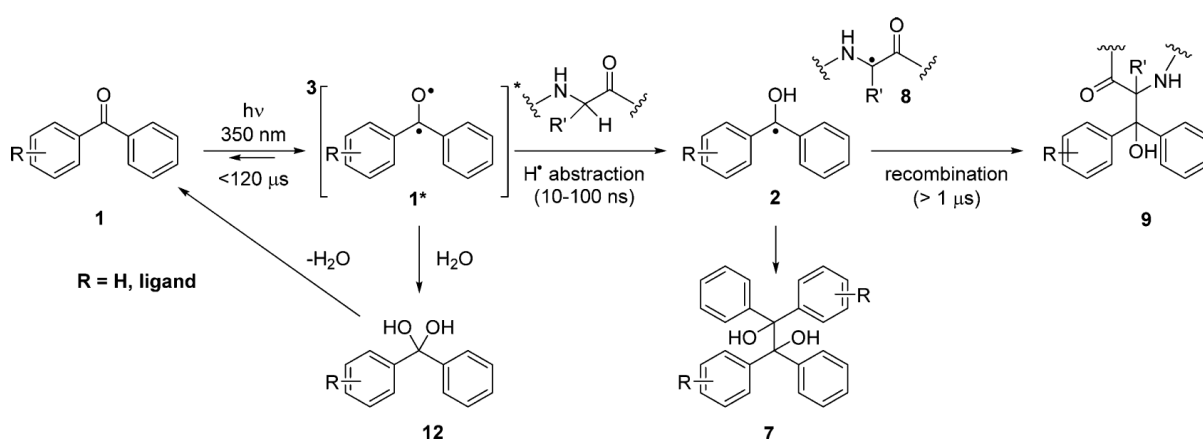


Figure 59. Example of the Bzp-induced photo-cross-linking on a protein substrate.<sup>203</sup>

The diradicaloid triplet state is the most reactive toward C–H bonds, forming relatively stable carbon radicals, thus it is particularly adapted to the cross-linking of lipid acyl chains. The radical stability drives the rate of  $H^\bullet$  abstraction. In that way, the  $H^\bullet$  abstraction kinetics is ranked in the order primary  $<$  cyclohexyl and secondary aliphatic  $<$  primary aliphatic and secondary benzylic  $<$  tertiary aliphatic hydrogens.<sup>203</sup> It can be noted that stability of the Bzp probe is convenient as it can be manipulated in ambient light.

Bzp-induced photo-cross-linking has been well characterized on peptidic molecules and is commonly used for protein cross-linking. The radical hydrogen abstraction reactivity of Bzp has also been used to determine the conformations of the flexible chains in membranes<sup>205,206</sup> and to induce cross-linking on lipid substrates in acetonitrile solutions.<sup>207</sup> More recently, this reactivity has been exploited to decipher the interaction of CPPs with model membranes, implying the photo-cross-linking reaction to occur in a complex system that is a lipid membrane.<sup>5</sup>

## 2.2. Paternò-Büchi reaction

The Paternò-Büchi (P-B) reaction consists in a [2+2] cycloaddition leading to oxetane formation on the double bond of unsaturated lipids.<sup>208–210</sup> It is a well described reaction and involves a UV-activated biradical carbonyl group of an aldehyde or a ketone, such as the one present in the Bzp (molecule **1\***), which further reacts in solution with C=C bond(s), as found in unsaturated lipids. If energy is applied to P-B products, retro Paternò-Büchi reaction (retro P-B) can happen *via* two pathways either leading back to the original reactants, or leading to cleavage of the C-C bond at the initial C=C bond position and the C-O bond of the initial carbonyl, thus forming a new olefin and ketone/aldehyde and leading to ions characteristic of the position of the double bond (see Figure 60).<sup>208,211,212</sup>

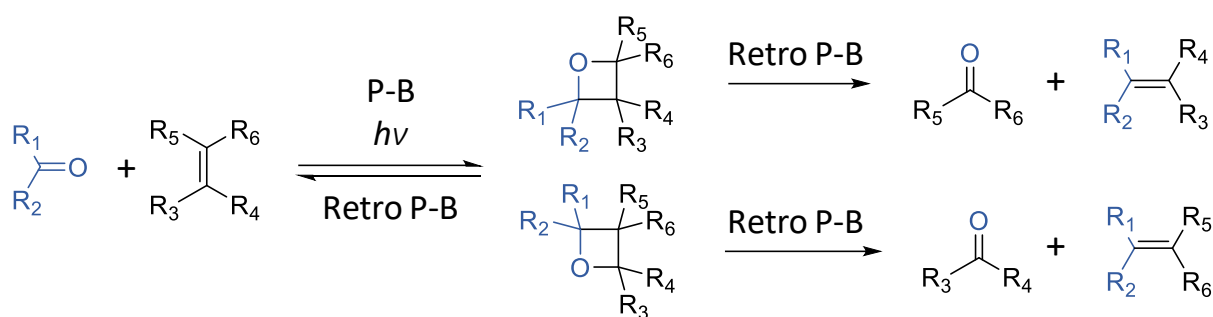


Figure 60. Paternò-Büchi (P-B) reaction between a ketone/aldehyde and olefin and possible retro P-B reactions.

Bzp has been recently described as a P-B reagent of choice for characterization and quantification of unsaturated lipids by MS/MS, gas-phase fragmentation of the P-B products leading to diagnostic ions of the position of the double bond.<sup>208,213,214</sup> Energy can be given by heating or collision with an inert gas during tandem MS experiments. These UV-induced reactions of the Bzp are well described on lipids in solution (P-B) or in the gas-phase (retro P-B).<sup>208,213</sup> P-B reaction coupled with MS/MS is used for identifying and quantifying unsaturated lipids in complex lipid mixtures.<sup>213,214</sup>

It is worth noting that the oxetane ring opening through retro P-B can be done by low collision energy in MS/MS, but also by heating<sup>213–215</sup> or acidic treatment since monosubstituted oxetanes are known to be unstable at pH 1.<sup>216</sup>

## 2.3. Triplet sensitized dimerization

Bzp can act as a photocatalyst by absorbing a photon and transferring it to a substrate *via* sensitization by energy or electron transfer.<sup>217</sup> Bzp-induced dimerization through photosensitization has been well described for biomolecular interactions with DNA. Bzp photoinduced reactions (photooxidation, P-B or retro P-B reactions, C-C bond formation, dimerization) often competes.<sup>203</sup> A study by Liu *et al.* on Bzp and pyrimidine bases revealed that the proportion of P-B reaction compared to dimerization *via* photosensitization, depends on the relative triplet energy ( $E_T$ ) levels of both entities.<sup>218</sup> When the  $E_T$  values of the Bzp and the pyrimidine are close, the two reactions occur concurrently.



## 2.4. Double bond formation

A less common reactivity of the Bzp chromophore can be considered as it is driven by the rigidity of the Bzp environment. As described in solution by Breslow,<sup>219,220</sup> Bzp can induce the formation of a double bond on a rigid and constrained substrate. In the system described by Breslow, rigidity is brought by the constrained molecular scaffold. This selective oxidation reaction of saturated carbons is directed by geometric control rather than intrinsic reactivity of the Bzp. A scaffold composed of a cholesterol molecule covalently bound to a Bzp *via* a more or less flexible  $(\text{CH}_2)_n$  alkane chain spacer was used to evaluate this reactivity (see Figure 61). The flexible substrate presenting a  $(\text{CH}_2)_n$  spacer with  $n=2$  shows a classical Bzp cross-linking reactivity, with formation of a C-C bond between the Bzp probe and the C7 or C14 of the cholesterol group.<sup>221</sup> With the inflexible substrate ( $n=1$ ), the reaction of the Bzp triplet excited state can also lead to an olefin product by dehydrogenation.<sup>220</sup> This UV-induced reaction consisting in the abstraction of two radical hydrogens (formal loss of  $\text{H}_2$ ) competes with the photo-cross-linking reaction leading to the C-C bond formation between Bzp and the substrate.

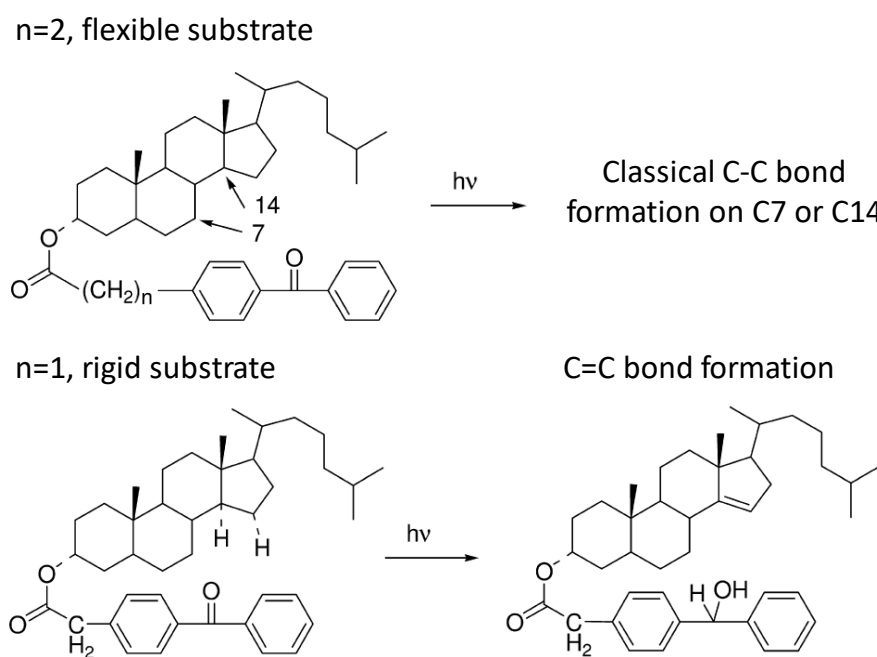


Figure 61. Bzp reactivity on the cholesterol substrate bound to the Bzp with a flexible spacer or in a rigid structure.<sup>220</sup>

### 3. Characterization of the Penetratin photoadducts in gas-phase fragmentation

The aim of this section is to describe the typical behavior of peptides subjected to MS/MS fragmentation, or tandem MS, in particular in MALDI TOF/TOF, which is the main instrument used in our experiments.

The MS process consists in sequential ionization, analysis and detection of analytes in the gas phase. Soft ionization techniques that do not induce fragmentation are required for MS analysis of biomolecules, such as electrospray ionization (ESI)<sup>222</sup> and matrix-assisted laser desorption ionization (MALDI)<sup>223</sup>. Tandem MS allows to refine the characterization of the analytes by gaining structural information. In the case of peptide MS analysis, it is a powerful tool to access the amino acid sequence.

The first step of an MS/MS experiment consists in the selection of the precursor ion of interest produced in the ion source. This ion is then activated, leading to its excitation (increase of its internal energy), and consecutive fragmentation when the required conditions are met. Afterwards, the fragment ions (daughter ions) are analyzed and detected. The actual experimental setup for MS/MS experiments can be very diverse. For MS/MS in space, two successive analyzers can be used, in different regions of the instrument (*i.e.* triple quadrupoles (TQ), Q/TOF, TOF/TOF). For MS/MS in time, successive sequences within the same enclosure are used (*i.e.* ion traps (IT), Fourier-transform ion cyclotron resonance, FT-ICR).

The activation of the accelerated precursor ion can occur in a collision cell filled with an inert gas such as nitrogen, argon or helium, leading to its excitation and potentially to its fragmentation. This type of dissociation is called collision-induced dissociation (CID) or collision-activated dissociation (CAD). Fragmentation can also be induced by capture of a low-energy electron < 1 eV (electron-capture dissociation, ECD) or electron transfer in a gas-phase ion-ion chemistry (electron-transfer dissociation, ETD). The odd-electron species formed then undergo rearrangement implying radical-type mechanism fragmentation.

In the case of CID fragmentation, before collisions with the gas, the initial internal energy of the precursor ion depends on the ionization process ( $E_{\text{int}}^0$ ). During the collision, energy is transferred to the center of mass ( $E_{\text{CM}}$ ) such that:

$$E_{\text{CM}} = E_{\text{k}} \times \frac{M_{\text{gas}}}{M_{\text{gas}} + M_{\text{incident precursor ion}}}$$

With  $E_{\text{k}}$  = kinetic energy of the incident precursor ion,  $M_{\text{gas}}$  = mass of the inert gas,  $M_{\text{incident precursor ion}}$  = mass of the incident precursor ion.

After collision, the precursor ion has an energy corresponding to the sum of the  $E_{\text{int}}^0$  and  $E_{\text{int}}^*$  the internal energy due to the collision itself. It represents a very small fraction of the  $E_{\text{CM}}$  especially if the  $E_{\text{k}}$  given to the precursor ion is low.

One can distinguish high and low collision energy fragmentation depending on the kinetic energy given to the parent ion, which determines the amount of energy given to the ion ( $E_{\text{int}}^0$ ).

Apart from the instrumental conditions used, the fragmentation pattern of a peptide depends on intrinsic factors such as the size of the peptide, the nature of the AAs and its charge state.

In this work, a MALDI-TOF/TOF instrument allowing CID fragmentation was used for the characterization of the Penetratin photoadducts induced by the Bzp-based photo-cross-linking. A scheme of the equipment is presented in Figure 62.

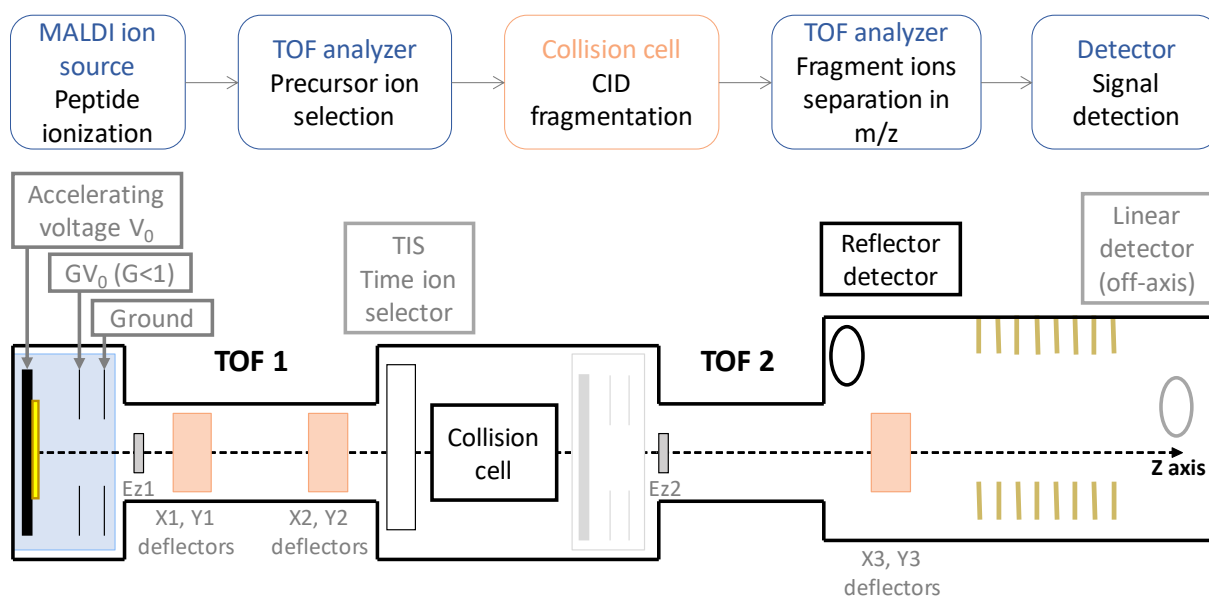


Figure 62. Scheme of a MALDI-TOF/TOF instrument.

In this equipment, high-energy CID fragmentation is performed. Ions are accelerated at a high kinetic energy of 1 keV, from 10 to 100-times higher than the usual values in ESI-trap-based fragmentation (20 eV). Ions with such a high internal energy are subjected to abundant fragmentations involving high-energy processes, leading to numerous consecutive dissociations. In general, high-energy CID allows the production of low-mass fragments like immonium ions that are usually not observed in low-energy CID.

### 3.1. Peptide fragmentation pathways

The aim of tandem MS is to produce a population of peptide fragment ions that differ in mass by an amino acid residue in order to characterize the amino acid sequence of the fragmented peptide, called the precursor peptide ion. A peptide bond can be fragmented at three different positions along the peptide backbone, giving different complementary ions. The commonly used nomenclature of the peptide bond fragmentation is represented in Figure 63. The N-term fragments are denoted by  $a_x$ ,  $b_x$ , and  $c_x$  where  $x$  is the number of amino acid residue  $\alpha$  carbons in the fragment ion. The complementary C-term fragment ions are denoted by  $x_z$ ,  $y_z$  and  $z_z$ , where  $(x + z)$  is the number of amino acid residues in the parent peptide ion.

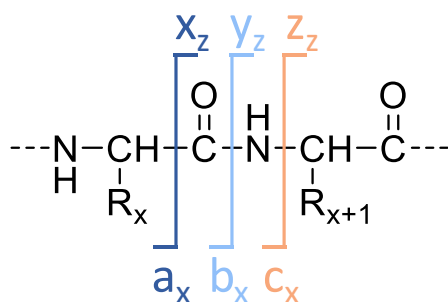


Figure 63. Peptide fragment ions nomenclature.<sup>224</sup>

CID dissociation consists in the collision of peptide cations with rare gas atoms. The gas collisions supply enough internal energy to the peptide cation to induce covalent bond cleavage. In these conditions, fragmentation occurs at the amide bonds, forming the structurally informative b and y ions that contain the N-term and the C-term, respectively (Figure 64).<sup>225–227</sup> Other consecutive neutral loss of water or ammonia are usually observed.

In electron-mediated dissociation (ExD) techniques, the radical fragmentation mechanisms are involved. These methods rely on the transfer of an electron from an appropriate donor to the protonated peptide. It leads to the formation of an even-electron c and odd-electron z<sup>\*</sup> ions (Figure 64).<sup>228</sup>

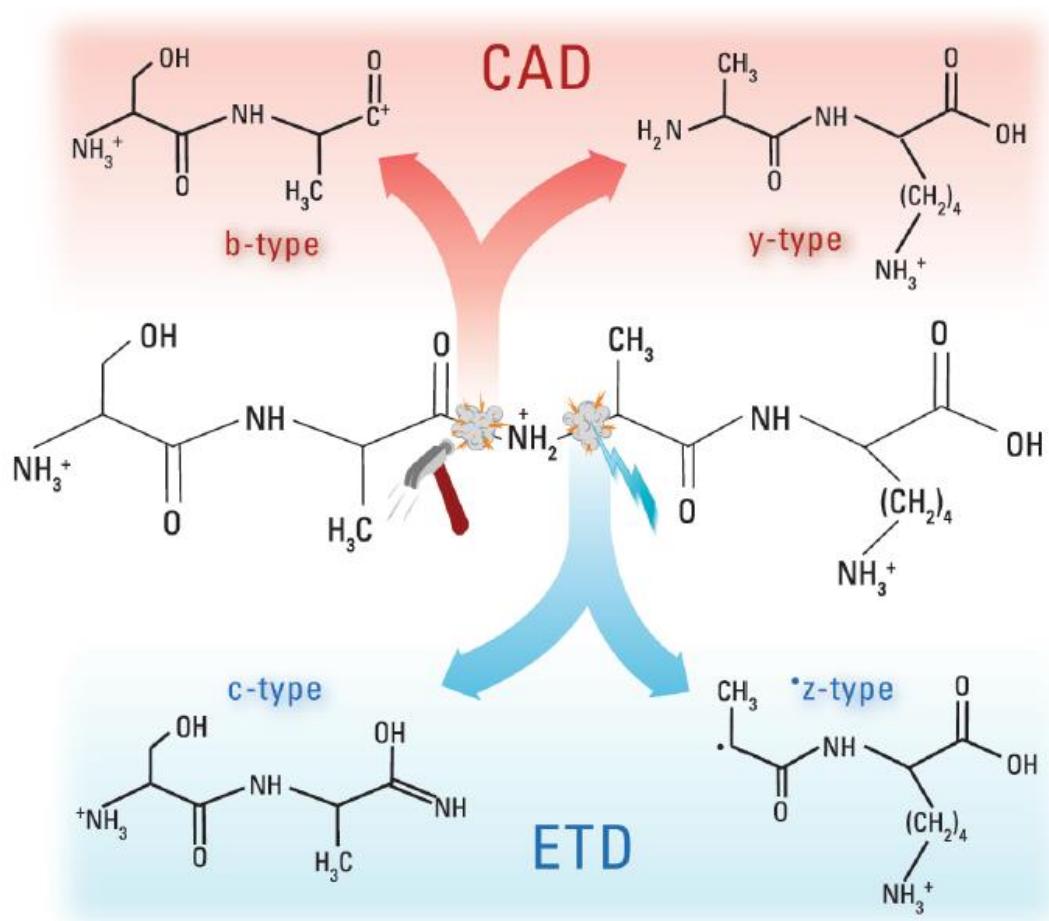


Figure 64. Fragment ion types produced from a multiprotonated parent ion following either CAD or ETD.<sup>228</sup>

An overview of the principal peptide fragmentation mechanisms by CID, leading to the formation of b and y ions, will be presented, as well as the main route for the formation of c and z ions in ExD. An emphasis will be made on the possible radical-type reactions, induced in the MALDI source by using a reducing matrix, that can also lead to c and z ions, usually typical of the electron-mediated dissociation.

### 3.1.1. CID fragmentation pathways, formation of b and y ions

#### THE MOBILE PROTON MODEL

Ionized peptides excited under CID collision conditions dissociate mainly by charge directed fragmentation.<sup>229</sup> Peptides can be protonated at various sites including side chain groups, N-term amino group, amide oxygens and nitrogens.

One or more protonation sites can be energetically and/or kinetically favored, leading to the sequestration of the additional proton, for example on a basic amino acid. In that case, an important energy is needed in order to mobilize the proton toward a less favored protonation site.

Moreover, molecular orbital calculations showed that the protonation on the amide nitrogen leads to a weakened amide bond, while the protonation on the amide oxygen stabilizes the amide bond.<sup>230</sup> However, the protonation on the amide nitrogen is thermodynamically unfavored compared to the protonation on the amide oxygen, on the N-term amino group or on a basic AA side chain.

Upon excitation by collision, the ions internal energy is increased, which can explain how the less favored protonation sites can be activated. The mobile proton model has been proposed by the group of Wysocki in 1996 to explain this phenomenon (Figure 65).<sup>231</sup> This model reflects the ability of the additional proton to migrate upon excitation toward various protonation sites before fragmentation. Thus, various isomers of the ionized peptide are assumed, leading to a larger population of fragments.

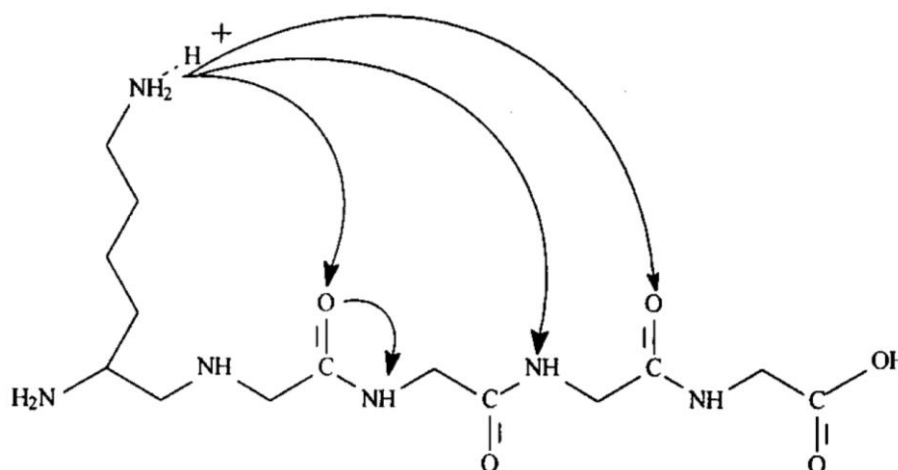


Figure 65. The mobile proton model.<sup>231</sup>

Under CID conditions most of the backbone cleavages of protonated amide bonds occur by rearrangement-type reactions. This is mainly due to the high energy needed for the direct bond

cleavage pathways to occur. Ions excited by CID do not have enough energy to fragment following these latter pathways. The majority of fragment ions are thus formed *via* rearrangement-type pathways.

The principal mechanisms for the formation of b and y ions involve an attack on the carbon center of the protonated amide bond either by the N-term neighbor amide oxygen<sup>232</sup> or by the nitrogen of the N-term AA group<sup>233</sup>. These two mechanisms are presented below, as well as an unconventional amide bond cleavage leading to the formation of a non-classical cyclic isoimide b ion.

#### THE CLASSICAL B<sub>x</sub>-Y<sub>z</sub> PEPTIDE FRAGMENTATION PATHWAY

The classical b<sub>x</sub>-y<sub>z</sub> fragmentation mechanism is depicted in Figure 66. The peptide protonation is first sequestered on the protonation site with the highest proton affinity, which can be the N-term amino group (as represented here) or a basic AA side chain.

The b<sub>x</sub>-y<sub>z</sub> fragmentation pathway is initiated by the transfer of the mobile added proton from the protonation site to the nitrogen of the amide bond where will occur the cleavage. The oxygen of the neighbor amide bond attacks the carbon center of the protonated amide bond *via* a nucleophilic attack, leading to the formation of a protonated oxazolone derivative.<sup>234–237</sup>

The rearrangement of the intermediate complex leads to a dimer of the two fragments sharing the added proton.<sup>232</sup> Dissociation of the proton-bound dimer is driven by the proton affinity of the fragment species, leading to a neutral fragment and a b<sub>x</sub> or y<sub>z</sub> ion. b<sub>x</sub> ions, as well as the neutral fragments complementary of the y<sub>z</sub> ions, are oxazolone derivatives.

Besides, y<sub>z</sub> ions have been reported to be protonated truncated peptides. They contain the added proton and the hydrogen coming from the nitrogen N-term of the cleaved amide bond, which migrated to the newly formed y<sub>z</sub> ion during the proton transfer step between the oxazolone derivative and the truncated peptide in the proton-bound dimer.<sup>233</sup>

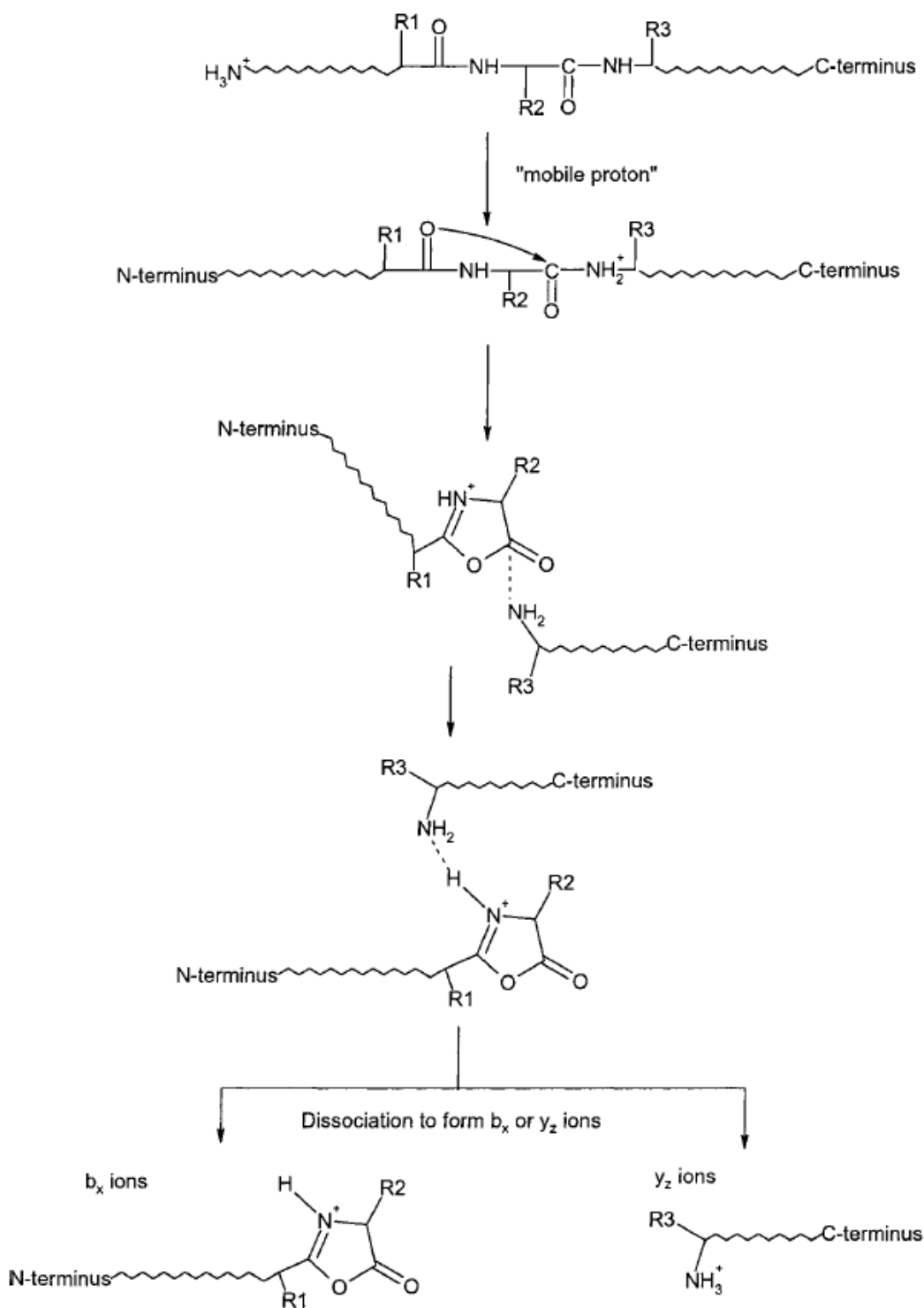
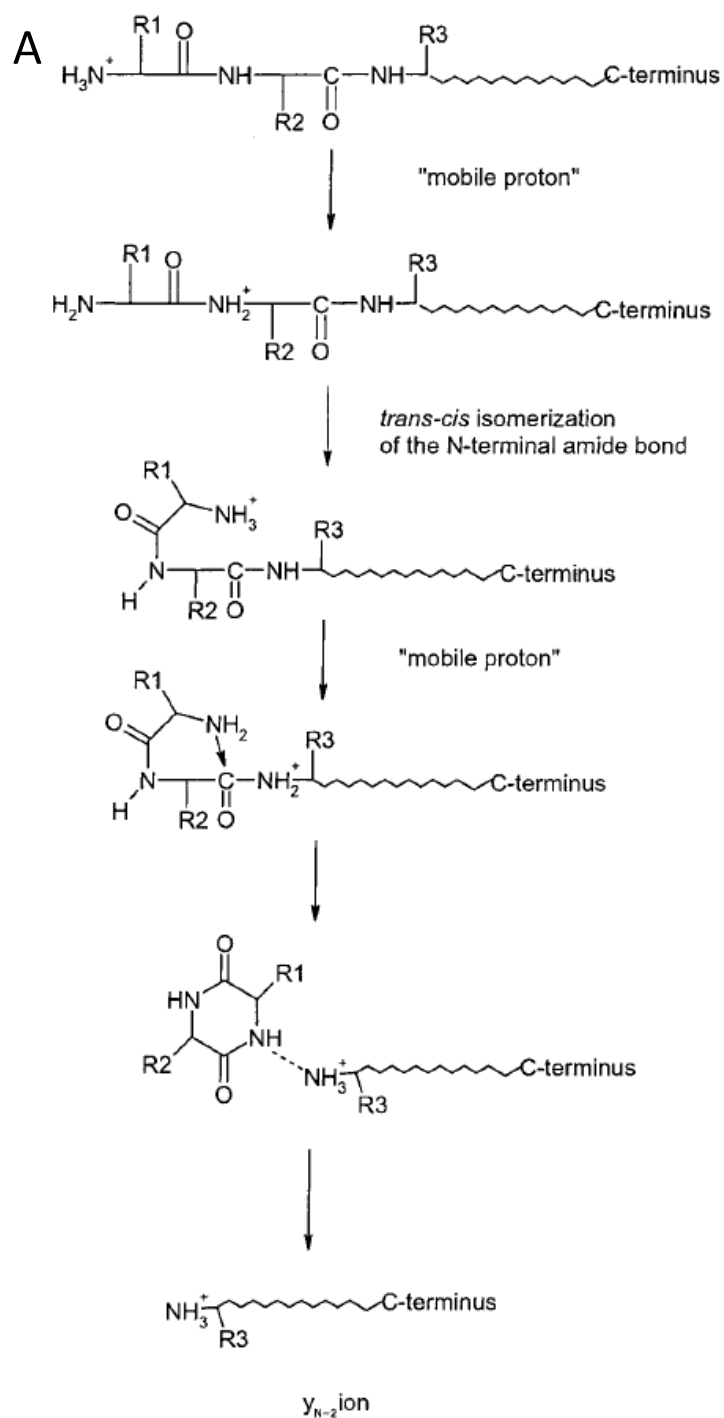


Figure 66. Classical fragmentation leading to the formation of the b (oxazolone) and y ions.<sup>229</sup>

#### THE DIKETOPIPERAZINE PEPTIDE FRAGMENTATION PATHWAYS

The classical b<sub>x</sub>-y<sub>z</sub> fragmentation mechanism cannot explain all observed fragment ions in CID MS/MS. In some cases, the neutral counterpart of the y<sub>z</sub> ion is a diketopiperazine derivative<sup>233</sup> (Figure 67). This pathway implies the mobilization of the added proton on the nitrogen of the amide bond to be cleaved. Actually, two diketopiperazine pathways exist, one leading to a y<sub>N-2</sub> ion (Figure 67A) and one leading to a y<sub>z</sub> or y<sub>N-n</sub> ion (when n>2, Figure 67B).

Diketopiperazine contains two cis amide bonds. Thus, *trans-cis* isomerization of the initially *trans* N-term amide bond is necessary in the diketopiperazine- $\gamma_{N-2}$  pathway, with protonation of the N-term amide bond.<sup>238</sup> The mobile proton is then moved to the nitrogen of the bond to be cleaved and the N-term amino group attacks the carbon center of the protonated amide bond. A loose complex is obtained, composed of the protonated diketopiperazine derivative and the leaving truncated peptide. Spontaneous proton transfer to the C-term fragment occurs, as the proton affinity of the obtained cyclic peptide is much lower than that of linear peptides. The complex dissociation thus leads to the  $\gamma_{N-2}$  ion and a neutral diketopiperazine derivative.





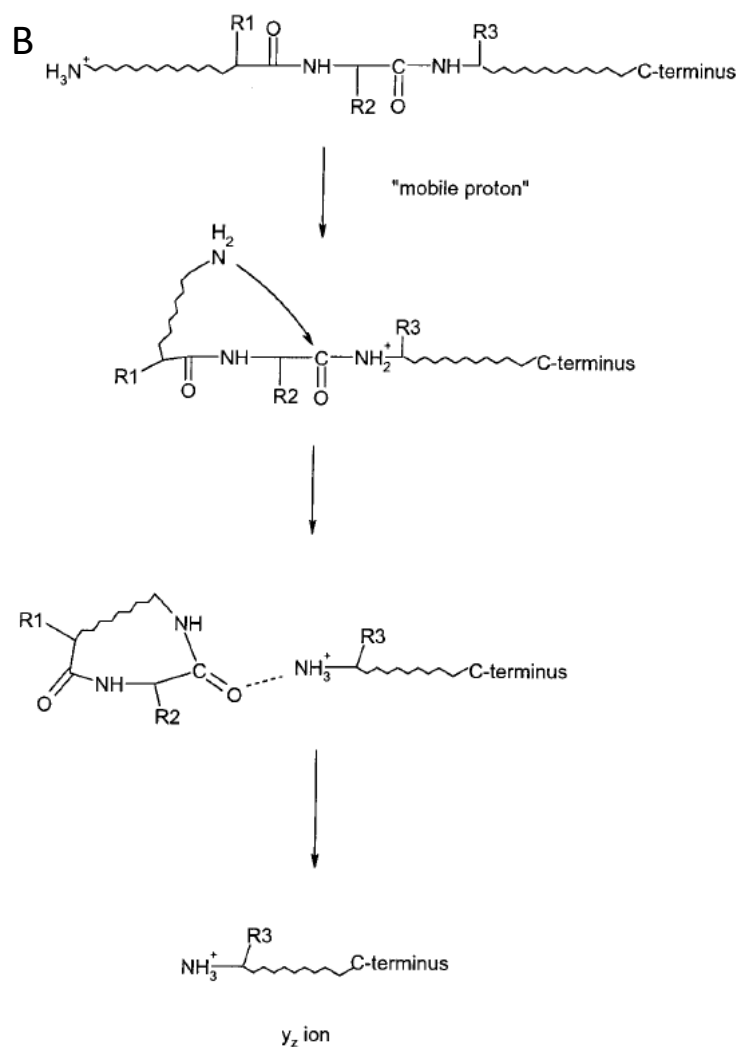


Figure 67. Diketopiperazine (A)  $y_{N-2}$  and (B)  $y_z$  or  $y_{N-n}$  pathway. N is the number of amino acid residues in the peptide and n is the amide bond cleaved.<sup>229</sup>

In the case of the  $y_{N-n}$  ion formation ( $n > 2$ ), the *cis-trans* isomerization is not necessary, as the neutral counterparts of the  $y_{N-n}$  ions are cyclic peptides that can adapt all of their amide bonds in the *trans* conformation.<sup>237</sup> This pathway is initiated by the mobilization of the added proton on the nitrogen of the amide bond to be cleaved. Nucleophilic attack of the N-term amino group on the carbon center of the protonated amide bond leads to the formation of the cyclic peptide in complex with the truncated  $y_{N-n}$  ion. Since the proton affinity of cyclic peptides is much lower than that of linear peptides, the added proton is transferred to the C-term fragment and the complex dissociates to form the  $y_{N-n}$  ( $n > 2$ ) ion and its complementary neutral cyclic peptide.

As it is the case for the classical  $b_x$ - $y_z$  fragmentation pathway, the  $y$  ions obtained by the diketopiperazine pathways are truncated protonated peptides. They contain the added proton and a hydrogen that was initially bound to a nitrogen N-term and was transferred to the truncated peptide upon cyclization of the N-term cyclic peptide during the formation of the diketopiperazine pathway complex.<sup>233</sup>

## PEPTIDE FRAGMENTATION PATHWAYS VIA NUCLEOPHILIC ATTACK OF SPECIFIC AMINO ACID SIDE CHAINS

Peptide fragmentation pathways can involve the interaction of the backbone functional groups, as previously presented, but some peptides can also dissociate *via* amide bond cleavage generated by nucleophilic attack of specific amino acid side chains to form non-classical  $b_x$  ions. This type of nucleophilic attack can be initiated by the side chains of histidine, glutamine, asparagine, lysine, and arginine residues located at the N-term neighbor of the considered protonated amide bond to be cleaved. It leads to various cyclic and non-classical N-term ions. Competition with the classical  $b_x$ - $y_z$  dissociation pathway can lead to a mixture of the two isomeric forms of the fragments N-term to the cleavage site, oxazolone-derivative type and non-classical  $b$  ion type. Generally, the classical  $b_x$ - $y_z$  dissociation is dominant but the side chain induced-cleavage at the C-term of histidine and glutamine residues can sometimes occur in significant proportions.

As Penetratin contains a glutamine and an asparagine, the fragmentation pathways induced by the amide oxygen of these two AAs side chains will be presented here.

The initiation of this pathway consists in the mobilization of the added proton on the nitrogen of the amide bond in C-term to the Gln or Asn residue (Figure 68). It is followed by the nucleophilic attack of the amide oxygen of the Gln or Asn side chain on the carbon center of the protonated amide bond. A non-classical cyclic isoimide derivative  $b$  ion is formed.<sup>229</sup> Similarly to the classical  $b_x$ - $y_z$  pathway, a relatively stable dimeric complex is formed, composed of the cyclic isoimide and of the truncated C-term peptide. This complex dissociated after rearrangement and proton transfer between the fragments, determined by the proton affinity of the species involved.

The same amide bond can also be dissociated by the classical  $b_x$ - $y_z$  pathway which leads to the oxazolone  $b_x$  ion and therefore it is possible to form isomers of the fragment  $b$  ion N-term to the cleavage site. Evidence of the co-existence of the two isomers in the mass spectrometer has been reported upon fragmentation of short Gln- or Asn-containing sequences.<sup>239-241</sup> These studies also revealed that the oxazolone isomer is more stable than the isoimide one for both the Gln- and Asn-containing  $b$  ions. Moreover, the relative energies of the two isomers are much closer for the Gln- than for the Asn-containing peptides. Also, cleavage of the amide bond C-term to Asn and Gln involving nucleophilic attack of the side chain amide nitrogen has been calculated to be energetically unfavored.

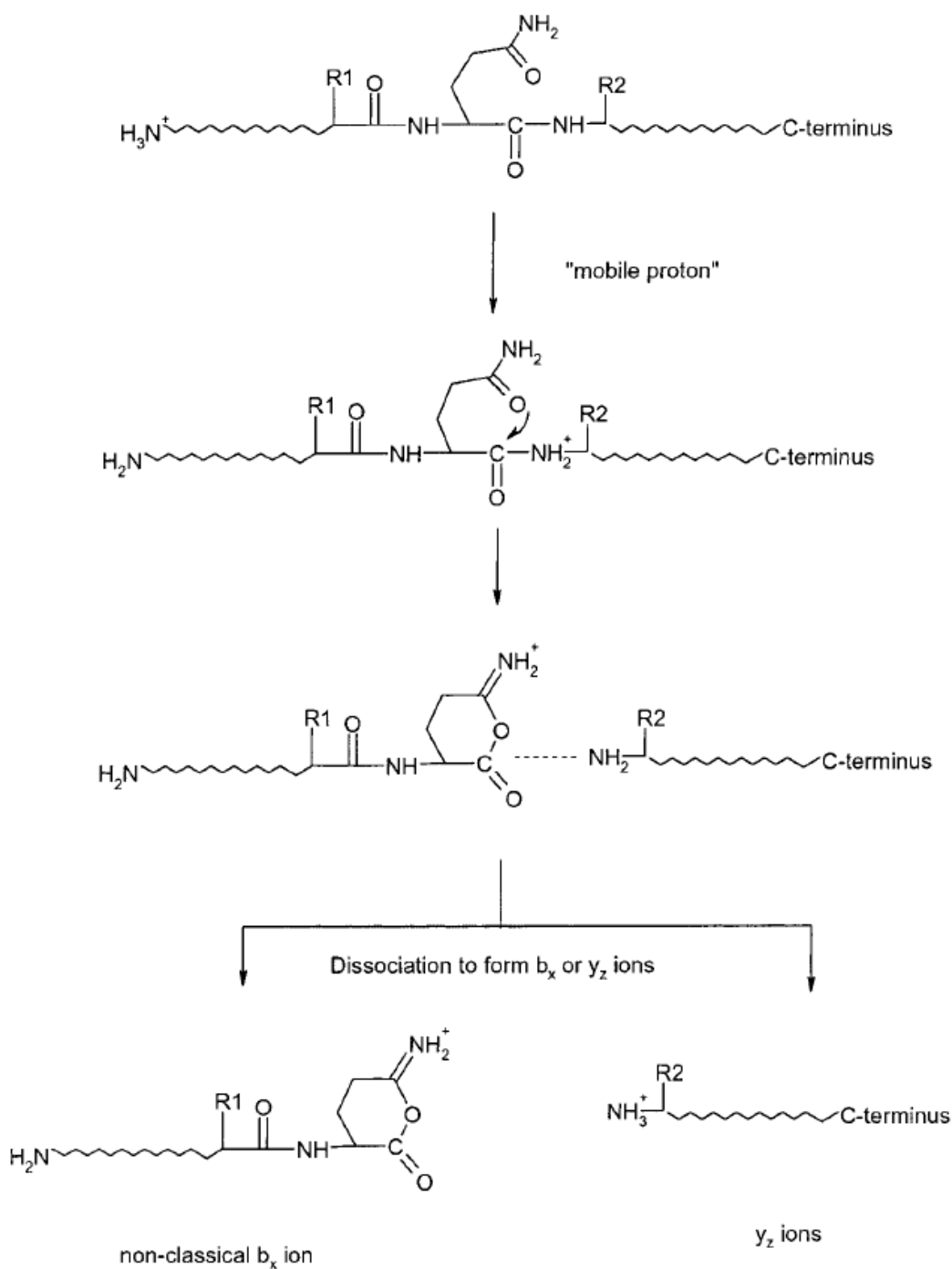
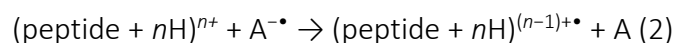
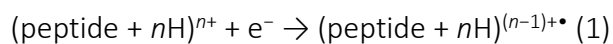


Figure 68. Non-classical amide bond cleavage initiated by the Gln side chain leading to the formation of a non-classical cyclic isoimide  $b$  ion.<sup>229</sup>

### 3.1.2. ExD and radical mechanisms, formation of $c$ and $z$ ions

Electron-mediated dissociation is initiated by the production of peptide cation radicals *via* collisional electron transfer from a suitable donor. The electron donor can be a simple electron flow (ECD),<sup>242</sup> a neutral atom or molecule (electron capture-induced dissociation, ECID) or a anion radical (ETD)<sup>243</sup> (see equations 1 to 3).<sup>244</sup>



ECD, ETD, and ECID can be referred to under the acronym of ExD. The association of an electron to the protonated peptide generates fragile radical species. Despite their differences, the ExD mechanisms all involve the formation of an aminoketyl radical intermediate that gives rise to radical-type of fragmentation pathways, and leads to the formation of c and z ions, as depicted on Figure 69.

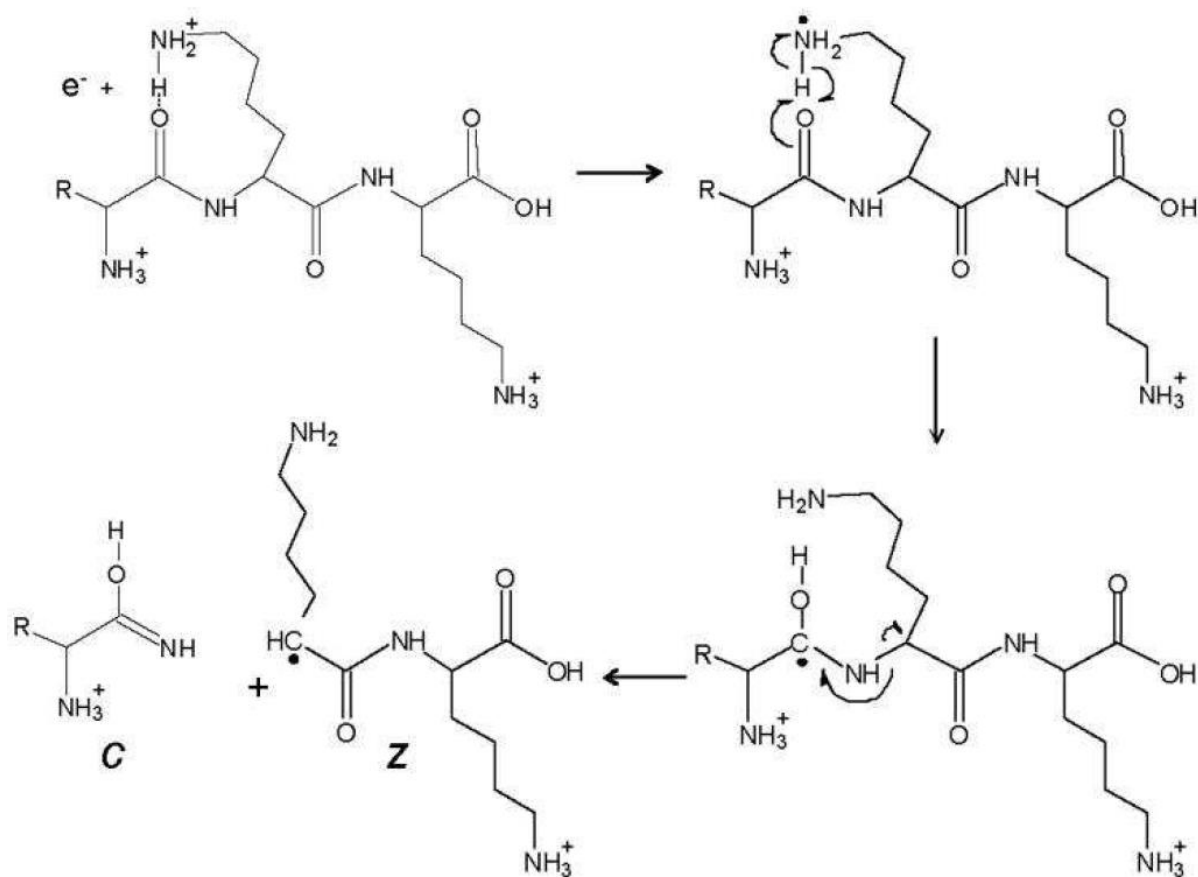


Figure 69. ETD fragmentation scheme. Fragmentation scheme of a multiply protonated peptide after reaction with a low energy electron to produce c- and z-type ions.<sup>245</sup>

### 3.1.3. Radical fragmentation induced by a reducing matrix

Usually observed in electron-induced dissociation, c and z ions can be less classically formed in the ion source when using a reducing matrix, promoting radical mechanisms. As they are formed in the MALDI source, these produced ions will be detected as a resolved ion signal at their expected m/z values. This type of reaction is called in-source decay (ISD) and can occur when using matrices able to release hydrogen radicals upon the UV-laser irradiation of the MALDI. The hydrogen radicals can react with the analyte peptide to produce radical species that can further undergo specific dissociations. They can lead to c and z ions by the mechanism presented in Figure 70.

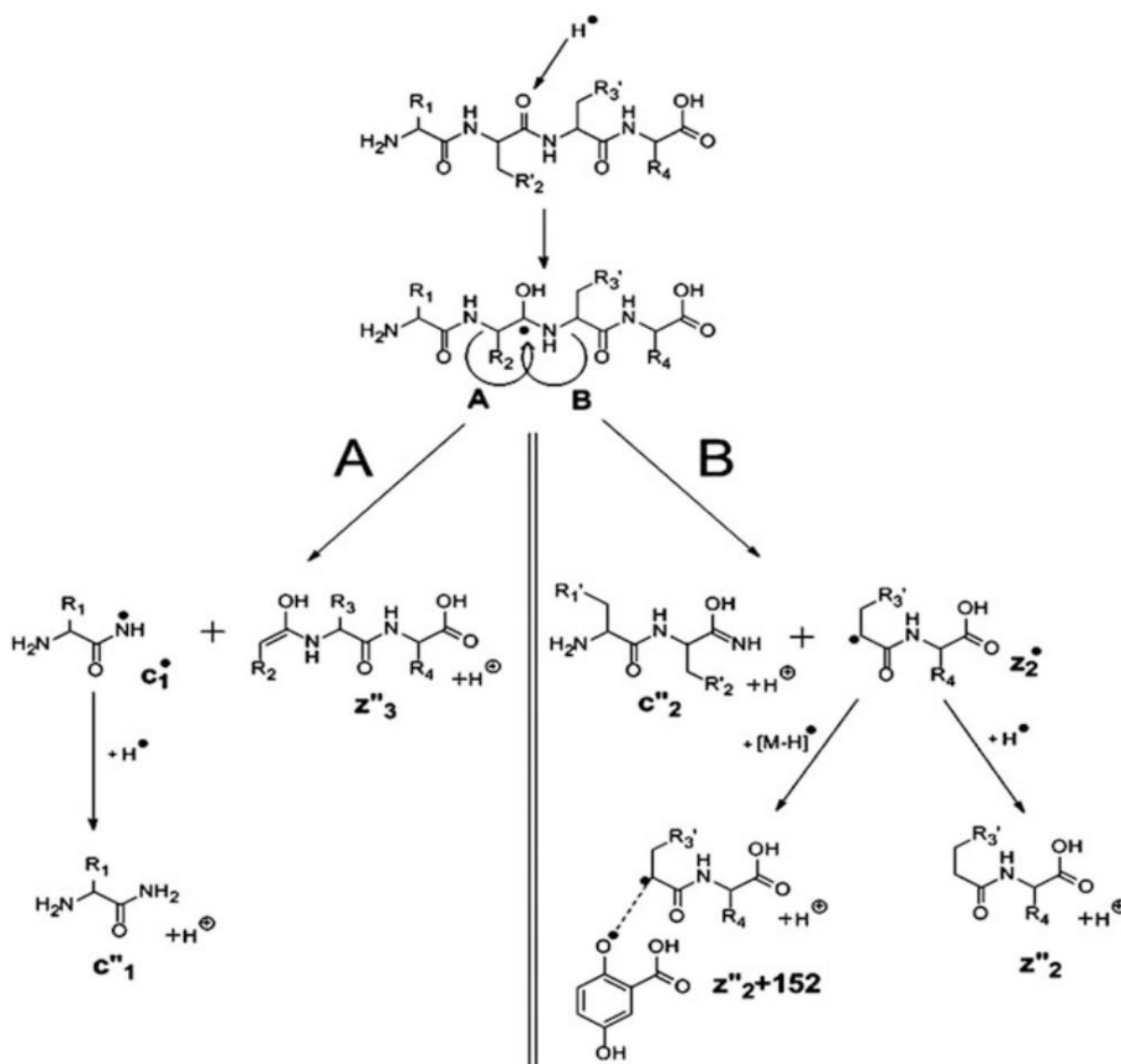


Figure 70. Radical mechanism for the formation of c- and z-fragments by a  $H^\bullet$  transfer from a reducing matrix.<sup>246</sup>

The 2,5-dihydroxybenzoic acid (2,5-DHB) was chosen as matrix for the analysis of the Bzp-induced photo-cross-linking because it is the matrix of choice to ionize lipids<sup>247,248</sup> and because it has been shown that it was also the best one for peptide-lipid photoadducts.<sup>5</sup> It is a reducing matrix, known to induce ISD in the MALDI ion source.<sup>246</sup> This process involves a prompt  $H^\bullet$  transfer from the 2,5-DHB matrix, which results in protonated radical species very similar to the ones produced by electron-mediated dissociation.

Apart from peptide cleavage, ISD induced by reducing matrices can also lead to the reduction of disulfide bonds due to the high hydrogen atom affinity of sulfur atoms. Cleavage of one disulfide bond implies the addition of two hydrogen radicals, resulting in +2u shift in the peptide mass, leading to the deformation of the isotopic distribution by an increased intensity of  $[M+2H+H]^+$ .<sup>249</sup>

The peptide structuration and insertion in the model membrane, the membrane composition, unsaturation degree and lamellar state are all important factors to consider when using the Bzp-induced photo-cross-linking method. The Bzp photoreactivity will be impacted by these parameters and the typical reactions of the Bzp triplet excited state, mainly reported in solution, will be observed in a more complex system that is a lipid membrane. Moreover, the peptide fragmentation pathways have to be kept in mind for a good characterization of the produced photoadducts species.

## Results and discussion

When used as a photo-cross-linking reagent, H<sup>•</sup> abstraction type reactivity is exploited to create a covalent C-C bond between two non-covalent interaction partners. This reaction is shown on Figure 71 in the specific context of a photoreactive Bzp-modified peptide and a lipid interaction partner (C-C bond, molecules **2** and **3**). Covalent bond formation can also occur through a [2+2] cycloaddition on a C=C double bond leading to an oxetane ring (P-B reaction), shown on Figure 71 (Oxetane, molecule **5**). Other secondary reactions have also been described, such as dimerization of molecules containing C=C double bonds (Figure 71, lipid dimer, molecule **7**) after sensitization of the corresponding molecule by triplet excited Bzp (Figure 71, molecule **6\***), or Bzp-assisted photooxidation through H<sup>•</sup> abstraction leading to the formation of a new C=C double bond (Figure 71, double bond, molecule **4**).<sup>219,220</sup> Most of these reactions are reported in the literature and were identified independently using small molecules in solution.<sup>250</sup> In the present study, we used Bzp photo-cross-linking coupled to MS to study the non-covalent interactions between CPPs and lipid bilayers.

Direct translocation is a purely physico-chemical process involving membrane destabilization by the CPP whereas endocytosis is thought to be more dependent on other membrane binding partners such as proteoglycans. Getting a precise molecular knowledge of CPP/lipids interactions is crucial for a better understanding of those internalization pathways.<sup>251</sup> Such non-covalent interactions can be studied by affinity photo-cross-linking using a peptide functionalized with a photoreactive probe.<sup>203</sup> Photo-cross-linking-based interactomics is a developing field, in particular for the study of protein or peptide-membrane interactions, using either photoreactive lipids,<sup>252–256</sup> or photoreactive peptides or proteins.<sup>257</sup> There are very few studies focusing on identification of CPPs membrane interaction partners. In 2016, the proteoglycan syndecan-4 was identified as a primary cell-surface target for octaarginine, using a diazirine-modified peptide.<sup>258</sup> Work from our group focused on Bzp-functionalized CPPs to identify lipid-type partners.<sup>5,259</sup> By comparing various photoactive probes, it showed that Bzp is the most adequate to study peptide/lipid interactions.<sup>259</sup> Its hydrophobicity, guaranteeing good insertion in lipid membranes, and its long history in lipids labelling, makes Bzp a photoprobe of choice for these systems. Upon irradiation, the photoreactive CPP functionalized with a Bzp can form a covalent C-C bond with a methylene group (CH<sub>2</sub>) of the lipid fatty acid chain in its immediate environment (Figure 71), as commonly described in the literature.<sup>203</sup> Kinetics for the radical hydrogen abstraction step vary according to the nature of the phospholipids acyl chains.<sup>181</sup> More recently, our group showed that the CPP Penetratin interacts more preferably with negatively charged phospholipids, with unsaturated and/or short fatty acid chains, using Bzp-based photo-cross-linking coupled to MS.<sup>5</sup>

The CPP properties of the Bzp-functionalized peptides will be evaluated on their internalization efficiency in cells and on their effect on the phase behavior of negatively charged liposomes. Photo-cross-linking efficiency of these peptides will also be estimated. Then, a mapping of the observed Bzp photoreactivity in lipid membranes will be presented. It will be highlighted how to exploit secondary reactions of the photo-cross-linking experiment to retrieve valuable information on the peptide-model membrane non-covalent interactions. An analytical

workflow for the interpretation of MS spectra will be presented, giving access to information on the CPP/lipid interaction at a molecular level such as depth of insertion or membrane fluidity in the CPP vicinity. An application of this workflow illustrates the role of cholesterol in the CPP/lipids interaction. In addition, observation of an unconventional CID gas-phase fragmentation of Penetratin by MALDI-TOF/TOF will be discussed. This work has been published in *Analytical Chemistry* in 2019 (in Appendix).<sup>6</sup>



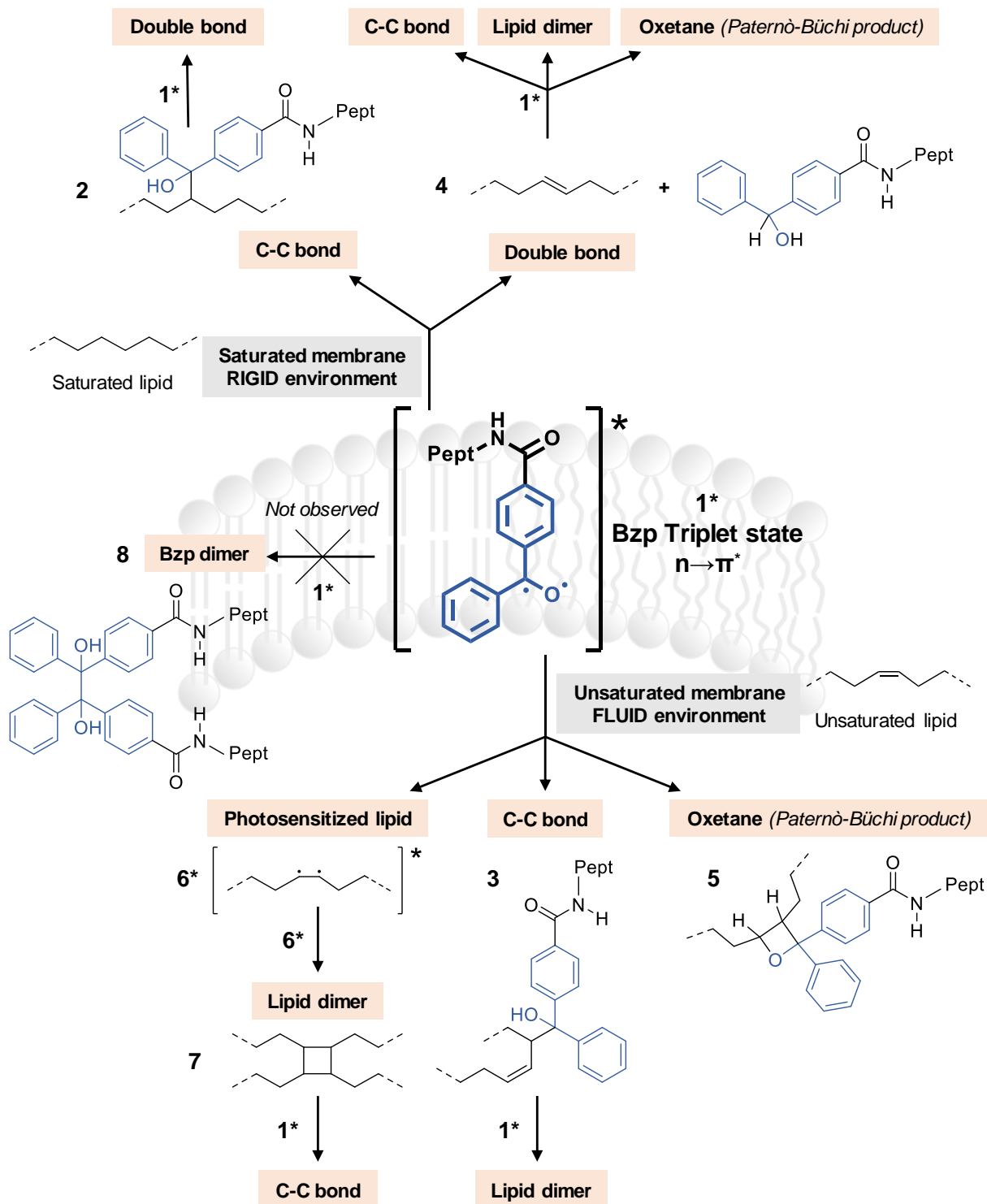


Figure 71. Observed Photochemical reactions of the Bzp triplet biradical ( $1^*$ ) in model membranes composed of saturated or unsaturated lipids (See text).

## 1. CPP properties of Bzp-functionalized peptides

The CPP Penetratin was functionalized with a Bzp probe for the photo-cross-linking experiment. The Bzp probe was either positioned at the N-term of the Penetratin sequence, or positioned inside the sequence, replacing the tryptophan 48. The first analogue is designed to keep intact the Penetratin sequence. The second aims to maintain a similar hydrophobicity of the peptide. In fact, the hydrophobic tryptophan residues are suspected to have a role in the internalization pathway by inserting between the hydrophobic tails of the membrane lipids. This second analogue is thus expected to have a membranotropic activity comparable with the one of Penetratin. Furthermore, incorporation of the aminopentanoic acid (Apa) spacer at the N-term of the peptide, between the biotin sulfone and the rest of the peptide, is supposed to induce better peptide recapture on streptavidin-coated magnetic beads. In total, 4 Penetratin analogues, and their corresponding deuterated versions containing 5 deuterated glycine residues, were synthesized for the photo-cross-linking experiments and internalization assays: Biot(O<sub>2</sub>)-G<sub>5</sub>-K(Bzp)-pen (referred as Pen in the manuscript), Biot(O<sub>2</sub>)-Apa-G<sub>5</sub>-K(Bzp)-pen (referred as ApaPen in the manuscript), Biot(O<sub>2</sub>)-G<sub>5</sub>-pen(K<sup>48</sup>Bzp) and Biot(O<sub>2</sub>)-Apa-G<sub>5</sub>-pen(K<sup>48</sup>Bzp). Penetratin analogues were tested in internalization experiments on CHO-K1 cells and their effect on thermotropic phase behavior of DMPC and PIP<sub>2</sub>-containing liposomes were measured in DSC. Photo-cross-linking experiments were also conducted with the (R/W)<sub>9</sub> CPP, which was functionalized with a Bzp placed at the N-term of the sequence: Biot(O<sub>2</sub>)-G<sub>5</sub>-K(Bzp)-(R/W)<sub>9</sub>.

### 1.1. Internalization efficiency of the Penetratin analogues

Internalization in cells of photoactivable Penetratin was quantified using the Burlina et al. method,<sup>175</sup> described in Part 1 of this manuscript. One million cells were incubated with peptides for 1 hour at 37°C. The membrane bound peptide was digested with trypsin. Extracellular concentration of peptides was 10 µM. It showed that Penetratin functionalization with a Bzp photoprobe does not reduce its cell penetration ability (Figure 72), but rather enhances it, probably due to the higher hydrophobicity of the Bzp-functionalized peptide.

Differences in internalized peptide quantity measured for Biot(O<sub>2</sub>)-G<sub>5</sub>-K(Bzp)-pen and Biot(O<sub>2</sub>)-G<sub>5</sub>-pen were highly significant ( $p < 0.001$ ). An enhancement of almost 7-fold of the internalization is observed with the Bzp on the peptide, probably due to a higher hydrophobicity of the peptide and thus a better insertion in the lipid membrane. As previously showed,<sup>4</sup> Bzp does not impair the CPP properties of Penetratin. Biot(O<sub>2</sub>)-G<sub>5</sub>-pen(K<sup>48</sup>Bzp) internalization properties are closer to the ones of Biot(O<sub>2</sub>)-G<sub>5</sub>-pen, as expected. Still, it shows 3 times more internalized peptide compared to the non-photoreactive peptide. The impact of Apa incorporation on the internalization is less clear. In the case of the Biot(O<sub>2</sub>)-Apa-G<sub>5</sub>-K(Bzp)-pen, presence of Apa spacer enhances the internalization efficiency by almost 2-fold, while in the case of Biot(O<sub>2</sub>)-Apa-G<sub>5</sub>-pen(K<sup>48</sup>Bzp), internalized peptide is decreased by a factor 2 compared to the same peptide without Apa. In all cases, the Bzp-functionalized Penetratin analogues show higher internalization efficiency than the non-photoreactive Penetratin.

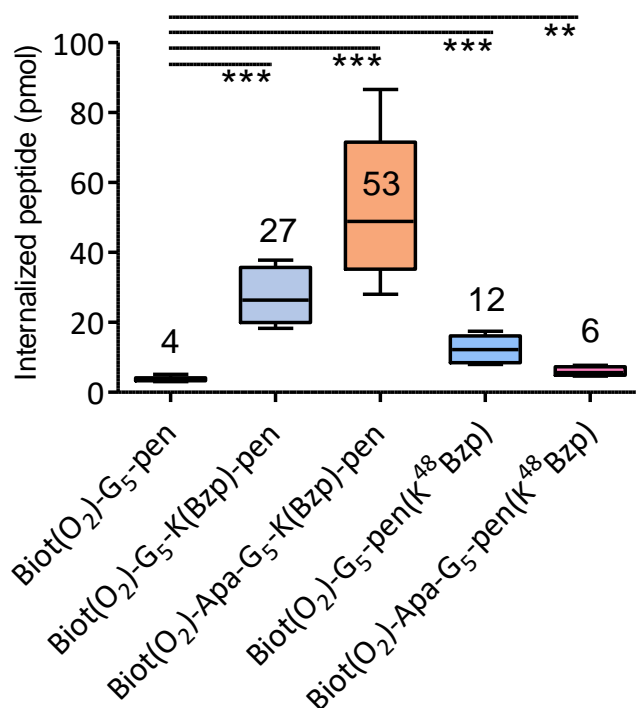


Figure 72. Quantification of internalized cell penetrating peptides Bzp-functionalized Penetratin analogues and Penetratin Biot(O<sub>2</sub>)-G<sub>5</sub>-pen in wild type CHO-K1 cells as described in <sup>175</sup>. (error bars correspond to standard deviation on 6 replicates from 2 independent experiments)

## 1.2. Effect of the Penetratin analogues on thermotropic phase behavior of PIP<sub>2</sub>-containing liposomes

The effect of the Bzp-functionalized Penetratin analogues on the phase transitions of PIP<sub>2</sub>-containing MLVs was measured by DSC, for a peptide/lipid ratio of 1/25. Thermograms are presented in Figure 73, and the related thermodynamic parameters are given in Table 7.

As for the non-photoreactive Pen (results in Part 1), the Penetratin analogues do not impact the phase transitions of DMPC liposomes. Their influence on DMPC/PIP<sub>2</sub> (95/5) are very similar. They induce a recovering of the pre-transition signal and an increase of the main transition temperature, like it was the case for the non-photoreactive Penetratin.

A clear decrease of the main transition enthalpy can be observed for all peptides, showing that the peptides insert in the lipid bilayer and perturb the van der Waals interactions between the fatty acid chains of the lipids. This effect is enhanced compared to the results obtained for the non-photoreactive Penetratin (Part 1). Thus, the presence of the Bzp probe induces a better insertion of the peptide in the bilayer, which is consistent with previous results showing that the internalization efficiency is enhanced by the Bzp-functionalization of Penetratin. Moreover, the decrease in enthalpy is even more important on peptide containing an Apa spacer, which seems to anchor even better the peptide to the membrane.

In the case of peptides Biot(O<sub>2</sub>)-G<sub>5</sub>-K(Bzp)-pen (Pen) and Biot(O<sub>2</sub>)-Apa-G<sub>5</sub>-K(Bzp)-pen (ApaPen), a shoulder can be observed, below the half maximum of the peaks. Bzp positioning at the N-term of the sequence, which increases the hydrophobicity of the peptide, seems to induce a

partitioning in the membrane. For the two other peptides, the main transition peaks are narrow and no shoulder or peak splitting are observed.

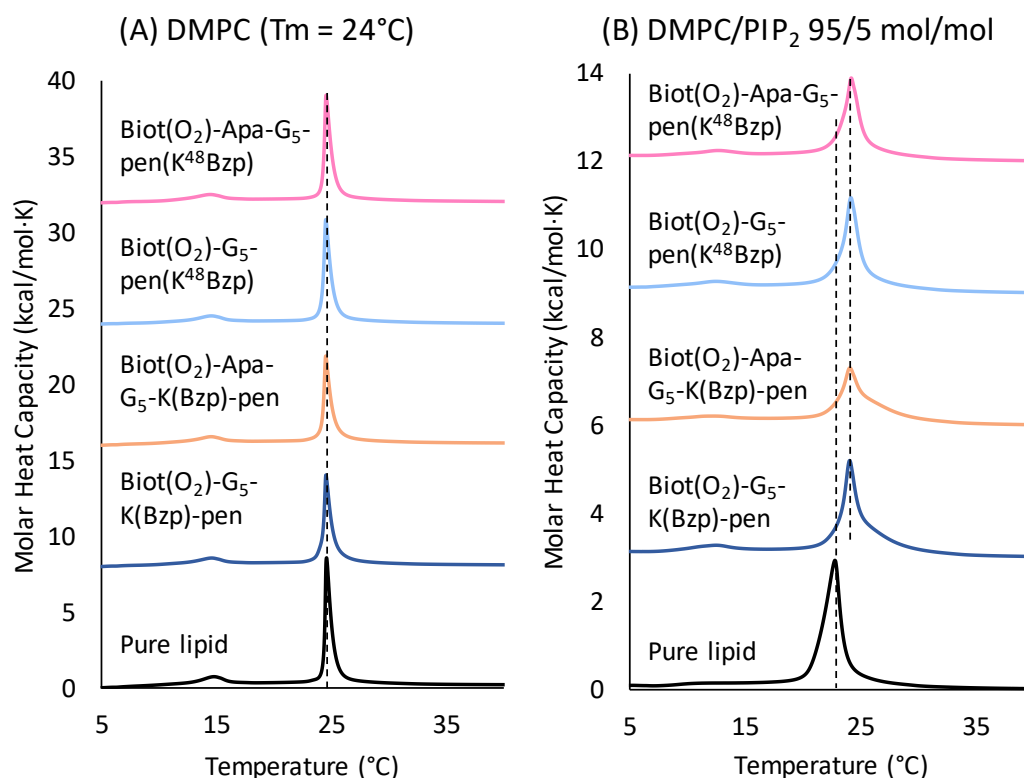


Figure 73. DSC heating scans illustrating the effect of the addition of Penetratin analogues on the thermotropic phase behavior of DMPC and PIP<sub>2</sub>-containing MLVs. The curves correspond to pure lipid and peptide to lipid ratio of 1/25.

Table 7. Thermodynamic parameters corresponding to DSC thermograms of phase behavior of DMPC and DMPC/Brain PIP<sub>2</sub> 5% (mol/mol) in presence of Bzp-functionalized Penetratin analogues, for ratios peptide/lipid of 1/25.

DMPC	T <sub>pre</sub> (°C)	T <sub>m</sub> (°C)	ΔH <sub>m</sub> (kJ/mol)	FWHM (°C)
Pure lipid	14.8	24.6	25.8	0.6
Biot(O <sub>2</sub> )-G <sub>5</sub> - pen(K <sup>48</sup> Bzp)	14.6	24.5	23.0	0.6
Biot(O <sub>2</sub> )-Apa-G <sub>5</sub> - pen(K <sup>48</sup> Bzp)	14.5	24.5	22.6	0.6
Biot(O <sub>2</sub> )-G <sub>5</sub> -K(Bzp)-pen	14.6	24.5	21.6	0.6
Biot(O <sub>2</sub> )-Apa-G <sub>5</sub> -K(Bzp)-pen	14.5	24.5	19.9	0.6
Pen/DMPC: PIP <sub>2</sub> 5% mol	T <sub>pre</sub> (°C)	T <sub>m</sub> (°C)	ΔH <sub>m</sub> (kJ/mol)	FWHM (°C)
Pure lipid	-	22.8	23.8	1.6
Biot(O <sub>2</sub> )-G <sub>5</sub> - pen(K <sup>48</sup> Bzp)	12.5	24.2	17.7	1.3
Biot(O <sub>2</sub> )-Apa-G <sub>5</sub> - pen(K <sup>48</sup> Bzp)	12.8	24.3	15.1	1.4
Biot(O <sub>2</sub> )-G <sub>5</sub> -K(Bzp)-pen	12.5	24.1	19.6	1.3
Biot(O <sub>2</sub> )-Apa-G <sub>5</sub> -K(Bzp)-pen	12.1	24.2	15.3	1.9

To resume, Bzp-functionalized Penetratin analogues show similar behavior in presence of lipid bilayers. Their internalization properties are not impaired by the presence of the Bzp probe and they have similar influence on the thermotropic phase behavior of liposomes composed of DMPC or DMPC/PIP<sub>2</sub> 95/5. Nevertheless, their behavior can be more or less pronounced depending on the Bzp positioning in the sequence and presence or not of an Apa spacer. Photo-cross-linking yields of these peptides should as well be influenced by these parameters.

### 1.3. Photo-cross-linking efficiency of the Bzp-functionalized Penetratin analogues on DMPG liposomes

The photo-cross-linking efficiency of the Bzp-functionalized Penetratin analogues was tested on DMPG liposomes. The theoretical masses and isotopic distributions for photoadducts containing myristic acid (MA) are presented in Figure 74, for each Penetratin analogue. MALDI-TOF spectra are shown in Figure 75.

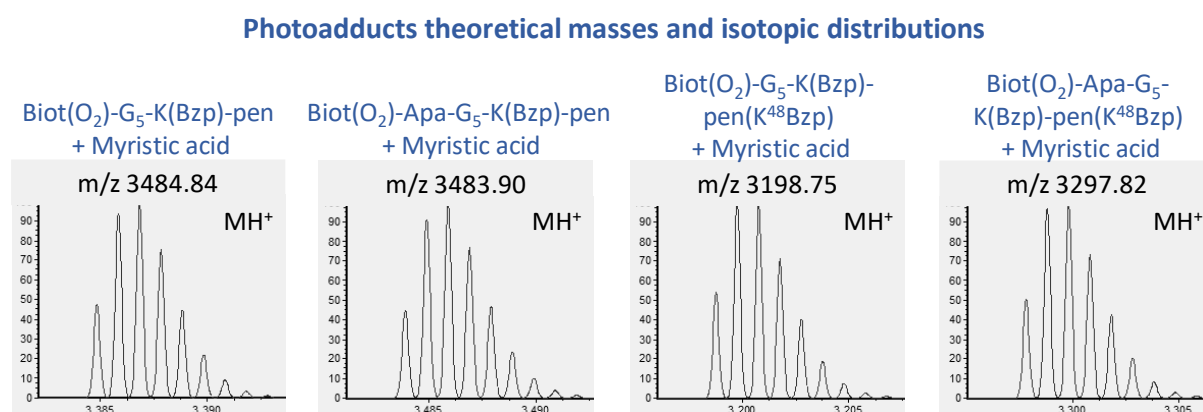


Figure 74. Photoadducts theoretical masses and isotopic distributions obtained with Isopro, corresponding to the Bzp-functionalized Penetratin analogues covalently bound to myristic acid.

Photoadducts containing the Penetratin analogue covalently bound to myristic acid are detected with high signal intensity. In all cases, the observed photoadduct is shifted to the lower mass and the first isotope is detected at - 2u in comparison to the theoretical one. This shift is very reproducible and is observed no matter the peptide sequence. It will be discussed more deeply in the following section, dealing with the mapping of the Bzp photoreactivity in lipid membranes.

Since MALDI ionization of the photoadducts only relies on the peptide moiety (no ionization site on the fatty acid part), the intensity of the ion species likely reflects the relative proportion between the photoadducts and the peptide in the MLVs.<sup>5</sup> Therefore, we assume that the relative intensities between Penetratin and photoadducts are proportional to the photolabeling yields.

The two peptides that contain the Apa spacer show slightly more intense signals for the photoadduct compared to the signal of the Penetratin alone. The Penetratin analogues show comparable properties that are more or less pronounced depending on the sequence considered. Thus, the choice of a Penetratin analogue can be adapted to the requested

experiment. For instance, the peptides containing the Apa spacer can be used for interaction partners identification when the interaction partner is present in low amounts in the liposomes. This allows to generate higher photo-cross-linking signals and improves the method sensitivity, as it is the case for the experiments conducted on PIP<sub>2</sub>-containing liposomes presented in Part 1 of this manuscript, where the Biot(O<sub>2</sub>)-Apa-G<sub>5</sub>-K(Bzp)-pen was used.

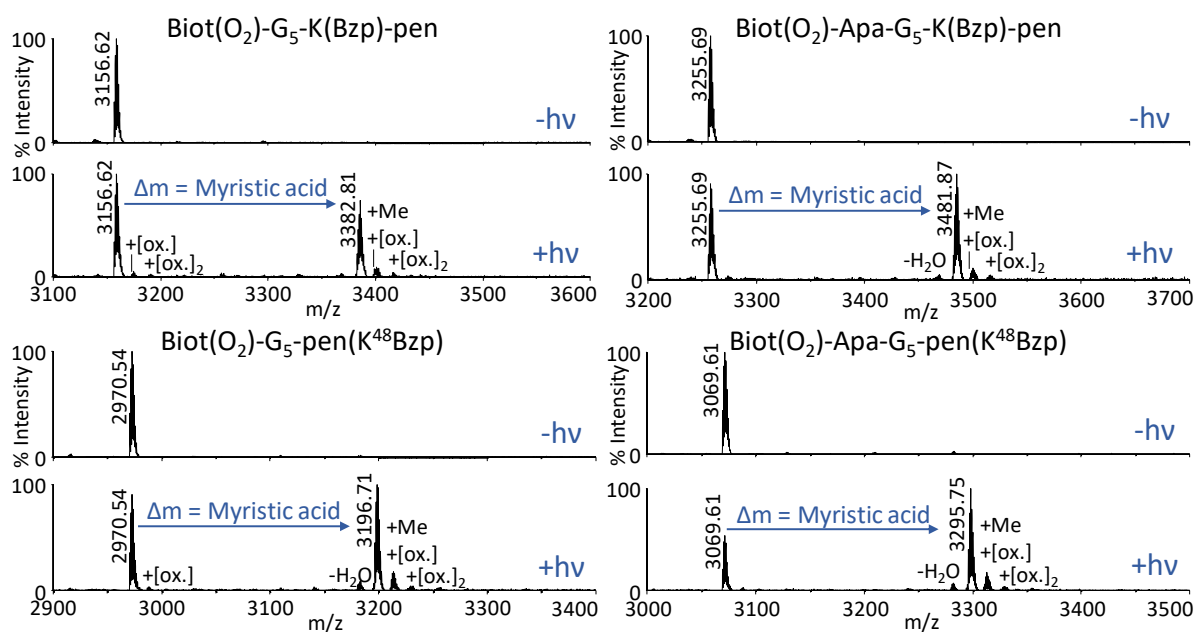


Figure 75. MALDI-TOF spectra (positive ions, reflector mode) of the Bzp-induced photo-cross-linking between Penetratin analogues and negatively charged MLVs of DMPG. Top to bottom: Control Pen without irradiation (-hv), Pen+DMPG+hv, for each Penetratin analogue sequence. Similar conditions of analysis were used in all spectra of the manuscript, 2,5-DHB is used as the matrix. Me: methylation, [ox.]: oxidation.

The Penetratin analogue Biot(O<sub>2</sub>)-G<sub>5</sub>-K(Bzp)-pen was chosen to conduct the protocol optimizations and the evaluation of the photoreactivity of Bzp in the context of a model membrane. These experiments were performed using 100% PG liposomes where the photo-cross-linking efficiency is high enough for good detection of the photoadducts. Also, the advantage of this sequence is that the integrity of the Penetratin sequence is maintained.

#### 1.4. Effect of Bzp-functionalized Penetratin and (R/W)<sub>9</sub> on thermotropic phase behavior of DMPG liposomes

Photo-cross-linking experiments optimization and study of the detailed photoreactivity of Bzp in model membranes was conducted on MLVs composed of 100% PG lipids. The peptides used for these experiments are Biot(O<sub>2</sub>)-G<sub>5</sub>-K(Bzp)-pen (Pen) and Biot(O<sub>2</sub>)-G<sub>5</sub>-K(Bzp)-(R/W)<sub>9</sub>. The effect of these peptides on the thermotropic phase behavior of DMPG liposomes was evaluated by DSC. Results are shown in Figure 76 and the corresponding thermodynamic parameters are presented in Table 8. Addition of the peptides to the MLVs suspension induces the loss of the pre-transition signal and an important enlargement of the main transition peak. Here, the main transition enthalpy is not decreased, suggesting that the peptides do not insert deeply in the PG membrane, as it has been previously shown in the literature.<sup>162,180</sup>

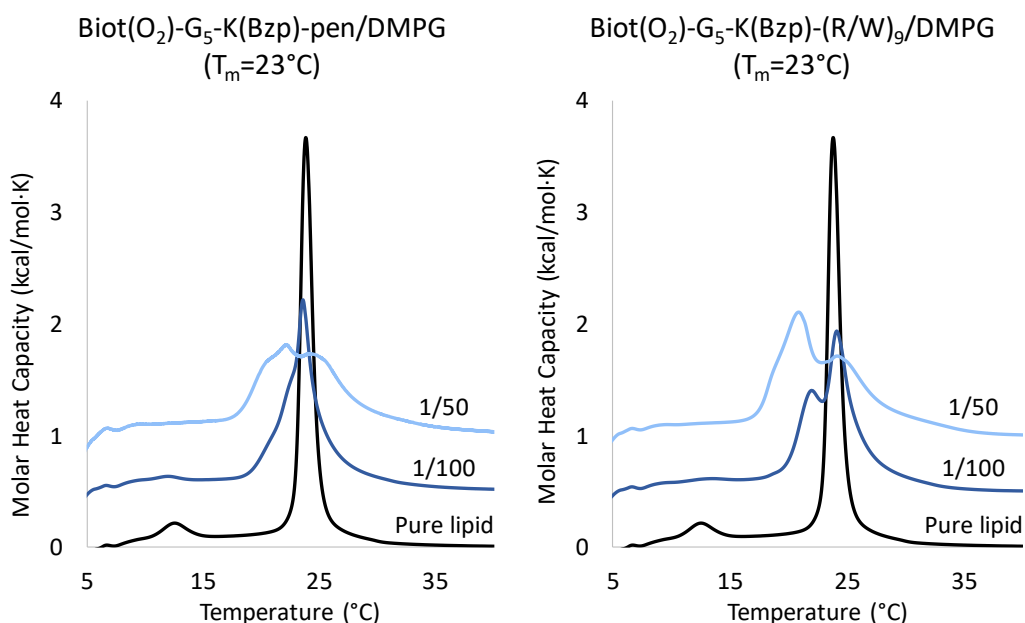


Figure 76. DSC heating scans illustrating the effect of the addition of Biot(O<sub>2</sub>)-G<sub>5</sub>-K(Bzp)-pen and Biot(O<sub>2</sub>)-G<sub>5</sub>-K(Bzp)-(R/W)<sub>9</sub> on the thermotropic phase behavior of DMPG MLVs. The curves correspond to pure lipid and peptide to lipid ratio of 1/100 and 1/50.

Table 8. Thermodynamic parameters corresponding to DSC thermograms of phase behavior of DMPG (mol/mol) in presence of Bzp-functionalized Penetratin and (R/W)<sub>9</sub> analogues, for ratios peptide/lipid of 1/100 and 1/50.

DMPG	T <sub>pre</sub> (°C)	T <sub>m</sub> (°C)	ΔH <sub>m</sub> (kJ/mol)	FWHM (°C)
Pure lipid	15.6	23.9	20.7	1.1
Biot(O <sub>2</sub> )-G <sub>5</sub> -K(Bzp)-pen 1/100	-	23.6	20.0	2.0
Biot(O <sub>2</sub> )-G <sub>5</sub> -K(Bzp)-pen 1/50	-	22.2	21.4	6.5
Biot(O <sub>2</sub> )-G <sub>5</sub> -K(Bzp)-(R/W) <sub>9</sub> 1/100	-	24.2	21.6	2.1
Biot(O <sub>2</sub> )-G <sub>5</sub> -K(Bzp)-(R/W) <sub>9</sub> 1/50	-	20.9	25.3	3.3

The shape of the main transition signal is greatly impacted by the presence of the peptides. Several domains are probably formed upon addition of the peptides to the MLVs. They can be lipid domains or peptide domains. As a pure lipid composition is considered here, the partitioning observed should be related to peptide-rich or peptide-poor domains. Indeed, (R/W)<sub>9</sub> is known to aggregate easily in solution and at the lipid membrane.<sup>260</sup> Peak deconvolution was performed on the main transition signals in presence of the peptides. Results are shown in Figure 77. It is clear that the transition signals are composed of different contributions. However, their composition obtained by peak deconvolution are quite complex and three contributions are needed to obtain a good correlation with the experimental curves. Still, an important trend can be highlighted from those simulations. It seems that, upon addition of increasing quantity of peptide, the contribution of a pure DMPG lipid region (T<sub>m</sub> observed here at 23.9°C) decreases (contribution peak in orange) in favor of the appearance of a contribution at a lower transition temperature (contribution peak in light blue). The effect is even more pronounced in the case of the (R/W)<sub>9</sub> peptide. A peptide-rich region would thus be

formed and would have a localized fluidifying effect on the lipid membrane (decrease of the transition temperature). By spreading in this localized region, lipids logically induce more compacity in the rest of the membrane, which explains the increase of transition temperature for the first contribution (in orange).

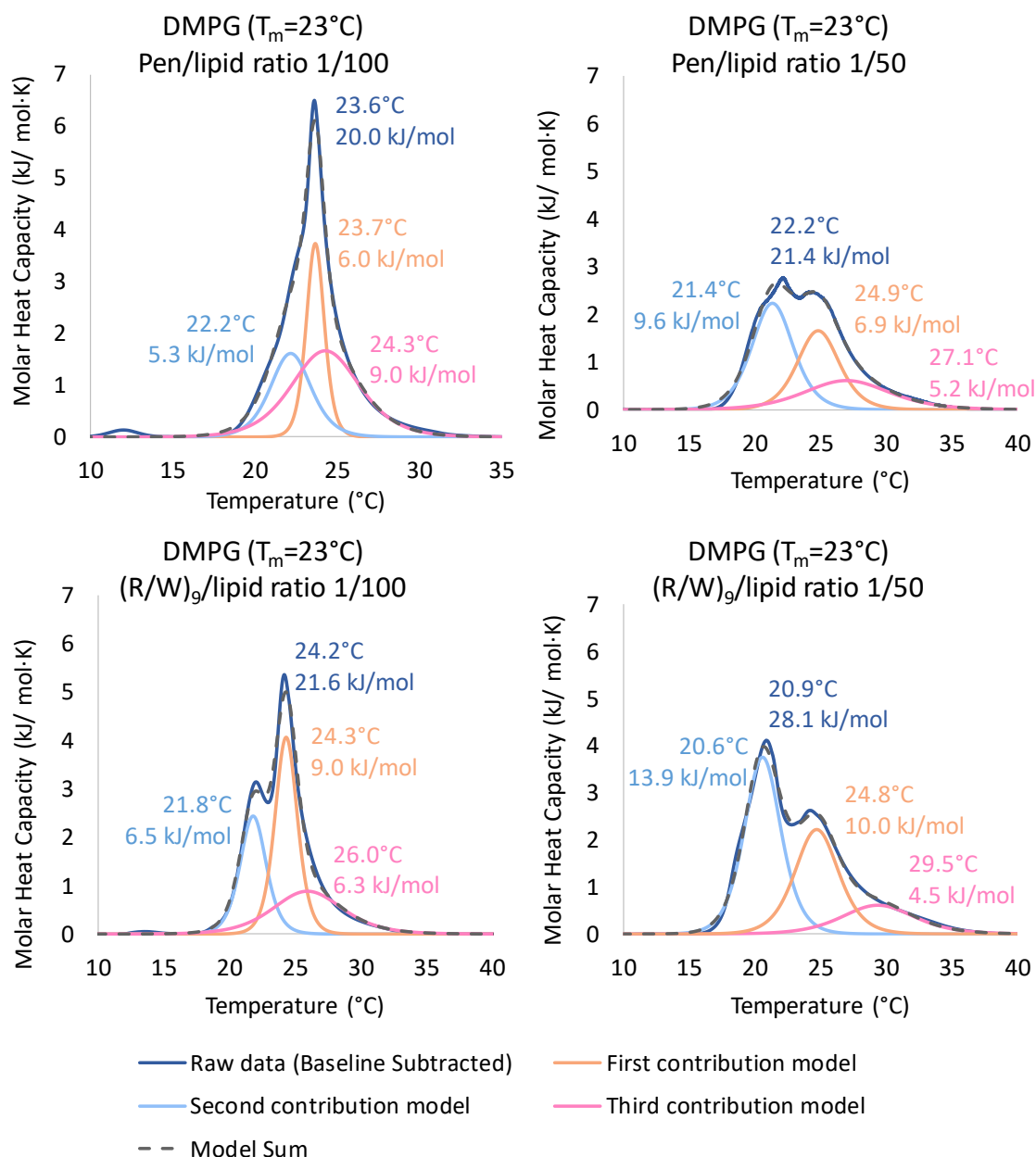


Figure 77. Deconvolution of the main transition signal of DSC thermograms obtain after Bzp-functionalized analogues of Penetratin (Biot(O<sub>2</sub>)-G<sub>5</sub>-K(εBzp)-pen) or (R/W)<sub>9</sub> (Biot(O<sub>2</sub>)-G<sub>5</sub>-K(εBzp)-(R/W)<sub>9</sub>) addition to MLVs of DMPG, at 1 mg/mL, for ratios peptide/lipid of 1/100 and 1/50. Experimental data, with corrected baseline, are in dark blue. The fitted model is shown as a dashed grey curve. Cooperativity of heterogeneous composition is modeled by three contributions, presented in orange, light blue and pink curves. The corresponding T<sub>m</sub> and ΔH<sub>m</sub> are also indicated on the graphs.

These results are well correlate to the literature on the interaction of Penetratin and (R/W)<sub>9</sub> with PG liposomes, evaluated by DSC measurements, whose thermograms aspect are very



similar to the ones we obtained with the Bzp-functionalized peptides. Indeed, Penetratin has been related to importantly impact the transition temperature, enthalpy and cooperativity of DMPG phase behavior, while it does not affect the phase transition of DMPC liposomes.<sup>145</sup> The same work also reports aggregation and precipitation effects of the peptide on the DMPG liposomes. As for the (R/W)<sub>9</sub> peptide, the main transition of DMPG liposomes is also greatly disturbed upon interaction with the peptide. (R/W)<sub>9</sub> induces a reduction of the phase transition temperature, cooperativity and pre-transition enthalpy until disappearance at peptide/lipid ratio 1/50, showing that the peptide interacts with the lipid polar heads of DMPG, favors the fluid phase. A broadening of the transition signal was also reported.<sup>261</sup>

To summarize, presence of a Bzp moiety covalently bound to the CPP has for effect to enhance the internalization properties of the peptide and does not change much the peptide effect on the thermotropic phase behavior of lipid membranes. Presence of the Bzp in the peptide sequence enhances the effect of the peptide on the phase transition of PIP<sub>2</sub>-containing liposomes in that the Bzp-functionalized peptide inserts deeper in this membrane, compared to the non-photoreactive peptide. In PG MLVs, the Bzp-functionalized peptides induce partitioning and seem to aggregate in some regions of the membrane. However, they do not insert deeply in PG membranes.

## 2. Mapping of the benzophenone photoreactivity in lipid membranes

In the present study, we fine-tuned the affinity photo-cross-linking protocol and MS detection parameters to significantly increase photo-cross-linking yields, and ions production and detection, resulting in high S/N MS spectra and improved sensitivity. By doing so, we detected secondary products of lower intensity compared to the photo-cross-linked ion species. These secondary reactions occurring during UV irradiation of the sample are highly informative.

Herein, we give a thorough mapping of the photoreactivity of Bzp coupled to two different CPPs (Penetratin and (R/W)<sub>9</sub>) to characterize their interaction with biomimetic lipid membranes. This model allowed to observe all the classical and less common reactivities of Bzp described on Figure 71 by direct MS analysis, either by MALDI (Figure 78) or ESI (Figure 79). We show that all these reactions can occur concomitantly in a single complex biological system: a membrane-active peptide inserted within a phospholipid bilayer. In particular, we show how they compete depending on the nature of the phospholipids we used and thus of the physicochemical state of the membrane surrounding the Bzp. Analysis of all the described reaction products can significantly improve characterization of CPP-membrane interactions using Bzp photo-cross-linking coupled to MS, by providing at least three types of information. First, identification of the classical C-C bond adduct(s) will give information on the nature of the lipids in the immediate peptide environment. Then, unusual isotopic distribution for the adduct peak can be used as a marker of membrane fluidity around the peptide. Finally, detection and identification of intermediate ions will provide information on the depth of insertion of the peptide in the membrane. All this information is obtained at the MS level directly, thus limiting the amounts of material needed. In particular, it allowed us to confirm that these CPPs favor interaction with fluid disordered regions of the membrane and do not insert deeply.<sup>180</sup> After a comprehensive description and characterization of all the side reaction products we observed, we will illustrate how to exploit them *via* a simple analytical workflow allowing direct MS spectra interpretation leading to information about interaction and insertion of this membrane-active peptide in lipid bilayer with binary mixtures. The final goal of this study is to understand how membrane permeability is influenced by a CPP sequence, how the lipids structure influences entry of CPP into cells and to locate preferred interaction sites between CPPs and lipids.

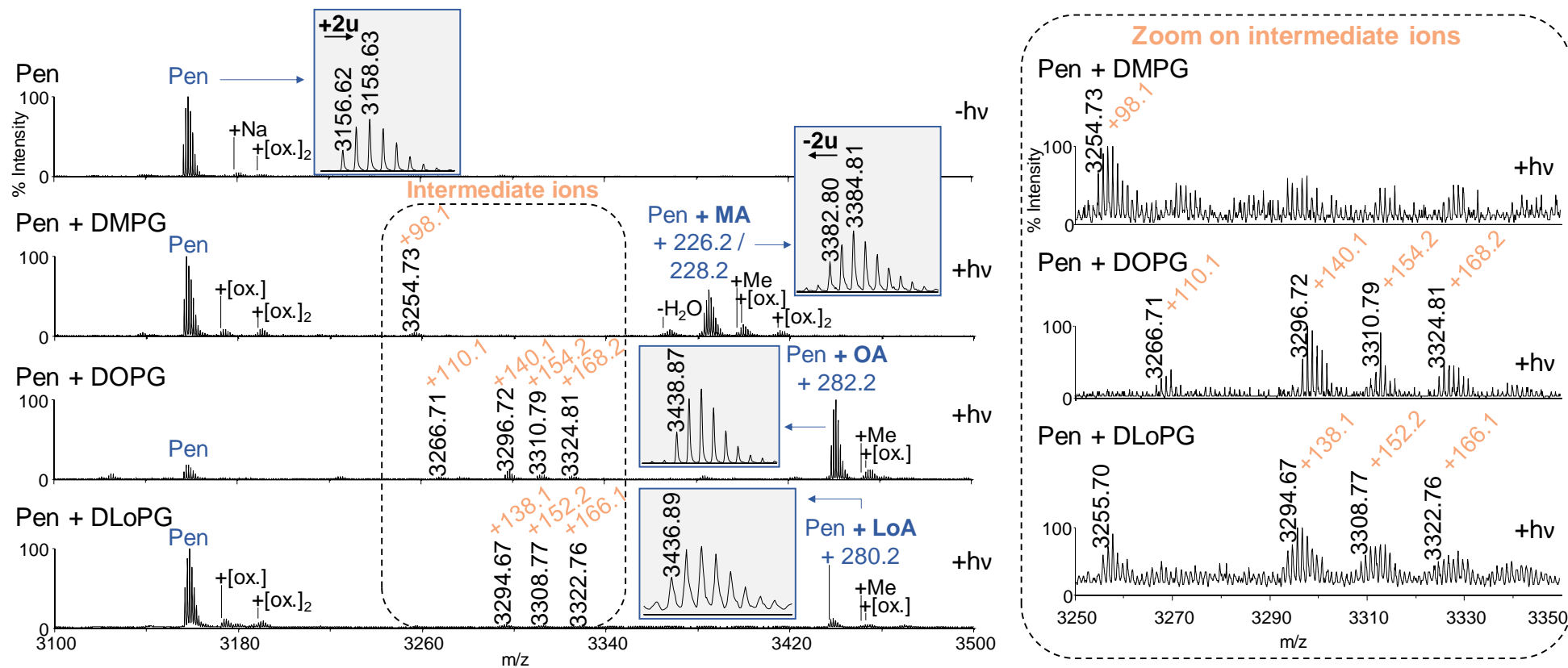


Figure 78. MALDI-TOF spectra (positive ions, reflector mode) of the Bzp-induced photo-cross-linking between Pen and negatively charged MLVs of various fatty acid chains. Top to bottom: Control Pen without irradiation (-hv), Pen+DMPG+hv, Pen+DOPG+hv, Pen+DLoPG+hv. Similar conditions of analysis were used in all spectra of the manuscript, 2,5-DHB is used as the matrix. Me: methylation, Na: sodium adduct, [ox.]: oxidation. The panel on the right is a zoom on the intermediate ions in the region 3250<m/z<3350.

## 2.1. General methodology

Our previous study<sup>5</sup> showed that Pen interacts preferably with negatively charged lipids so we chose to focus first on MLVs composed of PG phospholipids only for the full description of side reactions. In a second step we used binary mixtures of lipids: PG and cholesterol (Chol), to unveil Pen preferences according to bilayer fluidity properties. Photo-cross-linking using the photoreactive and biotinylated Pen and the rationally designed CPP (R/W)<sub>9</sub> was applied to MLVs composed of a single PG phospholipid and we varied the nature of the fatty acid chains. We used saturated DMPG (14:0) and DPPG (16:0), mono-unsaturated DOPG (18:1 *cis*  $\Delta^9$ ) and 18:1 (*trans*  $\Delta^9$ ) PG, and poly-unsaturated DLoPG (18:2 *cis*  $\Delta^9$ ,<sup>12</sup>).

The resulting photo-cross-linked species with intact phospholipids are heteroadducts known to be challenging to observe in MS. To allow a better MS ionization/detection yield, phospholipids saponification was performed on the photoadducts before affinity purification of the biotinylated species on streptavidin-coated magnetic beads and MALDI-TOF (Figure 78) or ESI-Orbitrap (Figure 79) analysis, thus leading to photoadducts composed of the peptide covalently linked to a simple fatty acid.<sup>5</sup> This step is crucial for the robustness of the setup. Measuring the mass shift ( $\Delta m$ ) between the ion signal of the non-crosslinked peptide (Pen, or (R/W)<sub>9</sub>) and the photoadducts allows identification of the fatty acid covalently linked to the peptide. Optimization of the photo-cross-linking protocol led to good quality ion signals corresponding to the expected peptide/fatty acid photoadducts as shown in the MALDI-MS spectra acquired using 2,5-DHB as the matrix (Figure 78).

Optimizations achieved on the protocol and on MS acquisition parameters are the following:

- Synthesis of fully oxidized peptides, using Biot(O<sub>2</sub>) and Met(O<sub>2</sub>)
- Use of a narrow spectrum UV-lamp
- Good temperature control and stability (45°C over 1h irradiation)
- Homogenous shaking of the samples over 1h
- Short saponification step with high NaOH concentration
- MALDI-TOF acquisition parameters in reflector mode were optimized on Insulin chain B (m/z 3494) for the detection of peptides around 3100-3500 u

Expected adducts, corresponding to a C-C bond formation (molecules **2** and **3**) between the photoreactive Pen and the different intact fatty acids are referred to in the manuscript as: Pen+myristic acid (MA; 14:0), Pen+oleic acid (OA; 18:1 *cis*  $\Delta^9$ ) Pen+linoleic acid (LoA; 18:2 *cis*  $\Delta^9$ ,<sup>12</sup>) or in SI Pen+palmitic acid (PA; 16:0), Pen+elaidic acid (EA; 18:1 *trans*  $\Delta^9$ ) (Figure 82). MS spectra obtained with Pen or (R/W)<sub>9</sub> (Figure 89) gave comparable results. All side reactions (P-B and oxidation products) observed for Pen were also observed when using (R/W)<sub>9</sub> for photo-cross-linking experiment.

High S/N ratio MALDI MS spectra allowed the unambiguous detection of low intense intermediate ions in the region between the m/z of the non-crosslinked Pen and the m/z of the intact photoadduct. These intermediate ions (highlighted in the dashed box and zoom in Figure 78) are only observed after photoirradiation (+hv spectra). Using an ESI ion source, these intermediate ions are even more intense (Figure 79). Therefore, these intermediate ions must

be treated as products of the UV-induced secondary reactions, and not occurring during the UV MALDI irradiation.

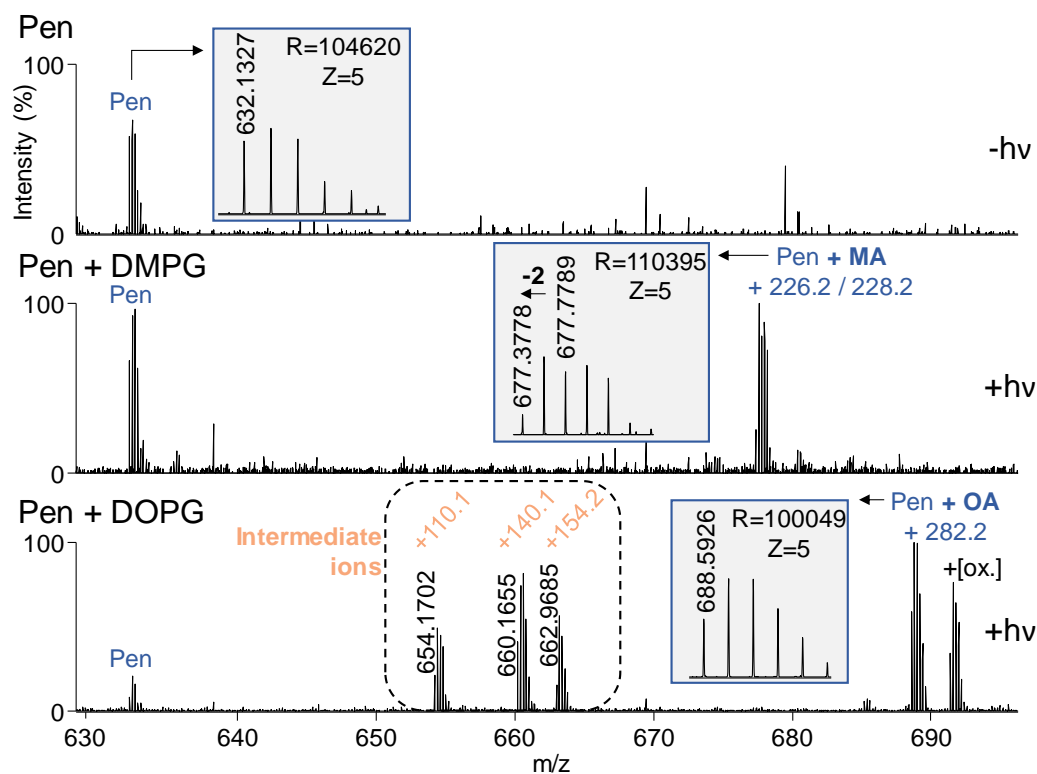


Figure 79. Flow injection analysis-ESI-Orbitrap MS spectra (positive ions) of the Bzp-induced photo-cross-linking between Pen and negatively charged MLVs of various fatty acid chains. Control Pen without irradiation (-hv), Pen+DMPG+hv, Pen+DOPG+hv. MA and OA stand for myristic acid and oleic acid respectively. Resolution (R) was set at 100000. Biotinylated species such as Pen or photoadducts are observed in the positive ions mode with different charge states  $z = 3, 4, 5$  and  $6$ . We chose to focus on the most abundant  $z = 5$  ion for this figure.

## 2.2. Benzophenone-induced in-source decay (ISD)

Focusing on the ion signals measured in MALDI-TOF MS (Figure 78), one can observe that the ion for Pen is not strictly identical to the theoretical one, predicted by IsoPro software. Pen experimental isotopic distribution (theoretical first isotope at  $m/z$  3156) contains a contribution at  $+2u$  ( $m/z$  3158) as clearly observed in Figure 78. On Figure 80A, left panel, we superimposed experimental isotopic distributions of the Pen ion signal obtained with 2,5-DHB as a MALDI matrix (blue dots), theoretical distribution as predicted by IsoPro (black triangles) and simulations of a massif resulting of two species with a  $+2u$  difference (grey diamonds). Isotopic pattern simulation showed that the species at  $+2u$  contributes for 25% to the experimental signal (Figure 80A, grey diamonds). This pattern was observed for uncross-linked Pen incubated alone or with lipids, with and without irradiation in MALDI MS spectra acquired in the same conditions (laser fluence and 2,5-DHB matrix) whereas ion signals in ESI were similar to the theory. We explain this unexpected isotopic distribution by a mechanism involving ISD in the MALDI source. The  $+2u$  contribution in the isotopic pattern of Pen is purely matrix-dependent since it is observed with 2,5-DHB (Figure 80A, blue dots) but not with CHCA ( $\alpha$ -cyano-4-

hydroxycinnamic acid) (Figure 80A, orange squares), in which case the isotopic distribution fits the theoretical ratio (Figure 80A, black triangles). Contrarily to CHCA, the reducing 2,5-DHB matrix is known to induce ISD in the MALDI ion source, as mentioned in the introduction.<sup>246</sup> This process involves a prompt H<sup>\*</sup> transfer from the 2,5-DHB leading to a complex isotopic distribution with two components: [M+H]<sup>+</sup> (75%) and [M+3H]<sup>+</sup> (25%). We performed a control experiment with a peptide without Bzp and no contribution at +2u was observed in either CHCA or DHB (Figure 80A, right panel). This strongly suggest that a reaction occurring on Bzp is responsible for this contribution and we propose a mechanism involving the specific reduction of the Bzp carbonyl by 2,5-DHB in the photoactivatable Pen ion (Figure 80B).

We can thus expect that ISD does not occur in the Pen-lipid complex, once the Bzp (in its reduced form) is covalently bound to a fatty acid. Indeed, we observe no contribution at +2u for intact photoadducts (Figures 78 and 81A). Moreover, photo-cross-linking data were also analyzed by ESI, where beads were eluted in 20 % formic acid. Results are presented in Figure 79, and ISD is not observed on the peptide isotopic pattern.

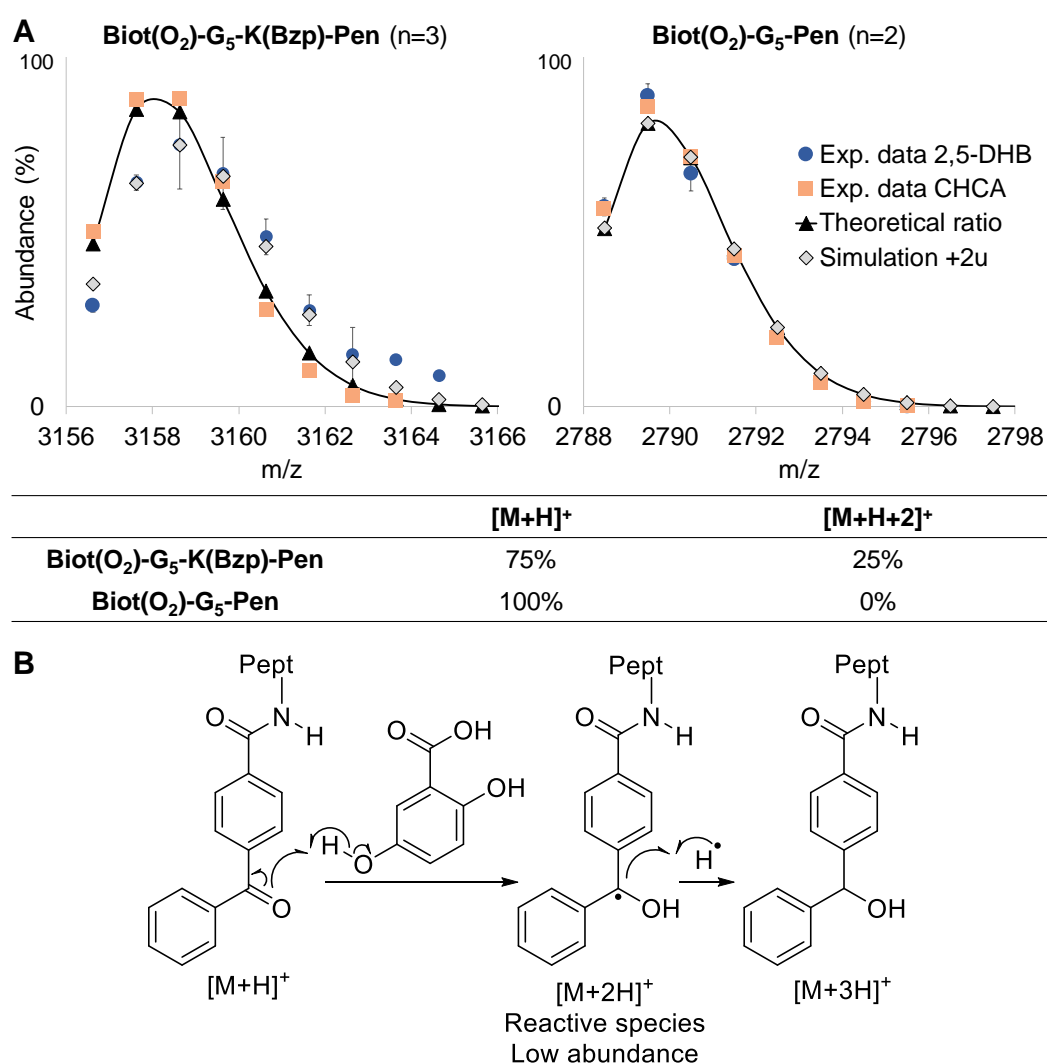


Figure 80. (A) Isotopic patterns of Pen with (left) or without (right) K(Bzp), acquired in 2,5-dihydroxybenzoic acid (2,5-DHB) or  $\alpha$ -cyano-4-hydroxycinnamic acid (CHCA) matrix (error bars correspond to standard deviation). (B) Proposed mechanism for the reduction on Bzp functionalized Pen using 2,5-DHB as matrix. (error bars correspond to standard deviation)

### 2.3. UV-induced redox reactions involving Bzp

The isotopic distribution of the Pen-MA photoadduct obtained with MALDI (Figure 78) and ESI (Figure 79) ion sources differs from the one predicted by the IsoPro software for the pure compound. The experimental isotopic distribution of Pen-MA photoadduct (theoretical first isotope at  $m/z$  3384) contains a contribution at  $-2u$  ( $m/z$  3382) as indicated in Figure 78. On Figure 81A, left panel, we superimposed the experimental isotopic distribution of the Pen-MA ion signal (blue dots), the theoretical distribution (black triangles) and simulation of a pattern resulting of two species with a  $-2u$  difference (orange diamonds).

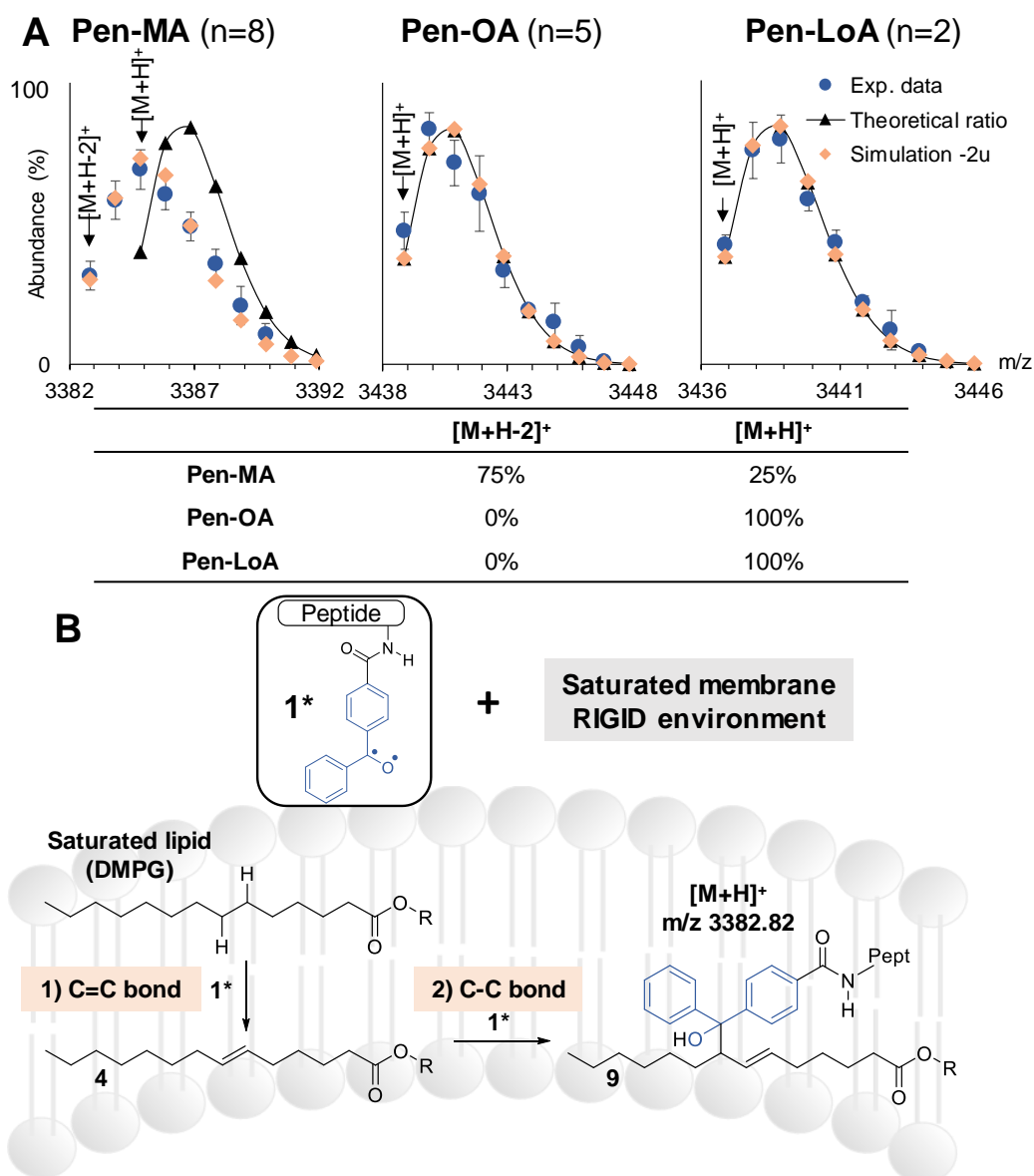


Figure 81. A) Isotopic ratios of the Pen-lipid photoadducts with MA (DMPG), OA (DOPG) and LoA (DLopG) (error bars correspond to standard deviation). B) UV-induced photoredox activity of the Bzp leading to double bond formation in a constrained DMPG MLV.

Isotopic pattern simulation showed that the species at  $-2u$  contributes for 75% to the experimental signal. This pattern is observed for Pen-MA in MALDI and ESI MS spectra showing

that this photoreactivity of the Bzp is not due to the UV laser ( $\lambda=355\text{nm}$ ) during the MALDI ionization process, but occurs in solution during the photolabeling step. This is also observed for the Pen-PA adduct (Figure 82) but not observed with Pen-OA (Figure 81A, middle panel), Pen-EA (Figure 82) or Pen-LoA adducts (Figure 81A, right panel).

We explain this shift towards lower  $m/z$  by specific redox photoreactivity of the Bzp towards saturated lipids. As described in solution by Breslow,<sup>219,220</sup> Bzp can induce the formation of a double bond on a rigid and constrained substrate. In Figure 81B, we propose such UV-induced mechanism occurring on the fatty acid chain of a lipid in a vesicle composed of saturated phospholipids that provides the constrained environment. In the system described by Breslow, rigidity is brought by the constrained molecular scaffold whereas in our system, rigidity is imposed by the saturated membrane. This UV-induced reaction consisting in the abstraction of two radical hydrogens (formal loss of  $\text{H}_2$ ) (molecule **4**, Figure 71) competes with the photo-cross-linking reaction leading to the C-C bond formation between Bzp and a fatty acid (molecule **2**, Figure 71). Considering the kinetics of  $\text{H}^\bullet$  abstraction by Bzp on secondary, allylic and doubly allylic hydrogens,<sup>181</sup> competitive formation of the double bond will be favored on saturated lipids (Figure 48). The combination of the lower rigidity of an unsaturated vs saturated lipid membrane and the favorable kinetics of the C-C bond formation on allylic or doubly allylic positions explains why the  $-2u$  contribution is not observed on photoadducts obtained with DOPG, *trans*-C18:1 and DLoPG.

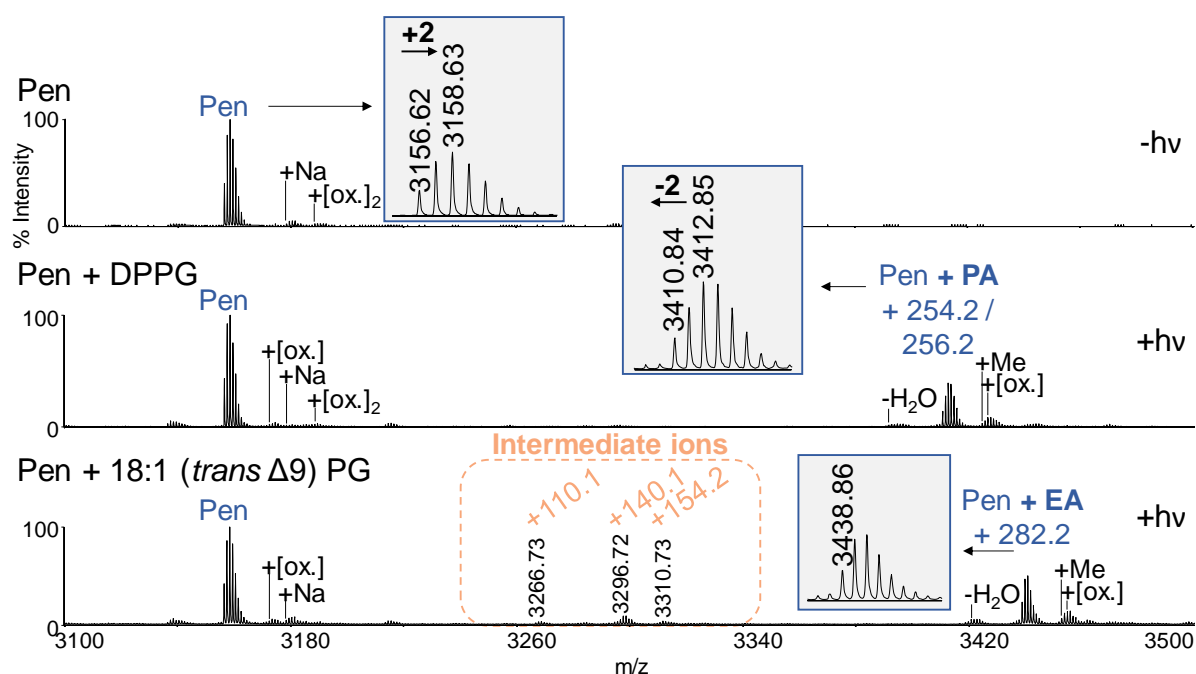


Figure 82. MALDI-TOF spectra positive ions, reflector mode of the Bzp-induced photo-cross-linking between Pen and negatively charged MLVs of various fatty acid chains. Control Pen without irradiation ( $-h\nu$ ), Pen+DPPG+ $h\nu$ , Pen+18:1 (*trans*  $\Delta 9$ ) PG+ $h\nu$ .

Once the double bond is formed on a saturated fatty acid (molecule **4**, Figure 81B), the photo-cross-linking reaction is favored on the newly-modified fatty acid (molecule **9**, Figure 81B). This consecutive reaction involves the presence of a second Pen with activated Bzp (molecule **1\***) in the close vicinity of the new unsaturation, which is highly probable in the conditions used for



the photo-cross-linking reaction (lipid/peptide ratio 10/1). Furthermore, since the membrane possibly becomes more fluid around the defect caused by the double bond, insertion of the Pen and the probe will be facilitated in this area. Indeed, as discussed in introduction, Pen is known to interact more favorably with lipids in fluid phase.<sup>162</sup>

It can be noted that other lipid species were used for photolabeling, in particular saturated DPPG and unsaturated 18:1 (*trans*  $\Delta^9$ ) PG. Data obtained by MALDI-TOF are shown in Figure 82. DPPG behaved strictly as DMPG, leading to palmitic acid (PA) as photoadduct, with a clear -2u contribution on the adduct peak, which supports our interpretation of the double bond formation on saturated lipids. 18:1 (*trans*  $\Delta^9$ ) PG behaved strictly as DOPG (18:1 *cis*  $\Delta^9$ ), giving an elaidic acid (EA) photoadduct, showing favored C-C bond formation on the allylic position of the fatty acid and no double bond formation. This shows the importance of kinetics of H<sup>•</sup> abstraction by Bzp over membrane fluidity for the double bond formation to occur.

## 2.4. UV-induced covalent bond formation and rupture

Intermediate ions (Figure 78) are noticed in the MS spectra whatever the ion source MALDI or ESI, showing that they are not produced by irradiation of the MALDI UV-laser. Tandem MS (MS/MS) was useful to characterize these ions. All intermediate ions and expected intact photoadducts were characterized by fragmentation using high energy CID (MALDI-TOF/TOF, gas N<sub>2</sub>, 1keV, selected window  $\pm 7u$ ) (Figure 83). Post-source decay (PSD) was also performed on intact photoadducts and gave the same information (Figure 84).

### 2.4.1. Peptide-lipid covalent bond stability

Gas-phase fragmentation of the intact photoadducts (Figures 83 and 84) shows a favored fragmentation pathway corresponding to the dissociation of the covalent bond formed between Pen and the fatty acids as previously observed for peptide-peptide photoadducts,<sup>204</sup> showing that they all contain the intact Pen sequence. Neutral loss leading to Pen fragment ion ( $m/z$  3156) corresponds to the loss of the lipid part covalently bound to Pen, confirming that the proton is located on the peptide. This is clearly visible with the CID MS/MS fragmentation of the Pen-LoA entire photoadduct. This highly intense fragment ion peak at the  $m/z$  of Pen shows that this newly-formed bond is unstable and can be easily broken during CID, or even afterwards in the flight tube (after reacceleration of the fragment ions) by PSD as shown by the broad fragmentation signal just next to the parent ion (Figure 83). Its fragility is probably increased compared to MA and OA because of the presence of multiple double bonds in the LoA, stabilizing the fragment ion resulting from the loss of the fatty acid (formation of a tertiary radical ion). This is in good agreement with the observed relative intensities of the photoadducts ion signals compared to the Pen ion signals (Figure 78), which are inversely proportional to the relative stability of the radical resulting from the fragmentation of the newly-formed C-C bond.

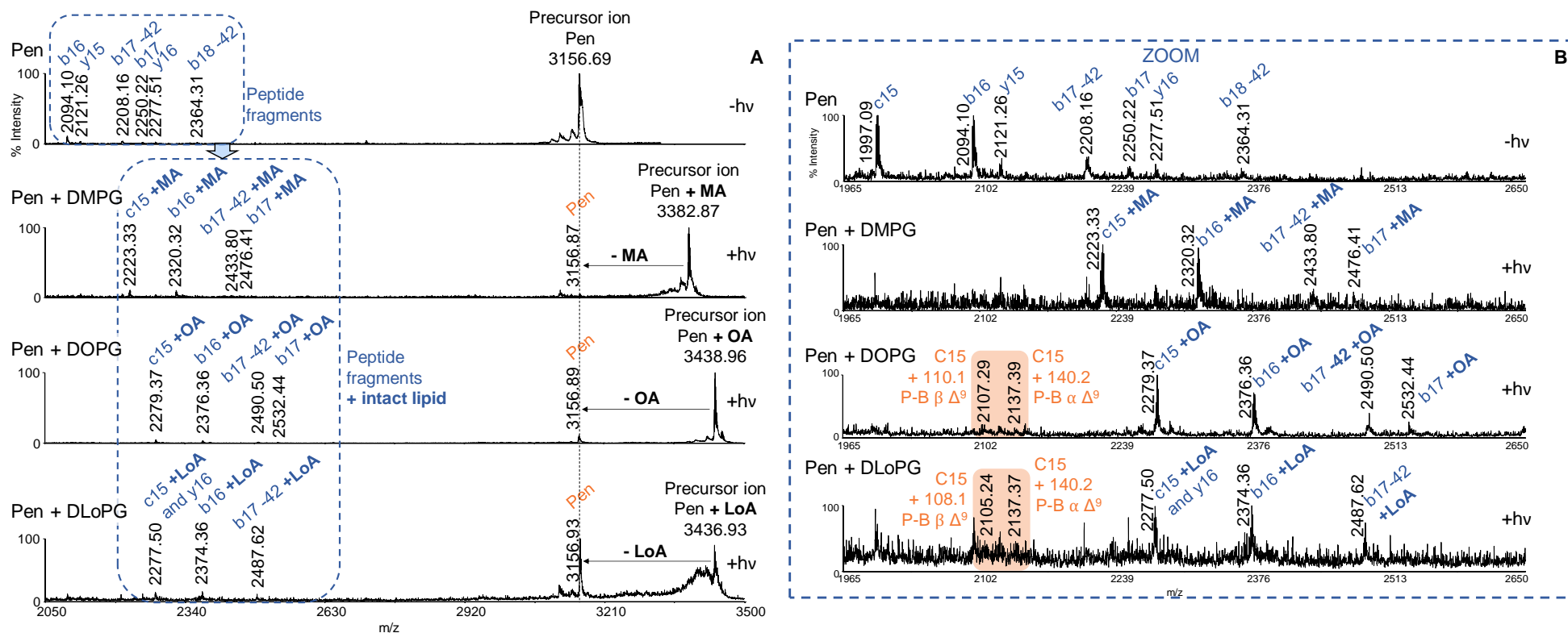


Figure 83. High mass range 2050 < m/z < 3500 MALDI-TOF/TOF spectra (gas N<sub>2</sub>, 1 keV, selection window ±7u) of the Bzp-induced photo-cross-linking between Pen and negatively charged MLVs of various fatty acid chains. Control Pen without irradiation (-hv), Pen+DMPG+hv, Pen+DOPG+hv, Pen+DLoPG+hv. MA, OA and LoA stand for myristic acid, oleic acid and linoleic acid respectively. (B) is a zoom in the mass range corresponding to the relevant fragment ion species which were present on MS/MS of the Penetratin alone (precursor ion m/z 3156.6) and on the MS/MS of the Penetratin + intact lipid with the corresponding mass increment of the intact lipid noted as +MA (precursor ion m/z 3382.8), +OA (precursor ion m/z 3438.9) and +LoA (precursor ion m/z 3436.9). A) High mass range of the MS/MS spectra (from 2050 to 3500 m/z), B) Magnification of the mass range 1965<m/z<2650.

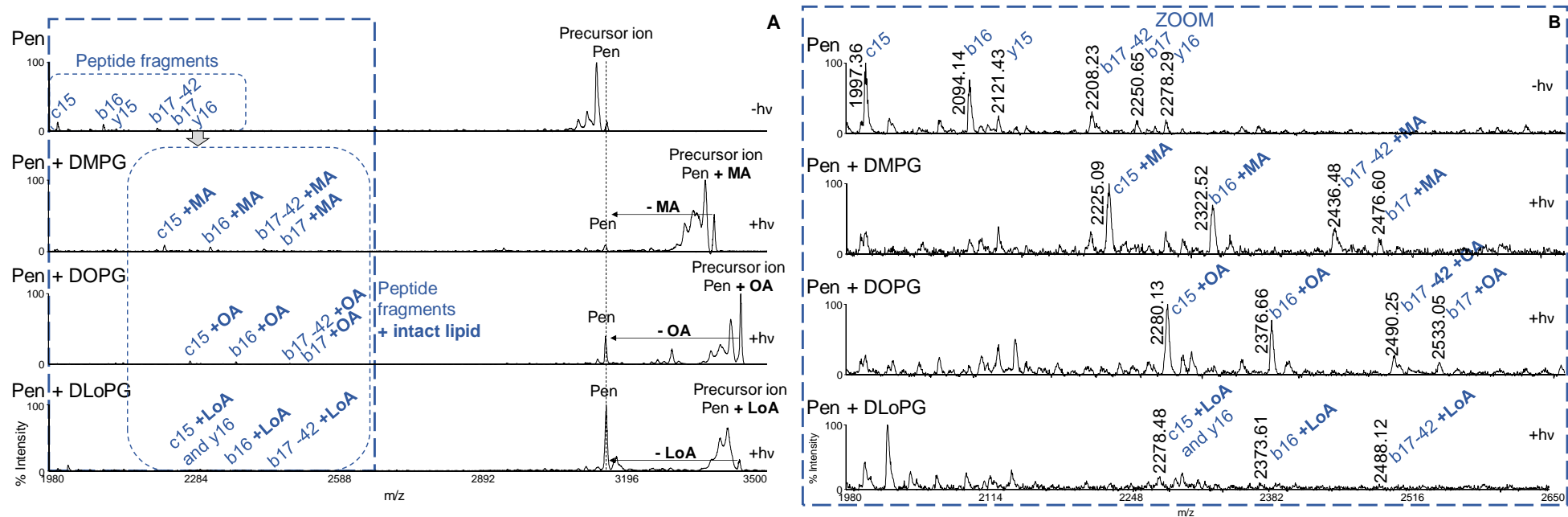


Figure 84. High mass range 1980 < m/z < 3500 MALDI-PSD spectra of the Bzp-induced photo-cross-linking between Pen and negatively charged MLVs of various fatty acid chains. Control Pen without irradiation (-hv) (precursor ion m/z 3156.6), Pen+DMPG+hv (precursor ion m/z 3382.8), Pen+DOPG+hv (precursor ion m/z 3438.9), Pen+DLoPG+hv (precursor ion m/z 3436.9). MA, OA and LoA stand for myristic acid, oleic acid and linoleic acid respectively.

A) High mass range of the MS/MS spectra (from 1980 to 3500 m/z), B) Magnification of the mass range 1980 < m/z < 2650.

#### 2.4.2. Information from Paternò-Büchi and retro Paternò-Büchi reactivities

Further MS/MS data analysis of the photoadducts revealed that the reactivity of Bzp and fatty acids is more complex than only the expected formation of a C-C bond. Indeed, it appears that the observed intact photoadducts actually mask two different photoinduced reactivities of the Bzp towards lipids: classical C-C bond formation (molecules **2** and **3**) and [2+2] cycloaddition leading to oxetane formation (P-B reaction, P-B) on unsaturated OA and LoA (molecule **5** and Figure 85).<sup>208–210</sup> These two pathways lead to products with the same elemental composition, which makes them undistinguishable at the MS level. They have the same *m/z* and identical isotopic pattern. It has to be noted that the oxetane formation on unsaturated lipids can also occur on oxidized MA that contains a double bond as described in the previous section. MS/MS spectra of the intact photoadducts therefore contain fragment ions originating from both species. These UV-induced reactions of the Bzp are well described on lipids in solution (P-B) or in the gas-phase (retro P-B) and are presented in introduction. In the present study, we describe the Paternò-Büchi reactivity of Bzp linked to a CPP in the context of lipid membranes, a constrained 2D molecular organization.

P-B reaction coupled with MS/MS is commonly used for identifying and quantifying unsaturated lipids in complex lipid mixtures. As it is induced by UV irradiation, this P-B reaction can occur in our system when unsaturated lipids are present, leading to two oxetane regioisomers as depicted in Figure 85. If we consider both products are formed (oxetane rings + C-C bond), these two populations of ions are selected and fragmented together during the MS/MS. The resulting MS/MS spectra contain fragment ions originating from both species. We observed fragment ions that could not be accounted for if only conventional C-C bond formation was occurring in our system and were consistent with P-B and retro P-B reactivities. We previously mentioned that the covalent bond formed between Bzp and the fatty acid is the most fragile bond in MS/MS analysis. This fragile Pen-lipid bond is a mixed population of both C-C bond and oxetane rings (two regioisomers). Interestingly, P-B and retro P-B reactivities could also explain certain so-far unidentified species in our MS spectra, *i.e.* the so-called intermediate ions described above (Figure 78, zoom).

The oxetane ring opening through retro P-B can be done by low collision energy in MS/MS, by heating<sup>213–215</sup> or acidic treatment.<sup>216</sup> Our experiment requires heating at 45°C for 1h during the photolabeling step in solution, and acidic pH (1-2) in the 2,5-DHB MALDI matrix or in the ESI solvent (formic acid 0.1%). There is also steric hindrance due to the presence of Pen on the Bzp. Therefore, both retro P-B  $\alpha$  and  $\beta$  products ( $\alpha$  and  $\beta$  ions schemed in Figure 85) can be observed at the MS level (dashed box, Figure 78) which is a real asset in our analytical approach.

Further MS/MS fragmentation applied to the P-B regioisomer products leads to diagnostic  $\gamma$  and  $\delta$  fragment ions (Figure 86, *m/z* at 319, 349 for the Pen-OA adduct, numbered peaks 5' and 7, respectively and *m/z* at 277, 317, 349 for the Pen-LoA adduct, numbered peaks 2, 5 and 7, respectively) offering structural information about the unsaturated lipids.

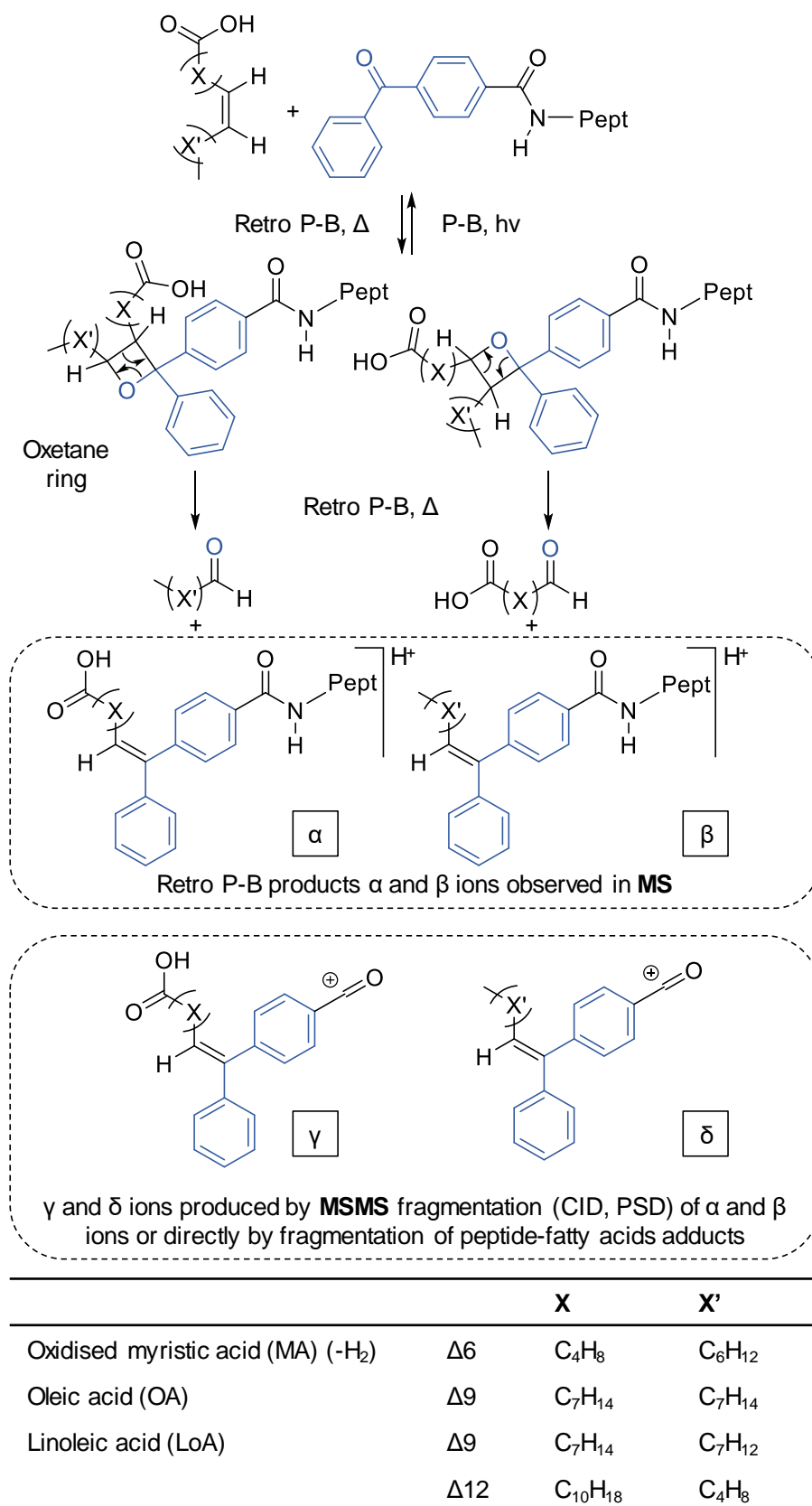


Figure 85. P-B and retro P-B reactions between photoreactive Pen and unsaturated lipids. Retro P-B products  $\alpha$ ,  $\beta$ ,  $\gamma$ ,  $\delta$  are obtained in MS and/or MS/MS when photoreactive Pen is crosslinked to unsaturated lipids.

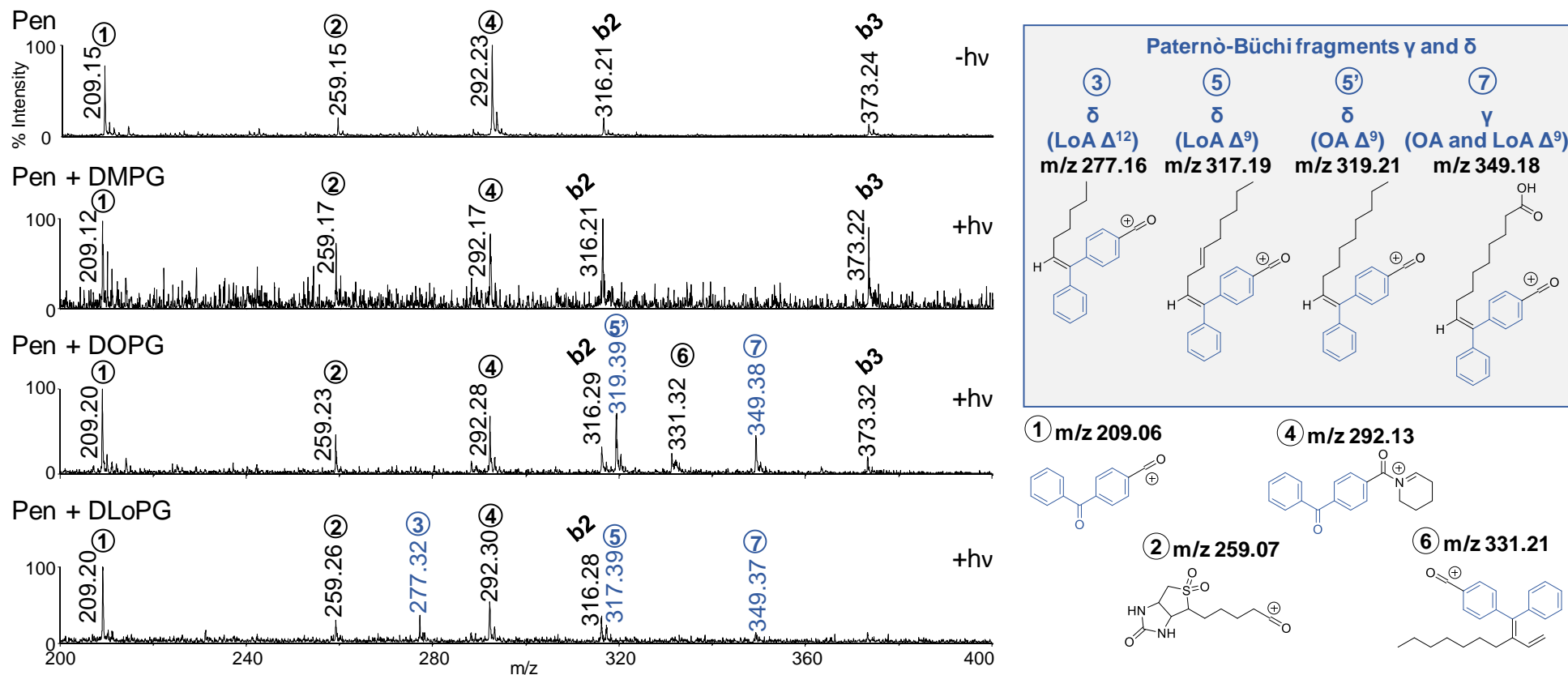


Figure 86. Low mass range  $200 < m/z < 400$  MALDI-TOF/TOF spectra of the Pen+fatty acids intact photoadducts precursor ions. Control Pen without irradiation (-hv), Pen+DMPG+hv, Pen+DOPG+hv, Pen+DLoPG+hv. Structures of ions are numbered from 1 to 7 and P-B fragments are highlighted in the grey box.

The  $\alpha$  and  $\beta$  ions are present in MS/MS with very low intensity and with consecutive fragments  $\gamma$  and  $\delta$  (Figure 85) in the low  $m/z$  region (Figure 86) proving that both C-C bond and oxetane ring formation coexist. The  $\gamma$  and  $\delta$  ions, requiring additional energy to be generated, are only observed using CID or PSD fragmentation.  $\gamma$  and  $\delta$  ions were observed in MS/MS spectra from both precursor ions: the intact photoadducts or the retro P-B products  $\alpha$  and  $\beta$  (Figures 85 and 86).  $\gamma$  and  $\delta$  are specific diagnostic ions of the existence of the P-B reaction, proving that both reactivities of Bzp occur in our system. They are absent in the control sample without irradiation (-hv) and their  $m/z$  is shifted according to the position and/or number of the double bond(s) in the fatty acid that is covalently linked to Bzp (Figure 86,  $\gamma$  and  $\delta$  ions 3, 5, 5' and 7). The  $m/z$  values of the  $\alpha$ ,  $\beta$ ,  $\gamma$  and  $\delta$  ions observed in MS and MS/MS are summarized and compared to expected  $m/z$  in Table 9. The  $m/z$  values observed in MS and MS/MS are highlighted in bold. P-B reaction can happen on unsaturated OA and LoA. Intermediate ions observed with DOPG at  $m/z$  3266.71 and 3296.71 (Figure 78) indeed match masses of the expected retro P-B products  $\beta$  and  $\alpha$ , respectively (Table 9).

We did not identify retro P-B products  $\alpha$  and  $\beta$  for DLoPG on MS spectra probably due to the fragility of the oxetane ring which leads back to the original reactants: Pen and LoA (Figure 85). However, MS/MS fragmentation of the expected intact photoadducts obtained with DOPG ( $m/z$  3438.88) and DLoPG ( $m/z$  3436.87) gives access to retro P-B fragments corresponding to products  $\gamma$  and  $\delta$  in the low mass range of the MS/MS spectra (Figure 86, retro P-B fragments 3, 5, 5' and 7) proving the presence of the oxetane ring photoproducts at  $m/z$  3438.88 and 3436.87. Retro P-B fragments  $\gamma$  and  $\delta$  at  $m/z$  349 and 319/317 show comparable relative intensities. This is in agreement with the P-B regioselectivity, which is mainly linked to steric hindrance of the substituents on the olefin and is not an issue in our case.<sup>262</sup> Both attacks of the carbonyl of the Bzp are equiprobable on the fatty acid double bond.

Other ions are reproducibly observed with similar relative intensities, in the low mass range in all MS/MS spectra. They correspond to Pen b-ions as well as ions at  $m/z$  209, 259, 292, the structures of which are schemed in Figure 86 (ions 1, 2, 4) according to mechanisms published in the literature.<sup>263</sup> A structure is also proposed for the ion at  $m/z$  331 (ion 6) observed with DOPG.

In Figure 83B, in the zoom in the mass range corresponding to the relevant fragment ion species obtained by MS/MS of the photoadducts, it can be noticed that very low intensity ions correspond to P-B fragments  $\alpha$  and  $\beta$  obtained on the photoadducts Pen+OA and Pen+LoA, with the peptide part being fragmented as to give an unconventional c15 ion. As previously commented, the oxetane bond is very fragile, thus it is very likely to be the first bond to be fragmented, and the remaining energy is sufficient to get supplemental fragmentations on the peptide backbone. Thus, the highly intense ions of the peptide fragment ions bound to the intact lipid part (c15, b16, etc.) probably correspond to fragments of the Pen-lipid adducts linked by a classical C-C bond formed by the photo-cross-linking reaction.

Table 9. Overview of possible Paternò-Büchi products obtained by Bzp functionalized peptide reaction on various unsaturated lipids. In bold: ions observed on the MS or MS/MS spectra realized (MALDI-TOF/TOF) on the photo-cross-linking reaction mixtures between Pen and various lipids: DMPG, DOPG and DLoPG after saponification and streptavidin purification of the biotinylated complexes. Mass error between expected and theoretical mass is lower than 20 ppm.

Lipid	P-B product				Retro P-B product in MS			After MS/MS			
	Observed [M+H] <sup>+</sup> m/z	Expected [M+H] <sup>+</sup> m/z	Adduct mass (Da)	$\Delta$	Observed [M+H] <sup>+</sup> m/z	Expected [M+H] <sup>+</sup> m/z	Adduct mass (Da)	Observed [M+H] <sup>+</sup> m/z	Expected [M+H] <sup>+</sup> m/z		
Oxidized myristic acid (-H <sub>2</sub> ) 14:1 ( $\Delta^6$ )	<b>3382.80</b>	3382.81	+226.19	$\Delta^6$	$\alpha$	<b>3254.73</b>	3254.69	+98.07	$\gamma$	307.13	
					$\beta$		3252.75	+96.13	$\delta$	305.19	
Oleic acid 18:1 ( $\Delta^9$ )	<b>3438.87</b>	3438.88	+282.26	$\Delta^9$	$\alpha$	<b>3296.72</b>	3296.74	+140.12	$\gamma$	<b>349.38</b>	349.18
					$\beta$	<b>3266.71</b>	3266.77	+110.14	$\delta$	<b>319.39</b>	319.21
Linoleic acid 18:2 ( $\Delta^{9,12}$ )	<b>3436.89</b>	3436.87	+280.24	$\Delta^9$	$\alpha$		3296.74	+140.12	$\gamma$	<b>349.37</b>	349.18
					$\beta$		3264.76	+108.13	$\delta$	<b>317.39</b>	317.10
					$\alpha$		3336.78	+180.15	$\gamma$		389.21
					$\beta$		3224.72	+68.09	$\delta$	<b>277.32</b>	277.16



More interestingly, P-B reaction can happen as a second step reaction on DMPG, after formation of the double bond as described previously. In fact, both C-C bond and oxetane rings (Figure 71) can be generated on the newly-formed unsaturated lipid ( $m/z$  3382, corresponding to the -2 u shift of the ion at 3384, Figure 78). The intermediate ion observed at  $m/z$  3254.74 on MS spectrum of Pen+DMPG+hv (Figure 78) matches the mass of the retro P-B product  $\alpha$  (Table 9). When subjected to MS/MS fragmentation, this ion does not lead to subsequent loss of the lipid part and thus, we do not observe any peak in the  $m/z$  region of Penetratin (Figure 87). Indeed, the oxetane fragmentation leading to a specific alkene structure (given in Figure 85), it is not possible to observe the intact Pen ion anymore after fragmentation. This is particularly interesting as the retro P-B product allows MS characterization of the position of the newly formed double bond on MA as being on C6-C7 (total mass of the retro P-B product ion corresponding to the mass of Pen + 98u), without further MS/MS fragmentation. In the case of saturated phospholipids, all positions having an equivalent reactivity towards  $H^\bullet$  abstraction by Bzp, the positioning of the double bond gives a direct indication of the insertion depth of Pen in the membrane.

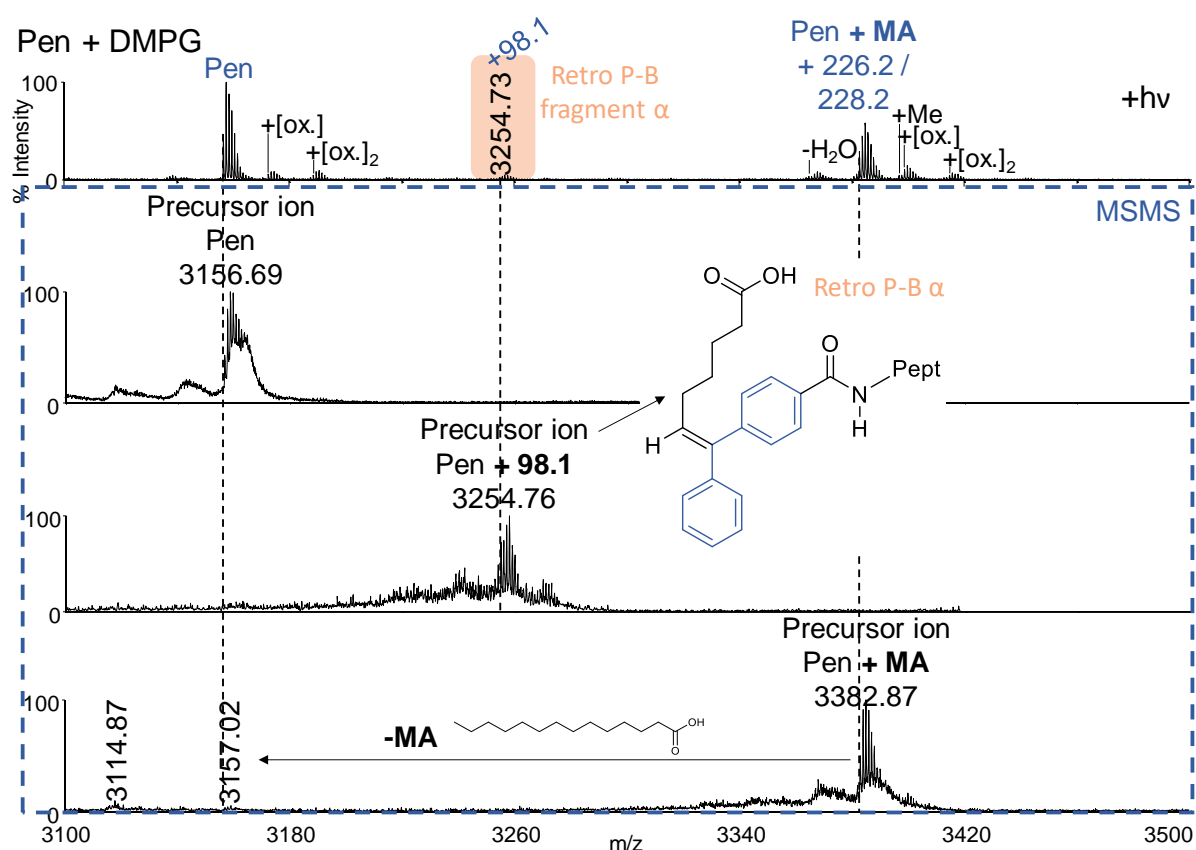


Figure 87. Mass spectra of the Bzp-induced photo-cross-linking between Pen and negatively charged MLVs of DMPG. Top to bottom: MALDI-TOF spectra (positive ions, reflector mode) Pen+DMPG+hv, MALDI-TOF/TOF spectra (gas  $N_2$ , 1 keV, selection window  $\pm 7u$ ) Pen+DMPG+hv precursor ion Pen, intermediate ion Pen+98.1 and photoadduct Pen+MA. Similar conditions of analysis were used in all spectra of the manuscript, 2,5-DHB is used as the matrix.

The C6-C7 position suggests a rather shallow insertion of the Pen in the lipid bilayer, which is consistent with what is known about Pen interactions with membranes.<sup>180</sup> Pen carries many

cationic residues and their deep insertion in the membrane would come with a very high energetic cost (see introduction). Furthermore, Pen carries two W residues, which are known to position themselves at water/lipid interfaces rather than inserting deeply within membranes.<sup>194</sup> Finally, Bzp-modified Pen has little effect on the fluidity and organization of a DMPG bilayer as probed by DSC.<sup>259</sup> No P-B fragments  $\gamma$  and  $\delta$  are observed in MS/MS with DMPG, probably due to the relatively low quantity of photoadduct at  $m/z$  3382, which impairs acquisition of MS/MS spectra with high S/N.

The same type of figure is presented for the Pen+OA photoadduct (Figure 88). Here, the more intense intermediate ion that can be subjected to MS/MS fragmentation is the one at the mass corresponding to Pen +140u. This mass actually reflects the contribution of two species: the retro P-B fragment  $\alpha$  and one of the products of the oxidation reactions on unsaturated lipids that will be described in a following paragraph. The structures of these two ions are given in Figure 88. As it is the case for the DMPG ion, the retro P-B product has a specific alkene structure that cannot lead to the intact Pen ion upon fragmentation. The observed Pen ion here must be due to the fragmentation of the oxidation product since they are both selected in the same selection window during the MS/MS experiment because they have the same  $m/z$ .

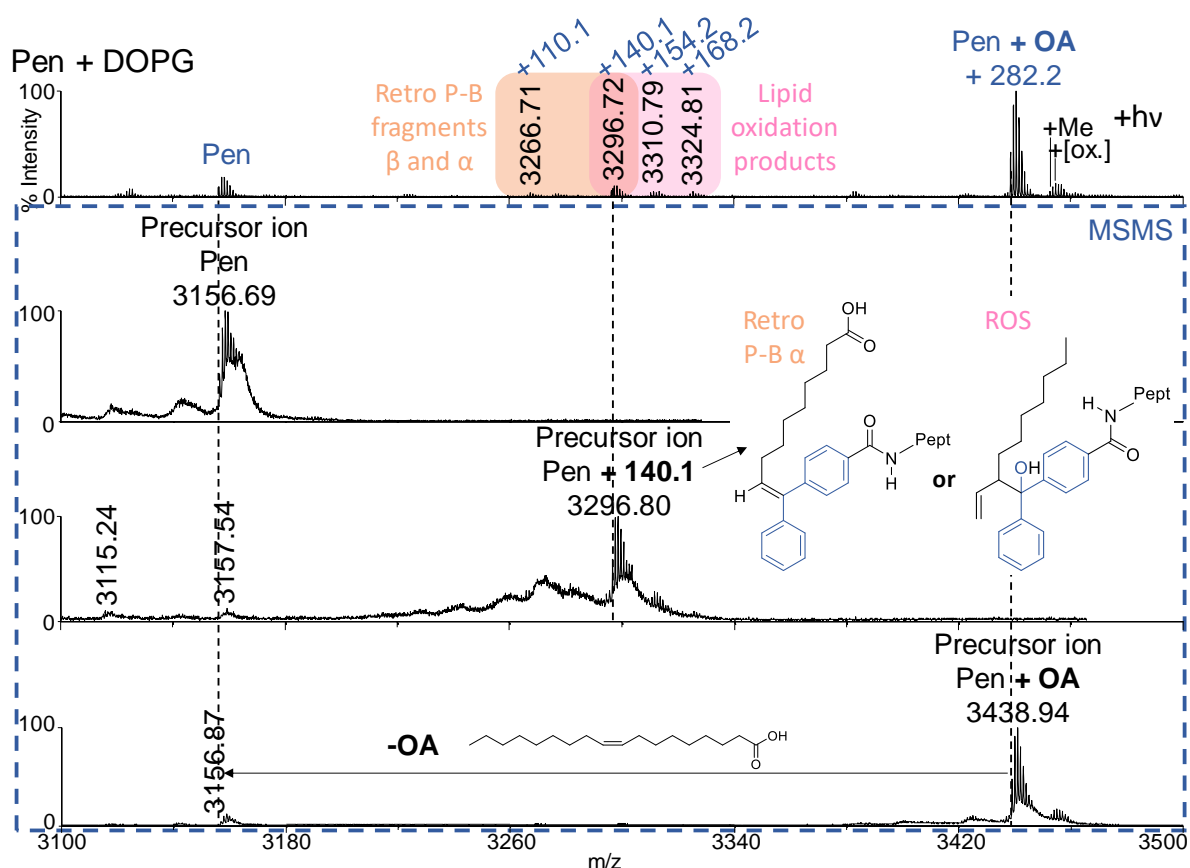


Figure 88. Mass spectra of the Bzp-induced photo-cross-linking between Pen and negatively charged MLVs of DOPG. Top to bottom: MALDI-TOF spectra (positive ions, reflector mode) Pen+DOPG+hv, MALDI-TOF/TOF spectra (gas N<sub>2</sub>, 1 keV, selection window  $\pm 7u$ ) Pen+DOPG+hv precursor ion Pen, intermediate ion Pen+140.1 and photoadduct Pen+OA. Similar conditions of analysis were used in all spectra of the manuscript, 2,5-DHB is used as the matrix.

In the MS/MS spectra deciphering work, it has been very useful to exploit the data acquired with the different sequences of Penetratin Pen and ApaPen. Indeed, the Apa spacer of mass 99u could be used as a tag to unequivocally identify the various fragment ions of the peptide-lipid adducts. The example of the b16 fragment ion is highlighted in the Figure 89.

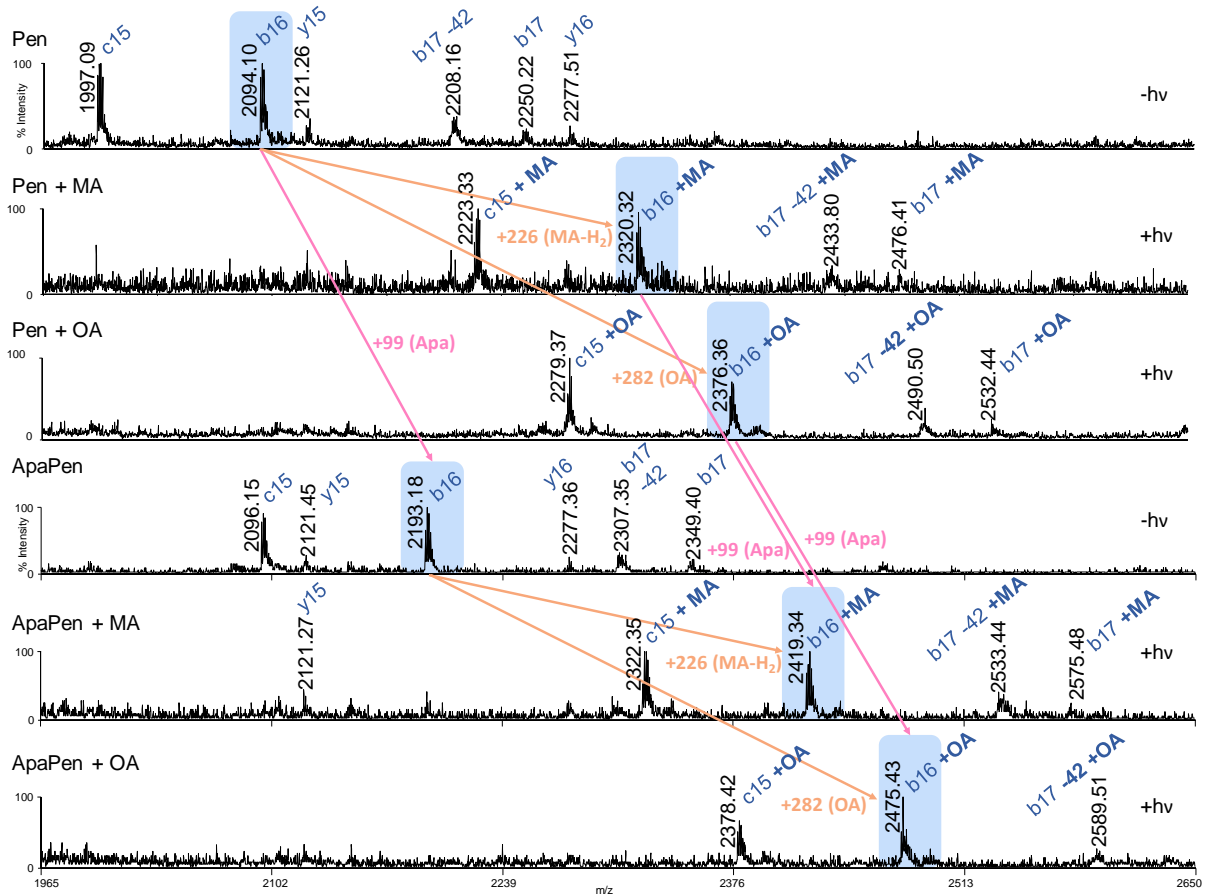


Figure 89. Zoom in the mass range  $1965 < m/z < 2650$  of MALDI-TOF/TOF spectra (gas  $N_2$ , 1 keV, selection window  $\pm 7u$ ) of the Bzp-induced photo-cross-linking between Pen and ApaPen and negatively charged MLVs of various fatty acid chains. Control Pen without irradiation (-hv), Pen+DMPG+hv, Pen+DOPG+hv, Control ApaPen without irradiation (-hv), ApaPen+DMPG+hv, ApaPen+DOPG+hv. MA and OA stand for myristic acid and oleic acid, respectively. MS/MS of the Pen alone (precursor ion  $m/z$  3156.6) and on the MS/MS of the Pen + intact lipid with the corresponding mass increment of the intact lipid noted as +MA (precursor ion  $m/z$  3382.8), +OA (precursor ion  $m/z$  3438.9). MS/MS of the ApaPen alone (precursor ion  $m/z$  3255.7) and on the MS/MS of the ApaPen + intact lipid with the corresponding mass increment of the intact lipid noted as +MA (precursor ion  $m/z$  3481.9), +OA (precursor ion  $m/z$  3537.9).

## 2.5. Bzp-induced photosensitization

In our experiments with DMPG or DOPG, we could reproducibly detect low intense covalent photoadducts corresponding to Pen covalently linked to two fatty acids in the higher  $m/z$  region. MALDI-TOF spectra illustrating lipid dimerization on DMPG are shown on Figure 90. One Bzp moiety cannot form two covalent bonds with two distinct fatty acids. The presence of such adducts can thus only be explained by dimerization of fatty acids due to Bzp-induced

photosensitization of an unsaturated fatty acid (Figure 71, molecules **6\*** and **7**). Two distinct activated Bzp moieties (**1\***) are involved: a crosslinker and a sensitizer.

This dimerization implies photosensitization of double bonds on the fatty acid and thus can only be observed on a previously oxidized myristic acid (loss of H<sub>2</sub>) bearing a newly-formed C=C bond. Isotopic distribution of the dimer adduct seems different from the theoretical one obtained for the pure compound with Isopro and a +2u contribution could help explain the observed isotopic pattern. However, low S/N does not allow us to have sufficient statistical accuracy to simulate a contribution at +2u, which would correspond to a single covalent bond between the two lipid chains.

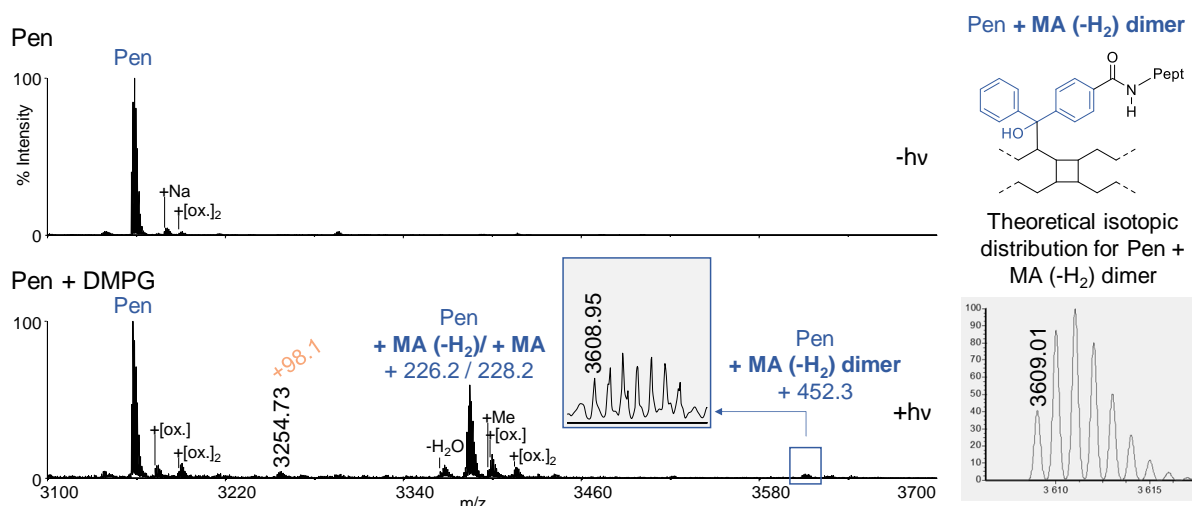


Figure 90. MALDI-TOF spectra positive ions, reflector mode of the Bzp-induced photo-cross-linking between Pen and negatively charged MLVs of DMPG. Control Pen without irradiation (-hv), Pen+DMPG+hv, with focus on the lipid dimer adduct at m/z 3608.95. Theoretical m/z for the protonated Pen+MA dimer is at m/z 3609.01 and the theoretical isotopic pattern is given in the grey box (Isopro).

Bzp-induced dimerization through photosensitization has been well described for biomolecular interactions with DNA. As discussed in introduction, Bzp photoinduced reactions (photooxidation, P-B or retro P-B reactions, C-C bond formation, dimerization) often competes (Figure 71).<sup>203</sup> In our case, the product of dimerization *via* Bzp photosensitization are always detected as low intensity ions compared to other Bzp photoinduced products, indicating that this pathway is probably not energetically favored, provided protonation occurring on the Pen moiety and therefore ionization yields comparable for all types of photoproducts.

Very interestingly, we observe fatty acid dimerization with DOPG, but also DMPG which confirms the photooxidation (loss of H<sub>2</sub>) of MA. Without this newly-formed unsaturation, photosensitized dimerization of MA would not occur.

Finally, it is described in the literature that UV irradiation of Bzp in solution in isopropanol leads to homodimerization of ketyl radicals to form benzopinacol. In our experiments in lipid membranes, we observed no homodimerization (Figure 71, molecule **8**) of Pen or (R/W)<sub>9</sub> either in the presence of liposomes or by irradiation of the control Pen or (R/W)<sub>9</sub> alone, which is consistent with the results reported for protein-Bzp<sup>203</sup> or peptide-Bzp<sup>204</sup>.

## 2.6. Radical oxygen species-induced oxidation reactions

Apart from P-B products  $\alpha$  and  $\beta$ , the intermediate ions region of MS spectra (Figure 78) contains species at +140.1/+138.1, +154.1/+152.1 and +168.1/+166.1 compared to the  $m/z$  of the non-crosslinked Pen for unsaturated DOPG and DLoPG. It is known that double bonds of (poly)unsaturated fatty acids can be cleaved during UV irradiation by reaction with radical oxygen species (ROS)<sup>264</sup> (Figure 91). Theoretically, we could observe these ions with DMPG after double bond formation, but none are observed, probably due to the higher acyl packing preventing penetration of water soluble radicals and oxidation.<sup>264</sup> These oxidation ions thus reflect membrane fluidity around the CPP. The scheme of this reactions is presented in Figure 91, explaining the oxidized intermediary ions observed in the MS spectra for DOPG.

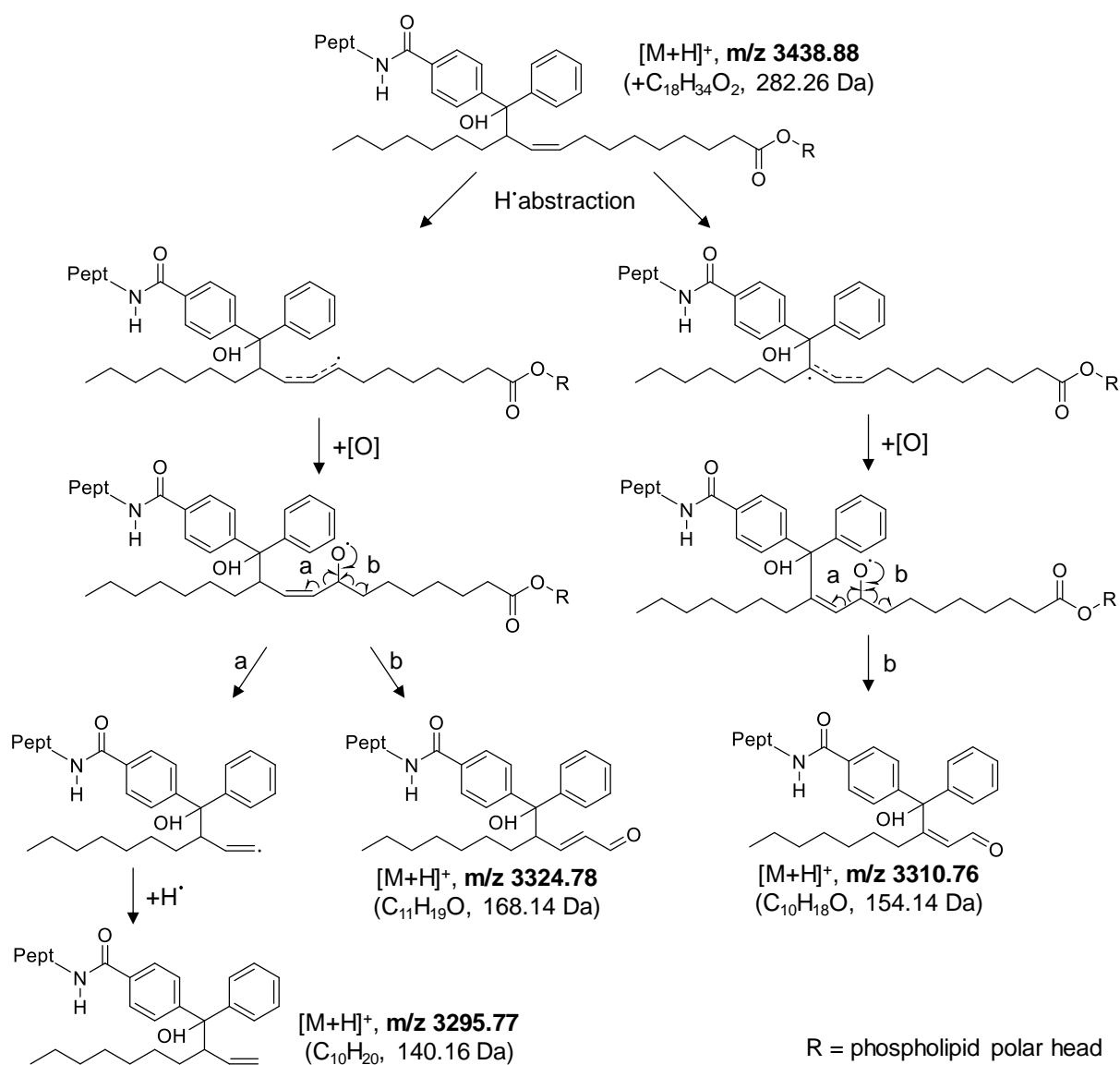


Figure 91. Scheme of the possible oxidation reactions occurring on the photoadducts between Pen and oleic acid when using DOPG vesicles for the photo-cross-linking experiment. These structures correspond to the intermediary ions observed in the MALDI-TOF spectra of the Figure 2 in the manuscript. Their  $m/z$  are highlighted in bold.

Minimizing dissolved O<sub>2</sub> by working under nitrogen atmosphere and using degassed buffers or not, containing or not an antioxidant (butylated hydroxytoluene, currently used to reduce lipid degradation by oxidation) led to the same results. Therefore, we assume that ROS-induced processes are probably intrinsic to our system.

### 2.6.1. (R/W)<sub>9</sub> photoadducts

(R/W)<sub>9</sub> showed a different behavior compared to Penetratin in MS and in MS/MS fragmentation (see Figures 92 and 93). Photo-cross-linking yields are different than with Pen. However, same trend is observed with a higher yield for unsaturated fatty acids. The peptide sequence has indeed an influence on the stability of the formed peptide-lipid adduct. For all adducts, fragmentation corresponding to the dissociation of the newly formed covalent bond between (R/W)<sub>9</sub> and the fatty acid is highly favored leading to an abundant fragment ion (base peak) at the m/z of the (R/W)<sub>9</sub> peptide (m/z 2392). Abundant losses arising from protonated arginine residues are observed at lower m/z for all fragment ions as well as for the parent ion, explaining the high noise observed in the region between the parent ion and the fragment ion at the m/z of (R/W)<sub>9</sub>. These losses are due to the high R content of the (R/W)<sub>9</sub> peptide (6R). The loss of 17u, which corresponds to the neutral loss of NH<sub>3</sub> from the R side chain is in competition with losses of 42 (NH=C=NH) and 59u (NH=C(NH<sub>2</sub>)<sub>2</sub>) from the guanidyl groups.<sup>265</sup> Most of the internal energy is consumed by both fragmentation pathways in the case of (R/W)<sub>9</sub>. Fragment ions (b- or y-ions) corresponding to fragmentation of the peptide backbone are observed with very low intensity. However, some P-B fragments are still produced in the low mass range of the MALDI-TOF/TOF spectra (Figure 93).

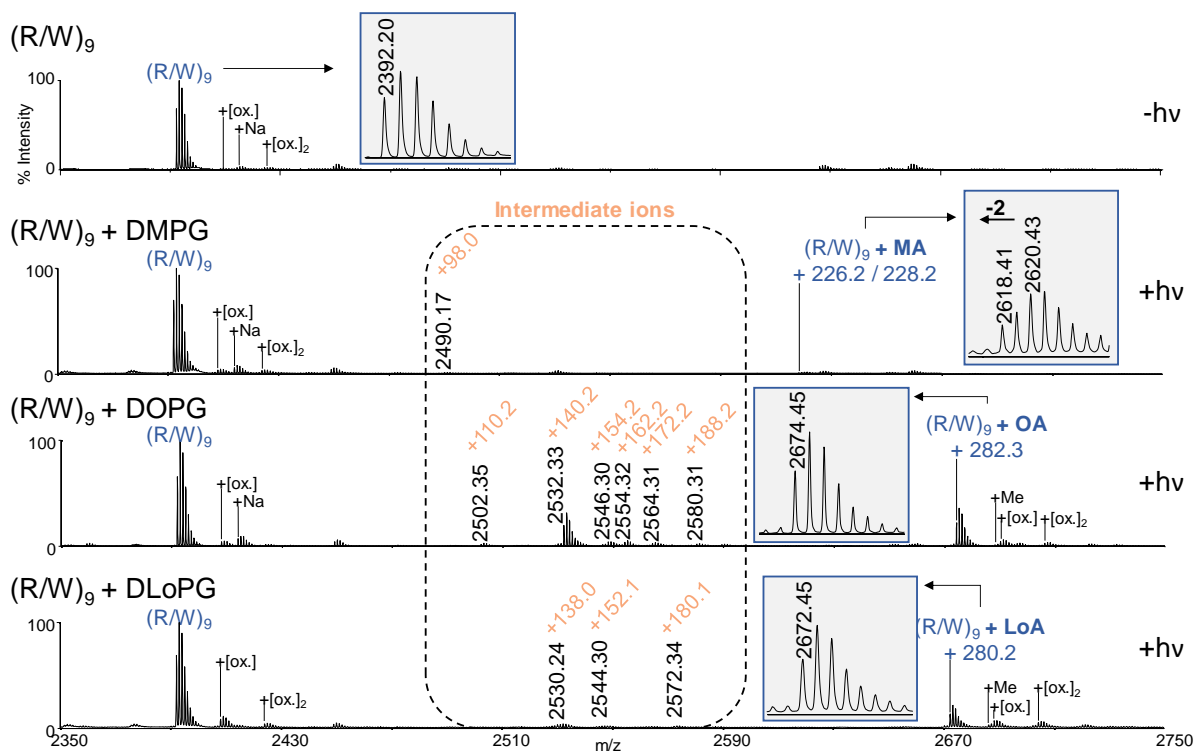


Figure 92. MALDI-TOF spectra positive ions, reflector mode of the Bzp-induced photo-cross-linking between Biot(O<sub>2</sub>)-G<sub>5</sub>-K(Bzp)-RRWRRR-NH<sub>2</sub> (R/W)<sub>9</sub> and negatively charged MLVs of various fatty acid chains. Control (R/W)<sub>9</sub> without irradiation (-hv), (R/W)<sub>9</sub>+DMPG+hv, (R/W)<sub>9</sub>+DOPG+hv, (R/W)<sub>9</sub>+DLoPG+hv.

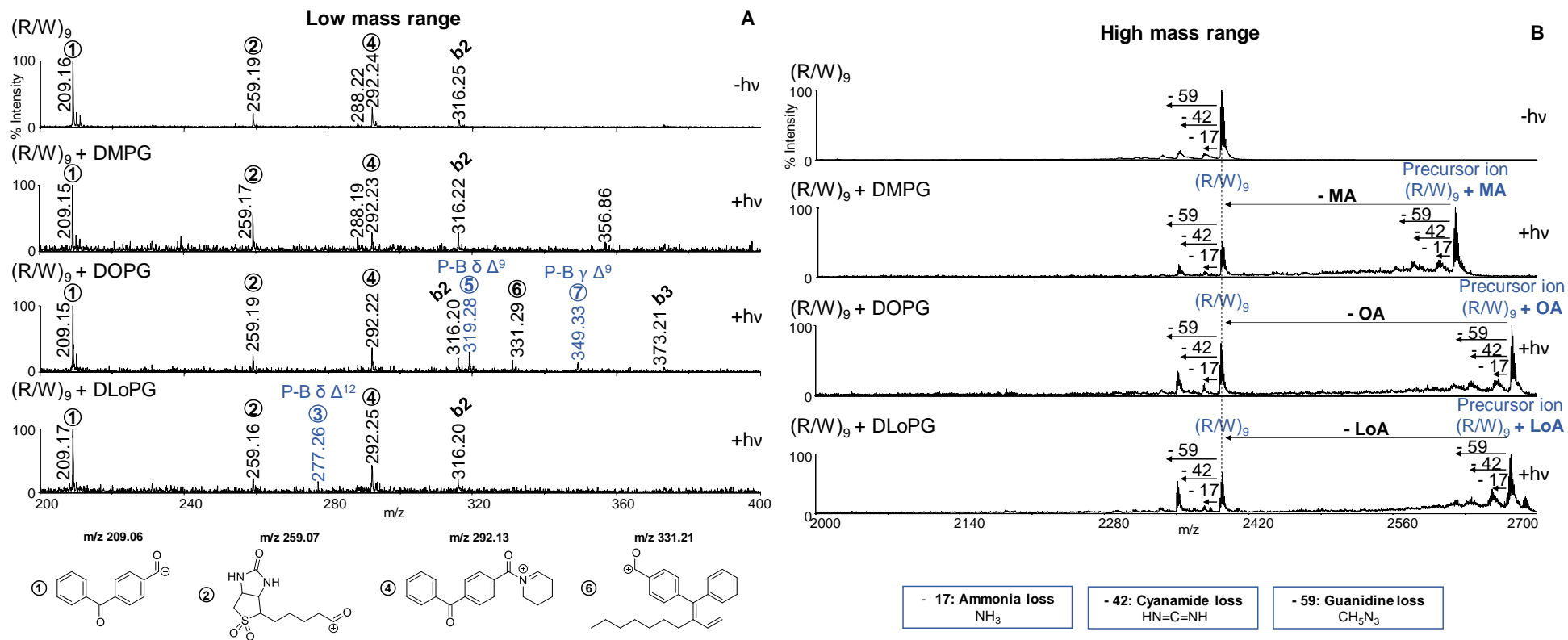


Figure 93. MALDI-TOF/TOF spectra (positive ions, reflector mode) of the Bzp-induced photo-cross-linking between Biot(O<sub>2</sub>)-G<sub>5</sub>-K(Bzp)-RRWWRRWRR-NH<sub>2</sub> (R/W)<sub>9</sub> and negatively charged MLVs of various fatty acid chains. Control (R/W)<sub>9</sub> without irradiation (-hv), (R/W)<sub>9</sub>+DMPG+hv, (R/W)<sub>9</sub>+DOPG+hv, (R/W)<sub>9</sub>+DLoPG+hv. A) MS/MS low mass range, B) MS/MS high mass range.

### 3. New insights in Pen preference for fluid-phase bilayers

After identifying all side-products and reactions, as described above, we go further on the characterization of CPP/lipids interaction in a membrane bilayer. Since MALDI ionization of the photoadducts only relies on the peptide moiety, the intensity of the ion species likely reflects the relative proportion between the photoadducts and the peptide in the MLVs.<sup>5</sup> Therefore, we assume that the relative intensities between Pen and photoadducts are proportional to the photolabeling yields, which are very different depending on the PG acyl chain (Figure 78 and 81). These photolabeling yields can be ranked as follows: OA > MA~PA~EA > LoA (or *cis* 18:1 > 14:0~16:0~*trans* 18:1 > *cis* 18:2). Pen-OA photoadduct shows the highest relative intensity compared to Pen. These results cannot be explained with the H<sup>•</sup> abstraction kinetics that are more rapid for doubly allylic over allylic and secondary hydrogens (kinetics given in Figure 48). The *cis* 18:1 unsaturation (OA) is indeed more cross-linked than the *trans* 18:1 one (EA). *Trans* fatty acids adopt a linear configuration similar to that of saturated fatty acid, while *cis* fatty acids have a bent configuration. *Trans* fatty acids are more packed than *cis* ones. This suggests that Pen shows preferential interactions with OA lipid chains found in fluid phase, as it has been previously reported (see introduction).<sup>162</sup> It is therefore not surprising that Pen-MA, Pen-PA and Pen-EA photoadducts show comparable relative intensities compared to Pen. These acyl chains being saturated or *trans*-unsaturated are indeed found in more packed membrane domains (see main transition temperatures given in the Experimental section). In addition, although DLoPG should give the fastest kinetics thanks to the doubly allylic H<sup>•</sup> abstraction<sup>181</sup> (Figure 48), the corresponding photoadduct (Pen-LoA) has the lowest intensity signal relative to the one of Pen (Figure 78). This is likely due to the low stability of the formed adduct compared to other acyl chains, as supported by tandem MS (MS/MS; Figure 83) whose data that have been discussed above.

Altogether, these first results, with PG acyl chains only, clearly establish that H<sup>•</sup> abstraction kinetics do not dominate photo-cross-linking reactions of PG MLVs with Pen and that other key parameters such as the membrane fluidity has to be taken into account to understand Pen photoadducts.



## 4. Analytical workflow and application of the methodology

On Figure 94, we propose a simple analytical workflow for the comprehensive interpretation of MS spectra of Bzp-based CPP/lipid photo-cross-linking experiments taking into account all the secondary reactions we described above.

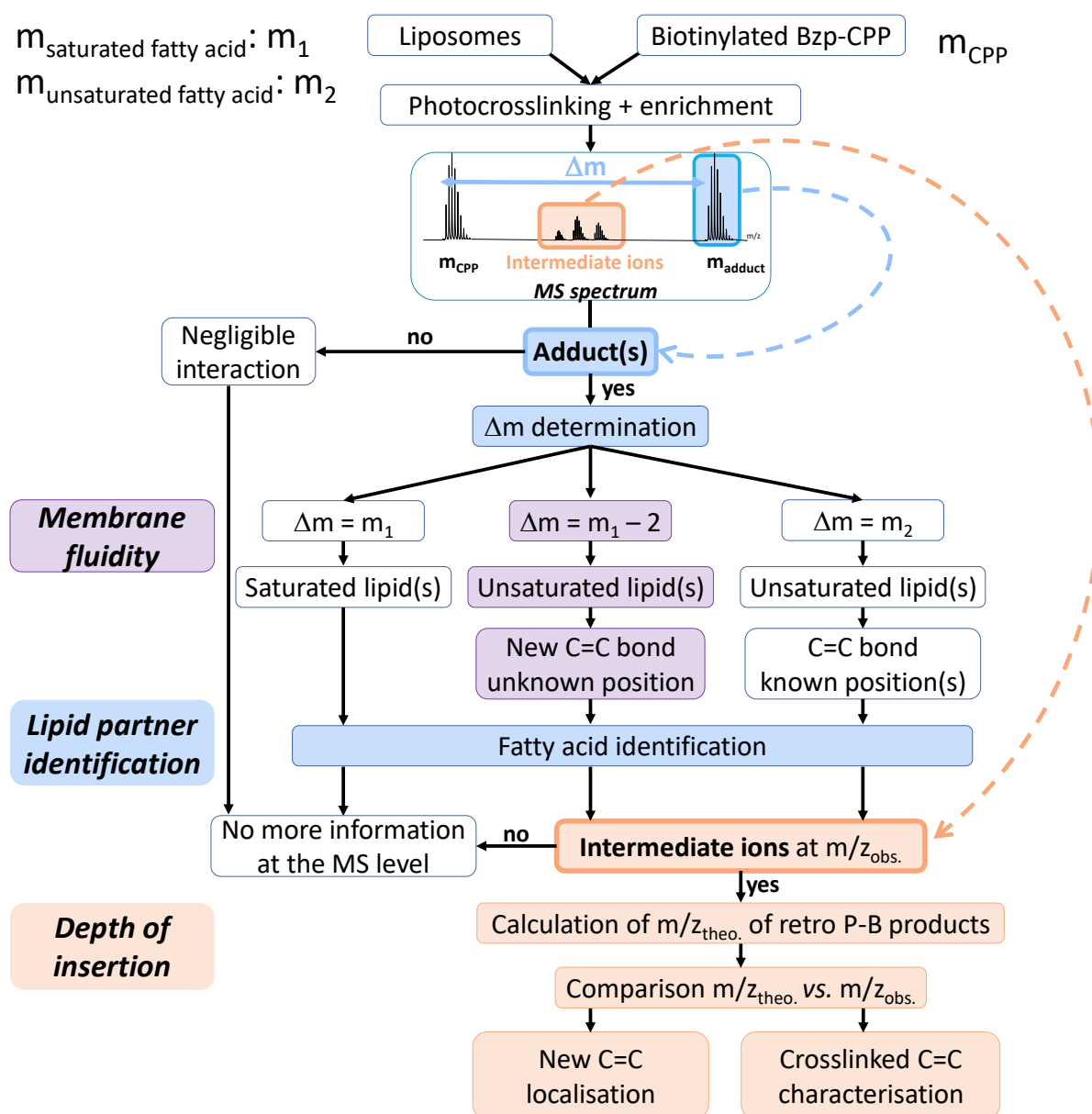


Figure 94. Analytical workflow for the comprehensive interpretation of the photo-cross-linking MS spectra.

Information on the interaction can be obtained at three levels. Identification of the CPP/fatty acid adduct(s) tells about lipid recognition preference by the CPP (Figure 94, blue boxes). Analysis of the isotope distribution of the adduct(s) peak(s) and in particular the presence of the first isotope at  $m-2u$  compared to the expected  $m/z$ , gives information about the fluidity of the membrane in the vicinity of the Bzp (Figure 94, purple boxes). Finally, careful identification of potential intermediate ions gives an indication on the depth of insertion of the Bzp probe in the membrane, as it allows determination of the position of the photo-cross-linked C=C bond

as well as the position of any potentially newly formed C=C bond on the crosslinked fatty acid (Figure 94, orange boxes).

To illustrate this workflow, we studied the interaction of ApaPen with binary membranes composed of DMPG/Chol or DOPG/Chol (75:25 mol/mol). It is indeed very interesting to study the interaction of CPPs with Chol-containing membranes as it was previously showed that Chol is involved in the internalization mechanisms of tryptophan-rich CPPs such as Pen or (R/W)<sub>9</sub>.<sup>129</sup> Chol is known to condense and rigidify lipid bilayers containing phospholipids with unsaturated fatty acyl chains such as DOPG. In contrast, it has been found that Chol has preferential interactions with saturated lipids,<sup>266</sup> and that it fluidizes bilayers of di-saturated phospholipids (see Part 1 introduction for more details).<sup>267</sup> The obtained MS spectra are presented on Figure 95 (DMPG/Chol) and Figure 96 (DOPG/Chol). For DMPG/Chol, two adducts are observed (m/z at 3481 and 3641), corresponding to ApaPen+MA and ApaPen+Chol respectively. This shows that Chol molecules are present in the close vicinity of the CPPs bound to the membrane, likely because the peptide prefers the more fluid phase of the DMPG/Chol mixture. On the other hand, with DOPG/Chol, no ApaPen+Chol could be observed. This suggests that the interaction between ApaPen and DOPG is tighter than with DMPG or that ApaPen tends to exclude Chol from its immediate environment in the more rigid DOPG/Chol bilayer, to stay in a more fluid phase.

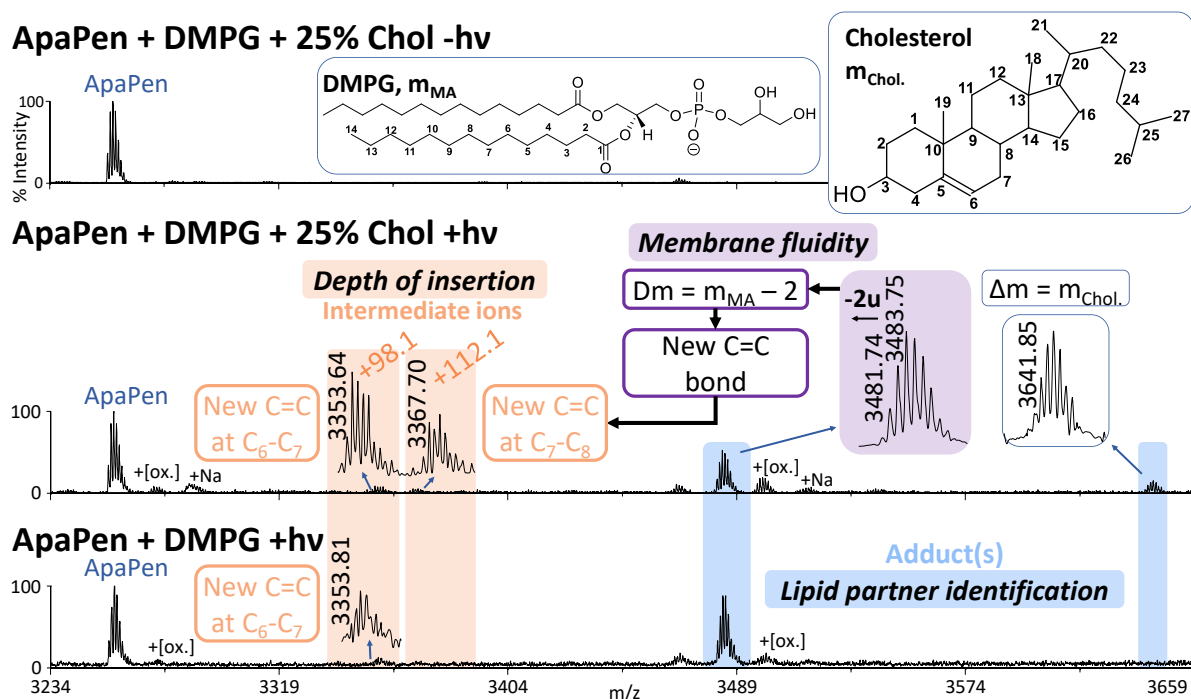
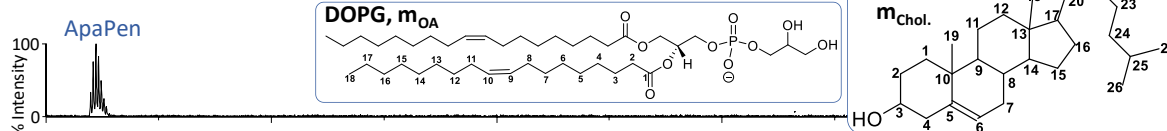


Figure 95. MALDI-TOF spectra (positive ions, reflector mode) of the Bzp-induced photo-cross-linking between ApaPen and binary MLVs of DMPG + 25% Chol. Top to bottom: Control ApaPen+DMPG+25% Chol without irradiation (-hv), ApaPen+DMPG+hv and ApaPen+DMPG+25% Chol+hv. Ions at 3353 and 3367 are  $\alpha$  retro P-B product ions with X= (CH<sub>2</sub>)<sub>4</sub> and X= (CH<sub>2</sub>)<sub>5</sub>, respectively. m<sub>MA</sub> = 228, m<sub>Chol</sub> = 386.

### ApaPen + DOPG + 25% Chol. -hv



### ApaPen + DOPG + 25% Chol. +hv

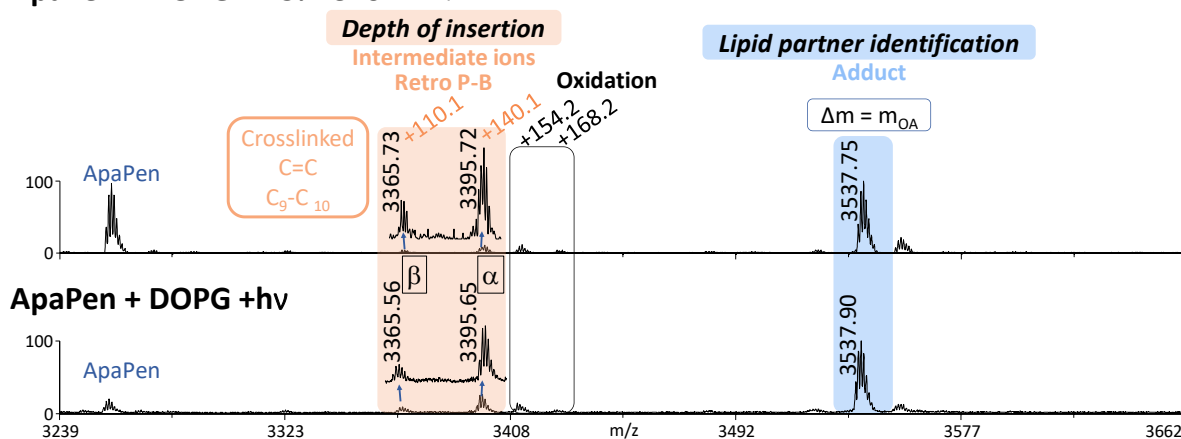


Figure 96. MALDI-TOF spectra (positive ions, reflector mode) of the Bzp-induced photo-cross-linking between ApaPen and binary MLVs of DOPG + 25% Chol. Controls ApaPen+DOPG+25% Chol. without irradiation (-hv) and ApaPen+DOPG+hv, ApaPen+DOPG+25% Chol.+hv. Na: sodium adduct, [ox.]: oxidation. Retro P-B products observed in the MS spectra are  $\alpha$  and  $\beta$  ions as presented in Figure 85. Intermediate ions at +110 are  $\beta$  ions and ions at +140 are  $\alpha$  ions with  $X' = (\text{CH}_2)_4$  and  $X = (\text{CH}_2)_4$ , respectively.  $m_{\text{OA}} = 282$ .

When looking at isotope distribution of the adduct signals, the Chol adduct is at the expected m/z and the MA adduct still contains a contribution at -2u. With DOPG, the OA adduct is at the expected m/z, showing that the presence of 25% of Chol in the membrane does not rigidify the membrane enough to allow the formation of an additional C=C bond on DOPG or that the peptide recruits DOPG (and excludes Chol) to stay in a more fluid environment.

Finally, when looking at the intermediate ions, two distinct retro P-B products are clearly identified with DMPG in the presence of 25% Chol (m/z at 3353 and 3367) whereas only one is detected in the absence of Chol (m/z at 3353). In the latter case, the intermediate ion corresponds to the formation of the C=C bond between C6 and C7. As described above, the C6-C7 position suggests a rather shallow insertion of ApaPen in the lipid bilayer, which is consistent with what is known about Pen interactions with membranes as deep insertion of Pen cationic residues in the membrane would imply high energetic cost. Also, Pen W residues are known to position themselves at water/lipid interfaces of membranes.<sup>194</sup> It has been previously showed that Bzp-modified Pen has little effect on the fluidity and organization of a DMPG bilayer as probed by DSC.<sup>259</sup>

In the presence of Chol, the additional intermediate ion corresponds to the formation of the C=C bond between C7 and C8, showing heterogeneous depth of insertion, with some Bzp moieties reaching deeper in the hydrophobic core of the membrane. This clearly shows that the presence of Chol has a disordering effect on the DMPG membrane and allows deeper insertion of the CPP. Because retro P-B on Chol would only lead to ring opening with no mass

modification compared to the Chol adduct, no information on the position of the formed covalent bond can be obtained. However, the most likely positions are the C4 and C7 allylic carbons on Chol. Labelling on C7 would be consistent with the position of Chol in a phospholipid membrane.<sup>268</sup>

## 5. Formation of unusual c ions during the fragmentation of the Penetratin sequence by high energy CID (MALDI-TOF/TOF)

Focusing on MALDI-TOF/TOF data (in the range  $1965 < m/z < 2650$ ) presented in the manuscript in Figure 83, we can observe conventional b and y ions (b16, b17, y15, y16) as well as the c15 ion from the Pen peptide without irradiation (-hv) and after irradiation (+hv) where same fragment ions are observed, crosslinked to the intact fatty acid as noted with +MA, +OA and +LoA for the adducts with myristic, oleic and linoleic acids, respectively. One can notice important losses of 42u (HN=C=NH) from b ions due to the presence of internal R residues<sup>265</sup> and the stable c15 ion, unusual for CID fragmentation. This c15 ion is highly intense and is even the base peak in the region of the peptide fragments (Figure 83, zoom on the peptide fragments). This stable c ion is unusual for CID fragmentation for which generally only b and y ions are observed in the case of peptide fragmentation. It can be noted that the complementary z8 ion is also observed at m/z 1160. c and z ions are generally described when peptides are fragmented by methods involving the use of electrons for fragmentation (ETD and ECD, see introduction).

An acetylated Penetratin sequence (Ac-RQIKIWFQNRRMKWKK-NH<sub>2</sub>) was used in order to assess whether the presence of this unconventional fragmentation is specific to the peptide sequence. The MS/MS spectrum is presented in Figure 97. The interpretation of the MALDI-TOF/TOF acetylated Penetratin fragmentation data allows us to observe the conventional b and y ions as well as highly intense c8 ion and its complementary z8 ion at the QN bond in the middle of the Penetratin sequence. We can thus be sure that the formation of these ions is not due to the presence of a lipid in the peptide/lipid photoadduct, to the Bzp photoprobe or to the biotin group. It is worth noting that c8 and z8 ions observation is independent on the matrix used. As previously mentioned, 2,5-DHB is a reducing matrix known to induce radical mechanisms in the ion source that could lead to the formation of c and z ions in CID. The unusual ions are observed in 2,5-DHB and CHCA matrices, dismissing the hypothesis of an ISD mechanism-type in the ion source involving a reducing matrix such as the ones presented in introduction.

Another interesting feature is that the fragmentation of the Engrailed homeodomain peptide, which has a very similar sequence to that of Penetratin (SQIKIWFQNKRAKIKK), does not lead to the observation of c or z ions.

The aim of this section is to understand how a c ion is produced and why specifically at the position between the residues Q and N of the Penetratin sequence. For this purpose, several shorter sequences of Penetratin were synthesized and analyzed in MALDI-TOF/TOF.

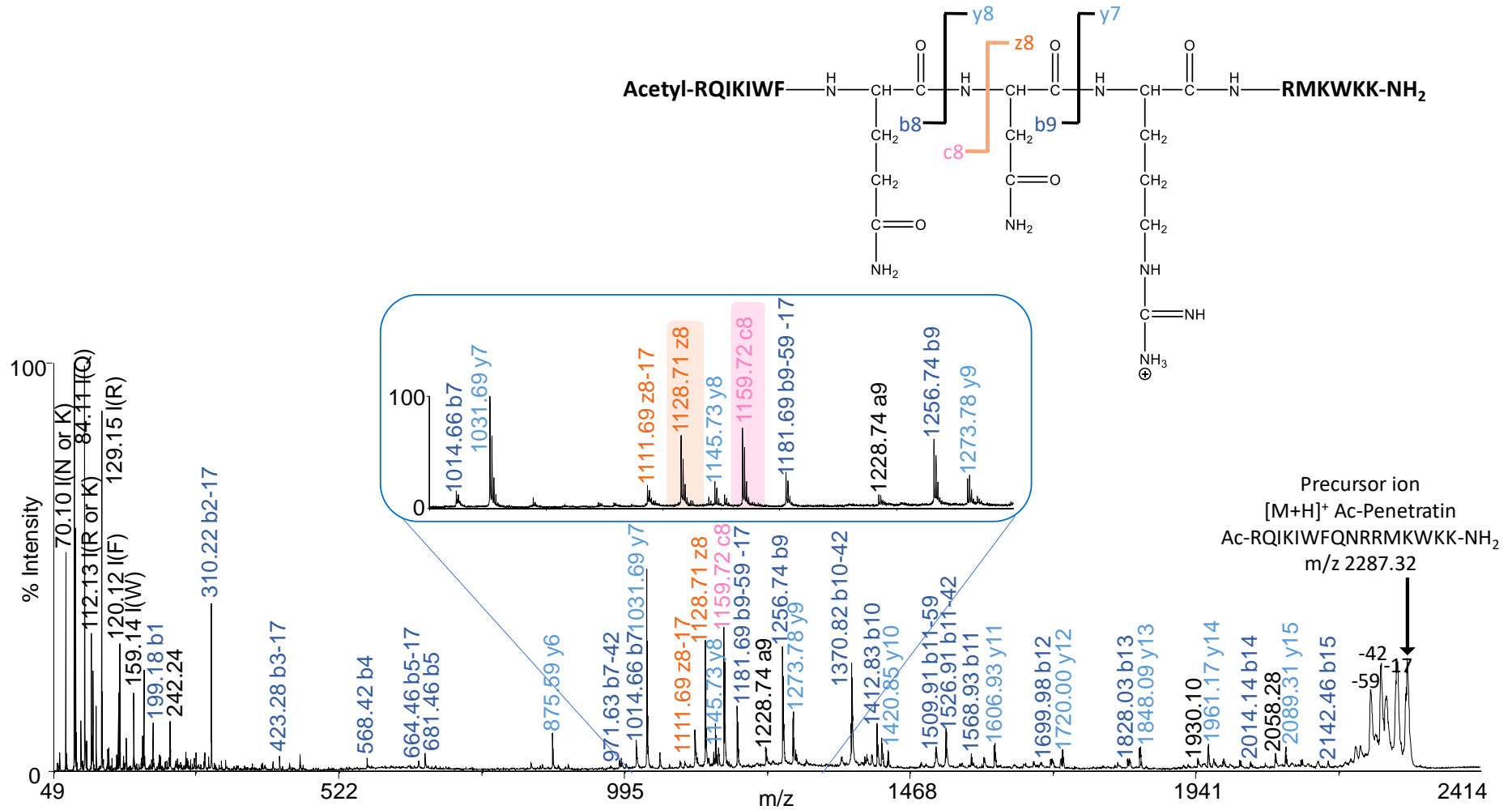


Figure 97. MALDI-TOF/TOF spectrum (gas N<sub>2</sub>, 1 keV, selection window ±7u) of the acetylated Penetratin (precursor ion m/z 2287.32). CHCA is used as the matrix. b ions are in dark blue, y ions are in light blue and unusual c8 and z8 ions are highlighted in pink and orange, respectively.

## 5.1. Mechanisms for the formation of c ions by CID MS/MS in the literature and comparison with our observations on the Penetratin sequence

In the literature, very few papers report the production of c ions by CID MS/MS and most of them concern the observation of c1 ions at the N-term of the peptide sequence. In this present case, the fragmentation occurs in the middle of the Penetratin sequence, between the glutamine and the asparagine residues (RQIKIWFQNRRRKMWKK).

It has been reported that the peptide primary structure is a prerequisite for the formation of c ions in high energy CID using a tandem magnetic-sector mass spectrometer, whatever the position of the cleaved bond is in the peptide sequence.<sup>269</sup> In this work, ions were accelerated from the source region into the magnetic sector by a 10 kV electric field. This acceleration is significantly greater (around 100 times) than the acceleration typical for a quadrupole instrument and in the same range as the acceleration used with a TOF (20 kV). This work showed that the cx ion formation is promoted by the nature of the amino acid at the C-term (x+1) to the cleavage position. In particular, the nature of the x+1 residue seems to influence the intensity of the produced cx ion, where the cx ion is the product ion of the cleavage between residues x and x+1. In some cases, the x+1 residue could offer a hydrogen atom in  $\beta$  of the residue amide bond that could be transferred to the nitrogen atom of the amide bond.<sup>269</sup> The mechanism is proposed in Figure 98, considering the shorter sequence of Penetratin, the decapeptide RQIKIWFQNR, which is sufficient to observe the c ion in question.

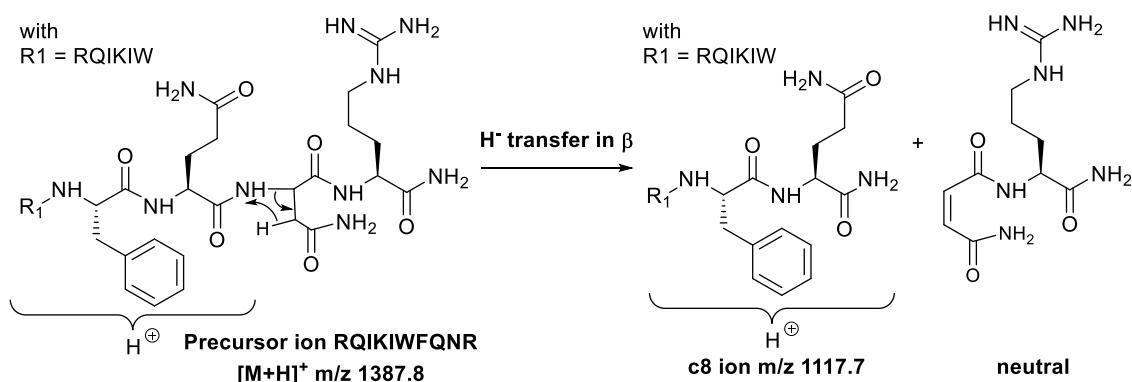


Figure 98. Proposed mechanism for the formation of the c8 ion upon fragmentation of the peptide RQIKIWFQNR, *via* a hydride transfer in  $\beta$ .

Their study on 168 peptides spectra acquired using high energy CID MS/MS allowed the correlation between formation of a cx ion and the nature of the residue in position x+1. They have demonstrated that having a threonine in the position x+1 considerably favors the cx cleavage. Also, to a lesser extent, tryptophan, lysine, serine and asparagine residues, in this order, favor the cx fragmentation directed at the N-term of these residues (Figure 99).

T>W>K>S>Q>C>N>L>D>Y>F>R>P>G>E>A>H>V>I>M  
 50                      20                      10                                      5                                      0%

Figure 99. Amino acid residues in decreasing order relative to the probability they occur at the x+1 position to cx cleavage (expressed as a percentage). Results from <sup>269</sup>.

The nature of the residue at the position x appeared to have little effect on the c ion formation. Still, they also propose a ranking of the amino acid residues favoring residues Q and R at the N-term of the produced c ion (Figure 100).

$$\begin{array}{cccc} \text{R} & > & \text{Q} & > & \text{P} & > & \text{W} \\ 28.2 & & 18.8 & & 1.3 & & 0\% \end{array}$$

Figure 100. Amino acid residues in decreasing order relative to the probability they occur at the x position to cx cleavage (expressed as a percentage). Results from <sup>269</sup>.

What emerges from this study is that the QN amino acids position seems likely to favor the c ion fragmentation, even though it is not the most favorable.

In addition to the nature of the amino acid residues in the vicinity of the cleavage site, the same work highlights the importance of the presence of an arginine residue on the N-term fragment, which would be a prerequisite to observe the c ion. This basic residue would retain the proton and direct the fragmentation. Indeed, fragmentation can occur without being observable, if the fragment thus formed is not charged. Thus, the presence of a protonatable basic residues on the peptide sequence conditions the observation of c and z ions. This could explain why we do not observe the c and z ions with the Engrailed-2 sequence, as the N-term residue is a serine, contrarily to the arginine of the Penetratin sequence. Thus, the lysine residue in position 4 of the sequence SQIKIWFQNKRAKIKK which is similar to Penetratin, does not seem to protonate. Decapeptides inspired from the Penetratin and the Engrailed sequences were synthesized and analyzed in high energy CID MALDI-TOF/TOF (1 keV, N<sub>2</sub> gas). Presence or not of the considered c and z ions are reported in Table 10. The c ion could be observed only if a residue with high proton affinity like an arginine was present on the N-term fragment. Thus, these results are well correlated to the literature. Also, it can be noted that the presence of a lysine in position 4 of the Penetratin is not sufficient to observe the c ion, thus this residue must not be protonated as in the SQIKIWFQNKRAKIKK sequence.

Table 10. Observation of the c and z ions corresponding to the cleavage at the position QN of decapeptides MALDI-TOF/TOF spectra.

Peptide sequence	QN c ion	QN z ion
RQIKIWFQNR	Yes	Yes
SQIKIWFQNR	No	Yes
RQIKIWFQNK	Yes	Yes
SQIKIWFQNK	No	Yes

Another work has shown the production of c1 ions from peptides containing a glutamine residue at the position 2 of their sequence, acquired with an ESI-Q/TOF instrument. These c1 ions were obtained by the rearrangement of a non-classical cyclic isoimide b2 ion, which was verified by H/D exchanges. However, the c ions observed show a relatively low intensity compared to the one observed in the case of Penetratin. The same type of mechanism could be considered with an asparagine as the x+1 residue to the cleavage site, as it can also lead to



the formation of a non-classical cyclic isoimide b ion (see introduction). This mechanism, adapted to the peptide RQIKIWFQNR, is presented in Figure 101.

The unconventional  $c_8$  ion would be produced by a sequence-specific reaction involving the N residue in position 9 of the sequence, by a rearrangement (hydride transfer in the gas phase) of a non-classical form of the  $b_9$  ion involving the formation of a cyclic isoimide form<sup>229</sup> in the gas-phase during CID. It can be noted that this mechanism involving the rearrangement of a b ion, does not allow the production of the complementary z ion observed on our spectra. The presence of the complementary z ion implies that a direct fragmentation pathway is involved. However, it is possible that the two mechanisms co-exist.

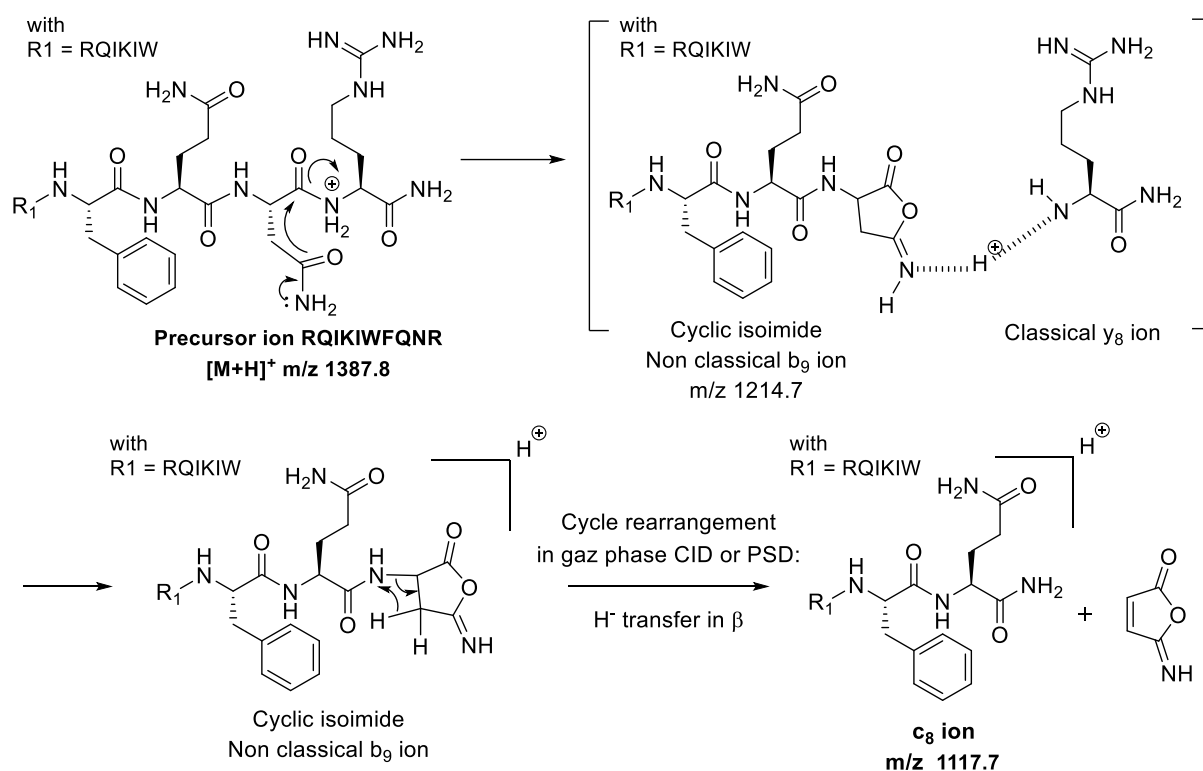


Figure 101. Proposed mechanism for  $c_8$  ion formation from a consecutive reaction occurring on the  $b_9$  ion of the peptide RQIKIWFQNR, *via* a cyclic isoimide intermediate.<sup>229,270</sup>

The nature of the second residue for the production of  $c_1$  ions has also been investigated by another group, using an ESI-Q/TOF instrument, who reports as well an influence of the peptide length.<sup>271</sup> They report that a glutamine or an asparagine residue in position 2 of the peptide sequence favors the formation of  $c_1$  ions. The effect of the nature of the first amino acid was tested and led to the conclusion that there is a correlation between the size of the residue of the amino acid in position 1 and the intensity of the  $c_1$  ion. It was not reproducible for every peptide sequences but, in general, intensity of the  $c_1$  ion increased with molecular weight of the residue in position 1. They explain this by the occurrence of different  $b_2$  ion structures, which result in different fragmentation behaviors and therefore variable intensities of the  $c_1$  ions.<sup>271</sup>

Using pentapeptides mimicking the  $c_8$  cleavage site of Penetratin, we tested the effect of various amino acid residues at the N-term position to the cleaved amide bond (Figure 102). We

find the same tendencies as the ones reported in the literature,<sup>269,271</sup> apart for the W residue in position x, which seems to lower the direct fragmentation reaction.

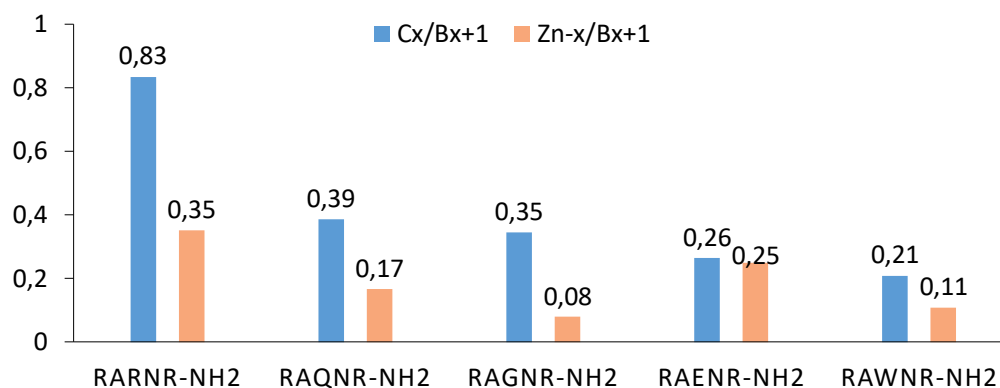


Figure 102. Relative intensities  $c_x/b_{x+1}$  and  $z_{n-1}/b_{x+1}$  observed in MALDI-TOF/TOF spectra (gas  $N_2$ , 1 keV, selection window  $\pm 7u$ ) of pentapeptides to investigate the c8 and z8 ions formation on the Penetratin sequence. Effect of the nature of the residue in position x, N-term to the cleavage site.

In their case, the c1 ions formation has been attributed to two competing mechanisms: one is a consecutive fragmentation of the b2 ion (the same as proposed in the previous paper<sup>270</sup>, Figure 101) and the other consists in a direct fragmentation forming the c1 ion and its complementary  $z_{max-1}$  ion. The later pathway implies the intervention of the mobile proton model, with the protonation of the nitrogen atom of the amide bond between the residues x and x+1. The amide bond would be cleaved by the nucleophilic attack from the  $-NH_2$  amide group of the lateral chain of a glutamine or an asparagine residue in position 2 of the peptide sequence, which leads to the production of the c1 ion. This mechanism is presented in Figure 103, considering the shorter sequence of Penetratin, the decapeptide RQIKIWFQNR, which is sufficient to observe the c and z ions in question. It can be noted that in our case, the nucleophilic attack would be initiated by the asparagine residue.

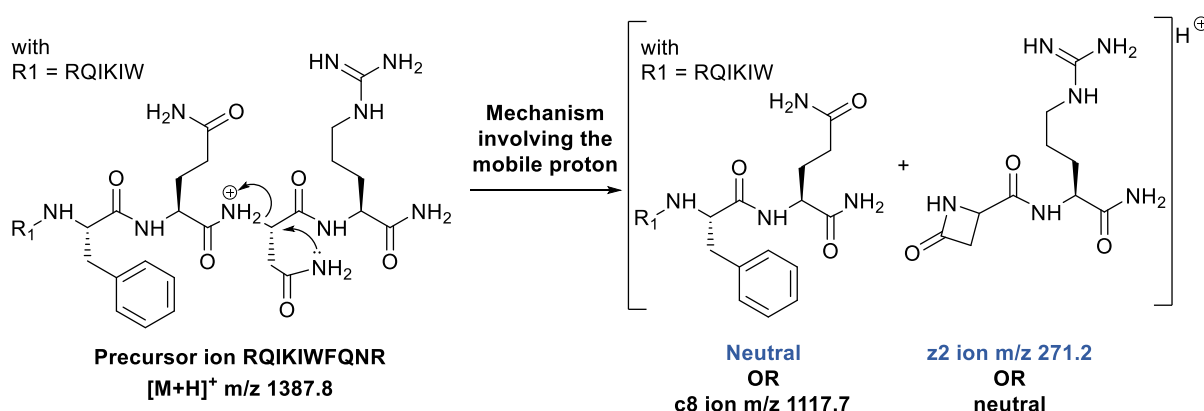


Figure 103. Proposed mechanism for the formation of c8/z2 ions from peptide RQIKIWFQNR, leading to a z2 fragment with a four-ring structure at the N-term residue. Adapted from <sup>271</sup>.

By comparing the intensity ratios of the c and z ions over the b2 ion intensity, they also showed that increasing the peptide length made the ratio of the c1 ion intensity over the b2 ion intensity decrease, showing that the direct mechanism is less favored. As their basic residue

was always positioned at the C-term of the peptide sequence, this could be an effect of the increasing distance of the mobile proton to the cleavage site.

In our case, using Penetratin analogues of various lengths (Figure 104), without changing the positions of the amino acids, we show that a longer peptide chain tends to make the c and z ions intensity increase, thus favoring a direct fragmentation pathway.

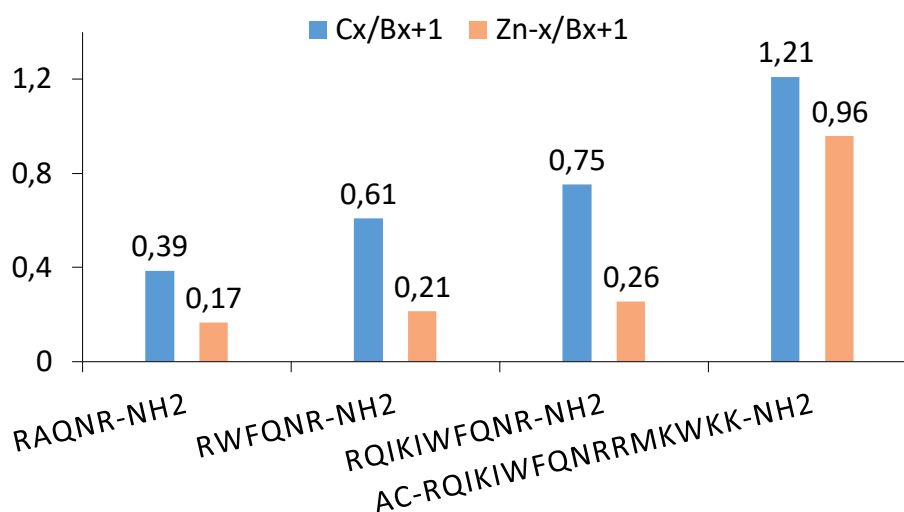


Figure 104. Relative intensities  $c_x/b_{x+1}$  and  $z_{n-1}/b_{x+1}$  observed in MALDI-TOF/TOF spectra (gas  $N_2$ , 1 keV, selection window  $\pm 7u$ ) of Penetratin analogues to investigate the c8 and z8 ions formation on the Penetratin sequence. Effect of peptide chain length.

Another fragmentation pathway has been proposed for the formation of c ions, this time not necessarily in position 1 of the peptide sequence. It would involve a positive charge localized on the N-term part of the peptide, and a glutamine, asparagine or lysine residue in position  $x+1$  to the cleaved bond.<sup>272</sup> They indeed observed  $c_x$  ions on model peptides having an N-term arginine residue upon low-energy CID, using an ESI-Q/TOF instrument. The protonated basic residue would sequester the positive charge and remote it from the cleavage site. They used amino acids substitutions, hydrogen-deuterium exchange and density functional theory calculations to provide a suitable pathway. It consists in a McLafferty-type rearrangement *via* a charge remote fragmentation. This pathway is presented in Figure 105, adapted to the sequence RQIKIWFQNR.

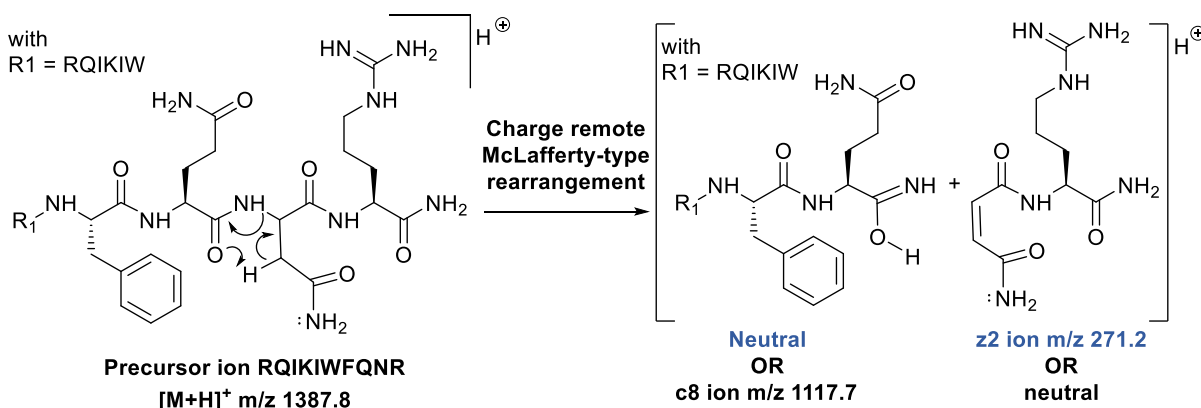


Figure 105. Proposed direct mechanism for the formation of c8/z2 ions from peptide RQIKIWFQNR *via* a charge remote McLafferty-type mechanism. Adapted from <sup>272</sup>.

In general, it is difficult to draw conclusions from these different studies. Some examples from the literature on the observation of c-ions in CID, as well as our experiments on shorter versions of Penetratin, suggest an importance of the peptide structure as well as the position of the amino acids in the sequence in relation to the fragmentation site. According to a study of the primary peptide structure, residues Q and N and their positioning would be favorable for the observation of such ions c.<sup>269</sup> A mechanism for the formation of ions c involving rearrangement from an ion b has also been proposed.<sup>270</sup> However, it would appear that the ion c observed in the case of Penetratin is at least partly derived from direct fragmentation since the corresponding ion z is also observed. Another study suggests that the production of c-ions is dependent on the amino acid in position 2 and the length of the peptide, and propose a mechanism for the direct fragmentation involving a mobile proton.<sup>271</sup> It should be noted that protonation sites should be taken into account in this type of study. Indeed, fragmentation can occur without being observable, if the fragment thus formed is not charged. Thus, the presence of protonable basic residues on the peptide sequence conditions the observation of c ions. Finally, a more recent article proposes a McLafferty-type mechanism induced at a distance by a localized N-terminal charge of the peptide.<sup>272</sup>

All these works result from the study of different peptide sequences in terms of nature of amino acids, peptide length and very probably 3D structure in the gas phase. It is thus quite difficult to retrieve a rational interpretation and to compare these results to each other and to our data. Besides, the c ions production seems to be the result of different routes of fragmentation that are in competition with each other.

## 5.2. Peptide protonation state

A work reports the MS/MS fragmentation of the Penetratin peptide, using an ESI-Q/TOF instrument and with varying the collision energy from 12 to 40 eV. Fragmentation of the multi-protonated peptide at charge +4 does not lead to the formation of c or z ions.<sup>273</sup> They observed the same b and y fragments whatever the collision energy used. In this paper, they estimated the probability of protonation for the different basic residues of the Penetratin sequence for the  $[M+4H]^{4+}$  form based on energies calculation. A comparison of the energy conformers is presented in Table 11.

In addition, they suggest that the peptide structuration in  $\alpha$ -helix would prevent the fragmentation of the central peptide domain. However, this hypothesis is based on the structure of Penetratin in membrane-like environments studied by NMR spectroscopy.<sup>100,189</sup> It has already been shown that Penetratin structures in an  $\alpha$ -helix in contact of a membrane. However, this is not the case in the context of gas-phase fragmentation of Penetratin.

Although these results could suggest that the absence of c and z ions on the Penetratin is due to the low energy collision used, our recent work using a CID ESI-TQ (40 eV, Ar) and an ESI-LTQ-Orbitrap (CID, NCE 20%, N<sub>2</sub>) instruments actually reveals a different tendency. In fact, the c and z ions could be observed only when fragmentation is performed on the Penetratin in the charge states  $[M+H]^+$  or  $[M+2H]^{2+}$ , with a higher intensity of the c ion fragment of  $[M+H]^+$ . Above these charge states, at  $[M+3H]^{3+}$  and  $[M+4H]^{4+}$ , the c and z ions were not observed. Still, cx ions have

a low intensity on the CID spectra obtained with the collision gas Ar and N<sub>2</sub> compared to the intensities observed in MALDI-TOF/TOF.

Table 11. Single-point energy calculations of Penetratin with four protons located at different positions using B3LYP/6-31G\*//HF/3-21G\*.<sup>273</sup>

Protonation site	$\Delta E$ (kcal/mol)	Protonation site	$\Delta E$ (kcal/mol)
R <sup>1</sup> R <sup>10</sup> R <sup>11</sup> K <sup>4</sup>	43.5	R <sup>1</sup> R <sup>11</sup> K <sup>4</sup> K <sup>16</sup>	50.8
R <sup>1</sup> R <sup>10</sup> R <sup>11</sup> K <sup>13</sup>	0	R <sup>1</sup> R <sup>11</sup> K <sup>4</sup> K <sup>15</sup>	54.3
R <sup>1</sup> R <sup>10</sup> R <sup>11</sup> K <sup>15</sup>	0.33	R <sup>1</sup> R <sup>11</sup> K <sup>4</sup> K <sup>13</sup>	57.9
R <sup>1</sup> R <sup>10</sup> R <sup>11</sup> K <sup>16</sup>	2.0	R <sup>1</sup> R <sup>11</sup> K <sup>13</sup> K <sup>15</sup>	22.3
R <sup>1</sup> R <sup>10</sup> K <sup>4</sup> K <sup>16</sup>	29.2	R <sup>1</sup> R <sup>11</sup> K <sup>13</sup> K <sup>16</sup>	24.8
R <sup>1</sup> R <sup>10</sup> K <sup>4</sup> K <sup>15</sup>	37.7	R <sup>1</sup> R <sup>11</sup> K <sup>15</sup> K <sup>16</sup>	29.8
R <sup>1</sup> R <sup>10</sup> K <sup>4</sup> K <sup>13</sup>	27.6	R <sup>10</sup> R <sup>11</sup> K <sup>13</sup> K <sup>15</sup>	26.6
R <sup>1</sup> R <sup>10</sup> K <sup>13</sup> K <sup>15</sup>	26.7	R <sup>10</sup> R <sup>11</sup> K <sup>13</sup> K <sup>16</sup>	21.1
R <sup>1</sup> R <sup>10</sup> K <sup>13</sup> K <sup>16</sup>	14.9	R <sup>10</sup> R <sup>11</sup> K <sup>15</sup> K <sup>16</sup>	29.3
R <sup>1</sup> R <sup>10</sup> K <sup>15</sup> K <sup>16</sup>	23.2		

These results might suggest an importance of the structure of the peptide in the gas phase for the direct fragmentation. Indeed, the multi-protonated state of Penetratin could favor charge repulsion and thus a different conformation of the peptide, impacting the fragmentation processes for the charge states above +2.

### 5.3. Peptide structuration

This leads us to the issue of the peptide structuration in the gas phase. Indeed, the charge repulsion above +2 leading to the loss of structure in the gas-phase, shows that the structure is needed for the c/z fragmentation to occur. Also, the fact that the c ions intensity is higher when the sequence is longer could indicate a mechanism dependent on the structure.

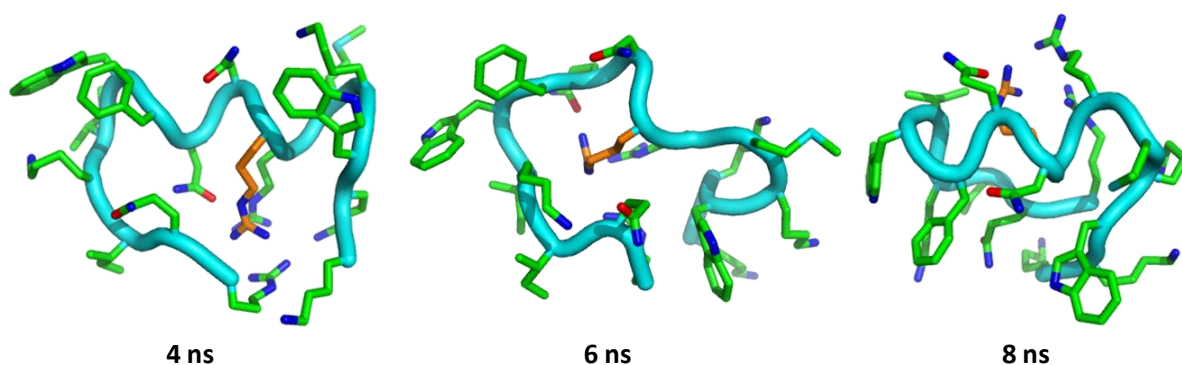
A collaboration with the NMR team of the laboratory allowed us getting some insight on this question by collecting molecular dynamics of the Penetratin peptide *in vacuum*, using the Amber force field ff14SB. This work was performed in the context of the Ph.D. project of Edward Chalouhi, supervised by Olivier Lequin. A simulation was acquired with a unique protonation site on the Arg 10, following the protonation sites probabilities mentioned earlier (Table 11) and based on our observations with the peptide SQIKIWFQNKRAKIKK which is similar to Penetratin and does not seem to protonate on Lys 4.<sup>273</sup> The simulation lasts 10 ns, starting from a conformation in  $\alpha$ -helix, and at T= 500 K. Snapshots of the simulation at 4 ns, 6 ns and 8 ns, as well as Ramachandran diagrams for each amino acid residue of the Penetratin sequence, numbered from position 43 to position 58 of the Antennapedia third helix sequence R<sup>43</sup>QIKIWFQNRMMKWKK<sup>58</sup>-NH<sub>2</sub>, are given in Figure 106.

The molecular dynamics results show that the region of the QN residues has a propension to structure in an  $\alpha$ -helix, whereas the rest of the sequence do not structure. Interestingly, the peptide would present a partial helix structure  $\alpha$ , precisely at the level of the residues at the center of the sequence, where the fragmentation giving the atypical c ion occurs. Indeed, the

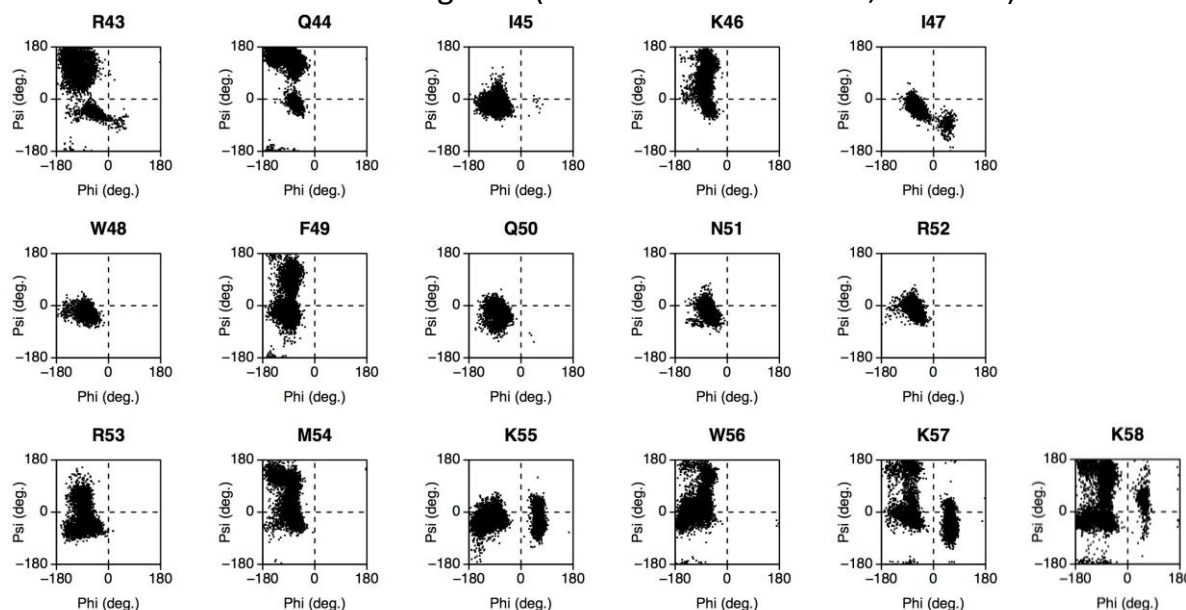
$\alpha$ -helix conformation is maintained throughout the simulation on the residues Trp 48, Gln 50, Asn 51 and Arg 52.

The structuration of this particular region of the peptide seems very interesting regards to the specific fragmentation observed in CID MS/MS. Further study on the peptide structure could help to understand this particular formation of the *c/z* fragment ions at the NQ position. Additional simulations of the Penetratin structuration *in vacuo*, with multi-protonation sites involved, are now studied, whose results will help deciphering the phenomenon.

Besides, additional experiments in ion mobility could provide interesting information on this point. Measuring the effective cross-section of Penetratin *in vacuo* could inform us, by comparing this effective cross-section with the theoretical cross-section for Penetratin in the form of an  $\alpha$ -helix, about the possible role of this structure in the fragmentation of the QN bond leading to the *c* ion.



Ramachandran diagrams (Helix domain Phi = -60, Psi = -40)



## Dynamic of Penetratin in *vacuum*

Protonation of R<sup>52</sup>, starting conformation: helix, simulation 10 ns, 500 K

Figure 106. Molecular dynamic simulation of the Penetratin *in vacuo* (Amber forcefield ff14SB).

#### 5.4. Pursuance of the project to elucidate the c ions formation

The comparative study of the fragmentation of Penetratin in the gas phase with various ions activation techniques (high and low energy CID, ExD) is the subject of a project directed by Emmanuelle Sachon and is currently in progress (TGE, *fédération de recherche* FT-ICR). Indeed, experiments to vary the collision energy or to apply other types of fragmentation by the use of FT-ICR mass spectrometers and electron fragmentations (ETD, ECD and EID) would provide additional information to better define this mechanism.

First experiments using an ESI-TQ instrument allowed to obtain more information about the mode of formation of the c ion at the QN position by using the parent ion mode. In this mode, all the precursor ions of the c ion formed by CID are searched. When an ion (Q1 in scanning mode) dissociates in the collision cell to give the c fragment, its m/z value is recorded. Therefore, even if it is always the same c fragment ion that reaches the detector (Q3 fixed value on the m/z of the c ion), the spectrum will provide all the precursor ions from which it is derived. It appeared that the cx ion is produced from the full peptide  $[M+H]^+$  and  $[M+2H]^{2+}$  but not from  $bx+1$ , using the sequence RWFQNR-NH<sub>2</sub>. In this specific sequence, fragmentation of the peptide backbone at the QN position between CH-NH leads to the c4 ion of interest at m/z 635 (Figure 107). In addition, MS<sup>3</sup> experiments performed on an ESI-LTQ-Orbitrap instrument showed that the  $bx+1$  ion does not produce the cx ion with RWFQNR-NH<sub>2</sub>, the  $bx+1$  ion produces the cx ion (low intensity) with RQIKIWFQNR-NH<sub>2</sub>, and the cx ion produces only b and a no c ion.

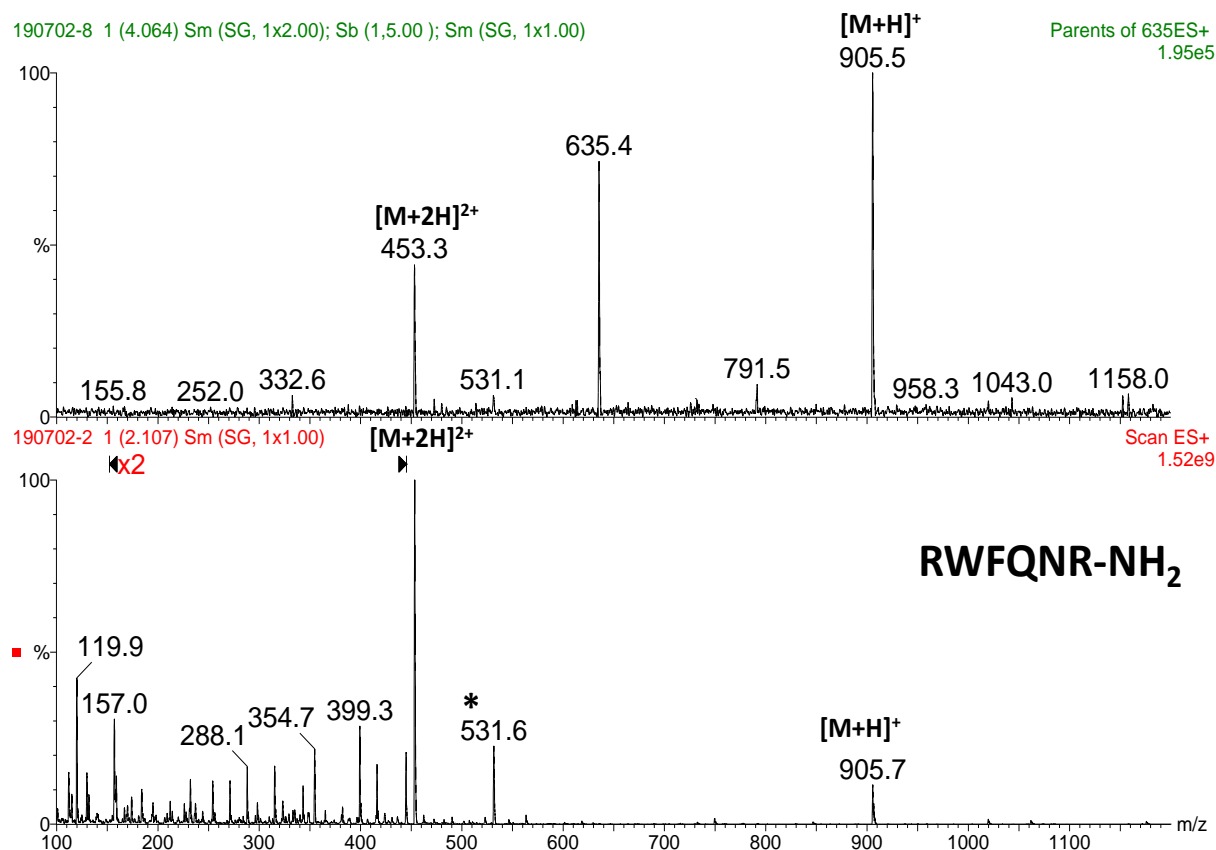


Figure 107. Parent ion mode of the c4 ion at m/z 635 (ESI-LTQ, 40 eV, Ar gas).

The use of an ESI-LTQ-Orbitrap instrument allows us to strengthen the hypothesis that the  $c_x$  ions are probably produced *via* two fragmentation pathways, especially in the case of the longer peptide chain, involving a direct fragmentation and a consecutive rearrangement of the  $b_{x+1}$  ion. In the case of shorter sequence (RWFQNR), it seems that only the direct mechanism leads to the  $c_x$  ion.

Still, many questions remain about the  $c$  ion formation specific to the QN position. How far is the peptide structuration implied in the fragmentation process? How does it impact the formation of the different structures of the  $b_{x+1}$  ion (oxazolone, diketopiperazine, cyclic isoimide) and can lead consecutively to the  $c_x$  ion?

The project will continue with the use of an FT-ICR instrument that allows the peptide fragmentation in the CID or in the EXD modes. Accessibility to the two modes of fragmentation on the same equipment allows to compare the ions production obtained without artefacts due to the use of different instruments of variable geometry and source conditions. The ExD fragmentation modes (ECD, ETD and EID) are electron-induced fragmentation that will allow to observe the production of  $c$  and  $z$  ions in a classical manner.

First observations using the ECD mode of fragmentation on the ESI-Q-FT-ICR shows that all the  $c$  ions are produced with similar intensity, and that the QN position is not particularly favored in the case of a fragmentation induced by electrons.



## Conclusion

In this study, we give a full description of Bzp photoreactivity within a lipid bilayer and illustrate how it can be exploited to study the interactions of two CPPs, Pen and (R/W)<sub>9</sub> with lipid interaction partners at the molecular level. The studied reactions encompass classical C-C bond formation, oxidation of the fatty acid chains *via* double bond C=C formation, Paternò-Büchi reaction as well as Bzp-induced photosensitization leading to unsaturated lipids dimerization. Additionally, oxidation reactions leading to double bond cleavage can be observed on unsaturated lipids. The occurrence of consecutive reactions on the same fatty acid chain, requiring more than one UV-activated Bzp suggests that CPPs accumulate in the same region and are close to each other.

Mapping of these secondary reactions is important, for at least three reasons, which we summarized on an analytical workflow showing how to extract the maximum information out of a simple MS spectrum.

First, ignoring the photoredox reactions involving Bzp could lead to false interpretations or photoadduct identification, especially when working with binary mixtures containing saturated and unsaturated lipids with the same chain length. Careful analysis of the isotopic distributions will allow to differentiate the two products. Indeed, the isotopic pattern of the unsaturated lipid adduct should fit with the theoretical one, while the isotopic pattern of the saturated lipid adduct should reflect the heterogeneous contributions of the intact lipid adduct and the oxidized lipid adduct at  $-2u$ .

Second, careful analysis of isotopic distribution can give information on membrane fluidity in the immediate environment of the CPP. Additionally, presence of ions resulting from ROS-induced oxidation of the CPP/lipids photoadducts gives an indication on membrane fluidity which influences penetration of water-soluble radicals and oxidation.

Finally, analysis of the retro P-B products allows finer characterization of the CPP/lipid interaction at the atomic level without using MS/MS, giving information on the depth of insertion of the CPP in the membrane. We illustrate this by analyzing the interaction of Penetratin with membranes composed of a binary mixture of PG and Chol.

Being aware of these side reactions and knowing how to extract the information they provide at the MS level will be an asset for studying interaction of CPPs or any membrane active peptide with complex biological membranes composed of multiple lipids. This is a great advantage when analyzing sub-picomolar amounts of a given species knowing that MS/MS requires more material than MS experiments.

Finally, this is the first report of Paternò-Büchi reactivity and Bzp-induced photosensitization in a Bzp-based lipid photo-cross-linking setup. Such reactivity was previously reported to occur with DNA,<sup>215,274</sup> suggesting the universality of this phenomenon, which should never be overlooked when studying biomolecular interactions with Bzp-based photo-cross-linking. In addition, our study shed new light on the insertion depth of CPPs with regard to membrane fluidity properties, and brings evidence for the relevance of such approach using liposomes as an intermediate study before going to cells.

An unconventional gas-phase fragmentation pathway of Penetratin, leading to the formation of c-ions in CID MS, was also observed, at the specific position QN in the middle of the peptide sequence. The cx ions are probably produced *via* multiple fragmentation pathways, involving at least a direct fragmentation and a consecutive rearrangement of the bx+1 ion structured in a non-classical cyclic isoimide form. Contribution of the structuration of the peptide to the atypical fragmentation has been discussed. The propension of the QN region of the peptide to structure in  $\alpha$ -helix *in vacuo* seems to play a role in the existence of the c/z fragmentation. This study is still on-going to elucidate the unconventional mechanism. This work consists in a fundamental study of peptides fragmentation mechanisms in the gas phase. The better understanding of mechanisms in the gas phase will allow an easier interpretation of peptides MS/MS spectra for *de novo* sequencing and also to improve the identification and characterization of proteins in proteomics.

Several students have worked on this part of the project as part as their internship graduating programs. Carla Kirschbaum has participated to the experiments and bibliography work on the Paternò-Büchi reactions occurring in the peptide/lipid membrane system during her Master 1 internship. Samy Leprévost, as part as his 3<sup>rd</sup> year Bachelor internship, has synthesized and analyzed in MALDI-TOF/TOF the short length sequences of the Penetratin for the elucidation of the c ions formation in CID MS/MS. Marine Cosset has participated to the production of control experiments on the 2,5-DHB-induced ISD as part as the publication process of the Analytical Chemistry article during her Master 2 internship and will continue to work on the identification of interaction partners of membranotropic peptides using the method of photo-cross-linking coupled to MS during her Ph.D. starting this year.

# GENERAL CONCLUSION

This Ph.D. work has consisted in the study of the interactions of the CPP Penetratin with lipid membranes from a molecular point of view. First, the contributions of PIP<sub>2</sub> to the internalization of Penetratin were evaluated, mainly by biophysical approaches. In a second step, the photoreactivity of Bzp in model membranes was investigated. Figure 108 resumes the main conclusions of the project.

In the first part of this manuscript, the contributions of PIP<sub>2</sub> in the internalization of the CPP Penetratin were highlighted. In particular, the interaction of Penetratin with model membranes containing PIP<sub>2</sub> has been better identified. These results showed that PIP<sub>2</sub> present in the intracellular membrane leaflet is involved in the mechanism of peptide entry into the cell, and that its blocking by interaction with the PH domain inhibits the internalization of Penetratin in CHO cells. In addition, experiments conducted in DSC have highlighted the interaction of Penetratin with the polar heads of PIP<sub>2</sub>, as well as its superficial insertion into the membranes. The same study also suggested that Penetratin recruits several PIP<sub>2</sub> molecules and induces stiffening of model membranes containing PIP<sub>2</sub>. These effects have not been observed on liposomes containing PC or PS. In addition, tryptophan fluorescence studies have shown that the binding affinity of Penetratin is higher for liposomes containing PIP<sub>2</sub> than for liposomes containing PS, with an equivalent overall charge. Finally, photo-cross-linking experiments coupled with MS have identified PIP<sub>2</sub> as a partner in the interaction of Penetratin in liposomes composed of PC, PS and PIP<sub>2</sub>. The clustering effect of Penetratin on PIP<sub>2</sub> lipids has been confirmed by a molecular modeling simulation, where 4 to 5 PIP<sub>2</sub> lipids were recruited by a Penetratin molecule, in a model membrane composed of PC, PS and PIP<sub>2</sub> at a proportion 80/15/5.

In the second part, the Bzp photoreactivity in the particular context of lipid membranes was pointed out. The revealed secondary reactions of Bzp occur simultaneously in a single complex biological system: a membranotropic peptide inserted in a phospholipid bilayer. This work represents a significant improvement for the interaction partners identification by photo-cross-linking, and shows how to exploit in an original way the different reactivities of Bzp in the context of a lipid membrane. We have proposed an analytical workflow for the interpretation of mass spectra, providing access to information on the CPP/lipid interaction at the molecular level such as insertion depth or membrane fluidity in the vicinity of the CPP. An application of our analytical workflow illustrates the role of cholesterol in CPP/lipid interaction. It showed that the presence of cholesterol, known to fluidify membranes composed of saturated lipids, allows a deeper insertion of the CPP into the lipid bilayer. Besides, the lipid partner identification by the classical photo-cross-linking reaction showed that the Penetratin interacts preferably with the fluid phase, as reported earlier in the literature. In addition, secondary reactions involving the intervention of several activated Bzp, such as lipid dimerization or double bond formation, suggest an aggregation of the CPP at the PG membrane, which has also been reported by DSC experiments.

Finally, the MS/MS fragmentation of Penetratin revealed the formation of c ions, atypical in CID fragmentation. Some avenues of reflection have been proposed in order to elucidate this fragmentation pathway occurring at a very precise location in the peptide sequence. In

particular, the relationship between structuration in the gas phase and fragmentation process has been pointed out, using different MS instruments and NMR structure-based simulation.

The peptide's ability to form PIP<sub>2</sub> clusters, favored interaction with the fluid phase state, deeper insertion in presence of membrane cholesterol and propension to aggregate embody as many features to better understand the interaction of Penetratin with the lipid bilayer and to give insights on the direct translocation pathway of the peptide through the plasma membrane. The Bzp photoreactivity seems to constitute a powerful tool for the molecular analysis of the membranotropic interaction with model membranes. Indeed, the versatility of the Bzp photoprobe allows to have access to various parameters such as insertion depth, sensitivity to the membrane lamellar state and interaction partner identification, representing a broad panel of information about the mode of interaction of the peptide with the lipid bilayer.

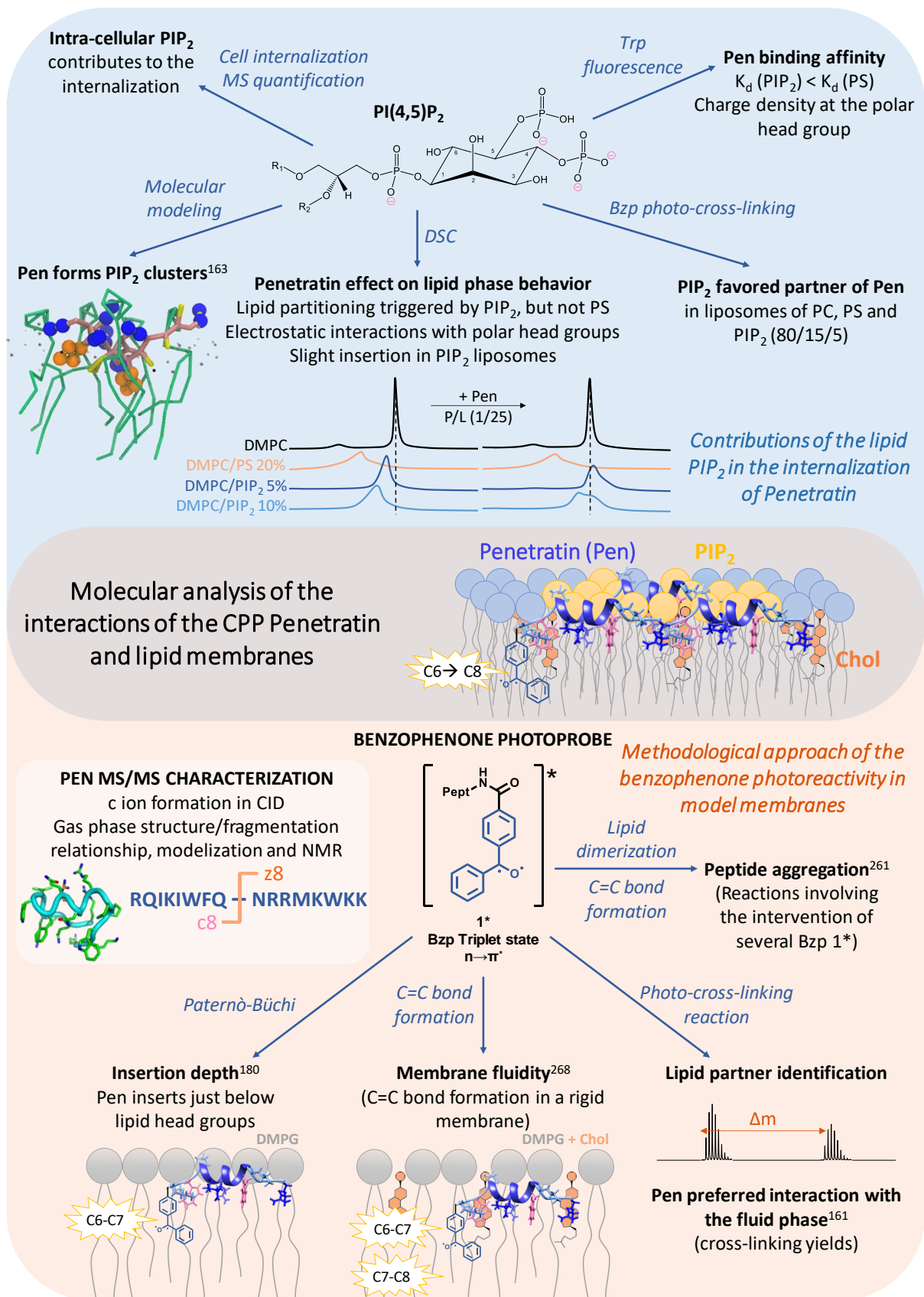


Figure 108. Illustration of the conclusions on the molecular analysis of the interactions of the CPP Penetratin and lipid membranes. *Contributions of the lipid PIP<sub>2</sub>, biophysical approaches and benzophenone photoreactivity in model membranes.*



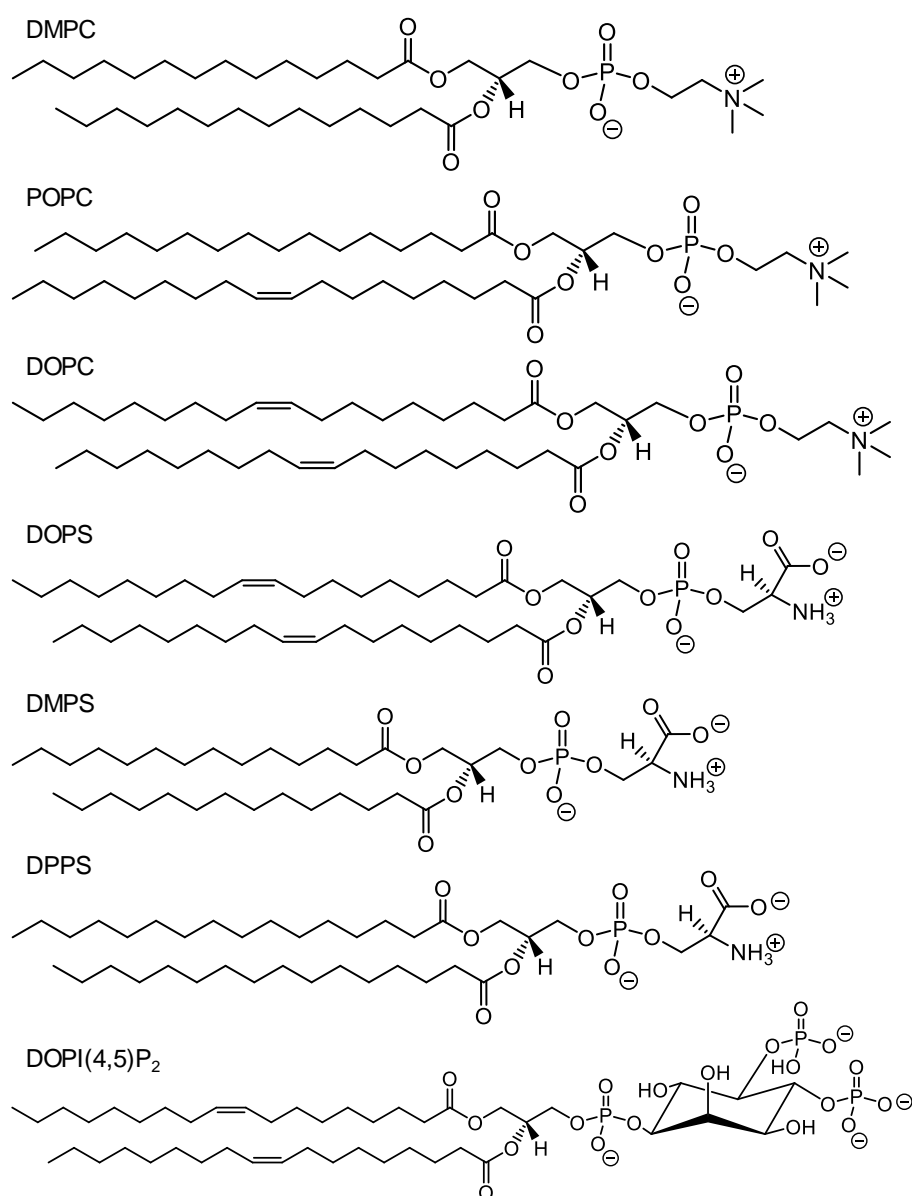
# MATERIAL AND METHODS

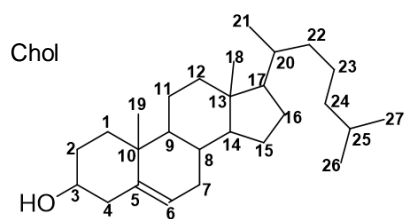
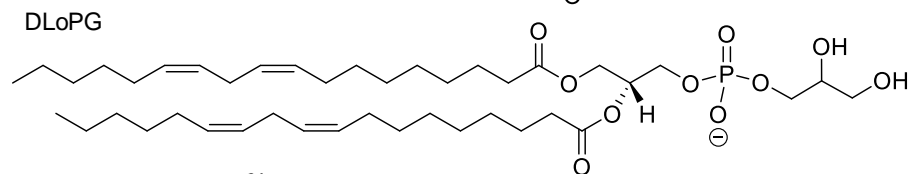
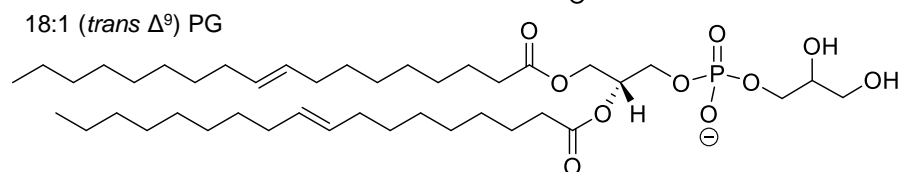
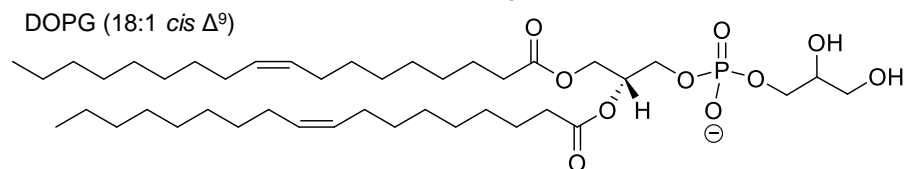
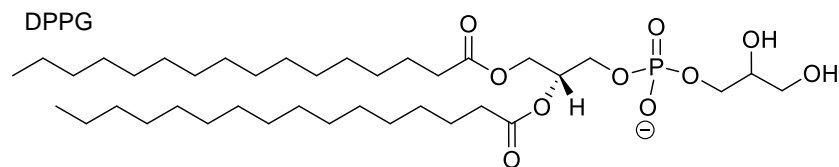
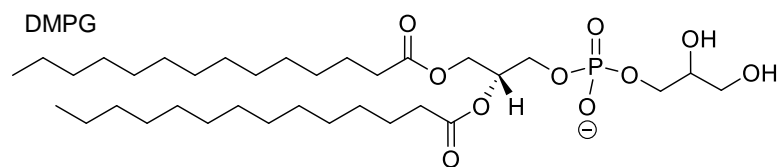
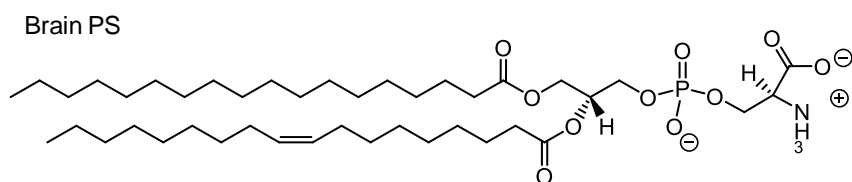
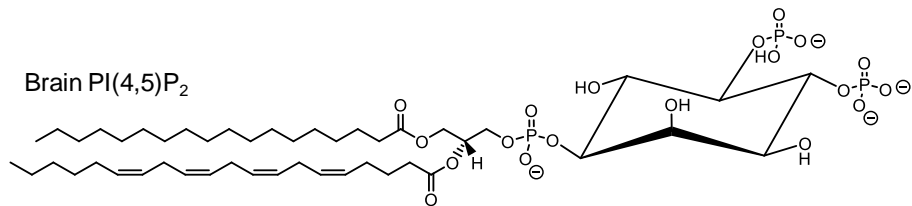
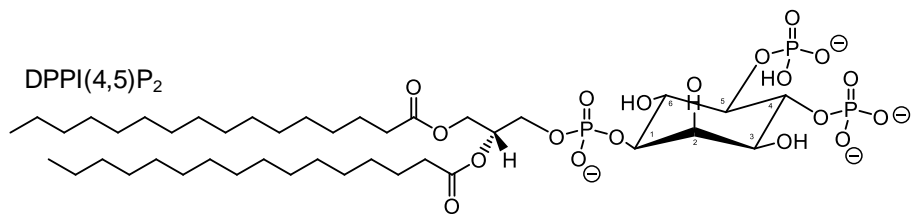


# 1. Material

## 1.1. Lipids

Dimyristoyl phosphatidylcholine (DMPC), Dipalmitoyl phosphatidylserine (DPPS), Dimyristoyl phosphatidylglycerol (DMPG) and Dipalmitoyl phosphatidylglycerol (DPPG) powders were purchased from Genzyme (Switzerland). Dioleoyl phosphatidylcholine (DOPC), 1-palmitoyl-2-oleoyl-phosphatidylcholine (POPC), Dioleoyl phosphatidylserine (DOPS), Dimyristoyl phosphatidylserine (DMPS), Brain PS, Brain PI(4,5)P<sub>2</sub>, Dioleoyl phosphatidylinositol-4,5-bisphosphate (DOPI(4,5)P<sub>2</sub>), Dipalmitoyl phosphatidylinositol-4,5-bisphosphate (DPPI(4,5)P<sub>2</sub>), Dioleoyl phosphatidylglycerol (DOPG), Dielaidoyl phosphatidylglycerol (18:1 (*trans* Δ<sup>9</sup>) PG), Dilinoleoyl phosphatidylglycerol (DLoPG) and cholesterol (Chol) powders were purchased from Avanti Polar Lipids (USA). Lipids structural formulas, and fatty acids compositions in the case of brain lipid extracts, are given in Figure 109. For Brain lipid extracts, the structural formula of the most representative fatty acid chain is given.





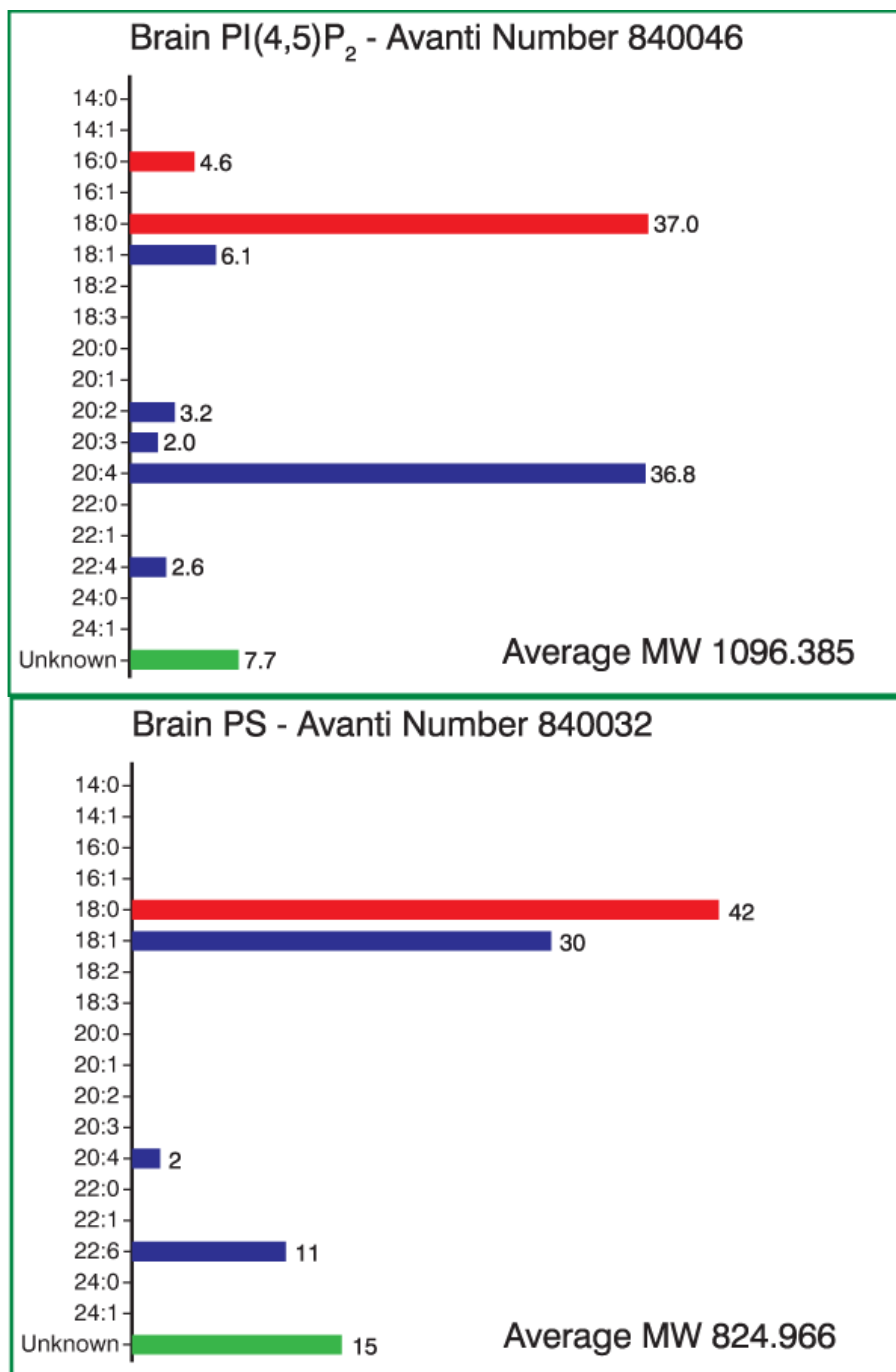


Figure 109. Structural formulas and fatty acids compositions for lipids used in the manuscript. Unsaturated fatty acids, except 18:1 (*trans*  $\Delta^9$ ) PG, are represented in their natural *cis* form.

## 1.2. Liposomes preparation

Chloroform was obtained from Carlo Erba.

## 1.3. Peptides

Standard Boc amino acids, MBHA resin and HBTU were purchased from Iris Biotech (Germany), benzoyl benzoic acid was obtained from Alfa Aesar (US). DMF (Peptide synthesis grade), acetonitrile (HPLC grade), TFA (Optical spectroscopy grade), DCM (Analysis grade) and piperidine (Peptide synthesis grade) were obtained from Carlo Erba (France). Hydrofluoric acid

(HF) was obtained from GHC Gerling Holz & Co. (Germany) and was handled in a HF teflon apparatus (Toho, Japan), anisole and dimethyl-sulfide were purchased from Sigma Aldrich (US).

Peptides used are obtained by peptide synthesis in solid phase, using Boc strategy. Penetratin N-terminal tags are adapted to the experiments carried out. Table 12 details all the peptides used, with their exact mass and the type of experiment for which they were designed and used.

Table 12. Detail of peptides sequences used for the different experiments. The mono-isotopic mass, calculated with Isopro, does not take in account the TFA counter-ion mass (M = 113 Da), present for each basic residue (R and K). (Bzp = benzophenone, Apa = aminopentanoic acid, Pen = RQIKIWFQNRRMKWKK)

Sequence	Use	Mono-isotopic exact mass
Biot(O <sub>2</sub> )-Apa-pen-NH <sub>2</sub>	DSC, Fluorescence spectroscopy	2601.44
Biot(O <sub>2</sub> )-G <sub>5</sub> -pen-NH <sub>2</sub>	Internalization MS	2787.48
Biot(O <sub>2</sub> )-G <sub>5</sub> (D,D)-pen-NH <sub>2</sub>		2797.56
Biot(O <sub>2</sub> )-G <sub>5</sub> -K(εBzp)-pen-NH <sub>2</sub>		3155.62
Biot(O <sub>2</sub> )-G <sub>5</sub> (D,D)-K(εBzp)-pen-NH <sub>2</sub>		3165.70
Biot(O <sub>2</sub> )-G <sub>5</sub> -pen(K48(εBzp))-NH <sub>2</sub>		2969.54
Biot(O <sub>2</sub> )-G <sub>5</sub> (D,D)-pen(K48(εBzp))-NH <sub>2</sub>		2979.62
Biot(O <sub>2</sub> )-Apa-G <sub>5</sub> -K(εBzp)-pen-NH <sub>2</sub>	MS-coupled photo-cross-linking	3254.69
Biot(O <sub>2</sub> )-Apa-G <sub>5</sub> (D,D)-K(εBzp)-pen-NH <sub>2</sub>		3264.76
Biot(O <sub>2</sub> )-Apa-G <sub>5</sub> -pen(K48(εBzp))-NH <sub>2</sub>		3068.61
Biot(O <sub>2</sub> )-Apa-G <sub>5</sub> (D,D)-pen(K48(εBzp))-NH <sub>2</sub>		3078.68
Biot(O <sub>2</sub> )-G <sub>5</sub> -K(εBzp)-RRWRRR-NH <sub>2</sub>		2391.20

#### 1.4. Photo-cross-linking reagents

Methanol, NaOH and NaCl were purchased from VWR. Triton X-100 and TRIS were obtained from Sigma Aldrich (US), SDS from Appli-Chem (US). PBS was purchased from Gibco. Acetonitrile (HPLC grade) was obtained from Carlo Elba (France).

#### 1.5. Cell transfection

We thank Jennifer Gallop, from the Gurdon Institute of Cambridge, who has provided the plasmid GFP-PH-PLC<sup>δ</sup> used for the transfection experiments. The plasmid map is given in Figure 110.

The Eugene transfection agent was purchased from Promega.

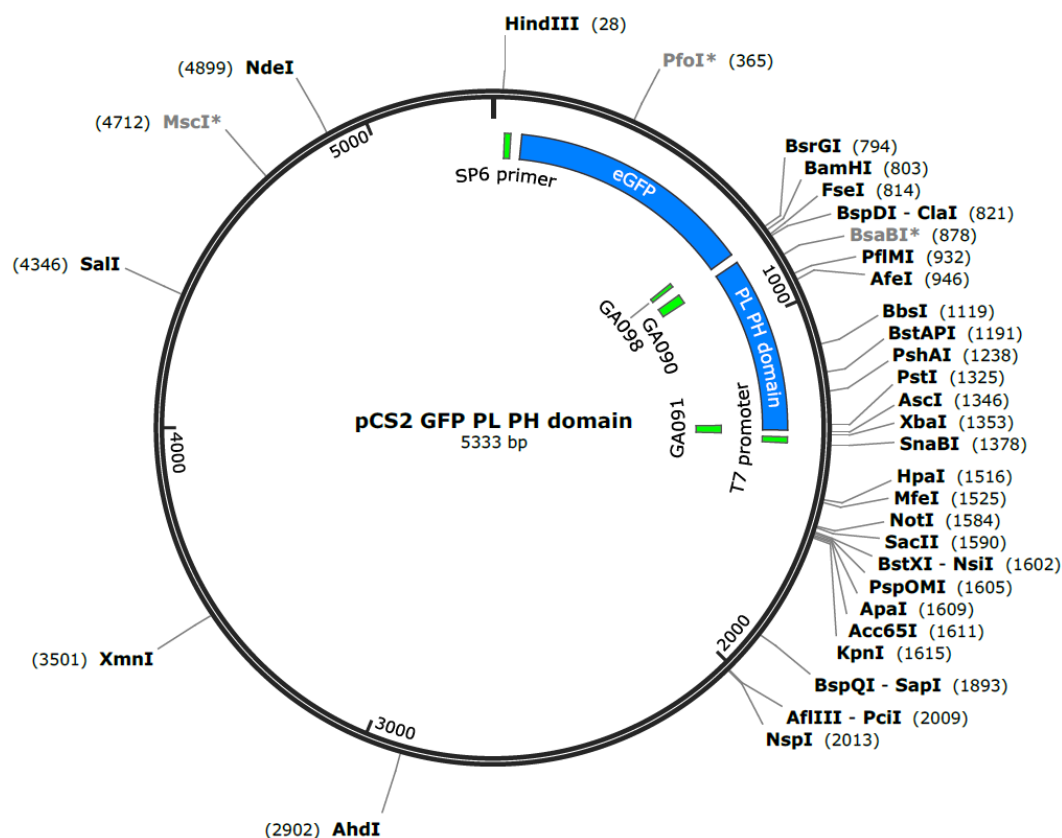


Figure 110. Map of the plasmid GFP-PH- PLC $\delta$ .

## 1.6. Mass spectrometry matrices

Acetonitrile (HPLC grade) and TFA (Optical spectroscopy grade) were purchased from Carlo Erba (France), phosphoric acid from Acros Organics, DHB from Fluka (Germany), and CHCA from Sigma Aldrich (US).

## 2. Peptide synthesis

Peptides were synthesized by Boc solid-phase peptide synthesis using DMF. Peptides were coupled manually on a Rink-amide MBHA-resin (amino acid activation by HBTU/DIEA). Peptides were cleaved from the resin with anhydrous HF treatment for 2h at 0°C, in the presence of anisole and dimethylsulfide. All peptides were HPLC purified (purity  $\geq 95\%$ ) and analyzed by MALDI-TOF (DE-Pro, Applied Biosystems) reflector, positive ions mode, using CHCA as the matrix.

Peptide synthesis in solid phase is realized on a MBHA resin, with a substitution rate of 0.53 mmol/g resin. Amino acids couplings are done manually, in a polypropylene syringe equipped with a sintered filter and a cap.

### Kaiser test

The Kaiser test is done after each coupling or deprotection step, in order to check the presence or not of a free amine group.<sup>275</sup>

Few resin beads are taken and transfer to a test tube. Few drops of each of the following solutions are added on the resin beads:

- Ninhydrin 5% in ethanol
- Phenol 0.32% in ethanol
- Potassium cyanide 0.02 mM in pyridine

The obtained suspension is heated at 100 °C for 3 min.

Beads color is checked:

- If the test is positive: Presence of a free  $\text{NH}_2$  → beads become blue.
  - After a deprotection: deprotection is complete.
  - After a coupling: coupling is not complete.
- If the test is negative: Absence of a free  $\text{NH}_2$  → beads are colorless.
  - After a deprotection: deprotection did not work properly, the peptide is protected.
  - After a coupling: coupling is complete.

### First amino acid coupling

Resin solvation	DMF for 1 hour
Deprotonation	DIEA 10% x 3
Coupling	The amino acid (6 equivalents) and the HBTU (5.8 eq.) are dissolved in DMF and 14 eq. DIEA are added. The activated amino acid solution is incubated for 1 hour on the resin at room temperature, under gentle stirring.
Washings	DMF x 3 DCM x 3
Kaiser test	Must be negative

### Couplings of the following amino acids

Boc deprotection	Incubation in TFA for 1 minute x 3
Washings	DCM x 3 DMF x 3
Kaiser test	Must be positive
Deprotonation	DIEA 10% x 3
Coupling	The amino acid (6 equivalents) and the HBTU (5.8 eq.) are dissolved in DMF and 14 eq. DIEA are added. The activated amino acid solution is incubated for 1 hour on the resin at room temperature, under gentle stirring.
Washings	DMF x 3 DCM x 3
Kaiser test	Must be negative

### Coupling of the biotin sulfone

Boc deprotection	Incubation in TFA for 1 minute x 3
Washings	DCM x 3 DMF x 3
Kaiser test	Must be positive

Deprotonation	DIEA 10% x 3
Coupling	The amino acid (6 equivalents) and the HBTU (5.8 eq.) are dissolved in DMF and 14 eq. DIEA are added. The activated amino acid solution is incubated overnight on the resin at room temperature, under gentle stirring.
Washings	DMF x 3 DCM x 3
Kaiser test	Must be negative

### Trp deformylation

Washings	DMF x 3
Deformylation	Resin incubation in piperidine at room temperature for: 1 min, 3 min, 5 min, 10 min, 15 min, 30 min, and 60 min.

### Resin drying

Washings	DMF x 3 DCM x 3 MeOH x 2
Drying	Under vacuum for 2 to 3 hours

### Hydrofluoric acid (HF) cleavage

Peptide cleavage by HF is done in presence of anisole (1.5 mL/g resin) and dimethyl sulfide (0.25 mL/g resin). The cleavage step is achieved at 0°C, under vacuum and under stirring, during 3 hours. After complete HF evaporation under vacuum, the peptide is recovered, precipitated and washed in cold ether, on a sintered filter. The peptide is then dissolved in a 10% acetic acid solution and recovered in the filtrate. It is lyophilized before conservation at -20°C.

### Purification

The peptide is purified by HPLC in reversed phase on a preparative column Nucleodur C18 HTec 5 µm (Macherey-Magel), with a linear gradient H<sub>2</sub>O/acetonitrile 0.1% TFA from 15% to 35% in acetonitrile 0.1% TFA over 20 min.

### Characterization

Peptides are characterized in MALDI-TOF MS (Applied Biosystems 4700) in positive ions reflector mode, using a CHCA matrix ( $\alpha$ -cyano-4-hydroxycinnamic acid).

## 3. Lipid vesicles preparation

### 3.1. Multilamellar vesicles (MLVs)

MLVs are prepared from lipid stock solutions in methanol or a mixture of chloroform/methanol (1:1) depending on the lipid solubility. The required volume of stock lipid solution is diluted in 1 mL chloroform, in a glass tube. The solvent is evaporated under a nitrogen flow, to form a homogeneous lipid film on the glass tube wall. Traces of solvent are dried under *vacuum* for 1

hour. The lipid film is then hydrated in 1 mL buffer and heated above the lipids transition temperature. The MLVs are formed by strong stirring on a vortex.

Suspensions of MLVs at 2 mM lipid concentration were prepared as follows. The appropriate amount of lipids was dissolved in chloroform alone or chloroform/methanol (1:1). Lipid films were formed on the wall of a glass tube by evaporating the solvent under nitrogen stream. Remaining solvent traces were removed under vacuum for 1 hour. Lipid films were then hydrated with a Phosphate Buffered Saline (PBS) solution pH 7.4, at a temperature above the lipid phase transition and vortexed extensively.

### 3.2. Large unilamellar vesicles (LUVs)

LUVs are prepared from a MLVs suspension. MLVs are frozen in liquid nitrogen and then defrost at room temperature. This freezing-defrosting cycle is repeated 5 times. The obtained lipid suspension is extruded on a polycarbonate membrane of 100 nm porosity. This step is performed thanks to the “Mini-Extruder” (Avanti Polar Lipids), by 15 passages through the membrane.

## 4. Penetratin interaction with model membranes

### 4.1. DSC

The calorimetry experiments were performed on a Nano DSC microcalorimeter (TA instruments). Series of DSC scans were acquired using a scan rate of 0.5 °C/min, with a delay of 10 min between sequential scans to allow thermal equilibration. Data analysis was performed with the program Nano Analyze provided by TA instruments. The total lipid concentrations used were around 1 mg/mL, considering full hydration of the phospholipids mixtures. The peptide was gradually added to the same sample of lipid MLVs to obtain peptide/lipid molar ratios of 1/100, 1/50, 1/25 and 1/10. For each peptide concentration, a minimum of three, and up to ten heating and cooling scans were performed for each analysis depending whether or not the spectra was reproducible.

### 4.2. Fluorescence spectroscopy

A Penetratin solution at 20 μM in PBS (150 μL in a quartz cell) was titrated by adding LUVs at increasing concentration, from 0 to 3.5 mM. A blank was measured using 150 μL PBS. Trp-fluorescence spectra were acquired using a FP 8300 Jasco fluorimeter. Emission spectra were recorded from 300 to 500 nm using a 280 nm excitation wavelength. The excitation and emission band-pass were set at 5 nm and 2.5 nm respectively. The temperature was regulated with a Peltier device at 25°C. The graphs and the statistical treatment of experiments was performed with GraphPad Prism software.

## 5. CPP internalization in cells and quantification by MALDI-TOF mass spectrometry

The quantification of the CPP internalization in cells was performed using the Burlina *et al.* protocol.<sup>175</sup>



For the classical internalization experiment,  $10^6$  adhering cells of wild type CHO-K1 or of xylose transferase deficient CHO-pgA 741 were plated in 12-well culture plate a day before the experiment. For the transfection experiment,  $10^5$  adhering cells of wild type CHO-K1 were plated in 12-well culture plate a day before the experiment.

### 5.1. Cells transfection with the plasmid GFP-PH

CHO-K1 cells were transfected with the GFP-PH plasmid using the Fugene transfection agent, for a ratio reagent/DNA of 3/1. The culture buffer was removed and replaced by 1mL OptiMEM per well. The transfection solution was prepared at  $0.020 \mu\text{g}/\mu\text{l}$  DNA in OptiMEM. The transfection agent was then added, with mixing carefully by pipetting 15 times by placing the pipette tip well in the center of the tube (without touching the tube wall with the pipette tip). The solution was incubated 5 to 10 min at room temperature. Then,  $50 \mu\text{L}/\text{well}$  of the transfection solution was added to the cell wells containing 1 mL OptiMEM. Cells were incubated for 24 hours at  $37^\circ\text{C}$ . The percentage of transfected cells was determined by flow cytometry.

### 5.2. Cells incubation with the peptide

Washings	HBSS 1 mL / well x 2 DMEM 1 mL / well
Internalization	Incubation with 0.5 mL / well peptide at $10 \mu\text{M}$ in DMEM
Washings	HBSS 1 mL / well x 2
Cells detachment	Trypsin 0.05% 500 $\mu\text{L}$ / well for 5 minutes
Trypsin inhibition	Place in ice Trypsin inhibitor (10 mg/mL) 100 $\mu\text{L}$ / well BSA (1 mg/mL) 100 $\mu\text{L}$ / well
Cells washing	Transfer cells into protein low-binding tubes Rinse the wells with TRIS 50mM and transfer in the tubes Pellet cells by centrifugation 2 min at 3000 rpm Eliminate the supernatant 1 mL buffer A and vortex Pellet cells by centrifugation 2 min at 3000 rpm Eliminate the supernatant
Cells lysis	Add [ $^2\text{H}$ ] peptide to the lysis buffer at a known concentration Lysis buffer (Triton 0.3%, NaCl 1 M) + deuterated peptide 150 $\mu\text{L}/\text{tube}$ Boil directly for 15 min
Lysate collection	Place in ice Pellet cell residues by centrifugation 5 min at 10 000 rpm Collect the supernatant 850 $\mu\text{L}$ buffer A and vortex Pellet cell residues by centrifugation 5 min at 10 000 rpm Collect the supernatant

### 5.3. Streptavidin-functionalized magnetic beads preparation

5  $\mu\text{L}$ /sample of a magnetic beads suspension (MyOne Streptavidin M280, Life Technologies) are taken. Beads are washed successively with 20  $\mu\text{L}$ /sample of buffer A (TRIS 50 mM, BSA 0.1 mg/mL), buffer B (TRIS 50 mM, BSA 0.1 mg/mL, 0.1 % SDS), buffer C (TRIS 50 mM, NaCl 1 M, BSA 0.1 mg/mL), and again with 20  $\mu\text{L}$ /sample of buffer A. Finally, beads are put back in suspension in 20  $\mu\text{L}$ /sample of buffer A.

### 5.4. Purification

Following the hydrolysis step, 20  $\mu\text{L}$  of the magnetic beads suspension previously prepared is added in each sample and the mixture is placed on gentle agitation during 1 hour, at room temperature), to capture the biotinylated peptides [ $^1\text{H}$ ] and [ $^2\text{H}$ ]. Samples are then placed on a magnetic holder and beads are washed successively with 200  $\mu\text{L}$  buffer A (2 times), 200  $\mu\text{L}$  buffer B (2 times), 200  $\mu\text{L}$  buffer C (2 times), 200  $\mu\text{L}$ , 100  $\mu\text{L}$ , and with 50  $\mu\text{L}$  distilled water. Samples are incubated with a biotin solution at 8  $\mu\text{M}$  (50  $\mu\text{L}$ ). Beads are washed with 200  $\mu\text{L}$  distilled water, 50  $\mu\text{L}$  and 10  $\mu\text{L}$  of  $\text{H}_2\text{O}$ :acetonitrile (ACN) (1:1). Beads are eluted with CHCA matrix at 10 mg/mL in  $\text{H}_2\text{O}$ /acetonitrile 0.1% TFA (1/1).

### 5.5. Mass spectrometry analysis.

MS spectra were acquired by MALDI-TOF MS on a 4700 Proteomics Analyzer (Applied Biosystems) or with an Autoflex III (Bruker Daltonics), in positive ions reflector mode, using a CHCA matrix at 10 mg/mL in  $\text{H}_2\text{O}$ /acetonitrile 0.1% TFA (1/1). MALDI-TOF acquisition parameters were optimized on Insulin chain B ( $m/z$  3494) for the detection of peptides around 3100-3500 u. Laser fluence was adjusted just above the ion production threshold. The amount of intact internalized [ $^1\text{H}$ ]CPP is calculated from the area ratio.

## 6. Identification of lipid interaction partner of Penetratin in $\text{PIP}_2$ -containing liposomes

### 6.1. Model membranes photo-cross-linking

Photo-cross-linking experiments were performed on samples containing 10 nmol peptide and 100 nmol lipid (MLVs) in PBS, 200  $\mu\text{L}$  total volume, as previously described.<sup>5</sup> Samples were placed under a 365 nm lamp (6 W, VWR) at 3 cm distance in open microtubes. Irradiation occurred for one hour at 45°C, at which all the lipids used are in fluid phase ( $T_m(\text{DMPC})=24^\circ\text{C}$ ,  $T_m(\text{DOPC})=-17^\circ\text{C}$ ,  $T_m(\text{DOPS})=-11^\circ\text{C}$ ,  $T_m(\text{DMPS})=35^\circ\text{C}$ ,  $T_m(\text{DPPS})=54^\circ\text{C}$ ,  $T_m(\text{DMPG})=23^\circ\text{C}$ ,  $T_m(\text{DPPG})=41^\circ\text{C}$ ,  $T_m(\text{DOPG})=-18^\circ\text{C}$ ,  $T_m(18:1 \text{ trans } \Delta 9) \text{ PG} \approx 12^\circ\text{C}$  and  $T_m(\text{DLPG}) \approx -57^\circ\text{C}$ ), under gentle stirring, using a thermostated multi-tube stirrer. Working under nitrogen atmosphere and using degassed buffers or not, with or without addition of an antioxidant (butylated hydroxytoluene) gave the same results.

After irradiation, samples were hydrolyzed by adding 200  $\mu\text{L}$  of 4 M NaOH in MeOH to each tube (2 M NaOH in  $\text{H}_2\text{O}$ /MeOH (1:1) final concentration) for 10 minutes. Samples pH was adjusted to pH 7 by addition of 48  $\mu\text{L}$  acetic acid (96%).

## 6.2. Streptavidin-functionalized magnetic beads preparation

5  $\mu\text{L}$ /sample of a magnetic beads suspension (MyOne Streptavidin M280, Life Technologies) are taken. Beads are washed successively with 20  $\mu\text{L}$ /sample of 0.1% Triton X100, TRIS 50 mM, TRIS 50 mM 0.1% SDS, TRIS 50 mM 1 M NaCl and again with 20  $\mu\text{L}$ /sample of 0.1% Triton X100. Finally, beads are put back in suspension in 20  $\mu\text{L}$ /sample of 0.1% Triton X100.

## 6.3. Purification

Following the hydrolysis step, 20  $\mu\text{L}$  of the magnetic beads suspension previously prepared is added in each sample and the mixture is placed on gentle agitation during 1 hour, at room temperature, in the presence of 0.1% Triton X100, to capture the biotinylated peptides and their attached photoadducts. Samples are then placed on a magnetic holder and beads are washed successively with 200  $\mu\text{L}$  TRIS 50 mM (2 times), 200  $\mu\text{L}$  TRIS 50 mM 0.1% SDS (2 times), 200  $\mu\text{L}$  TRIS 50 mM 1 M NaCl (2 times), 200  $\mu\text{L}$ , 100  $\mu\text{L}$ , and with 50  $\mu\text{L}$  distilled water. Samples are incubated with a biotin solution at 8  $\mu\text{M}$ . Beads are washed with 200  $\mu\text{L}$  distilled water, 50  $\mu\text{L}$  and 10  $\mu\text{L}$  of  $\text{H}_2\text{O}:\text{ACN}$  (1:1).

## 6.4. Photoadduct characterization

Beads were then eluted for 5-10 min at room temperature (beads were resuspended during incubation using vortex) with 3  $\mu\text{L}$  of 20 mg/mL 2,5-DHB supplemented with 1% phosphoric acid in water/acetonitrile (1:1). On the magnetic sample holder, 1  $\mu\text{L}$  of supernatant is taken and deposited on a MALDI plate. Complete protocol is summarized on Figure 110. In the case of ESI analysis, beads were eluted in 3  $\mu\text{L}$  of 20 % formic acid to be compatible with ions production and 1 to 2.5  $\mu\text{L}$  were loaded onto the injection loop of 20  $\mu\text{L}$ . It is worth mentioning that recovery from the beads was less efficient than with 2,5-DHB.

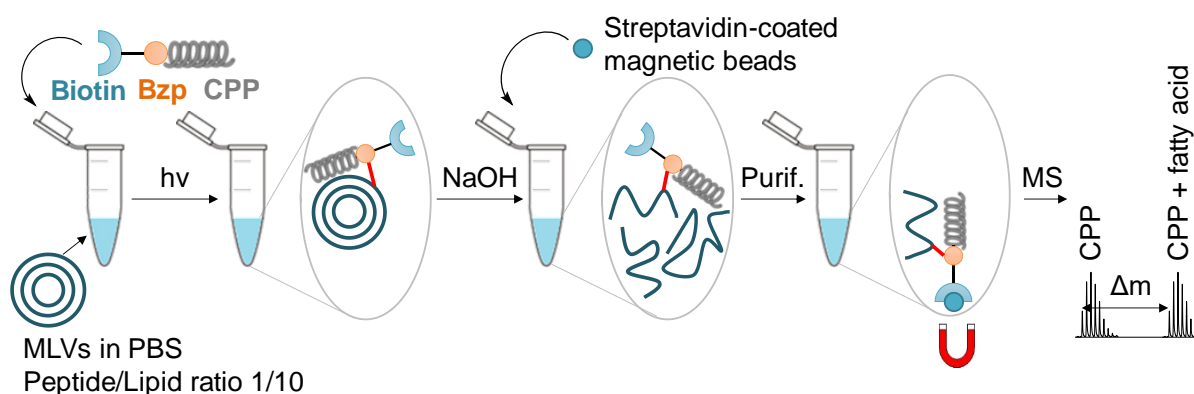


Figure 111. Protocol for Bzp-induced photo-cross-linking between a biotinylated and photoreactive CPP and MLVs.

Samples are analyzed by MALDI-TOF MS on a Voyager DEPro or on a 4700 Proteomics Analyzer (Applied Biosystems), in positive reflector mode. The mass difference between the isotopic massifs of the peptide-lipid photoadduct and of the peptide alone indicates us about the nature of the lipid partner.

Significant optimizations were achieved on the published protocol and on MS acquisition parameters on the following points:

- Synthesis of fully oxidized peptides, using Biot(O<sub>2</sub>) and Met(O<sub>2</sub>)
- Use of a narrow spectrum UV-lamp (6 W, VWR)
- Good temperature control and stability (45°C over 1h irradiation)
- Homogenous shaking of the samples over 1h
- Short saponification step (10 min) with high NaOH concentration (2 M)
- MALDI-TOF acquisition parameters in reflector mode were optimized on Insulin chain B (m/z 3494) for the detection of peptides around 3100-3500 u

### 6.5. Mass spectrometry analysis.

MS spectra were acquired by MALDI-TOF MS on a 4700 Proteomics Analyzer (Applied Biosystems) or with an Autoflex III (Bruker Daltonics), in positive ions reflector mode, using a 2,5-DHB matrix at 20 mg/mL in H<sub>2</sub>O/acetonitrile (1/1), supplemented with phosphoric acid at 1%. MALDI-TOF acquisition parameters were optimized on Insulin chain B (m/z 3494) for the detection of peptides around 3100-3500 u. Laser fluence was adjusted just above the ion production threshold. For high energy CID (N<sub>2</sub> gas, 1 keV) MS/MS experiments (MALDI-TOF/TOF), the precursor ion selection window was adjusted +/- 7u. For MALDI PSD experiments (Laser induced dissociation, post-source decay fragmentation), the analyzer was operated in LIFT mode, the selection window was automatically chosen at +/- 10% of the m/z of the precursor ion. For ESI flow-injection analysis (FIA), the solvent used was acetonitrile/H<sub>2</sub>O (20/80) containing 0.1% formic acid, flow rate 30 µL/min. Spectra were acquired with a high resolution (R=100000) using the Orbitrap mass analyzer (Thermo Scientific). ESI-MS/MS acquisition was impaired due to very low amount of material recovered after beads elution using 20% formic acid.

### 6.6. Studies and simulations of isotopic distributions.

Theoretical isotopic distributions were calculated with the Isopro 3.0 software for the pure molecules. Theoretical distributions were shifted to the desired m/z (-2u or +2u). Simulations were obtained by combining these new distributions to the theoretical ones, with the percentage of contribution of the two species. Contribution percentage were adjusted by comparing visually the simulations to the experimental isotopic distributions. Data treatment was performed with Excel.

# REFERENCES

- (1) Delaroche, D.; Cantrelle, F. X.; Subra, F.; Van Heijenoort, C.; Guittet, E.; Jiao, C. Y.; Blanchoin, L.; Chassaing, G.; Lavielle, S.; Auclair, C.; et al. Cell-Penetrating Peptides with Intracellular Actin-Remodeling Activity in Malignant Fibroblasts. *J. Biol. Chem.* **2010**, *285* (10), 7712–7721. <https://doi.org/10.1074/jbc.M109.045872>.
- (2) Clavier, S. Effet Moléculaire Du Peptide Vecteur (RW)9 Sur Le Phénotype de Cellules Modèles Du Sarcome d'Ewing, Étude Protéomique, Université Pierre et Marie Curie, 2016.
- (3) Alves, I. D.; Jiao, C. Y.; Aubry, S.; Aussedat, B.; Burlina, F.; Chassaing, G.; Sagan, S. Cell Biology Meets Biophysics to Unveil the Different Mechanisms of Penetratin Internalization in Cells. *Biochim. Biophys. Acta - Biomembr.* **2010**, *1798* (12), 2231–2239. <https://doi.org/10.1016/j.bbamem.2010.02.009>.
- (4) Jiao, C. Y.; Delaroche, D.; Burlina, F.; Alves, I. D.; Chassaing, G.; Sagan, S. Translocation and Endocytosis for Cell-Penetrating Peptide Internalization. *J. Biol. Chem.* **2009**, *284* (49), 33957–33965. <https://doi.org/10.1074/jbc.M109.056309>.
- (5) Jiao, C.-Y.; Sachon, E.; Alves, I. D.; Chassaing, G.; Bolbach, G.; Sagan, S. Exploiting Benzophenone Photoreactivity To Probe the Phospholipid Environment and Insertion Depth of the Cell-Penetrating Peptide Penetratin in Model Membranes. *Angew. Chemie Int. Ed.* **2017**, *56* (28), 8226–8230. <https://doi.org/10.1002/anie.201703465>.
- (6) Bechtella, L.; Kirschbaum, C.; Cosset, M.; Clodic, G.; Matheron, L.; Bolbach, G.; Sagan, S.; Walrant, A.; Sachon, E. Benzophenone Photoreactivity in a Lipid Bilayer To Probe Peptide/Membrane Interactions: Simple System, Complex Information. *Anal. Chem.* **2019**, *91* (14), 9102–9110. <https://doi.org/10.1021/acs.analchem.9b01584>.
- (7) Singel, S. J.; Nicolson, G. L. The Fluid Mosaic Model of the Structure of Cell Membranes. *Science (80-. )*. **1972**, *175* (4023), 720–731.
- (8) Nicolson, G. L. Biochimica et Biophysica Acta The Fluid — Mosaic Model of Membrane Structure : Still Relevant to Understanding the Structure , Function and Dynamics of Biological Membranes after More than 40 Years ☆. *BBA - Biomembr.* **2014**, *1838* (6), 1451–1466. <https://doi.org/10.1016/j.bbamem.2013.10.019>.
- (9) Simons, K.; Ikonen, E. Functional Rafts in Cell Membranes. **1997**, 569–572.
- (10) Brown, D. A.; London, E. Structure of Detergent-Resistant Membrane Domains : Does Phase Separation Occur in Biological Membranes ? **1997**, *7* (240), 1–7.
- (11) Simons, K.; Toomre, D. Lipid Rafts and Signal Transduction. **2000**, *1* (October).
- (12) Simons, K.; Gerl, M. J. New Tools and Insights. *Nat. Publ. Gr.* **2010**, *11* (10), 688–699. <https://doi.org/10.1038/nrm2977>.
- (13) Head, B. P.; Patel, H. H.; Insel, P. A. Biochimica et Biophysica Acta Interaction of Membrane / Lipid Rafts with the Cytoskeleton : Impact on Signaling and Function ☆ Membrane / Lipid Rafts , Mediators of Cytoskeletal Arrangement and Cell Signaling. *BBA - Biomembr.* **2014**, *1838* (2), 532–545. <https://doi.org/10.1016/j.bbamem.2013.07.018>.
- (14) Gennis, R. B. Gennis 1989 - Chapter 1 Introduction The Structure and Composition of Biomembranes, Biomembranes Molecular Structure and Function.Pdf. In *Biomembranes*; Springer, Ed.; New-York, 1989; pp 1–35.
- (15) Ridgway, N. D.; McLeod, R. S. *Biochemistry of Lipids, Lipoproteins and Membranes*; Elsevier, 2015.
- (16) Cullis, P. R.; Fenske, D. B.; Hope, M. J. Physical Properties and Functional Roles of Lipids in Membranes. *Biochem. Lipids, Lipoproteins Membr.* **1996**, 1–33. <https://doi.org/10.1016/S0167->

7306(08)60508-6.

- (17) Gennis, R. B. *Biomembranes: Molecular Structure and Function.*; Springer Science & Business Media, 2013.
- (18) Eeman, M.; Deleu, M. From Biological Membranes to Biomimetic Model Membranes. **2010**, *14* (4), 719–736.
- (19) Heimburg, T. A Model for the Lipid Pretransition: Coupling of Ripple Formation with the Chain-Melting Transition. *Biophys. J.* **2000**, *78* (3), 1154–1165. [https://doi.org/10.1016/S0006-3495\(00\)76673-2](https://doi.org/10.1016/S0006-3495(00)76673-2).
- (20) Lemmich, J.; Mortensen, K.; Ipsen, J. H.; Hønger, T.; Bauer, R.; Mouritsen, O. G. The Effect of Cholesterol in Small Amounts on Lipid-Bilayer Softness in the Region of the Main Phase Transition. *Eur. Biophys. J.* **1997**, *25* (4), 293–304. <https://doi.org/10.1007/s002490050041>.
- (21) Contreras, F. X.; Sánchez-Magraner, L.; Alonso, A.; Goñi, F. M. Transbilayer (Flip-Flop) Lipid Motion and Lipid Scrambling in Membranes. *FEBS Lett.* **2010**, *584* (9), 1779–1786. <https://doi.org/10.1016/j.febslet.2009.12.049>.
- (22) Bevers, E. M.; Williamson, P. L. Getting to the Outer Leaflet: Physiology of Phosphatidylserine Exposure at the Plasma Membrane. *Physiol. Rev.* **2016**, *96* (2), 605–645. <https://doi.org/10.1152/physrev.00020.2015>.
- (23) Zachowski, A. Phospholipids in Animal Eukaryotic Membranes: Transverse Asymmetry and Movement. *Biochem. J.* **1993**, *294* (1), 1–14. <https://doi.org/10.1042/bj2940001>.
- (24) Steck, T. L.; Lange, Y. Transverse Distribution of Plasma Membrane Bilayer Cholesterol : Picking Sides. **2018**, No. May, 750–760. <https://doi.org/10.1111/tra.12586>.
- (25) Sezgin, E.; Levental, I.; Mayor, S.; Eggeling, C. The Mystery of Membrane Organization: Composition, Regulation and Roles of Lipid Rafts. *Nat. Rev. Mol. Cell Biol.* **2017**, *18* (6), 361–374. <https://doi.org/10.1038/nrm.2017.16>.
- (26) Yu, J.; Fischman, D. A.; Steck, T. L. Selective Solubilization of Proteins and Phospholipids from Red Blood Cell Membranes by Nonionic Detergents. *J. Supramol. Cell. Biochem.* **1973**, *1* (3), 233–248. <https://doi.org/10.1002/jss.400010308>.
- (27) Bagatolli, L. A.; Ipsen, J. H.; Simonsen, A. C.; Mouritsen, O. G. Progress in Lipid Research An Outlook on Organization of Lipids in Membranes : Searching for a Realistic Connection with the Organization of Biological Membranes. *Prog. Lipid Res.* **2010**, *49* (4), 378–389. <https://doi.org/10.1016/j.plipres.2010.05.001>.
- (28) Bagatolli, L. A.; Mouritsen, O. G. Is the Fluid Mosaic (and the Accompanying Raft Hypothesis) a Suitable Model to Describe Fundamental Features of Biological Membranes? What May Be Missing? *Front. Plant Sci.* **2013**, *4* (November), 1–6. <https://doi.org/10.3389/fpls.2013.00457>.
- (29) Simons, K.; Vaz, W. L. C. Model Systems, Lipid Rafts, and Cell Membranes. *Annu. Rev. Biophys. Biomol. Struct.* **2004**, *33* (1), 269–295. <https://doi.org/10.1146/annurev.biophys.32.110601.141803>.
- (30) Pike, L. J. Rafts Defined: A Report on the Keystone Symposium on Lipid Rafts and Cell Function. *J. Lipid Res.* **2006**, *47* (7), 1597–1598. <https://doi.org/10.1194/jlr.e600002-jlr200>.
- (31) Raghupathy, R.; Anilkumar, A. A.; Polley, A.; Singh, P. P.; Yadav, M.; Johnson, C.; Suryawanshi, S.; Saikam, V.; Sawant, S. D.; Panda, A.; et al. Transbilayer Lipid Interactions Mediate Nanoclustering of Lipid-Anchored Proteins. *Cell* **2015**, *161* (3), 581–594. <https://doi.org/10.1016/j.cell.2015.03.048>.

- (32) Kiessling, V.; Wan, C.; Tamm, L. K. Domain Coupling in Asymmetric Lipid Bilayers. *Biochim. Biophys. Acta - Biomembr.* **2009**, *1788* (1), 64–71. <https://doi.org/10.1016/j.bbamem.2008.09.003>.
- (33) Parton, R. G.; Simons, K. The Multiple Faces of Caveolae. *Nat. Rev. Mol. Cell Biol.* **2007**, *8* (3), 185–194. <https://doi.org/10.1038/nrm2122>.
- (34) Pomorski, T.; Menon, A. K. Lipid Flippases and Their Biological Functions. *Cell. Mol. Life Sci.* **2006**, *63* (24), 2908–2921. <https://doi.org/10.1007/s00018-006-6167-7>.
- (35) Steck, T. L.; Ye, J.; Lange, Y. Probing Red Cell Membrane Cholesterol Movement with Cyclodextrin. *Biophys. J.* **2002**, *83* (4), 2118–2125. [https://doi.org/10.1016/S0006-3495\(02\)73972-6](https://doi.org/10.1016/S0006-3495(02)73972-6).
- (36) Hamilton, J. A. Fast Flip-Flop of Cholesterol and Fatty Acids in Membranes: Implications for Membrane Transport Proteins. *Curr. Opin. Lipidol.* **2011**, 263–271. <https://doi.org/10.1097/01.mol.0000073507.41685.9b>.
- (37) Sprong, H.; Van Der Sluijs, P.; Van Meer, G. How Proteins Move Lipids and Lipids Move Proteins. *Nat. Rev. Mol. Cell Biol.* **2001**, *2* (7), 504–513. <https://doi.org/10.1038/35080071>.
- (38) Berr, F.; Meier, P. J.; Stieger, B. Evidence for the Presence of a Phosphatidylcholine Translocator in Isolated Rat Liver Canalicular Plasma Membrane Vesicles. *J. Biol. Chem.* **1993**, *268* (6), 3976–3979.
- (39) Lipids and Membrane Proteins in Biological Membranes [http://csls-text.c.u-tokyo.ac.jp/inactive/05\\_02.html](http://csls-text.c.u-tokyo.ac.jp/inactive/05_02.html).
- (40) MacKenzie, K. R. A Transmembrane Helix Dimer: Structure and Implications. *Science (80-. )*. **1997**, *276* (5309), 131–133. <https://doi.org/10.1126/science.276.5309.131>.
- (41) Pinho, S. S.; Reis, C. A. Glycosylation in Cancer: Mechanisms and Clinical Implications. *Nat. Rev. Cancer* **2015**, *15* (9), 540–555. <https://doi.org/10.1038/nrc3982>.
- (42) Moremen, K. W.; Tiemeyer, M.; Nairn, A. V. Vertebrate Protein Glycosylation: Diversity, Synthesis and Function. *Nat. Rev. Mol. Cell Biol.* **2012**, *13* (7), 448–462. <https://doi.org/10.1038/nrm3383>.
- (43) Ma, J.; Hart, G. W. O-GlcNAc Profiling: From Proteins to Proteomes. *Clin. Proteomics* **2014**, *11* (1), 8. <https://doi.org/10.1186/1559-0275-11-8>.
- (44) Luther, K. B.; Haltiwanger, R. S. Role of Unusual O-Glycans in Intercellular Signaling. *Int. J. Biochem. Cell Biol.* **2009**, *41* (5), 1011–1024. <https://doi.org/10.1016/j.biocel.2008.10.001>.
- (45) Lodish, M. H.; Berk, M. A.; Matsudaira, P. *Biologie Moléculaire de La Cellule.*; De Boeck Supérieur, Ed.; 2005.
- (46) Sorkin, A. The Endocytosis Machinery: Poster. *J. Cell Sci.* **2000**, *113 Pt 24*, 4375–4376.
- (47) Mayor, S.; Pagano, R. E. Pathways of Clathrin-Independent Endocytosis. *Nat. Rev. Mol. Cell Biol.* **2007**, *8* (8), 603–612. <https://doi.org/10.1038/nrm2216>.
- (48) Doherty, G. J.; McMahon, H. T. Mechanisms of Endocytosis. *Annu. Rev. Biochem.* **2009**, *78*, 857–902. <https://doi.org/10.1146/annurev.biochem.78.081307.110540>.
- (49) Kaksonen, M.; Roux, A. Mechanisms of Clathrin-Mediated Endocytosis. *Nat. Rev. Mol. Cell Biol.* **2018**, *19* (5), 313–326. <https://doi.org/10.1038/nrm.2017.132>.
- (50) Zhou, C.; Garigapati, V.; Roberts, M. F. Short-Chain Phosphatidylinositol Conformation and Its Relevance to Phosphatidylinositol-Specific Phospholipase C. *Biochemistry* **1997**, *36* (50), 15925–



15931. <https://doi.org/10.1021/bi9716175>.
- (51) Bradshaw, J. P.; Bushby, R. J.; Giles, C. C. D.; Saunders, M. R. Orientation of the Headgroup of Phosphatidylinositol in a Model Biomembrane as Determined by Neutron Diffraction. *Biochemistry* **1999**, *38* (26), 8393–8401. <https://doi.org/10.1021/bi990338+>.
- (52) Mclaughlin, S.; Wang, J.; Gambhir, A.; Murray, D. PIP<sub>2</sub> AND PROTEINS: Interactions, Organization, and Information Flow. *Annu. Rev. Biophys.* **2002**, *31*, 151–175. <https://doi.org/10.1146/annurev.biophys.31.082901.134259>.
- (53) van Paridon, P. A.; de Kruijff, B.; Ouwerkerk, R.; Wirtz, K. W. A. Polyphosphoinositides Undergo Charge Neutralization in the Physiological PH Range: A <sup>31</sup>P-NMR Study. *Biochim. Biophys. Acta (BBA)/Lipids Lipid Metab.* **1986**, *877* (1), 216–219. [https://doi.org/10.1016/0005-2760\(86\)90137-2](https://doi.org/10.1016/0005-2760(86)90137-2).
- (54) Vanhaesebroeck, B.; Leeyers, S. J.; Ahmadi, K.; Timms, J.; Katso, R.; Driscoll, P. C.; Woscholski, R.; Parker, P. J.; Waterfield, M. D. Synthesis and Function of 3-Phosphorylated Inositol Lipids. *Annu. Rev. Biochem.* **2001**, *70*, 535–602.
- (55) Gascard, P.; Tran, D.; Sauvage, M.; Sulpice, J. C.; Fukami, K.; Takenawa, T.; Claret, M.; Giraud, F. Asymmetric Distribution of Phosphoinositides and Phosphatidic Acid in the Human Erythrocyte Membrane. *Biochim. Biophys. Acta* **1991**, *1069* (1), 27–36.
- (56) Pike, L. J.; Miller, J. M. Cholesterol Depletion Delocalizes Phosphatidylinositol Bisphosphate and Inhibits Hormone-Stimulated Phosphatidylinositol Turnover. *J. Biol. Chem.* **1998**, *273* (35), 22298–22304. <https://doi.org/10.1074/jbc.273.35.22298>.
- (57) Martin, T. F. J. PI(4,5)P<sub>2</sub> Regulation of Surface Membrane Traffic. *Curr. Opin. Cell Biol.* **2001**, *13* (4), 493–499. [https://doi.org/10.1016/S0955-0674\(00\)00241-6](https://doi.org/10.1016/S0955-0674(00)00241-6).
- (58) Balla, T.; Bondeva, T.; Várnai, P. How Accurately Can We Image Inositol Lipids in Living Cells? *Trends Pharmacol. Sci.* **2000**, *21* (7), 238–241. [https://doi.org/10.1016/S0165-6147\(00\)01500-5](https://doi.org/10.1016/S0165-6147(00)01500-5).
- (59) Tall, E. G.; Spector, I.; Pentylala, S. N.; Bitter, I.; Rebecchi, M. J. Dynamics of Phosphatidylinositol 4,5-Bisphosphate in Actin-Rich Structures. *Curr. Biol.* **2000**, *10* (12), 743–746. [https://doi.org/10.1016/S0960-9822\(00\)00541-8](https://doi.org/10.1016/S0960-9822(00)00541-8).
- (60) Botelho, R. J.; Teruel, M.; Dierckman, R.; Anderson, R.; Wells, A.; York, J. D.; Meyer, T.; Grinstein, S. Localized Biphasic Changes in Phosphatidylinositol-4,5-Bisphosphate at Sites of Phagocytosis. *J. Cell Biol.* **2000**, *151* (7), 1353–1367. <https://doi.org/10.1083/jcb.151.7.1353>.
- (61) Laux, T.; Fukami, K.; Thelen, M.; Golub, T.; Frey, D.; Caroni, P. Gap43, Marcks, and Cap23 Modulate PI(4,5)P<sub>2</sub> at Plasmalemmal Rafts, and Regulate Cell Cortex Actin Dynamics through a Common Mechanism. *J. Cell Biol.* **2000**, *149* (7), 1455–1472. <https://doi.org/10.1083/jcb.149.7.1455>.
- (62) Liu, A. P.; Fletcher, D. A. Actin Polymerization Serves as a Membrane Domain Switch in Model Lipid Bilayers. *Biophys. J.* **2006**, *91* (11), 4064–4070. <https://doi.org/10.1529/biophysj.106.090852>.
- (63) Janmey, P. A.; Bucki, R.; Radhakrishnan, R. Regulation of Actin Assembly by PI(4,5)P<sub>2</sub> and Other Inositol Phospholipids: An Update on Possible Mechanisms. *Biochem. Biophys. Res. Commun.* **2018**, *506* (2), 307–314. <https://doi.org/10.1016/j.bbrc.2018.07.155>.
- (64) Czech, M. P. PIP<sub>2</sub> and PIP<sub>3</sub>: Complex Roles at the Cell Surface. *Cell* **2000**, *100* (6), 603–606. [https://doi.org/10.1016/S0092-8674\(00\)80696-0](https://doi.org/10.1016/S0092-8674(00)80696-0).
- (65) McLaughlin, S.; Murray, D. Plasma Membrane Phosphoinositide Organization by Protein

- Electrostatics. *Nature* **2005**, *438* (7068), 605–611. <https://doi.org/10.1038/nature04398>.
- (66) Simonsen, A.; Wurmser, A. E.; Emr, S. D.; Stenmark, H. The Role of Phosphoinositides in Membrane Transport. *Curr. Opin. Cell Biol.* **2001**, *13* (4), 485–492. [https://doi.org/10.1016/S0955-0674\(00\)00240-4](https://doi.org/10.1016/S0955-0674(00)00240-4).
- (67) Haucke, V. Phosphoinositide Regulation of Clathrin-Mediated Endocytosis. *Biochem. Soc. Trans.* **2005**, *33* (6), 1285. <https://doi.org/10.1042/BST20051285>.
- (68) Kale, S. D.; Gu, B.; Capelluto, D. G. S.; Dou, D.; Feldman, E.; Rumore, A.; Arredondo, F. D.; Hanlon, R.; Fudal, I.; Rouxel, T.; et al. External Lipid PI3P Mediates Entry of Eukaryotic Pathogen Effectors into Plant and Animal Host Cells. *CELL\*\*\** **2010**, *142* (2), 284–295. <https://doi.org/10.1016/j.cell.2010.06.008>.
- (69) Thapa, N.; Anderson, R. A. PIP2 Signaling, an Integrator of Cell Polarity and Vesicle Trafficking in Directionally Migrating Cells. *Cell Adhes. Migr.* **2012**, *6* (5), 409–412. <https://doi.org/10.4161/cam.21192>.
- (70) Tsuji, T.; Takatori, S.; Fujimoto, T. Definition of Phosphoinositide Distribution in the Nanoscale. *Curr. Opin. Cell Biol.* **2019**, *57*, 33–39. <https://doi.org/10.1016/j.ceb.2018.10.008>.
- (71) Ferguson, K. M.; Lemmon, M. A.; Schlessinger, J.; Sigler, P. B. Structure of the High Affinity Complex of Inositol Trisphosphate with a Phospholipase C Pleckstrin Homology Domain. *Cell* **1995**, *83* (6), 1037–1046. [https://doi.org/10.1016/0092-8674\(95\)90219-8](https://doi.org/10.1016/0092-8674(95)90219-8).
- (72) LEMMON, M. A.; FERGUSON, K. M. Signal-Dependent Membrane Targeting by Pleckstrin Homology (PH) Domains. *Biochem. J.* **2000**, *350* (1), 1–18. <https://doi.org/10.1042/bj3500001>.
- (73) Lemmon, M. A.; Ferguson, K. M.; O'Brien, R.; Sigler, P. B.; Schlessinger, J. Specific and High-Affinity Binding of Inositol Phosphates to an Isolated Pleckstrin Homology Domain. *Proc. Natl. Acad. Sci. USA* **1995**, *92* (23), 10472–10476. <https://doi.org/10.1073/pnas.92.23.10472>.
- (74) Gillyooly, D. J.; Stenmark, H. A Lipid Oils the Endocytosis Machine. *Science (80-. )*. **2001**, *291* (5506), 993–994.
- (75) Howard, B. Lipid Monolayers: Why Use Half a Membrane to Characterize Protein Membrane Interactions? *Curr. Opin. Struct. Biol.* **1999**, *9*, 438–443.
- (76) Maget-Dana, R. *The Monolayer Technique: A Potent Tool for Studying the Interfacial Properties of Antimicrobial and Membrane-Lytic Peptides and Their Interactions with Lipid Membranes*; 1999; Vol. 1462.
- (77) Peetla, C.; Stine, A.; Labhasetwar, V. Biophysical Interactions with Model Lipid Membranes: Applications in Drug Discovery and Drug Delivery. *Mol. Pharm.* **2009**, *6* (5), 1264–1276. <https://doi.org/10.1021/mp9000662>.
- (78) Walrant, A.; Saxton, D. S.; Correia, G. P.; Gallop, J. L. *Triggering Actin Polymerization in Xenopus Egg Extracts from Phosphoinositide-Containing Lipid Bilayers*; Elsevier Ltd, 2015; Vol. 128. <https://doi.org/10.1016/bs.mcb.2015.01.020>.
- (79) Marquardt, D.; Geier, B.; Pabst, G. Asymmetric Lipid Membranes: Towards More Realistic Model Systems. *Membranes (Basel)*. **2015**, *5* (2), 180–196. <https://doi.org/10.3390/membranes5020180>.
- (80) Doktorova, M.; Heberle, F. A.; Eicher, B.; Standaert, R. F.; Katsaras, J.; London, E.; Pabst, G.; Marquardt, D. Preparation of Asymmetric Phospholipid Vesicles for Use as Cell Membrane Models. *Nat. Protoc.* **2018**, *13* (9), 2086–2101. <https://doi.org/10.1038/s41596-018-0033-6>.

- (81) Wesolowska, O.; Michalak, K.; Maniewska, J.; Hendrich, A. B. Giant Unilamellar Vesicles - a Perfect Tool to Visualize Phase Separation and Lipid Rafts in Model Systems. *Acta Biochim. Pol.* **2009**, *56* (1). [https://doi.org/10.18388/abp.2009\\_2514](https://doi.org/10.18388/abp.2009_2514).
- (82) Rodriguez, N.; Pincet, F.; Cribier, S. Giant Vesicles Formed by Gentle Hydration and Electroformation: A Comparison by Fluorescence Microscopy. *Colloids Surfaces B Biointerfaces* **2005**, *42* (2), 125–130. <https://doi.org/10.1016/j.colsurfb.2005.01.010>.
- (83) Bagatolli, L. A.; Parasassi, T.; Gratton, E. Giant Phospholipid Vesicles: Comparison among the Whole Lipid Sample Characteristics Using Different Preparation Methods: A Two Photon Fluorescence Microscopy Study. *Chem. Phys. Lipids* **2000**, *105* (2), 135–147.
- (84) Levental, I.; Byfield, F. J.; Chowdhury, P.; Gai, F.; Baumgart, T.; Janmey, P. A. Cholesterol-Dependent Phase Separation in Cell-Derived Giant Plasma-Membrane Vesicles. *Biochem. J.* **2009**, *424* (2), 163–167. <https://doi.org/10.1042/BJ20091283>.
- (85) Baumgart, T.; Hammond, A. T.; Sengupta, P.; Hess, S. T.; Holowka, D. A.; Baird, B. A.; Webb, W. W. Large-Scale Fluid/Fluid Phase Separation of Proteins and Lipids in Giant Plasma Membrane Vesicles. *Proc. Natl. Acad. Sci.* **2007**, *104* (9), 3165 LP – 3170. <https://doi.org/10.1073/pnas.0611357104>.
- (86) Sezgin, E.; Kaiser, H.-J.; Baumgart, T.; Schwille, P.; Simons, K.; Levental, I. Elucidating Membrane Structure and Protein Behavior Using Giant Plasma Membrane Vesicles. *Nat. Protoc.* **2012**, *7*, 1042.
- (87) Green, M.; Loewenstein, P. M. Autonomous Functional Domains of Chemically Synthesized Human Immunodeficiency Virus Tat Trans-Activator Protein. *Cell* **1988**, *55* (6), 1179–1188. [https://doi.org/10.1016/0092-8674\(88\)90262-0](https://doi.org/10.1016/0092-8674(88)90262-0).
- (88) Frankel, A. D.; Pabo, C. O. Cellular Uptake of the Tat Protein from Human Immunodeficiency Virus. *Cell* **1988**, *55* (6), 1189–1193. [https://doi.org/10.1016/0092-8674\(88\)90263-2](https://doi.org/10.1016/0092-8674(88)90263-2).
- (89) Joliot, A.; Pernelle, C.; Deagostini-Bazin, H.; Prochiantz, A. Antennapedia Homeobox Peptide Regulates Neural Morphogenesis. *Proc. Natl. Acad. Sci.* **1991**, *88* (5), 1864–1868. <https://doi.org/10.1073/pnas.88.5.1864>.
- (90) Derossi, D.; Joliot, A. H.; Chassaing, G.; Prochiantz, A. The Third Helix of the Antennapedia Homeodomain Translocates through Biological Membranes. *J. Biol. Chem.* **1994**, *269* (14), 10444–10450. [https://doi.org/10444-50](https://doi.org/10.1073/pnas.88.5.1864).
- (91) Agrawal, P.; Bhalla, S.; Usmani, S. S.; Singh, S.; Chaudhary, K.; Raghava, G. P. S.; Gautam, A. CPPsite 2.0: A Repository of Experimentally Validated Cell-Penetrating Peptides. *Nucleic Acids Res.* **2016**, *44* (D1), D1098–D1103. <https://doi.org/10.1093/nar/gkv1266>.
- (92) Guidotti, G.; Brambilla, L.; Rossi, D. Cell-Penetrating Peptides: From Basic Research to Clinics. *Trends Pharmacol. Sci.* **2017**, *38* (4), 406–424. <https://doi.org/10.1016/j.tips.2017.01.003>.
- (93) El-Sayed, A.; Futaki, S.; Harashima, H. Delivery of Macromolecules Using Arginine-Rich Cell-Penetrating Peptides: Ways to Overcome Endosomal Entrapment. *AAPS J.* **2009**, *11* (1), 13–22. <https://doi.org/10.1208/s12248-008-9071-2>.
- (94) Zhu, W. L.; Shin, S. Y. Antimicrobial and Cytolytic Activities and Plausible Mode of Bactericidal Action of the Cell Penetrating Peptide Penetratin and Its Lys-Linked Two-Stranded Peptide. *Chem. Biol. Drug Des.* **2009**, *73* (2), 209–215. <https://doi.org/10.1111/j.1747-0285.2008.00769.x>.
- (95) Gallo, M.; Defaus, S.; Andreu, D. 1988–2018: Thirty Years of Drug Smuggling at the Nano Scale.

- Challenges and Opportunities of Cell-Penetrating Peptides in Biomedical Research. *Arch. Biochem. Biophys.* **2019**, *661* (October 2018), 74–86. <https://doi.org/10.1016/j.abb.2018.11.010>.
- (96) Gehring, W. J.; Qian, Y. Q.; Billeter, M.; Furukubo-Tokunaga, K.; Schier, A. F.; Resendez-Perez, D.; Affolter, M.; Otting, G.; Wüthrich, K. Homeodomain-DNA Recognition. *Cell* **1994**, *78* (2), 211–223. [https://doi.org/10.1016/0092-8674\(94\)90292-5](https://doi.org/10.1016/0092-8674(94)90292-5).
- (97) Le Roux, I.; Joliot, A. H.; Bloch-Gallego, E.; Prochiantz, A.; Volovitch, M. Neurotrophic Activity of the Antennapedia Homeodomain Depends on Its Specific DNA-Binding Properties. *Proc. Natl. Acad. Sci.* **1993**, *90* (19), 9120–9124. <https://doi.org/10.1073/pnas.90.19.9120>.
- (98) Magzoub, M.; Eriksson, L. E. G.; Gräslund, A. Conformational States of the Cell-Penetrating Peptide Penetratin When Interacting with Phospholipid Vesicles: Effects of Surface Charge and Peptide Concentration. *Biochim. Biophys. Acta - Biomembr.* **2002**, *1563* (1–2), 53–63. [https://doi.org/10.1016/S0005-2736\(02\)00373-5](https://doi.org/10.1016/S0005-2736(02)00373-5).
- (99) Eiríksdóttir, E.; Konate, K.; Langel, Ü.; Divita, G.; Deshayes, S. Secondary Structure of Cell-Penetrating Peptides Controls Membrane Interaction and Insertion. *Biochim. Biophys. Acta - Biomembr.* **2010**, *1798* (6), 1119–1128. <https://doi.org/10.1016/j.bbamem.2010.03.005>.
- (100) Czajlik, A.; Meskó, E.; Penke, B.; Perczel, A. Investigation of Penetratin Peptides. Part 1. The Environment Dependent Conformational Properties of Penetratin and Two of Its Derivatives. *J. Pept. Sci.* **2002**, *8* (4), 151–171. <https://doi.org/10.1002/psc.380>.
- (101) Madani, F.; Lindberg, S.; Langel, Ü.; Futaki, S.; Gräslund, A. Mechanisms of Cellular Uptake of Cell-Penetrating Peptides. *J. Biophys.* **2011**, *2011*. <https://doi.org/10.1155/2011/414729>.
- (102) Ziegler, A. Thermodynamic Studies and Binding Mechanisms of Cell-Penetrating Peptides with Lipids and Glycosaminoglycans. *Adv. Drug Deliv. Rev.* **2008**, *60* (4–5), 580–597. <https://doi.org/10.1016/j.addr.2007.10.005>.
- (103) Milletti, F. Cell-Penetrating Peptides: Classes, Origin, and Current Landscape. *Drug Discov. Today* **2012**, *17* (15–16), 850–860. <https://doi.org/10.1016/j.drudis.2012.03.002>.
- (104) Gallo, M.; Defaus, S.; Andreu, D. 1988–2018: Thirty Years of Drug Smuggling at the Nano Scale. Challenges and Opportunities of Cell-Penetrating Peptides in Biomedical Research. *Arch. Biochem. Biophys.* **2019**, *661* (October 2018), 74–86. <https://doi.org/10.1016/j.abb.2018.11.010>.
- (105) Pooga, M.; Langel, Ü. *Cell-Penetrating Peptides - Methods and Protocols*; 2015. [https://doi.org/10.1007/978-1-4939-2806-4\\_1](https://doi.org/10.1007/978-1-4939-2806-4_1).
- (106) Pooga, M.; Hällbrink, M.; Zorko, M.; Langel, Ü. Cell Penetration by Transportan. *FASEB J.* **1998**, *12* (1), 67–77. <https://doi.org/10.1096/fasebj.12.1.67>.
- (107) Morris, M. C.; Depollier, J.; Mery, J.; Heitz, F.; Divita, G. A Peptide Carrier for the Delivery of Biologically Active Proteins into Mammalian Cells. *Nat. Biotechnol.* **2001**, *19* (12), 1173–1176. <https://doi.org/10.1038/nbt1201-1173>.
- (108) Morris, M. C.; Vidal, P.; Chaloin, L.; Heitz, F.; Divita, G. A New Peptide Vector for Efficient Delivery of Oligonucleotides into Mammalian Cells. *Nucleic Acids Res.* **1997**, *25* (14), 2730–2736. <https://doi.org/10.1093/nar/25.14.2730>.
- (109) Delaroche, D.; Aussedat, B.; Aubry, S.; Chassaing, G.; Burlina, F.; Clodic, G.; Bolbach, G.; Lavielle, S.; Sagan, S. Tracking a New Cell-Penetrating (W/R) Nonapeptide, through an Enzyme-Stable Mass Spectrometry Reporter Tag. *Anal. Chem.* **2007**, *79* (5), 1932–1938.

<https://doi.org/10.1021/ac061108l>.

- (110) Oehlke, J.; Scheller, A.; Wiesner, B.; Krause, E.; Beyermann, M.; Klauschenz, E.; Melzig, M.; Bienert, M. Cellular Uptake of an  $\alpha$ -Helical Amphipathic Model Peptide with the Potential to Deliver Polar Compounds into the Cell Interior Non-Endocytically. *Biochim. Biophys. Acta - Biomembr.* **1998**, *1414* (1–2), 127–139. [https://doi.org/10.1016/S0005-2736\(98\)00161-8](https://doi.org/10.1016/S0005-2736(98)00161-8).
- (111) Elmquist, A.; Lindgren, M.; Bartfai, T.; Langel, Ü. Ve-Cadherin-Derived Cell-Penetrating Peptide, PVEC with Carrier Functions. *Exp. Cell Res.* **2001**, *269* (2), 237–244. <https://doi.org/10.1006/excr.2001.5316>.
- (112) Johansson, H. J.; El-Andaloussi, S.; Holm, T.; Mäe, M.; Jänes, J.; Maimets, T.; Langel, Ü. Characterization of a Novel Cytotoxic Cell-Penetrating Peptide Derived from P14ARF Protein. *Mol. Ther.* **2008**, *16* (1), 115–123. <https://doi.org/10.1038/sj.mt.6300346>.
- (113) Vivès, E.; Brodin, P.; Lebleu, B. A Truncated HIV-1 Tat Protein Basic Domain Rapidly Translocates through the Plasma Membrane and Accumulates in the Cell Nucleus. *J. Biol. Chem.* **1997**, *272* (25), 16010–16017. <https://doi.org/10.1074/jbc.272.25.16010>.
- (114) Futaki, S.; Suzuki, T.; Ohashi, W.; Yagami, T.; Tanaka, S.; Ueda, K.; Sugiura, Y. Arginine-Rich Peptides An Abundant Source of Membrane-Permeable Peptides Having Potential as Carriers for Intracellular Protein Delivery. *J. Biol. Chem.* **2001**, *276* (8), 5836–5840. <https://doi.org/10.1074/jbc.m007540200>.
- (115) Mitchell, D. J.; Kim, D. T.; Steinman, L.; Fathman, C. G.; Rothbard, J. B. Polyarginine Enters Cells More Efficiently than Other Polycationic Homopolymers. *J. Pept. Res.* **2000**, *56* (5), 318–325. <https://doi.org/10.1034/j.1399-3011.2000.00723.x>.
- (116) Han, K.; Jeon, M. J.; Kim, K. A.; Park, J.; Choi, S. Y. Efficient Intracellular Delivery of GFP by Homeodomains of Drosophila Fushi-Tarazu and Engrailed Proteins. *Mol. Cells* **2000**, *10* (6), 728–732. <https://doi.org/10.1007/s10059-000-0728-7>.
- (117) Rhee, M.; Davis, P. Mechanism of Uptake of C105Y, a Novel Cell-Penetrating Peptide. *J. Biol. Chem.* **2006**, *281* (2), 1233–1240. <https://doi.org/10.1074/jbc.M509813200>.
- (118) Gao, C.; Mao, S.; Ditzel, H. J.; Farnaes, L.; Wirsching, P.; Lerner, R. A.; Janda, K. D. A Cell-Penetrating Peptide from a Novel PVII-PIX Phage-Displayed Random Peptide Library. *Bioorganic Med. Chem.* **2002**, *10* (12), 4057–4065. [https://doi.org/10.1016/S0968-0896\(02\)00340-1](https://doi.org/10.1016/S0968-0896(02)00340-1).
- (119) Taylor, B. N.; Mehta, R. R.; Yamada, T.; Lekmine, F.; Christov, K.; Chakrabarty, A. M.; Green, A.; Bratescu, L.; Shilkaitis, A.; Beattie, C. W.; et al. Noncationic Peptides Obtained from Azurin Preferentially Enter Cancer Cells. *Cancer Res.* **2009**, *69* (2), 537–546. <https://doi.org/10.1158/0008-5472.CAN-08-2932>.
- (120) Neves-Coelho, S.; Eleutério, R. P.; Enguita, F. J.; Neves, V.; Castanho, M. A. R. B. A New Noncanonical Anionic Peptide That Translocates a Cellular Blood-Brain Barrier Model. *Molecules* **2017**, *22* (10). <https://doi.org/10.3390/molecules22101753>.
- (121) Tünnemann, G.; Ter-Avetisyan, G.; Martin, R. M.; Stöckl, M.; Herrmann, A.; Cardoso, M. C. Live-Cell Analysis of Cell Penetration Ability and Toxicity of Oligo-Arginines. *J. Pept. Sci.* **2008**, *14* (4), 469–476. <https://doi.org/10.1002/psc.968>.
- (122) Wender, P. a; Mitchell, D. J.; Pattabiraman, K.; Pelkey, E. T.; Steinman, L.; Rothbard, J. B. The Design, Synthesis, and Evaluation of Molecules That Enable or Enhance Cellular Uptake: Peptoid Molecular Transporters. *Proc. Natl. Acad. Sci.* **2000**, *97* (24), 13003–13008. <https://doi.org/10.1073/pnas.97.24.13003>.

- (123) Nakase, I.; Takeuchi, T.; Tanaka, G.; Futaki, S. Methodological and Cellular Aspects That Govern the Internalization Mechanisms of Arginine-Rich Cell-Penetrating Peptides. *Adv. Drug Deliv. Rev.* **2008**, *60* (4–5), 598–607. <https://doi.org/10.1016/j.addr.2007.10.006>.
- (124) Rothbard, J. B.; Jessop, T. C.; Lewis, R. S.; Murray, B. A.; Wender, P. A. Role of Membrane Potential and Hydrogen Bonding in the Mechanism of Translocation of Guanidinium-Rich Peptides into Cells. *J. Am. Chem. Soc.* **2004**, *126* (31), 9506–9507.
- (125) Verdurmen, W. P. R.; Brock, R. Biological Responses towards Cationic Peptides and Drug Carriers. *Trends Pharmacol. Sci.* **2011**, *32* (2), 116–124. <https://doi.org/10.1016/j.tips.2010.11.005>.
- (126) Prochiantz, A. Getting Hydrophilic Compounds into Cells: Lessons from Homeopeptides. *Curr. Opin. Neurobiol.* **1996**, *6* (5), 629–634.
- (127) Christiaens, B.; Symoens, S.; Vanderheyden, S.; Engelborghs, Y.; Joliot, A.; Prochiantz, A.; Vandekerckhove, J.; Rosseneu, M.; Vanloo, B. Tryptophan Fluorescence Study of the Interaction of Penetratin Peptides with Model Membranes. *Eur. J. Biochem.* **2002**, *269* (12), 2918–2926. <https://doi.org/10.1046/j.1432-1033.2002.02963.x>.
- (128) Drin, G.; Mazel, M.; Clair, P.; Mathieu, D.; Kaczorek, M.; Tamsamani, J. Physico-Chemical Requirements for Cellular Uptake of PANTp Peptide: Role of Lipid-Binding Affinity. *Eur. J. Biochem.* **2001**, *268* (5), 1304–1314. <https://doi.org/10.1046/j.1432-1327.2001.01997.x>.
- (129) Bechara, C.; Pallerla, M.; Burlina, F.; Illien, F.; Cribier, S.; Sagan, S. Massive Glycosaminoglycan-Dependent Entry of Trp-Containing Cell-Penetrating Peptides Induced by Exogenous Sphingomyelinase or Cholesterol Depletion. *Cell. Mol. Life Sci.* **2015**, *72* (4), 809–820. <https://doi.org/10.1007/s00018-014-1696-y>.
- (130) Thorén, P. E. G.; Persson, D.; Esbjörner, E. K.; Goksör, M.; Lincoln, P.; Nordén, B. Membrane Binding and Translocation of Cell-Penetrating Peptides. *Biochemistry* **2004**, *43* (12), 3471–3489. <https://doi.org/10.1021/bi0360049>.
- (131) Walrant, A.; Bechara, C.; Alves, I. D.; Sagan, S. Molecular Partners for Interaction and Cell Internalization of Cell-Penetrating Peptides: How Identical Are They? *Nanomedicine (Lond)*. **2012**, *7* (1), 133–143. <https://doi.org/10.2217/nnm.11.165>.
- (132) Sagan, S.; Burlina, F.; D. Alves, I.; Bechara, C.; Dupont, E.; Joliot, A. Homeoproteins and Homeoprotein-Derived Peptides: Going in and Out. *Curr. Pharm. Des.* **2013**, *19* (16), 2851–2862. <https://doi.org/10.2174/1381612811319160002>.
- (133) Oehlke, J.; Krause, E.; Wiesner, B.; Beyermann, M.; Bienert, M. Extensive Cellular Uptake into Endothelial Cells of an Amphipathic  $\beta$ -Sheet Forming Peptide. *FEBS Lett.* **1997**, *415* (2), 196–199. [https://doi.org/10.1016/S0014-5793\(97\)01123-X](https://doi.org/10.1016/S0014-5793(97)01123-X).
- (134) Marks, J. R.; Placone, J.; Hristova, K.; Wimley, W. C. Spontaneous Membrane-Translocating Peptides by Orthogonal High-Throughput Screening. *J. Am. Chem. Soc.* **2011**, *133* (23), 8995–9004. <https://doi.org/10.1021/ja2017416>.
- (135) Gomez, J. A.; Chen, J.; Ngo, J.; Hajkova, D.; Yeh, I. J.; Gama, V.; Miyagi, M.; Matsuyama, S. Cell-Penetrating Penta-Peptides (CPP5s): Measurement of Cell Entry and Protein-Transduction Activity. *Pharmaceuticals* **2010**, *3* (12), 3594–3613. <https://doi.org/10.3390/ph3123594>.
- (136) Schafmeister, C. E.; Po, J.; Verdine, G. L. An All-Hydrocarbon Cross-Linking System for Enhancing the Helicity and Metabolic Stability of Peptides [8]. *J. Am. Chem. Soc.* **2000**, *122* (24), 5891–5892. <https://doi.org/10.1021/ja000563a>.
- (137) Ochocki, J. D.; Mullen, D. G.; Wattenberg, E. V.; Distefano, M. D. Evaluation of a Cell Penetrating

- Prenylated Peptide Lacking an Intrinsic Fluorophore via in Situ Click Reaction. *Bioorganic Med. Chem. Lett.* **2011**, 21 (17), 4998–5001. <https://doi.org/10.1016/j.bmcl.2011.04.138>.
- (138) O'Callaghan, K.; Kuliopulos, A.; Covic, L. Turning Receptors on and off with Intracellular Pepducins: New Insights into G-Protein-Coupled Receptor Drug Development. *J. Biol. Chem.* **2012**, 287 (16), 12787–12796. <https://doi.org/10.1074/jbc.R112.355461>.
- (139) Derossi, D.; Calvet, S.; Trembleau, A.; Brunissen, A.; Chassaing, G.; Prochiantz, A. Cell Internalization of the Third Helix of the Antennapedia Homeodomain Is Receptor-Independent. *J. Biol. Chem.* **1996**, 271 (30), 18188–18193. <https://doi.org/10.1074/jbc.271.30.18188>.
- (140) Mueller, J.; Kretschmar, I.; Volkmer, R.; Boisguerin, P. Comparison of Cellular Uptake Using 22 CPPs in 4 Different Cell Lines. *Bioconjug. Chem.* **2008**, 19 (12), 2363–2374. <https://doi.org/10.1021/bc800194e>.
- (141) Kristensen, M.; Birch, D.; Nielsen, H. M. Applications and Challenges for Use of Cell-Penetrating Peptides as Delivery Vectors for Peptide and Protein Cargos. *Int. J. Mol. Sci.* **2016**, 17 (2). <https://doi.org/10.3390/ijms17020185>.
- (142) Järver, P.; Mäger, I.; Langel, Ü. In Vivo Biodistribution and Efficacy of Peptide Mediated Delivery. *Trends Pharmacol. Sci.* **2010**, 31 (11), 528–535. <https://doi.org/10.1016/j.tips.2010.07.006>.
- (143) Killian, J. A.; Timmermans, J. W.; Keur, S.; de Kruijff, B. The Tryptophans of Gramicidin Are Essential for the Lipid Structure Modulating Effect of the Peptide. *Biochim. Biophys. Acta* **1985**, 820, 154–156.
- (144) Berlose, J.-P.; Convert, O.; Derossi, D.; Brunissen, A.; Chassaing, G. Conformational and Associative Behaviours of the Third Helix of Antennapedia Homeodomain in Membrane-Mimetic Environments. *Eur. J. Biochem.* **1996**, 242 (2), 372–386.
- (145) Alves, I. D.; Goasdoué, N.; Correia, I.; Aubry, S.; Galanth, C.; Sagan, S.; Lavielle, S.; Chassaing, G. Membrane Interaction and Perturbation Mechanisms Induced by Two Cationic Cell Penetrating Peptides with Distinct Charge Distribution. *Biochim. Biophys. Acta - Gen. Subj.* **2008**, 1780 (7–8), 948–959. <https://doi.org/10.1016/j.bbagen.2008.04.004>.
- (146) Cardoso, A. M. S.; Trabulo, S.; Cardoso, A. L.; Lorents, A.; Morais, C. M.; Gomes, P.; Nunes, C.; Lúcio, M.; Reis, S.; Padari, K.; et al. S4(13)-PV Cell-Penetrating Peptide Induces Physical and Morphological Changes in Membrane-Mimetic Lipid Systems and Cell Membranes: Implications for Cell Internalization. *Biochim. Biophys. Acta - Biomembr.* **2012**, 1818 (3), 877–888. <https://doi.org/10.1016/j.bbamem.2011.12.022>.
- (147) Binder, H.; Lindblom, G. Charge-Dependent Translocation of the Trojan Peptide Penetratin across Lipid Membranes. *Biophys. J.* **2003**, 85 (2), 982–995. [https://doi.org/10.1016/S0006-3495\(03\)74537-8](https://doi.org/10.1016/S0006-3495(03)74537-8).
- (148) Sakai, N.; Takeuchi, T.; Futaki, S.; Matile, S. Direct Observation of Anion-Mediated Translocation of Fluorescent Oligoarginine Carriers into and across Bulk Liquid and Anionic Bilayer Membranes. *ChemBioChem* **2005**, 6 (1), 114–122. <https://doi.org/10.1002/cbic.200400256>.
- (149) Sakai, N.; Matile, S. Anion-Mediated Transfer of Polyarginine across Liquid and Bilayer Membranes. *J. Am. Chem. Soc.* **2003**, 125 (47), 14348–14356. <https://doi.org/10.1021/ja037601l>.
- (150) Esbjörner, E. K.; Lincoln, P.; Nordén, B. Counterion-Mediated Membrane Penetration: Cationic Cell-Penetrating Peptides Overcome Born Energy Barrier by Ion-Pairing with Phospholipids. *Biochim. Biophys. Acta - Biomembr.* **2007**, 1768 (6), 1550–1558. <https://doi.org/10.1016/j.bbamem.2007.03.004>.

- (151) Herce, H. D.; Garcia, A. E.; Litt, J.; Kane, R. S.; Martin, P.; Enrique, N.; Rebolledo, A.; Milesi, V. Arginine-Rich Peptides Destabilize the Plasma Membrane, Consistent with a Pore Formation Translocation Mechanism of Cell-Penetrating Peptides. *Biophys. J.* **2009**, *97* (7), 1917–1925. <https://doi.org/10.1016/j.bpj.2009.05.066>.
- (152) Herce, H. D.; Garcia, A. E. Molecular Dynamics Simulations Suggest a Mechanism for Translocation of the HIV-1 TAT Peptide across Lipid Membranes. *Proc. Natl. Acad. Sci.* **2007**, *104* (52), 20805–20810. <https://doi.org/10.1073/pnas.0706574105>.
- (153) Brogden, K. A. Antimicrobial Peptides: Pore Formers or Metabolic Inhibitors in Bacteria? *Nat. Rev. Microbiol.* **2005**, *3* (3), 238–250. <https://doi.org/10.1038/nrmicro1098>.
- (154) Clayton, A. H. A.; Atcliffe, B. W.; Howlett, G. J.; Sawyer, W. H. Conformation and Orientation of Penetratin in Phospholipid Membranes. *J. Pept. Sci.* **2006**, *12* (3), 233–238. <https://doi.org/10.1002/psc.715>.
- (155) Bechara, C.; Sagan, S. Cell-Penetrating Peptides: 20 Years Later, Where Do We Stand? *FEBS Lett.* **2013**, *587* (12), 1693–1702. <https://doi.org/10.1016/j.febslet.2013.04.031>.
- (156) Ghibaudi, E.; Boscolo, B.; Inserra, G.; Laurenti, E.; Traversa, S.; Barbero, L.; Ferrari, R. P.; M, D. C. I. F. The Interaction of the Cell-Penetrating Peptide Penetratin with Heparin, Heparansulfates and Phospholipid Vesicles Investigated by ESR Spectroscopy. **2005**, *409* (December 2004), 401–409. <https://doi.org/10.1002/psc.633>.
- (157) Madani, F.; Perálvarez-Marín, A.; Gräslund, A. Liposome Model Systems to Study the Endosomal Escape of Cell-Penetrating Peptides: Transport across Phospholipid Membranes Induced by a Proton Gradient. *J. Drug Deliv.* **2011**, *2011*, 1–7. <https://doi.org/10.1155/2011/897592>.
- (158) Binder, H.; Lindblom, G. Charge-Dependent Translocation of the Trojan Peptide Penetratin across Lipid Membranes. *Biophys. J.* **2003**, *85* (2), 982–995. [https://doi.org/10.1016/S0006-3495\(03\)74537-8](https://doi.org/10.1016/S0006-3495(03)74537-8).
- (159) Rothbard, J. B.; Jessop, T. C.; Jones, L.; Goun, E.; Shinde, R.; Contag, C. H.; Wender, P. A. Mechanistic Insights into Guanidinium-Rich Transporters Entering Cells. In *Handbook of Cell-Penetrating Peptides 2nd edition*; 2007; pp 353–374.
- (160) Afonin, S.; Frey, A.; Bayerl, S.; Fischer, D.; Wadhvani, P.; Weinkauff, S.; Ulrich, A. S. The Cell-Penetrating Peptide TAT(48-60) Induces a Non-Lamellar Phase in DMPC Membranes. *ChemPhysChem* **2006**, *7* (10), 2134–2142. <https://doi.org/10.1002/cphc.200600306>.
- (161) Alves, I. D.; Bechara, C.; Walrant, A.; Zaltsman, Y.; Jiao, C.-Y.; Sagan, S. Relationships between Membrane Binding, Affinity and Cell Internalization Efficacy of a Cell-Penetrating Peptide: Penetratin as a Case Study. *PLoS One* **2011**, *6* (9), e24096. <https://doi.org/10.1371/journal.pone.0024096>.
- (162) Joanne, P.; Galanth, C.; Goasdoué, N.; Nicolas, P.; Sagan, S.; Lavielle, S.; Chassaing, G.; El Amri, C.; Alves, I. D. Lipid Reorganization Induced by Membrane-Active Peptides Probed Using Differential Scanning Calorimetry. *Biochim. Biophys. Acta - Biomembr.* **2009**, *1788* (9), 1772–1781. <https://doi.org/10.1016/j.bbamem.2009.05.001>.
- (163) Golebiewska, U.; Gambhir, A.; Hangyás-Mihályné, G.; Zaitseva, I.; Rädler, J.; McLaughlin, S. Membrane-Bound Basic Peptides Sequester Multivalent (PIP<sub>2</sub>), but Not Monovalent (PS), Acidic Lipids. *Biophys. J.* **2006**, *91* (2), 588–599. <https://doi.org/10.1529/biophysj.106.081562>.
- (164) Gambhir, A.; Hangyás-Mihályné, G.; Zaitseva, I.; Cafiso, D. S.; Wang, J.; Murray, D.; Pentylala, S. N.; Smith, S. O.; McLaughlin, S. Electrostatic Sequestration of PIP<sub>2</sub> on Phospholipid Membranes by Basic/Aromatic Regions of Proteins. *Biophys. J.* **2004**, *86* (4), 2188–2207.



[https://doi.org/10.1016/S0006-3495\(04\)74278-2](https://doi.org/10.1016/S0006-3495(04)74278-2).

- (165) Steringer, J. P.; Lange, S.; Čujová, S.; Šachl, R.; Poojari, C.; Lolicato, F.; Beutel, O.; Müller, H.-M.; Unger, S.; Coskun, Ü.; et al. Key Steps in Unconventional Secretion of Fibroblast Growth Factor 2 Reconstituted with Purified Components. *Elife* **2017**, *6*, 1–36. <https://doi.org/10.7554/eLife.28985>.
- (166) Charlier, L.; Louet, M.; Chaloin, L.; Fuchs, P.; Martinez, J.; Muriaux, D.; Favard, C.; Floquet, N. Coarse-Grained Simulations of the HIV-1 Matrix Protein Anchoring: Revisiting Its Assembly on Membrane Domains. *Biophys. J.* **2014**, *106* (3), 577–585. <https://doi.org/10.1016/j.bpj.2013.12.019>.
- (167) Nakase, I.; Tadokoro, A.; Kawabata, N.; Takeuchi, T.; Katoh, H.; Hiramoto, K.; Negishi, M.; Nomizu, M.; Sugiura, Y.; Futaki, S. Interaction of Arginine-Rich Peptides with Membrane-Associated Proteoglycans Is Crucial for Induction of Actin Organization and Macropinocytosis †. *Biochemistry* **2007**, *46* (2), 492–501. <https://doi.org/10.1021/bi0612824>.
- (168) Gerbal-Chaloin, S.; Gondeau, C.; Aldrian-Herrada, G.; Heitz, F.; Gauthier-Rouvière, C.; Divita, G. First Step of the Cell-Penetrating Peptide Mechanism Involves Rac1 GTPase-Dependent Actin-Network Remodelling. *Biol. Cell* **2007**, *99* (4), 223–238. <https://doi.org/10.1042/BC20060123>.
- (169) Clavier, S.; Illien, F.; Sagan, S.; Bolbach, G.; Sachon, E. Proteomic Comparison of the EWS-FLI1 Expressing Cells EF with NIH-3T3 and Actin Remodeling Effect of (R/W)9 Cell-Penetrating Peptide. *EuPA Open Proteomics* **2016**, *10*, 1–8. <https://doi.org/10.1016/j.euprot.2015.10.002>.
- (170) Rayne, F.; Debaisieux, S.; Yezid, H.; Lin, Y.-L.; Mettling, C.; Konate, K.; Chazal, N.; Arold, S. T.; Pugnère, M.; Sanchez, F.; et al. Phosphatidylinositol-(4,5)-Bisphosphate Enables Efficient Secretion of HIV-1 Tat by Infected T-Cells. *EMBO J.* **2010**, *29* (8), 1348–1362. <https://doi.org/10.1038/emboj.2010.32>.
- (171) Lin, T. Mécanismes Du Transfert Intercellulaire Des Homéoprotéines, 2015.
- (172) Arbuzova, A.; Martushova, K.; Hangyás-Mihályiné, G.; Morris, A. J.; Ozaki, S.; Prestwich, G. D.; McLaughlin, S. Fluorescently Labeled Neomycin as a Probe of Phosphatidylinositol-4,5-Bisphosphate in Membranes. *Biochim. Biophys. Acta - Biomembr.* **2000**, *1464* (1), 35–48. [https://doi.org/10.1016/S0005-2736\(99\)00243-6](https://doi.org/10.1016/S0005-2736(99)00243-6).
- (173) Goodyear, R. J.; Gale, J. E.; Ranatunga, K. M.; Kros, C. J.; Richardson, G. P. Aminoglycoside-Induced Phosphatidylserine Externalization in Sensory Hair Cells Is Regionally Restricted, Rapid, and Reversible. *J. Neurosci.* **2008**, *28* (40), 9939–9952. <https://doi.org/10.1523/JNEUROSCI.1124-08.2008>.
- (174) Burlina, F.; Sagan, S.; Bolbach, G.; Chassaing, G. Quantification of the Cellular Uptake of Cell-Penetrating Peptides by MALDI-TOF Mass Spectrometry. *Angew. Chem. Int. Ed. Engl.* **2005**, *44* (27), 4244–4247. <https://doi.org/10.1002/anie.200500477>.
- (175) Burlina, F.; Sagan, S.; Bolbach, G.; Chassaing, G. A Direct Approach to Quantification of the Cellular Uptake of Cell-Penetrating Peptides Using MALDI-TOF Mass Spectrometry. *Nat. Protoc.* **2006**, *1* (1), 200–205. <https://doi.org/10.1038/10.1038/nprot.2006.30>.
- (176) Aubry, S.; Aussedat, B.; Delaroche, D.; Jiao, C.-Y.; Bolbach, G.; Lavielle, S.; Chassaing, G.; Sagan, S.; Burlina, F. MALDI-TOF Mass Spectrometry: A Powerful Tool to Study the Internalization of Cell-Penetrating Peptides. *Biochim. Biophys. Acta* **2010**, *1798* (12), 2182–2189. <https://doi.org/10.1016/j.bbamem.2009.11.011>.
- (177) Riske, K. A.; Barroso, R. P.; Veqi-Suplicy, C. C.; Germano, R.; Henriques, V. B.; Lamy, M. T. Lipid Bilayer Pre-Transition as the Beginning of the Melting Process. *Biochim. Biophys. Acta -*

- Biomembr.* **2009**, *1788* (5), 954–963. <https://doi.org/10.1016/j.bbamem.2009.01.007>.
- (178) Jobin, M.-L.; Alves, I. D. The Contribution of Differential Scanning Calorimetry for the Study of Peptide/Lipid Interactions; 2019; Vol. 1964, pp 3–15. [https://doi.org/10.1007/978-1-4939-9179-2\\_1](https://doi.org/10.1007/978-1-4939-9179-2_1).
- (179) McElhaney, R. N. Differential Scanning Calorimetric Studies of Lipid-Protein Interactions in Model Membrane Systems. *Biochim. Biophys. Acta* **1986**, *864* (3–4), 361–421. [https://doi.org/10.1016/0304-4157\(86\)90004-3](https://doi.org/10.1016/0304-4157(86)90004-3).
- (180) Jobin, M. L.; Blanchet, M.; Henry, S.; Chaignepain, S.; Manigand, C.; Castano, S.; Lecomte, S.; Burlina, F.; Sagan, S.; Alves, I. D. The Role of Tryptophans on the Cellular Uptake and Membrane Interaction of Arginine-Rich Cell Penetrating Peptides. *Biochim. Biophys. Acta - Biomembr.* **2015**, *1848* (2), 593–602. <https://doi.org/10.1016/j.bbamem.2014.11.013>.
- (181) Lala, A. K.; Kumar, E. R. Orientation of the Benzophenone Group at Various Depths in Bilayers. *J. Am. Chem. Soc.* **1993**, *115* (10), 3982–3988. <https://doi.org/10.1021/ja00063a018>.
- (182) Corradi, V.; Mendez-Villuendas, E.; Ingólfsson, H. I.; Gu, R.-X.; Siuda, I.; Melo, M. N.; Moussatova, A.; DeGagné, L. J.; Sejdiu, B. I.; Singh, G.; et al. Lipid-Protein Interactions Are Unique Fingerprints for Membrane Proteins. *ACS Cent. Sci.* **2018**, *4* (6), 709–717. <https://doi.org/10.1021/acscentsci.8b00143>.
- (183) Marrink, S. J.; Risselada, H. J.; Yefimov, S.; Tieleman, D. P.; de Vries, A. H. The MARTINI Force Field: Coarse Grained Model for Biomolecular Simulations. *J. Phys. Chem. B* **2007**, *111* (27), 7812–7824. <https://doi.org/10.1021/jp071097f>.
- (184) Monticelli, L.; Kandasamy, S. K.; Periole, X.; Larson, R. G.; Tieleman, D. P.; Marrink, S.-J. The MARTINI Coarse-Grained Force Field: Extension to Proteins. *J. Chem. Theory Comput.* **2008**, *4* (5), 819–834. <https://doi.org/10.1021/ct700324x>.
- (185) Futaki, S.; Nakase, I. Cell-Surface Interactions on Arginine-Rich Cell-Penetrating Peptides Allow for Multiplex Modes of Internalization. *Acc. Chem. Res.* **2017**, *50* (10), 2449–2456. <https://doi.org/10.1021/acs.accounts.7b00221>.
- (186) Persson, D.; Thorén, P. E. G.; Nordén, B. Penetratin-Induced Aggregation and Subsequent Dissociation of Negatively Charged Phospholipid Vesicles. *FEBS Lett.* **2001**, *505* (2), 307–312. [https://doi.org/10.1016/S0014-5793\(01\)02843-5](https://doi.org/10.1016/S0014-5793(01)02843-5).
- (187) Ye, J.; Fox, S. A.; Cudic, M.; Rezler, E. M.; Lauer, J. L.; Fields, G. B.; Terentis, A. C. Determination of Penetratin Secondary Structure in Live Cells with Raman Microscopy. *J. Am. Chem. Soc.* **2010**, *132* (3), 980–988. <https://doi.org/10.1021/ja9043196>.
- (188) Lättig-Tünnemann, G.; Prinz, M.; Hoffmann, D.; Behlke, J.; Palm-Apergi, C.; Morano, I.; Herce, H. D.; Cardoso, M. C. Backbone Rigidity and Static Presentation of Guanidinium Groups Increases Cellular Uptake of Arginine-Rich Cell-Penetrating Peptides. *Nat. Commun.* **2011**, *2* (May), 453. <https://doi.org/10.1038/ncomms1459>.
- (189) Lindberg, M.; Biverstahl, H.; Gräslund, A.; Mäler, L. Structure and Positioning Comparison of Two Variants of Penetratin in Two Different Membrane Mimicking Systems by NMR. *Eur. J. Biochem.* **2003**, *270* (14), 3055–3063. <https://doi.org/10.1046/j.1432-1033.2003.03685.x>.
- (190) Balayssac, S.; Burlina, F.; Convert, O.; Bolbach, G.; Chassaing, G.; Lequin, O. Comparison of Penetratin and Other Homeodomain-Derived Cell-Penetrating Peptides: Interaction in a Membrane-Mimicking Environment and Cellular Uptake Efficiency †. *Biochemistry* **2006**, *45* (5), 1408–1420. <https://doi.org/10.1021/bi0518390>.

- (191) Zhang, W.; Smith, S. O. Mechanism of Penetration of Antp(43–58) into Membrane Bilayers †. *Biochemistry* **2005**, *44* (30), 10110–10118. <https://doi.org/10.1021/bi050341v>.
- (192) Magzoub, M.; Eriksson, L. E. G.; Gräslund, A. Comparison of the Interaction, Positioning, Structure Induction and Membrane Perturbation of Cell-Penetrating Peptides and Non-Translocating Variants with Phospholipid Vesicles. *Biophys. Chem.* **2003**, *103* (3), 271–288. [https://doi.org/10.1016/S0301-4622\(02\)00321-6](https://doi.org/10.1016/S0301-4622(02)00321-6).
- (193) Christiaens, B.; Grooten, J.; Reusens, M.; Joliot, A.; Goethals, M.; Vandekerckhove, J.; Prochiantz, A.; Rosseneu, M. Membrane Interaction and Cellular Internalization of Penetratin Peptides. *Eur. J. Biochem.* **2004**, *271* (6), 1187–1197. <https://doi.org/10.1111/j.1432-1033.2004.04022.x>.
- (194) Killian, J. A.; Heijne, G. Von. How Proteins Adapt to a Membrane–Water Interface. **2000**, *0004* (September), 429–434. [https://doi.org/10.1016/S0968-0004\(00\)01626-1](https://doi.org/10.1016/S0968-0004(00)01626-1).
- (195) Almeida, C.; Lamazière, A.; Filleau, A.; Corvis, Y.; Espeau, P.; Ayala-Sanmartin, J. Membrane Re-Arrangements and Rippled Phase Stabilisation by the Cell Penetrating Peptide Penetratin. *Biochim. Biophys. Acta - Biomembr.* **2016**, *1858* (11), 2584–2591. <https://doi.org/10.1016/j.bbamem.2016.07.012>.
- (196) Almeida, C.; Maniti, O.; Di Pisa, M.; Swiecicki, J.-M.; Ayala-Sanmartin, J. Cholesterol Re-Organisation and Lipid de-Packing by Arginine-Rich Cell Penetrating Peptides: Role in Membrane Translocation. *PLoS One* **2019**, *14* (1), e0210985. <https://doi.org/10.1371/journal.pone.0210985>.
- (197) Lamazière, A.; Chassaing, G.; Trugnan, G.; Ayala-Sanmartin, J. Tubular Structures in Heterogeneous Membranes Induced by the Cell Penetrating Peptide Penetratin. *Commun. Integr. Biol.* **2009**, *2* (3), 223–224. <https://doi.org/10.4161/cib.2.3.8073>.
- (198) Clerc, S. G.; Thompson, T. E. Permeability of Dimyristoyl Phosphatidylcholine/Dipalmitoyl Phosphatidylcholine Bilayer Membranes with Coexisting Gel and Liquid-Crystalline Phases. *Biophys. J.* **1995**, *68* (6), 2333–2341. [https://doi.org/10.1016/S0006-3495\(95\)80415-7](https://doi.org/10.1016/S0006-3495(95)80415-7).
- (199) Komatsu, H.; Okada, S. Increased Permeability of Phase-Separated Liposomal Membranes with Mixtures of Ethanol-Induced Interdigitated and Non-Interdigitated Structures. *Biochim. Biophys. Acta - Biomembr.* **1995**, *1237* (2), 169–175. [https://doi.org/10.1016/0005-2736\(95\)00098-N](https://doi.org/10.1016/0005-2736(95)00098-N).
- (200) Menger, F. M.; Seredyuk, V. A.; Kitaeva, M. V.; Yaroslavov, A. A.; Melik-Nubarov, N. S. Migration of Poly- L -Lysine through a Lipid Bilayer. *J. Am. Chem. Soc.* **2003**, *125* (10), 2846–2847. <https://doi.org/10.1021/ja021337z>.
- (201) Baumgärtner, P.; Geiger, M.; Zieseniss, S.; Malleier, J.; Huntington, J. A.; Hochrainer, K.; Bielek, E.; Stoeckelhuber, M.; Lauber, K.; Scherfeld, D.; et al. Phosphatidylethanolamine Critically Supports Internalization of Cell-Penetrating Protein C Inhibitor. *J. Cell Biol.* **2007**, *179* (4), 793–804. <https://doi.org/10.1083/jcb.200707165>.
- (202) Murayama, T.; Masuda, T.; Afonin, S.; Kawano, K.; Takatani-Nakase, T.; Ida, H.; Takahashi, Y.; Fukuma, T.; Ulrich, A. S.; Futaki, S. Loosening of Lipid Packing Promotes Oligoarginine Entry into Cells. *Angew. Chemie Int. Ed.* **2017**, *56* (26), 7644–7647. <https://doi.org/10.1002/anie.201703578>.
- (203) Dormán, G.; Nakamura, H.; Pulsipher, A.; Prestwich, G. D. The Life of Pi Star: Exploring the Exciting and Forbidden Worlds of the Benzophenone Photophore. *Chem. Rev.* **2016**, *116* (24), 15284–15398. <https://doi.org/10.1021/acs.chemrev.6b00342>.
- (204) Clavier, S.; Bolbach, G.; Sachon, E. Photocross-Linked Peptide-Protein Complexes Analysis: A Comparative Study of CID and ETD Fragmentation Modes. *J. Am. Soc. Mass Spectrom.* **2015**, *26*

- (6), 1014–1026. <https://doi.org/10.1007/s13361-015-1095-0>.
- (205) Czarniecki, M. F.; Breslow, R. Photochemical Probes for Model Membrane Structures. *J. Am. Chem. Soc.* **1979**, *101* (13), 3675–3676. <https://doi.org/10.1021/ja00507a052>.
- (206) Breslow, R.; Kitabatake, S.; Rothbard, J. Photoreactions of Charged Benzophenone with Amphiphiles in Micelles and Multicomponent Aggregates as Conformational Probes. *J. Am. Chem. Soc.* **1978**, *100* (26), 8156–8160. <https://doi.org/10.1021/ja00494a022>.
- (207) Andreu, I.; Neshchadin, D.; Rico, E.; Griesser, M.; Samadi, A.; Morera, I. M.; Gescheidt, G.; Miranda, M. A. Probing Lipid Peroxidation by Using Linoleic Acid and Benzophenone. *Chem. - A Eur. J.* **2011**, *17* (36), 10089–10096. <https://doi.org/10.1002/chem.201100983>.
- (208) Xu, T.; Pi, Z.; Song, F.; Liu, S.; Liu, Z. Benzophenone Used as the Photochemical Reagent for Pinpointing C=C Locations in Unsaturated Lipids through Shotgun and Liquid Chromatography–Mass Spectrometry Approaches. *Anal. Chim. Acta* **2018**, *1028*, 32–44. <https://doi.org/10.1016/j.aca.2018.04.046>.
- (209) Bednařík, A.; Bölsker, S.; Soltwisch, J.; Dreisewerd, K. An On-Tissue Paternò–Büchi Reaction for Localization of Carbon–Carbon Double Bonds in Phospholipids and Glycolipids by Matrix-Assisted Laser-Desorption–Ionization Mass-Spectrometry Imaging. *Angew. Chemie - Int. Ed.* **2018**, *57* (37), 12092–12096. <https://doi.org/10.1002/anie.201806635>.
- (210) Esch, P.; Heiles, S. Charging and Charge Switching of Unsaturated Lipids and Apolar Compounds Using Paternò–Büchi Reactions. *J. Am. Soc. Mass Spectrom.* **2018**, *29* (10), 1971–1980. <https://doi.org/10.1007/s13361-018-2023-x>.
- (211) Jeck, V.; Korf, A.; Vosse, C.; Hayen, H. Localization of Double-Bond Positions in Lipids by Tandem Mass Spectrometry Succeeding High-Performance Liquid Chromatography with Post-Column Derivatization. *Rapid Commun. Mass Spectrom.* **2018**, No. May, 1–9. <https://doi.org/10.1002/rcm.8262>.
- (212) Wäldchen, F.; Becher, S.; Esch, P.; Kompauer, M.; Heiles, S. Selective Phosphatidylcholine Double Bond Fragmentation and Localisation Using Paternò–Büchi Reactions and Ultraviolet Photodissociation. *Analyst* **2017**, *142* (24), 4744–4755. <https://doi.org/10.1039/c7an01158j>.
- (213) Ma, X.; Xia, Y. Pinpointing Double Bonds in Lipids by Paternò–Büchi Reactions and Mass Spectrometry. *Angew. Chemie Int. Ed.* **2014**, *53* (10), 2592–2596. <https://doi.org/10.1002/anie.201310699>.
- (214) Stinson, C. A.; Xia, Y. A Method of Coupling the Paternò–Büchi Reaction with Direct Infusion ESI-MS/MS for Locating the CC Bond in Glycerophospholipids. *Analyst* **2016**, *141* (12), 3696–3704. <https://doi.org/10.1039/c6an00015k>.
- (215) Nakatani, K.; Yoshida, T.; Saito, I. Photochemistry of Benzophenone Immobilized in a Major Groove of DNA: Formation of Thermally Reversible Interstrand Cross-Link. *J. Am. Chem. Soc.* **2002**, *124* (10), 2118–2119.
- (216) Burkhard, J. A.; Wuitschik, G.; Rogers-Evans, M.; Müller, K.; Carreira, E. M. Minireviews Oxetanes as Versatile Elements in Drug Discovery and Synthesis. *Angew. Chemie Int. Ed.* **2010**, *49*, 9052–9067. <https://doi.org/10.1002/anie.200907155>.
- (217) Weinberger, M.; Wagenknecht, H.-A. Synthesis of a Benzophenone C-Nucleoside as Potential Triplet Energy and Charge Donor in Nucleic Acids. *Synthesis (Stuttg.)* **2012**, *2012* (04), 648–652. <https://doi.org/10.1055/s-0031-1289672>.
- (218) Liu, X. L.; Wang, J. B.; Tong, Y.; Song, Q. H. Regioselectivity and Competition of the Paternò–Büchi

- Reaction and Triplet-Triplet Energy Transfer between Triplet Benzophenones and Pyrimidines: Control by Triplet Energy Levels. *Chem. - A Eur. J.* **2013**, *19* (39), 13216–13223. <https://doi.org/10.1002/chem.201300958>.
- (219) Breslow, R.; Baldwin, S.; Reichtner, T.; Kalicky, P.; Liu, S.; Washburnle, W. Remote Oxidation. *J. Am. Chem. Soc.* **1973**, *95* (3), 3251–3262.
- (220) Breslow, R. *Artificial Enzymes*; Breslow, R., Ed.; Wiley, 2005. <https://doi.org/10.1002/3527606645>.
- (221) Breslow, R.; Baldwin, S.; Flechtner, T.; Kalicky, P.; Liu, S.; Washburn, W. Remote Oxidation of Steroids by Photolysis of Attached Benzophenone Groups. *J. Am. Chem. Soc.* **1973**, *95* (10), 3251–3262. <https://doi.org/10.1021/ja00791a031>.
- (222) Fenn, J.; Mann, M.; Meng, C.; Wong, S.; Whitehouse, C. Electrospray Ionization for Mass Spectrometry of Large Biomolecules. *Science (80-. )*. **1989**, *246* (4926), 64–71. <https://doi.org/10.1126/science.2675315>.
- (223) Karas, M.; Hillenkamp, F. Laser Desorption Ionization of Proteins with Molecular Masses Exceeding 10,000 Daltons. *Anal. Chem.* **1988**, *60* (20), 2299–2301. <https://doi.org/10.1021/ac00171a028>.
- (224) Roepstorff, P.; Fohlman, J. Proposal for a Common Nomenclature for Sequence Ions Inmass Spectra of Peptides. *Biomed. Mass Spectrom.* **1984**, *11* (11), 601–601. <https://doi.org/10.1002/bms.1200111109>.
- (225) Hunt, D. F.; Yates, J. R.; Shabanowitz, J.; Winston, S.; Hauer, C. R. Protein Sequencing by Tandem Mass Spectrometry. *Proc. Natl. Acad. Sci.* **1986**, *83* (17), 6233–6237. <https://doi.org/10.1073/pnas.83.17.6233>.
- (226) Biemann, K. Contributions of Mass Spectrometry to Peptide and Protein Structure. *Biol. Mass Spectrom.* **1988**, *16* (1–12), 99–111. <https://doi.org/10.1002/bms.1200160119>.
- (227) Papayannopoulos, I. A. The Interpretation of Collision-Induced Dissociation Tandem Mass Spectra of Peptides. *Mass Spectrom. Rev.* **1995**, *14* (1), 49–73. <https://doi.org/10.1002/mas.1280140104>.
- (228) Coon, J. J. Collisions or Electrons? Protein Sequence Analysis in the 21st Century. *Anal. Chem.* **2009**, *81* (9), 3208–3215. <https://doi.org/10.1021/ac802330b>.
- (229) Paizs, B.; Suhai, S. Fragmentation Pathways of Protonated Peptides. *Mass Spectrom. Rev.* **2005**, *24* (4), 508–548. <https://doi.org/10.1002/mas.20024>.
- (230) Somogyi, Á.; Wysocki, V. H.; Mayer, I. The Effect of Protonation Site on Bond Strengths in Simple Peptides: Application of Ab Initio and Modified Neglect of Differential Overlap Bond Orders and Modified Neglect of Differential Overlap Energy Partitioning. *J. Am. Soc. Mass Spectrom.* **1994**, *5* (8), 704–717. [https://doi.org/10.1016/1044-0305\(94\)80002-2](https://doi.org/10.1016/1044-0305(94)80002-2).
- (231) Dongré, A. R.; Jones, J. L.; Somogyi, Á.; Wysocki, V. H. Influence of Peptide Composition, Gas-Phase Basicity, and Chemical Modification on Fragmentation Efficiency: Evidence for the Mobile Proton Model. *J. Am. Chem. Soc.* **1996**, *118* (35), 8365–8374. <https://doi.org/10.1021/ja9542193>.
- (232) Paizs, B.; Suhai, S. Combined Quantum Chemical and RRKM Modeling of the Main Fragmentation Pathways of Protonated GGG. II. Formation of B2, Y1, and Y2 Ions. *Rapid Commun. Mass Spectrom.* **2002**, *16* (5), 375–389. <https://doi.org/10.1002/rcm.586>.
- (233) Cordero, M. M.; Houser, J. J.; Wesdemiotis, C. Neutral Products Formed during Backbone

- Fragmentations of Protonated Peptides in Tandem Mass Spectrometry. *Anal. Chem.* **1993**, *65* (11), 1594–1601. <https://doi.org/10.1021/ac00059a019>.
- (234) Yalcin, T.; Csizmadia, I. G.; Peterson, M. R.; Harrison, A. G. The Structure and Fragmentation of B<sub>n</sub> (N≥3) Ions in Peptide Spectra. *J. Am. Soc. Mass Spectrom.* **1996**, *7* (3), 233–242. [https://doi.org/10.1016/1044-0305\(95\)00677-X](https://doi.org/10.1016/1044-0305(95)00677-X).
- (235) Yalcin, T.; Khouw, C.; Csizmadia, I. G.; Peterson, M. R.; Harrison, A. G. Why Are B Ions Stable Species in Peptide Spectra? *J. Am. Soc. Mass Spectrom.* **1995**, *6* (12), 1165–1174. [https://doi.org/10.1016/1044-0305\(95\)00569-2](https://doi.org/10.1016/1044-0305(95)00569-2).
- (236) Paizs, B.; Lendvay, G.; Vékey, K.; Suhai, S. Formation of B<sub>2</sub><sup>+</sup> Ions from Protonated Peptides: An Ab Initio Study. *Rapid Commun. Mass Spectrom.* **1999**, *13* (6), 525–533. [https://doi.org/10.1002/\(SICI\)1097-0231\(19990330\)13:6<525::AID-RCM519>3.0.CO;2-O](https://doi.org/10.1002/(SICI)1097-0231(19990330)13:6<525::AID-RCM519>3.0.CO;2-O).
- (237) Polce, M. J.; Ren, D.; Wesdemiotis, C. Dissociation of the Peptide Bond in Protonated Peptides. *J. Mass Spectrom.* **2000**, *35* (12), 1391–1398. [https://doi.org/10.1002/1096-9888\(200012\)35:12<1391::AID-JMS85>3.0.CO;2-1](https://doi.org/10.1002/1096-9888(200012)35:12<1391::AID-JMS85>3.0.CO;2-1).
- (238) Paizs, B.; Suhai, S. Combined Quantum Chemical and RRKM Modeling of the Main Fragmentation Pathways of Protonated GGG. I. Cis-Trans Isomerization around Protonated Amide Bonds. *Rapid Commun. Mass Spectrom.* **2001**, *15* (23), 2307–2323. <https://doi.org/10.1002/rcm.507>.
- (239) Farrugia, J. M.; O’Hair, R. A. .; Reid, G. E. Do All B<sub>2</sub> Ions Have Oxazolone Structures? Multistage Mass Spectrometry and Ab Initio Studies on Protonated N-Acyl Amino Acid Methyl Ester Model Systems. *Int. J. Mass Spectrom.* **2001**, *210–211*, 71–87. [https://doi.org/10.1016/S1387-3806\(01\)00421-3](https://doi.org/10.1016/S1387-3806(01)00421-3).
- (240) Harrison, A. G. Fragmentation Reactions of Protonated Peptides Containing Glutamine or Glutamic Acid. *J. Mass Spectrom.* **2003**, *38* (2), 174–187. <https://doi.org/10.1002/jms.427>.
- (241) Jonsson, A. P.; Bergman, T.; Jörnvall, H.; Griffiths, W. J. Gln-Gly Cleavage: A Dominant Dissociation Site in the Fragmentation of Protonated Peptides. *Rapid Commun. Mass Spectrom.* **2001**, *15* (9), 713–720. <https://doi.org/10.1002/rcm.289>.
- (242) Zubarev, R. A.; Kelleher, N. L.; McLafferty, F. W. Electron Capture Dissociation of Multiply Charged Protein Cations. A Nonergodic Process. *J. Am. Chem. Soc.* **1998**, *120* (13), 3265–3266. <https://doi.org/10.1021/ja973478k>.
- (243) Syka, J. E. P.; Coon, J. J.; Schroeder, M. J.; Shabanowitz, J.; Hunt, D. F. Peptide and Protein Sequence Analysis by Electron Transfer Dissociation Mass Spectrometry. *Proc. Natl. Acad. Sci.* **2004**, *101* (26), 9528–9533. <https://doi.org/10.1073/pnas.0402700101>.
- (244) Tureček, F.; Julian, R. R. Peptide Radicals and Cation Radicals in the Gas Phase. *Chem. Rev.* **2013**, *113* (8), 6691–6733. <https://doi.org/10.1021/cr400043s>.
- (245) Elviri, L. ETD and ECD Mass Spectrometry Fragmentation for the Characterization of Protein Post Translational Modifications. In *Tandem Mass Spectrometry - Applications and Principles*; InTech, 2012. <https://doi.org/10.5772/35277>.
- (246) Debois, D.; Smargiasso, N.; Demeure, K.; Asakawa, D.; Zimmerman, T. A.; Quinton, L.; De Pauw, E. MALDI In-Source Decay, from Sequencing to Imaging. In *Applications of MALDI-TOF Spectroscopy*; Springer, 2012; pp 117–141. [https://doi.org/10.1007/128\\_2012\\_363](https://doi.org/10.1007/128_2012_363).
- (247) Schiller, J.; Arnhold, J.; Benard, S.; Mu, M.; Reichl, S.; Arnold, K. Lipid Analysis by Matrix-Assisted Laser Desorption and Ionization Mass Spectrometry: A Methodological Approach. *Anal. Biochem.* **1999**, *267*, 46–56.

- (248) Schiller, J.; Süß, R.; Fuchs, B.; Müller, M.; Petkovic, M.; Zschörnig, O.; Waschipky, H. The Suitability of Different DHB Isomers as Matrices for the MALDI-TOF MS Analysis of Phospholipids : Which Isomer for What Purpose? *Eur. Biophys. J.* **2007**, *36* (4–5), 517–527. <https://doi.org/10.1007/s00249-006-0090-6>.
- (249) Asakawa, D. Principles of Hydrogen Radical Mediated Peptide/Protein Fragmentation during Matrix-Assisted Laser Desorption/Ionization Mass Spectrometry. *Mass Spectrom. Rev.* **2016**, *35* (4), 535–556. <https://doi.org/10.1002/mas.21444>.
- (250) Fréneau, M.; Hoffmann, N. The Paternò-Büchi Reaction—Mechanisms and Application to Organic Synthesis. *J. Photochem. Photobiol. C Photochem. Rev.* **2017**, *33*, 83–108. <https://doi.org/10.1016/j.jphotochemrev.2017.10.002>.
- (251) Walrant, A.; Cardon, S.; Burlina, F.; Sagan, S. Membrane Crossing and Membranotropic Activity of Cell-Penetrating Peptides: Dangerous Liaisons? *Acc. Chem. Res.* **2017**, *50* (12), 2968–2975. <https://doi.org/10.1021/acs.accounts.7b00455>.
- (252) Haberkant, P.; Raijmakers, R.; Wildwater, M.; Sachsenheimer, T.; Brügger, B.; Maeda, K.; Houweling, M.; Gavin, A. C.; Schultz, C.; Van Meer, G.; et al. In Vivo Profiling and Visualization of Cellular Protein-Lipid Interactions Using Bifunctional Fatty Acids. *Angew. Chemie - Int. Ed.* **2013**, *52* (14), 4033–4038. <https://doi.org/10.1002/anie.201210178>.
- (253) Xia, Y.; Peng, L. Photoactivatable Lipid Probes for Studying Biomembranes by Photoaffinity Labeling. *Chem. Rev.* **2013**, *113* (10), 7880–7929. <https://doi.org/10.1021/cr300419p>.
- (254) Gubbens, J.; Ruijter, E.; de Fays, L. E. V.; Damen, J. M. A.; de Kruijff, B.; Slijper, M.; Rijkers, D. T. S.; Liskamp, R. M. J.; de Kroon, A. I. P. M. Photocrosslinking and Click Chemistry Enable the Specific Detection of Proteins Interacting with Phospholipids at the Membrane Interface. *Chem. Biol.* **2009**, *16* (1), 3–14. <https://doi.org/10.1016/j.chembiol.2008.11.009>.
- (255) Kölbel, K.; Ihling, C. H.; Sinz, A. Analysis of Peptide Secondary Structures by Photoactivatable Amino Acid Analogues. *Angew. Chemie - Int. Ed.* **2012**, *51* (50), 12602–12605. <https://doi.org/10.1002/anie.201205308>.
- (256) Peng, T.; Yuan, X.; Hang, H. C. Turning the Spotlight on Protein-Lipid Interactions in Cells. *Curr. Opin. Chem. Biol.* **2014**, *21*, 144–153. <https://doi.org/10.1016/j.cbpa.2014.07.015>.
- (257) Kramer, K.; Sachsenberg, T.; Beckmann, B. M.; Qamar, S.; Boon, K. L.; Hentze, M. W.; Kohlbacher, O.; Urlaub, H. Photo-Cross-Linking and High-Resolution Mass Spectrometry for Assignment of RNA-Binding Sites in RNA-Binding Proteins. *Nat. Methods* **2014**, *11* (10), 1064–1070. <https://doi.org/10.1038/nmeth.3092>.
- (258) Kawaguchi, Y.; Takeuchi, T.; Kuwata, K.; Chiba, J.; Hatanaka, Y.; Nakase, I.; Futaki, S. Syndecan-4 Is a Receptor for Clathrin-Mediated Endocytosis of Arginine-Rich Cell-Penetrating Peptides. *Bioconjug. Chem.* **2016**, *27* (4), 1119–1130. <https://doi.org/10.1021/acs.bioconjchem.6b00082>.
- (259) Jiao, C. Y.; Alves, I. D.; Point, V.; Lavielle, S.; Sagan, S.; Chassaing, G. Comparing Lipid Photo-Cross-Linking Efficacy of Penetratin Analogues Bearing Three Different Photoprobes: Dithienyl Ketone, Benzophenone, and Trifluoromethylaryldiazirine. *Bioconjug. Chem.* **2010**, *21* (2), 352–359. <https://doi.org/10.1021/bc900466q>.
- (260) Bechara, C.; Pallerla, M.; Zaltsman, Y.; Burlina, F.; Alves, I. D.; Lequin, O.; Sagan, S. Tryptophan within Basic Peptide Sequences Triggers Glycosaminoglycan- Dependent Endocytosis. *FASEB J.* **2013**, *27* (2), 738–749. <https://doi.org/10.1096/fj.12-216176>.
- (261) Walrant, A.; Correia, I.; Jiao, C. Y.; Lequin, O.; Bent, E. H.; Goasdoué, N.; Lacombe, C.; Chassaing, G.; Sagan, S.; Alves, I. D. Different Membrane Behaviour and Cellular Uptake of Three Basic

- Arginine-Rich Peptides. *Biochim. Biophys. Acta - Biomembr.* **2011**, *1808* (1), 382–393. <https://doi.org/10.1016/j.bbamem.2010.09.009>.
- (262) Kumarasamy, E.; Raghunathan, R.; Kandappa, S. K.; Sreenithya, A.; Jockusch, S.; Sunoj, R. B.; Sivaguru, J. Transposed Paternò-Büchi Reaction. *J. Am. Chem. Soc.* **2017**, *139* (2), 655–662. <https://doi.org/10.1021/jacs.6b05936>.
- (263) Atik, A. E.; Hernandez, O.; Maître, P.; Yalcin, T. Specific Rearrangement Reactions of Acetylated Lysine Containing Peptide Bn (N=4-7) Ion Series. *J. Mass Spectrom.* **2014**, *49* (12), 1290–1297. <https://doi.org/10.1002/jms.3462>.
- (264) Reis, A.; Spickett, C. M. Biochimica et Biophysica Acta Chemistry of Phospholipid Oxidation. *Biochim. Biophys. Acta - Biomembr.* **2012**, *1818* (10), 2374–2387. <https://doi.org/10.1016/j.bbamem.2012.02.002>.
- (265) Forbes, M. W.; Jockusch, R. A.; Young, A. B.; Harrison, A. G. Fragmentation of Protonated Dipeptides Containing Arginine. Effect of Activation Method. *J. Am. Soc. Mass Spectrom.* **2007**, *18* (11), 1959–1966. <https://doi.org/10.1016/j.jasms.2007.08.003>.
- (266) Radhakrishnan, A.; McConnell, H. Condensed Complexes in Vesicles Containing Cholesterol and Phospholipids. *Proc. Natl. Acad. Sci.* **2005**, *102* (36), 12662–12666. <https://doi.org/10.1073/pnas.0506043102>.
- (267) Maxfield, F. R.; van Meer, G. Cholesterol, the Central Lipid of Mammalian Cells. *Curr. Opin. Cell Biol.* **2010**, *22* (4), 422–429. <https://doi.org/10.1016/j.ceb.2010.05.004>.
- (268) Ermilova, I.; Lyubartsev, A. P. Cholesterol in Phospholipid Bilayers: Positions and Orientations inside Membranes with Different Unsaturation Degrees. *Soft Matter* **2019**, *15* (1), 78–93. <https://doi.org/10.1039/C8SM01937A>.
- (269) Downard, K. M.; Biemann, K. Amino Acid Sequence Prerequisites for the Formation of Cn Ions. *J. Am. Soc. Mass Spectrom.* **1993**, *4* (11), 874–831. [https://doi.org/10.1016/1044-0305\(93\)87005-W](https://doi.org/10.1016/1044-0305(93)87005-W).
- (270) Lee, Y. J.; Lee, Y. M. Formation of C1 Fragment Ions in Collision-Induced Dissociation of Glutamine-Containing Peptide Ions: A Tip for de Novo Sequencing. *Rapid Commun. Mass Spectrom.* **2004**, *18* (18), 2069–2076. <https://doi.org/10.1002/rcm.1593>.
- (271) Winter, D.; Seidler, J.; Hahn, B.; Lehmann, W. D. Structural and Mechanistic Information on C1 Ion Formation in Collision-Induced Fragmentation of Peptides. *J. Am. Soc. Mass Spectrom.* **2010**, *21* (10), 1814–1820. <https://doi.org/10.1016/j.jasms.2010.06.020>.
- (272) Wang, B.; Liu, J.; Cao, J.; Wang, H.; Guan, X.; Wei, Z.; Guo, X. Investigation of c Ions Formed by N-Terminally Charged Peptides upon Collision-Induced Dissociation. *J. Mass Spectrom.* **2016**, *51* (11), 989–997. <https://doi.org/10.1002/jms.3841>.
- (273) Peng, J.; Zu, L.; Fang, W.; Huang, L.; Wang, Y.; He, D. Selective Cleavage of Protonated Penetratin and Its Substitutes under Low-Energy Collision-Induced Dissociation Condition. *J. Mass Spectrom.* **2010**, *45* (6), n/a-n/a. <https://doi.org/10.1002/jms.1748>.
- (274) Verga, D.; Hamon, F.; Poyer, F.; Bombard, S.; Teulade-Fichou, M. P. Photo-Cross-Linking Probes for Trapping G-Quadruplex DNA. *Angew. Chemie - Int. Ed.* **2014**, *53* (4), 994–998. <https://doi.org/10.1002/anie.201307413>.
- (275) Kaiser, E.; Colecott, R. L.; Bossinger, C. D.; Cook, P. I. Color Test for Detection of Free Terminal Amino Groups in the Solid-Phase Synthesis of Peptides. *Anal. Biochem.* **1970**, *34* (2), 595–598. [https://doi.org/10.1016/0003-2697\(70\)90146-6](https://doi.org/10.1016/0003-2697(70)90146-6).





# APPENDIX